



UNIVERSIDAD DE VALLADOLID ESCUELA DE INGENIERIAS INDUSTRIALES

Grado en Ingeniería Energética

DESIGN OF A ZERO-EMISSION BUILDING WITH RENEWABLE ENERGY SOURCES IN SIMULINK/MATLAB

Autor:

Fernández Alonso, Yago

Responsable de Intercambio en la Uva Daniel Moriñigo Sotelo

Technical University of Crete

Valladolid, julio 2025.

TFG REALIZADO EN PROGRAMA DE INTERCAMBIO

TÍTULO: Design of a zero-emission building with renewable energy

sources in Simulink/MATLAB

ALUMNO: Yago Fernández Alonso

FECHA: 9 de julio de 2025

CENTRO: Universidad de Valladolid

UNIVERSIDAD: Technical University of Crete

TUTOR: Eftychios Koutroulis





DESIGN OF A ZERO-EMISSION BUILDING WITH RENEWABLE ENERGY SOURCES IN SIMULINK/MATLAB

JUNE 28, 2025 YAGO FERNÁNDEZ ALONSO Technical University of Crete

©2025 Yago Fernández Alonso All rights reserved.

INDEX

Ack	nowledgments	3
Abs	tract	4
List	of tables	5
List	of figures	6
Non	menclature	. 13
Cha	pter I: Introduction	. 14
В	ackground	. 14
0	Objectives	. 15
N	Лethodology	. 16
0	Outline	. 18
Cha	pter II: Theoretical Background	. 20
1		
2	. Basic Principles of Energy in Buildings	. 20
	The Zeroth Law of Thermodynamics	. 21
	The First Law of Thermodynamics	. 21
	The Second Law of Thermodynamics	. 23
	Heat transfer mechanisms	. 28
3	. Renewable energy generation: solar power and energy storage	. 30
	3.1 Photovoltaic Panels	. 30
	3.2 Battery Energy Storage	. 43
4	. Ideal Compression cycle	. 50
5	. Efficient Thermal Systems: Heat Pumps and Four-Way Valves	. 54
	5.1 Reversible Heat Pumps for Residential Applications	. 55
	5.2 Four-Way Valves	. 59
	5.3 Refrigerant: R-410A Properties and Considerations	. 60
6	-	
	pter III: Modelling Setup	
	Characteristics of the model	65
,	CHALACTERS II COLLINE MODEL	n >

8	. MATLAB model	68
	8.1 Original scenario	70
	8.2 Consumption optimization	78
	8.3 Economic optimization	83
	8.4 Comparison of results	87
9	. Simulink model	100
	9.1 System Architecture and Overview	102
	9.2 Control System Architecture and Logic	107
	9.3 Heat Exchanger Subsystems	110
	9.4 Refrigerant Circuit and Flow Control	111
	9.5 Compressor System and Mechanical Components	111
	9.6 Control System Integration and Operation	113
	9.7 Performance Monitoring and Analysis	113
Cha	pter IV: Results	115
T	ypical day	116
T	he coldest day	138
T	he hottest day	158
Cha	pter V: Conclusions and future work	180
C	omparison between the cases of study	180
	EV Charging	180
	Batteries	181
	Solar production and consumption	182
	Economic cost	183
	Energy flows	185
	Comparison conclusion	186
F	uture work	188
Refe	erences	191

Acknowledgments

I don't even know where to begin — and words have never really been my thing.

First and foremost, I want to thank the people who have always stood by me—my friends and, above all, my family.

Especially Laura, David, Ángela, my cousin, my aunt, my mother, my father, and most of all, my brother.

They've always been there for me, no matter what or when, and I know I can always count on them. I truly don't know what I would do without them.

I also want to thank all the people who shared this Erasmus experience with me—because without you, none of it would have made sense. In such a short time, you've become a truly important part of my life. I've had so much fun, and I owe it all to you.

Words can't express how happy and grateful I am to have met you and to have been able to share this precious time that I will never forget.

Even though time will pass, and our paths may part, I will always remember the moments we shared.

To all of you — Domenico, Emma, Hugo, Jannik, Laila, Paul, Markus, Oleg, David, Joel, Alba, Adrián, Loreto and Magdalena —

just thank you for making this experience unforgettable.

Grazie, Danke, Gracias

Love to you all

Yago

Abstract

This study focuses on designing and simulating a residential zero-emission building (ZEB) integrated with Renewable Energy Sources (RES), such as photovoltaic (PV) panels, and an energy management algorithm. The aim is to optimize energy performance by increasing the self-consumption of locally generated RES and minimizing reliance on the grid. A dynamic simulation model was created in MATLAB/Simulink to mimic real building energy behaviour, accounting for heating, ventilation, air conditioning (HVAC), and household appliances. The energy management algorithm balances supply and demand, improves efficiency, and maximizes economic benefits. The simulation was tested on a building in Valladolid, considering three weather conditions: typical day, coldest day, and hottest day of the year. The results showed that energy deficits were reduced by up to 62%, demonstrating that smart energy management can effectively reduce energy waste and unmet demand, enhancing both environmental and economic performance in residential buildings.

Keywords: Zero-emission building (ZEB), Renewable Energy Source (RES), Energy management algorithm, Photovoltaic panels, Energy efficiency.

Resumen:

Este estudio aborda el diseño y la simulación de un edificio residencial de cero emisiones (ZEB) con fuentes de energía renovable (FER), como paneles fotovoltaicos (FV), y un algoritmo de gestión energética. El objetivo es optimizar el rendimiento energético del edificio, maximizando el autoconsumo de energía renovable y minimizando la dependencia de la red eléctrica. Se desarrolló un modelo dinámico en MATLAB/Simulink para simular el comportamiento energético del edificio, considerando cargas como calefacción, ventilación, aire acondicionado (HVAC) y electrodomésticos. Un algoritmo inteligente de gestión energética se implementó para equilibrar la oferta y la demanda, mejorar la eficiencia y maximizar los beneficios económicos. El modelo se aplicó a un edificio en Valladolid bajo tres condiciones climáticas. Los resultados mostraron una mejora significativa en la reducción de déficits energéticos, alcanzando hasta un 62%. Este enfoque contribuye a la mejora ambiental y económica en la edificación residencial.

Palabras clave: Edificio cero emisiones (ZEB), fuente de energía renovable, algoritmo de gestión energética, paneles fotovoltaicos, eficiencia energética.

List of tables

Table 1. Electricity prices	71
Table 2. Thermal Characteristics of the roof	. 104
Table 3. Thermal characteristics of the exterior walls	. 105
Table 4. Thermal characteristics of the interior walls	. 105
Table 5. Thermal characteristics of the windows	. 105
Table 6. Typical day hourly solar data	. 116
Table 7. Typical day energy consumption	. 120
Table 8. Typical day EV parameters	. 128
Table 9. Typical day batteries parameters summary	. 131
Table 10. Typical day economic cost comparison	. 133
Table 11. Typical day Energy Flows summary	. 137
Table 12. The coldest day hourly solar data	. 138
Table 13. The coldest day energy consumption	. 142
Table 14. The coldest day EV parameters	. 148
Table 15. The coldest day batteries parameters summary	. 151
Table 16. The coldest day economic cost comparison	. 153
Table 17. The coldest day Energy Flows summary	. 157
Table 18. The hottest day hourly solar data	. 158
Table 19. The hottest day energy consumption	. 162
Table 20. The hottest day EV parameters	. 170
Table 21. The hottest day batteries parameter summary	. 173
Table 22. The hottest day economic cost comparison	. 175
Table 23. The hottest day Energy Flows summary	. 179
Table 28. Solar production and energy consumption summary	. 182

List of figures

Figure 1. Clausius statement. Source: (Vega Maza, 2022) 24
Figure 2. Kelvin – Plack Statement. Source: (Vega Maza, 2022)24
Figure 3. The photovoltaic effect
Figure 4. Pn-junction diode. Source: (Chamarro Camazón, 2023)
Figure 5. Principle of operation of a photovoltaic cell
Figure 6. Photovoltaic panel I-V characteristic derivation. Source: (Chamarro Camazón
2023)
Figure 7. I-V Curve of a photovoltaic panel. Source: (Stuart Bowden & Christians
Honsberg, 2025)
Figure 8. The effect of temperature on the I-V characteristics of a solar cell. Source
(Stuart Bowden & Christiana Honsberg, 2025)
Figure 9. The effect of irradiance on the I-V characteristics of a solar cell. Source: (Stuar
Bowden & Christiana Honsberg, 2025)
Figure 10. Performance I-V curves for two identical solar cells connected in series
Source: (Fedkin, 2025)
Figure 11. Performance I-V curves for two identical solar cells connected in parallel
Source: (Fedkin, 2025)
Figure 12. Types of inverters output waveforms. Source: (Kansagara, 2025) 43
Figure 13. Types of single-axis solar tracking. Source: (Gestor, 2025)
Figure 14. Parts of a lithium-ion battery. Source: (Chapman, 2025)
Figure 15. Discharge of a lithium-ion battery. Source: (Chapman, 2025) 45
Figure 16. Charge of a lithium-ion battery. Source: (Chapman, 2025)
Figure 17. Block diagram of the Compression Cycle
Figure 18. Ideal Compression Cycle. Source: (Tejero González, 2024) 52
Figure 19. Comparison between the ideal inverse Rankine cycle and the real inverse
Rankine cycle
Figure 20. Approximated Real Inverse Rankine Cycle. Source: (Brenner, 2025) 54
Figure 21. Operating scheme of a heat pump/refrigerating machine 50
Figure 22. Inverse Carnot Cycle

Figure 23. Four-way valve operating modes. Source: (GROUP, 2025)	60
Figure 24. Diagram of the overall system.	64
Figure 25. Diagram of the software model	66
Figure 26. MATLAB code flowchart	70
Figure 27. Example of plot with temperature of the panel and ambient temperature.	72
Figure 28. Example of plot with PV production and solar irradiance	73
Figure 29. Example plot of EV consumption	74
Figure 30. Example plot of EV SOC.	74
Figure 31. Example plot of hourly energy consumption.	76
Figure 32. Example plot of energy balance.	78
Figure 33. Example plot of battery SOC	78
Figure 34. Flowchart of the consumption optimization.	79
Figure 35. Economic optimization flowchart.	84
Figure 36. Example plot of battery SOC for economic optimization	86
Figure 37. Example plot of EV SOC for economic optimization	86
Figure 38. Example of binary activation of appliances for economic optimization	87
Figure 39. Example of binary activation of EV charging for economic optimization	87
Figure 40. Example of original Energy balance	88
Figure 41.Example plot of energy balance for optimization for minimum consumpti	on.
	89
Figure 42. Example plot of energy balance comparison for optimization for maximum	net
economic benefit	89
Figure 43. Example plot of original energy consumption	90
Figure 44. Example plot of energy consumption for optimization for minim	um
consumption	90
Figure 45. Example plot of energy consumption for optimization for maximum	net
economic benefit	91
Figure 46. Example of original appliances binary activation.	92
Figure 47. Example of appliances binary activation for minimum energy consumpti	on.
	92
Figure 48. Example of appliance binary activation for maximum net economic bene	efit.
	93

Figure 49. Example of original consumption and schedule of the EV	94
Figure 50. Example of EV binary charging for optimization for minimum	n energy
consumption	94
Figure 51. Example of EV binary charging for optimization for maximum net e	economic
benefit	94
Figure 52. Example of EV SOC comparison	95
Figure 53. Example of battery SOC comparison.	96
Figure 54. Example of hourly net cost for weekdays comparison	97
Figure 55. Example of hourly net cost for holidays comparison	97
Figure 56. Example of original energy flows	98
Figure 57. Example of energy flows for optimization for minimum consumption	ı 99
Figure 58. Example of energy flows for optimization for maximum net economic	c benefit.
	99
Figure 59. Example plot of HVAC mode switching	100
Figure 60. Example plot of setpoint temperature, temperature indoors and	ambient
temperature	101
Figure 61. Example plot of HVAC energy consumption	101
Figure 62. Simulink Reversible heat pump model. Source: (MATLABWorks, 2025)	5) 102
Figure 63. Simulink house block.	103
Figure 64. Simulink system architecture and logic blocks.	107
Figure 65. Simulink HVAC mode block	108
Figure 66. Simulink EXV Control block	109
Figure 67. Simulink Compressor control block	110
Figure 68. Simulink compressor parameters.	112
Figure 69. Simulink Ambient temperature block	113
Figure 70. Typical day plot with Temperature of the Panel and Ambient Tem	perature.
	118
Figure 71. Typical day plot with PV Production and Irradiance	118
Figure 72. Typical day scheduling of controllable appliances	119
Figure 73. Typical day EV SOC and Consumption.	119
Figure 74. Typical day hourly energy consumption	120
Figure 75. Typical day HVAC mode.	122

Figure 76 Typical day plot of setpoint temperature, temperature indoors and ambient
temperature
Figure 77. Typical day Energy Balance
Figure 78. Typical day Battery SOC
Figure 79. Typical day Energy Flows
Figure 80. Typical day original scheduling of controllable appliances
Figure 81. Typical day scheduling of controllable appliances for optimization for
minimum consumption
Figure 82. Typical day scheduling of controllable appliances for optimization for
maximum net economic benefit
Figure 83. Typical day EV consumption and charging schedule
Figure 84. Typical day EV charging schedule for optimization for minimum consumption.
Figure 85. Typical day EV charging schedule for optimization for maximum net economic
benefit
Figure 86. Typical day EV SOC comparison
Figure 87. Typical day original energy consumption
Figure 88. Typical day energy consumption for optimization for minimum energy
consumption
Figure 89. Typical day energy consumption for optimization for maximum net economic
benefit
Figure 90. Typical day Battery SOC comparison
Figure 91. Typical day hourly net cost comparison for weekdays 132
Figure 92. Typical day hourly net cost comparison for holidays 133
Figure 93. Typical day Original Energy Balance
Figure 94. Typical day Energy Balance for optimization for minimum consumption 135
Figure 95, Typical day Energy Balance for optimization for maximum net economic
benefit
Figure 96. Typical day original Energy Flows
Figure 97. Typical day Energy Flows for optimization for minimum consumption 136
Figure 98. Typical day Energy Flows for optimization for maximum net economic benefit.

Figure 99. The coldest day plot with Temperature of the Panel and Ambient Temperature	ure.
	139
Figure 100. The coldest day plot with PV Production and Irradiance.	140
Figure 101. The coldest day scheduling of controllable appliances.	141
Figure 102. The coldest day EV SOC and Consumption	141
Figure 103. The coldest day hourly energy consumption.	142
Figure 104. The coldest day HVAC mode	143
Figure 105. The coldest day plot of setpoint temperature, temperature indoors,	and
ambient temperature.	143
Figure 106. The coldest day Energy Balance.	144
Figure 107. The coldest day Battery SOC.	145
Figure 108. The coldest day Energy Flows.	145
Figure 109. The coldest day scheduling of controllable appliances for optimization	for
minimum consumption.	146
Figure 110. The coldest day scheduling of controllable appliances for optimization	for
maximum net economic benefit.	146
Figure 111. The coldest day EV charging schedule for optimization for minim	ıum
consumption	147
Figure 112. The coldest day EV charging schedule for optimization for maximum	net
economic benefit	147
Figure 113. The coldest day EV SOC comparison.	148
Figure 114. The coldest day original energy consumption	149
Figure 115. The coldest day energy consumption for optimization for minimum energy	ergy
consumption	150
Figure 116. The coldest day energy consumption for optimization for maximum	net
economic benefit	150
Figure 117. The coldest day Battery SOC comparison	151
Figure 118. The coldest day hourly net cost comparison for weekdays	152
Figure 119. The coldest day hourly net cost comparison for holidays.	153
Figure 120. The coldest day original Energy Balance.	154
Figure 121. The coldest day Energy Balance for optimization for minimum consumpt	ion
	155

Figure 122. The coldest day Energy Balance for optimization for maximum net economic
benefit
Figure 123. The coldest day original Energy Flows
Figure 124. The coldest day Energy Flows for optimization for minimum consumption
Figure 125. The coldest day Energy Flows for optimization for maximum net economic
benefit
Figure 126. The hottest day plot with Temperature of the Panel and Ambien
Temperature
Figure 127. The hottest day plot with PV Production and Irradiance
Figure 128. The hottest day scheduling of controllable appliances
Figure 129. The hottest day EV SOC and Consumption
Figure 130. The hottest day hourly energy consumption
Figure 131. The hottest day HVAC mode
Figure 132. The hottest day plot of setpoint temperature, temperature indoors and
ambient temperature
Figure 133. The hottest day Energy Balance
Figure 134. The hottest day Battery SOC
Figure 135. The hottest day Energy Flows
Figure 136. The hottest day scheduling of controllable appliances for optimization fo
minimum consumption
Figure 137. The hottest day scheduling of controllable appliances for optimization fo
maximum net economic benefit
Figure 138. The hottest day EV charging schedule for optimization for minimum
consumption
Figure 139. The hottest day EV charging schedule for optimization for maximum ne
economic benefit
Figure 140. The hottest day EV SOC comparison
Figure 141. The hottest day original energy consumption
Figure 142. The hottest day energy consumption for optimization for minimum energy
consumption

Figure 143. The hottest day energy consumption for optimization for maximum net
economic benefit
Figure 144. The hottest day Battery SOC comparison
Figure 145. The hottest day hourly net cost comparison for weekdays 174
Figure 146. The hottest day hourly net cost comparison for holidays 175
Figure 147. The hottest day original Energy Balance
Figure 148. The hottest day Energy Balance for optimization for minimum energy
consumption
Figure 149. The hottest day Energy Balance for optimization for maximum net economic
benefit
Figure 150. The hottest day original Energy Flows
Figure 151. The hottest day Energy Flows for optimization for minimum energy
consumption
Figure 152. The hottest day Energy Flows for optimization for maximum net economic
benefit

Nomenclature

PV	Photovoltaic	EV	Electric Vehicle
NOCT	Nominal Operating Cell	ZEB	Zero Emission Building
	Temperature (°C)		
RES	Renewable Energy Sources	ES	Energy Storage
SOC	State of Charge	DC	Direct Current
AC	Alternating Current	GHG	Greenhouse Gas
GWP	Global Warming Potential	ODP	Ozone Depletion Potential
HVAC	Heating Ventilation Air	CA	Controllable Appliances
	Conditioning		
N-CA	Non-Controllable Appliances	DOD	Depth Of Discharge
P _{real}	Real power generated by the solar	T_c	Temperature of the panel (°C)
	panels (Wh)		
1	Irradiance (W/m²)	T_{env}	Ambient temperature (°C)
T _{ref}	Reference temperature (°C)	β	Temperature coefficient (%/°C)
η	Efficiency of the solar panel	η_{ref}	Reference efficiency of the solar panel
I _{SC}	Short-circuit current	V_{OC}	Open-circuit voltage
FF	Fill Factor	I_{ph}	Illumination current
I _D	Dark current	MPP	Maximum Power Point
СОР	Coefficient of Performance	EER	Energy Efficiency Ratio
dQ	Differential Heat exchanged	ΔU	Internal energy exchange in the system
W	Work transferred to the system	ΔS	Difference of entropy

Chapter I: Introduction

Background

The significance of zero-emission buildings has grown dramatically over the past few decades, rooted in a broader historical context of environmental awareness, energy crises, and evolving climate science. In the mid-20th century, rapid industrialization and urbanization led to a massive increase in global energy consumption, much of which was powered by fossil fuels. Buildings —residential, commercial, and industrial—became major energy consumers, accounting for a significant percentage of greenhouse gas (GHG) emissions due to heating, cooling, lighting, and appliance use. What's more the building sector is responsible for nearly 40% of global energy-related carbon dioxide emissions.

The 1970s energy crisis was a pivotal moment that first brought widespread attention to the vulnerability of relying on non-renewable energy sources. During this period, architects and engineers began exploring energy-efficient design principles, giving rise to early concepts of sustainable architecture. However, it wasn't until the late 20th and early 21st centuries that the urgency of climate change, backed by increasingly robust scientific evidence, shifted sustainability from a niche concern to a global imperative.

International agreements such as the Kyoto Protocol (1997) and the Paris Agreement (2015) marked major milestones in global climate action, setting targets for emissions reductions that required sweeping changes across all sectors, including the built environment. These accords emphasized the need for countries to decarbonize their economies and reduce reliance on fossil fuels, prompting governments, industries, and communities to reimagine how buildings are designed, constructed, and operated.

In recent years, the concept of zero-emission building structures that produce no net carbon emissions during operation has gained momentum as a key solution to climate change. This shift has been fuelled by advances in green technologies such as solar panels, high-efficiency insulation materials, heat pumps, and smart energy management systems, making it increasingly feasible to design buildings that meet strict environmental standards. Moreover, growing public awareness of climate issues,

coupled with policy incentives and stricter building codes, has accelerated the adoption of zero-emission principles in construction and urban planning.

The COVID-19 pandemic also contributed to this shift by highlighting the importance of indoor air quality, energy resilience, and sustainable urban environments. As cities around the world recover and rebuild, zero-emission buildings are being recognized not just as a climate solution, but as a pathway to healthier, more efficient, and more resilient communities.

Thus, the movement toward zero-emission buildings represents not only a technological evolution but also a profound transformation in how societies understand and respond to environmental responsibility. From early efforts in energy conservation to today's integrated climate strategies, the built environment has become a central focus in the global pursuit of a sustainable and carbon-neutral future.

Objectives

The main objectives of this thesis are as follows:

- To develop a dynamic simulation model of a residential zero-emission building (ZEB) using MATLAB and Simulink, integrating both energy generation from Renewable Energy Sources (RES) and the building's energy consumption profiles.
- 2. **To model and analyse the energy loads** of the building, including key systems such as heating, ventilation, air conditioning (HVAC), and electrical appliances, in order to reflect realistic consumption behaviour.
- To design and implement an energy management algorithm capable of optimizing the use of locally generated renewable energy, enhancing selfconsumption and minimizing reliance on the external electricity grid.
- 4. To evaluate the building's energy and environmental performance under different operational scenarios, assessing the potential for reducing net energy consumption and approaching zero-emission targets.

5. **To explore the economic benefits** associated with optimized energy management, considering factors such as electricity costs, grid feed-in tariffs, and financial returns from surplus energy export.

Methodology

This research aims to evaluate and optimize the energy consumption distribution of a residential building in order to approach zero-emission building (ZEB) performance. To achieve this, a simulation-based methodology has been adopted, utilizing MATLAB and Simulink to model the energy behaviour of the building under real environmental and consumption conditions.

The methodology can be divided into the following key stages:

1. Data Collection.

Real-world data sets form the foundation of the simulation model.

 Meteorological data: Ambient temperature and solar irradiance data were obtained from reliable local weather stations or databases covering an entire year, with an hourly resolution.

2. Model Development in MATLAB/Simulink.

A dynamic simulation model of the building was developed in MATLAB and Simulink, integrating:

- Thermal behaviour modelling: the heat transfer through the building envelope, and internal heat gains were modelled using thermal network principles.
- Energy systems: The simulation includes models of HVAC systems, photovoltaic (PV) energy generation, battery storage, and domestic appliances.
- Control strategies: Load shifting, smart scheduling, and demand-side management techniques were implemented to evaluate various consumption distribution scenarios.

3. Scenario Definition and Simulation.

Multiple simulation scenarios were defined to explore different consumption distributions, including:

- Baseline (non-optimized usage).
- Load shifting.
- Enhanced energy utilization.

Each scenario was simulated over a representative daily cycle.

4. Optimization Process.

Using custom algorithms, the model was iteratively adjusted to:

- Consumption optimization: the first objective focuses on minimizing the building's net energy consumption from non-renewable sources and reducing associated carbon emissions. This is achieved by maximizing self-consumption of photovoltaic energy, implementing load-shifting strategies, and optimizing the operation of energy systems (e.g., energy storage).
- Economic optimization: In addition to the consumption objective, an
 economic optimization function was implemented to maximize the
 financial benefit derived from the energy system. This function considers:
 - The cost of electricity imported from the grid is based on time-ofuse tariffs.
 - Revenue from surplus energy exported back to the grid, under the conditions of the local feed-in tariff scheme.
 - The trade-off between consuming self-generated energy versus exporting it for profit.

The optimization algorithms evaluate various consumption and generation scenarios to find a balanced strategy that not only reduces emissions but also improves the building's economic performance. These dual objectives are subject to real-world constraints, including occupant comfort, equipment limitations, appliance operating schedules,

battery capacity, grid availability, and daily usage patterns, all of which were carefully considered to ensure realistic implementation potential.

This methodological framework allows for a comprehensive and realistic analysis of how energy consumption in a building can be managed and optimized to align with zero-emission targets through simulation-based design and control strategies.

Outline

This thesis is organized into five main chapters, each of which contributes to a comprehensive understanding of the modelling and optimization of a residential building to achieve near zero-emission performance.

Chapter I: Introduction

This chapter presents the general background of the research, emphasizing the growing global relevance of Zero-Emission Buildings (ZEBs) in the context of climate change and sustainable development. It outlines the main goals of the thesis, and the methodology used to achieve them. Finally, the chapter provides a roadmap of the thesis structure.

Chapter II: Theoretical Background

This chapter reviews the theoretical principles underlying Zero-Emission Buildings. Topics covered include energy efficiency in buildings, renewable energy integration (especially solar PV), energy storage systems, and smart load management.

Chapter III: Modelling Setup

This chapter presents the development and implementation of the simulation model used to analyse and optimize the energy performance of residential buildings. The model is based on real physical and operational characteristics of the building, including thermal envelope properties, internal heat gains, HVAC systems, photovoltaic generation, and typical load profiles. MATLAB was used to handle data preprocessing,

implement control logic, and define optimization algorithms, while Simulink provided a dynamic environment to simulate the building's thermal behaviour and energy flows in response to varying environmental conditions. The model integrates weather data (ambient temperature and solar irradiance), real electricity consumption profiles, and energy system parameters to replicate realistic operating conditions. The combined MATLAB/Simulink setup enables scenario analysis and optimization by simulating the effects of various consumption distributions and control strategies on both environmental and economic performance.

Chapter IV: Results

This chapter presents and analyses the simulation outcomes obtained from the MATLAB/Simulink model under various energy consumption and control scenarios. Initially, the baseline scenario—representing the building's non-optimized energy usage—was simulated to establish a reference point. Subsequent simulations applied consumption and economic optimization strategies aimed at minimizing energy deficit and maximizing financial returns, respectively. Key performance indicators such as net energy demand, grid interaction, and economic savings were evaluated for each scenario. The results demonstrate how the optimized distribution of consumption, aligned with periods of high solar generation and favourable tariff structures, significantly improves both energy and economic performance. The optimal scenario, which balances deficit reduction and cost efficiency, is discussed in detail, highlighting the potential of smart control and optimization in approaching zero-emission building standards.

Chapter V: Conclusion and Future Work

This chapter summarizes the key findings and contributions of the research. It presents the practical implications of the proposed approach and identifies the limitations of the current model. Suggestions for future improvements, such as integrating real-time control, are also discussed.

Chapter II: Theoretical Background

This chapter establishes the theoretical framework that underpins the research carried out in this thesis. It begins by introducing the concept of Zero-Emission Buildings (ZEBs), highlighting their growing importance in the context of global efforts to reduce greenhouse gas emissions and promote energy efficiency in the built environment. The chapter also examines the integration of Renewable Energy Sources (RES), with a particular emphasis on photovoltaic (PV) systems, which are commonly used to supply on-site electricity in residential ZEBs. In addition to energy generation, the chapter explores key technologies that contribute to the reduction of energy demand, including high-efficiency systems such as reversible heat pumps. These systems provide both heating and cooling functions, significantly improving the building's thermal performance while reducing reliance on conventional fossil-fuel-based systems. The role of smart energy management is also discussed, particularly in terms of optimizing the interaction between energy consumption and renewable generation. Lastly, this chapter reviews commonly used optimization methods in the context of building energy modelling.

1. Definition of a Zero Emission Building

A Zero Emission Building (ZEB) is a construction that, on an annual basis, does not generate net carbon dioxide (CO₂) emissions associated with its operation. This is achieved through a combination of energy efficiency strategies, on-site renewable energy generation, and, in some cases, energy storage and smart demand management. The concept may vary depending on regulations or calculation methodologies, considering different scopes such as operational emissions only or full life-cycle analysis including embodied emissions.

ZEBs not only aim to minimize energy consumption, but also to interact with the electrical grid in a sustainable way, promoting decarbonization in the building sector.

2. Basic Principles of Energy in Buildings

The energy analysis of buildings is fundamentally grounded in the principles of **thermodynamics** and the study of **heat transfer mechanisms**. A comprehensive understanding of the thermal behaviour of a building requires knowledge of key thermodynamic laws and the ways in which heat is transferred across different media. These principles help in modelling the thermal performance of the building, evaluating thermal losses, optimizing insulation, and analysing the efficiency of active systems such as HVAC (Heating, Ventilation, and Air Conditioning).

The Zeroth Law of Thermodynamics

If two systems are each in thermal equilibrium with a third system, then they are in thermal equilibrium with each other.

The First Law of Thermodynamics

Often referred to as the law of energy conservation, it asserts that energy cannot be created or destroyed but can only change forms. In the context of buildings, this principle plays a critical role in understanding the movement and storage of energy within the structure. For instance, the energy inputs to a building include external factors such as solar radiation, electrical energy used for lighting and HVAC systems, and fuel used for heating. The energy output involves thermal energy lost through the building's envelope (walls, windows, roof) and the energy used by the building's internal systems (such as lighting, mechanical processes, or air conditioning). To maintain thermal comfort and minimize energy consumption, it is essential to strike a balance between these inputs and outputs. Efficient insulation, high-performance windows, and airtight construction contribute to reducing unnecessary energy losses, ensuring that the energy conservation principle is upheld.

First principle of thermodynamics for a closed system at rest:

$$dU = \delta Q - \delta W^1 \tag{1}$$

$$\Delta U = Q - W \tag{2}$$

where:

dU, ΔU , change in internal energy (J),

 δQ , Q, energy transferred as heat (J),

 δW , W, energy transferred as work (J).

First principle of thermodynamics for a closed system in motion:

$$dE = \delta Q - \delta W \tag{3}$$

$$\Delta E = Q - W \tag{4}$$

$$\Delta E = \Delta U + \Delta E_C + \Delta E_P \tag{5}$$

where:

dE, ΔE , change in total energy (J),

 δQ , energy transferred as heat (J),

 δW , energy transferred as work (J),

 ΔU , change in internal energy (J),

 ΔE_C , change in kinetic energy (J),

 ΔE_P , change in potential energy (J).

¹ Exact differential (d): Used to denote changes in state functions. A state function is a property of a system that depends only on the current state of the system and not on how the system arrived at that state. The internal energy (U) is a state function, which means that the change in internal energy (dU) depends only on the initial and final states of the system and not on the path followed to get from one state to the other. Inaccurate differential (δ): Used to denote changes in quantities that are not state functions, such as work (W) and heat (Q). Work and heat depend on the path followed during the thermodynamic process. This means that the amount of work done, or heat transferred depends on the specific path the system follows from one state to another.

First principle of thermodynamics for an open system in non-stationary regime:

$$\dot{Q_{VC}} - \dot{W}_{VC} = \frac{dE_{VC}}{dt} + \sum \dot{m}_{out} \left(h_{out} + \frac{c_{out}^2}{2} + gz_{out} \right) - \sum \dot{m}_{in} \left(h_{in} + \frac{c_{in}^2}{2} + gz_{in} \right)$$
(6)

where:

 $\dot{Q_{VC}}$, heat flux through the control volume (W),

 \dot{W}_{VC} , work flux through the control volume (W),

 $\frac{dE_{VC}}{dt}$, rate of change of internal, kinetic, and potential energy inside the control volume (W),

 \dot{m}_{out} , \dot{m}_{in} , mass flux into or out of the control volume (kg/s),

 h_{out} , h_{in} , specific enthalpy (J/kg),

 $\frac{c_{out}^2}{2}$, $\frac{c_{in}^2}{2}$, specific kinetic energy (J/kg),

 gz_{out} , gz_{in} , specific potential energy (J/kg).

This final expression is the most general form of the First Law of Thermodynamics and is applicable to all types of systems. Depending on the specific case, certain simplifications can be made — such as assuming stationary flow, a closed system, negligible kinetic and potential energy, an adiabatic process, or no work being done on or by the system can be applied.

The Second Law of Thermodynamics

The second Law of Thermodynamics introduces the concept of entropy, which refers to the natural tendency of systems to evolve toward a state of greater disorder. This law states that energy conversions are inherently inefficient, meaning that some energy is always lost to the surroundings, primarily as heat. In building design, this concept is crucial for understanding the limitations of energy systems, such as HVAC systems, in their efficiency. One of the primary consequences of this law is the inevitable heat flow from warmer to cooler areas within a building. For example, in the winter, heat will naturally be transferred from the warm interior to the colder external environment through the building envelope. Conversely, in the summer, heat from the outside will be

transferred into the building if the air conditioning system is not functioning efficiently. This principle underscores the importance of optimizing energy systems and improving the thermal performance of the building's envelope to reduce energy wastage and maintain a comfortable indoor climate with minimal energy consumption.

Clausius statement: 'It is impossible for a system to exist that can operate in such a way that its only effect is the transfer of energy in the form of heat from a cold body to a hotter one'. The Clausius statement can be seen in Fig. 1.

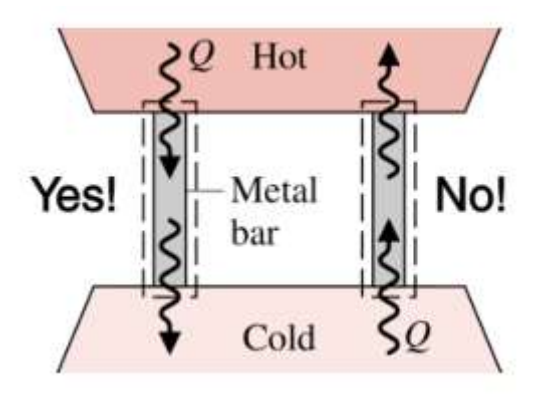


Figure 1. Clausius statement. Source: (Vega Maza, 2022).

Kelvin-Planck statement: 'It is impossible to construct a system which, operating according to a thermodynamic cycle, yields a net amount of energy to its environment while receiving energy in the form of heat from a single (thermal) source'. The Kelvin-Plank statement can be seen in Fig.2.

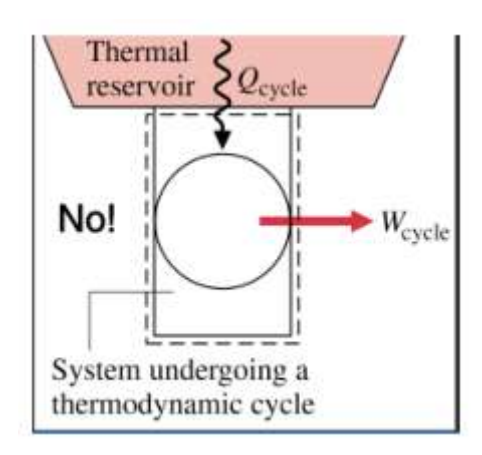


Figure 2. Kelvin – Plack Statement. Source: (Vega Maza, 2022).

Another thermal reservoir is required to yield work to its environment while receiving energy from a thermal source.

The following equations correspond to the First Law of Thermodynamics applied to a closed cycle:

$$\oint dU = \oint \delta Q - \oint \delta W \tag{7}$$

where:

 $\oint dU$, net internal energy change in a cycle (J),

 $\oint \delta Q$, net heat received in a cycle (J),

 $\oint \delta W$, net work produced in a cycle (J).

Since the system returns to its initial state, the net change in internal energy is zero. This means that the total heat absorbed during the cycle is converted into net useful work:

$$0 = Q_{cvcle} - W_{cvcle} \tag{8}$$

where:

 Q_{cvcle} , total heat received during a cycle (J),

 W_{cycle} , total work output from the system during the cycle (J).

According to the Kelvin – Plack Statement, if $W_{cycle} > 0$, this is not possible with one thermal reservoir, another thermal source is required to make the cycle physically feasible.

$$W_{cyle} \le 0$$
 (for a single reservoir) (9)

where:

 W_{cvcle} , total work output from the system during the cycle (J).

Irreversible process: Additional energy is required to return the system and its environment to its initial conditions (real process). The causes of the irreversibility are dissipation of work into internal energy and lack of balance. Dissipation of work can be result of electrical resistance, friction, viscosity etc. (Vega Maza, 2022).

Lack of balance can be due to:

Mechanical: pressure difference.

Thermal: temperature difference.

- Matter: concentration difference, mixture, and chemical reaction.

Total entropy never decreases in an irreversible process; this is mathematically expressed as:

$$\Delta S_{total} \ge 0$$
 (10)

where:

 ΔS_{total} , is the change of total entropy of the system and the surroundings (J/K).

For an isolated system it holds that:

$$\Delta S_{system} \ge 0$$
 (11)

where:

 ΔS_{system} , change in entropy of an isolated system (J/K).

Another way to express the second law is in terms of the Clausius inequality, which states that for any thermodynamic cycle:

$$\oint \frac{dQ}{T} \le 0$$
(12)

where:

 $\oint \frac{dQ}{T}$, is the infinitesimal amount of heat transferred to the system at a temperature T during a cycle (J/K).

The equality holds for reversible processes, while the inequality holds for irreversible processes.

Entropy balance for a closed system is described by:

$$\Delta S_{system} = S_Q + \sigma; \ \sigma \ge 0 \ with \ S_Q = \int \left(\frac{\delta Q}{T}\right)_{ext}$$
 (13)

where:

 ΔS_{system} , change in entropy of an isolated system (J/K),

 S_O , entropy flux associated with the heat transfer (J/K),

 σ , generated entropy (J/K),

 $\int \left(\frac{\delta Q}{T}\right)_{ext}$, is the infinitesimal amount of heat transferred to the system at an external temperature (J/K).

For the result of generated entropy (σ) holds that:

 $\sigma > irreversible process$

 $\sigma = 0$ reversible process

 $\sigma < 0$ imposible process

The entropy balance to a closed system from the global point of view is expressed as:

$$\Delta S_{total} = \Delta S_{system} + \Delta S_{surroundings} \rightarrow \Delta S_{total} \ge 0$$
 (14)

where:

 ΔS_{total} , is the change of total entropy of the system and the surroundings (J/K),

 ΔS_{system} , change in entropy of a system (J/K),

 $\Delta S_{surroundings}$, change in entropy of the surroundings (J/K).

While the entropy balance to a closed system from the system's point of view is expressed as:

$$\sigma = S_2 - S_1 - \int_1^2 \left(\frac{\delta Q}{T}\right)_{ext} \tag{15}$$

where:

 σ , generated entropy (J/K),

 $\int_{1}^{2} \left(\frac{\delta Q}{T}\right)_{ext}$, entropy flux associated with the heat transfer (J/K),

 $S_2 - S_1$, change in entropy (J/K).

According to the entropy balance for an open system in non-stationary regime, it holds that:

$$\dot{\sigma} = \frac{dS_{VC}}{dt} + \sum \dot{m}_{out} s_{out} - \sum \dot{m}_{in} s_{in} - \sum \dot{S}_{Q} \ge 0 \qquad (16)$$

where:

 $\dot{\sigma}$, generated entropy (W/K),

 $\frac{dS_{VC}}{dt}$, rate of change of entropy in the control volume (W/K),

 \dot{m}_{out} , \dot{m}_{in} , mass flow through the control volume (kg/s),

 s_{out} , s_{in} , specific entropy (J/kg*K),

 \dot{S}_{O} , entropy flux associated with the heat transfer (W/K).

The entropy changes when matter is transferred ($\sum \dot{m}_{out} s_{out} - \sum \dot{m}_{in} s_{sin}$), heat is transferred ($\sum \dot{S}_Q$), and entropy is generated, because of the irreversibility of the process ($\dot{\sigma}$).

The entropy balance applied to an open, adiabatic, stationary system is defined as follows:

$$\sum \dot{m}_{out} s_{out} \ge \sum \dot{m}_{in} s_{in} \tag{17}$$

where:

 \dot{m}_{out} , \dot{m}_{in} , mass flow through the control volume (kg/s),

 s_{out} , s_{in} , specific entropy (J/kg*K).

Heat transfer mechanisms

Heat transfer within buildings occurs via three primary mechanisms: **conduction**, **convection**, and **radiation**. These mechanisms are responsible for the transfer of thermal energy through various building elements and are integral to the building's overall energy efficiency.

Conduction: Heat Transfer Through Solid Elements

Conduction is the process by which heat is transferred through solid materials (such as walls, roofs, floors, and windows) due to a temperature gradient. The rate of heat transfer via conduction is determined by the thermal conductivity of the materials involved, the thickness of the material, and the temperature difference between the interior and exterior surfaces. For example, heat will flow through a wall with poor insulation at a higher rate than it would through a wall made of highly insulating materials, leading to greater energy losses.

Conduction is a critical factor in energy analysis because it directly affects the building's thermal resistance (R-value). A higher R-value corresponds to better insulation and reduced heat transfer. Effective insulation materials are essential for minimizing thermal losses through conduction, ensuring that the interior temperature remains stable without excessive reliance on mechanical heating or cooling systems.

- Convection: Heat Exchange Between Surfaces and Air

Convection refers to the transfer of heat between a surface (e.g., a wall or window) and the air surrounding it. This process occurs when air particles in contact with a heated surface gain energy and rise, while cooler air moves in to take its place, creating a convective current. In buildings, convection plays a significant role in both natural convection (driven by temperature differences) and forced convection (induced by mechanical systems like fans or air handlers).

For example, in a room with a heated radiator, the hot air near the radiator will rise, and cooler air from the rest of the room will be drawn in to replace it. This interaction is critical for managing indoor thermal comfort and energy use. A building's design should take into account the placement of heating and cooling systems to optimize the convective heat transfer process and minimize energy wastage.

- Radiation: Transfer Between Bodies via Electromagnetic Waves

Radiation is the transfer of heat in the form of electromagnetic waves, typically infrared radiation, between surfaces that do not have to be in direct contact with each other. All objects emit radiation depending on their temperature; warmer objects emit more radiation. In buildings, radiation can lead to heat gains or losses, depending on the temperature and material properties of the building's surfaces.

For example, solar radiation is a key factor in determining the amount of heat entering a building through windows and walls. The design of windows, shading devices, and materials with low solar heat gain coefficients can help control the amount of radiation entering the building, thereby reducing the need for active cooling. Similarly, radiant heating systems, which heat a surface that then radiates warmth to the surrounding air, are used in some buildings to provide more energy-efficient heating.

These principles allow for modelling thermal losses, insulation behaviour, and the performance of active HVAC systems and their efficiency.

3. Renewable energy generation: solar power and energy storage

3.1 Photovoltaic Panels

Photovoltaic (PV) panels convert solar radiation into electricity through the photovoltaic effect. Solar cells, typically made of silicon, generate direct current (DC) electricity when exposed to sunlight. This energy is then converted into alternating current (AC) using DC/AC converters (inverters), allowing it to be used in the building or fed into the grid.

3.1.1 Photovoltaic effect

When photons from sunlight strike a semiconductor material (typically silicon), they transfer their energy to electrons, exciting them from the valence band to the conduction band. This creates electron-hole pairs, generating a flow of electric current when the material is connected to an external circuit. The photovoltaic effect is shown in Fig. 3.

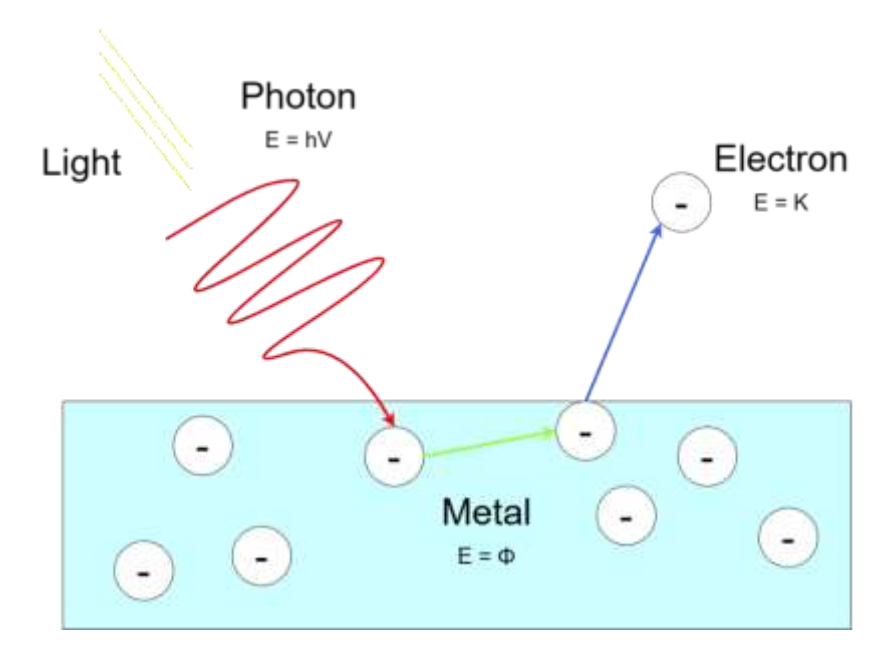


Figure 3. The photovoltaic effect.

The basic structure consists of two layers of doped silicon: an n-type layer (negatively doped with phosphorus, with 5 e⁻ in the valence shell - in this shell, there is a larger number of free electrons than in a pure silicon shell) and a p-type layer (positively doped with boron, with 3 e⁻ in the valence shell, there is a smaller number of free electrons than in a pure silicon shell). When the pn-bond is created, the free electrons in the n-shell enter the p-shell and recombine with the holes in the p-region, creating an electric field. The pn-junction is shown in Fig. 4.

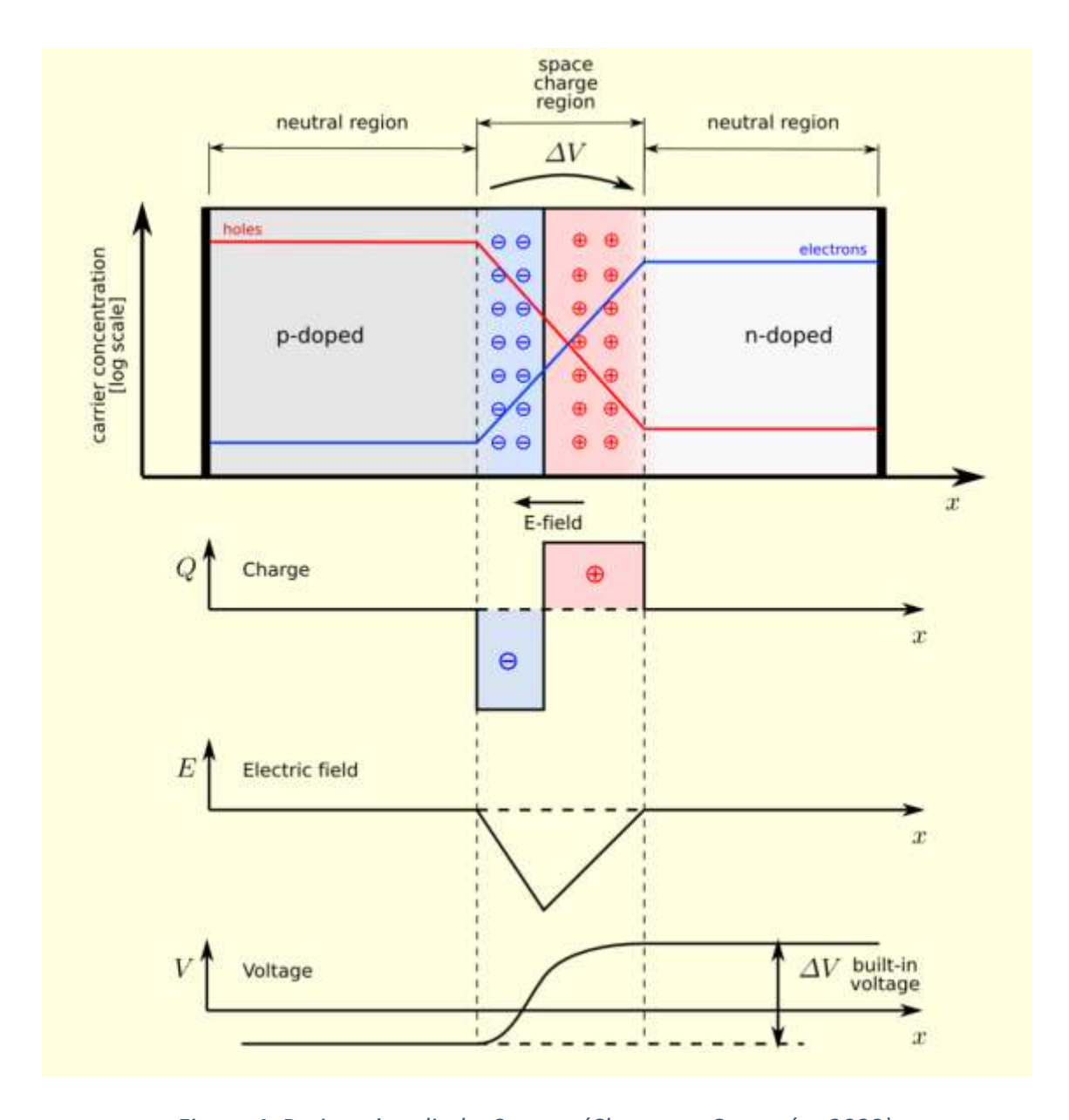


Figure 4. Pn-junction diode. Source: (Chamarro Camazón, 2023).

When light strikes the photovoltaic cell, the electrons are released. The electrons are repelled by the electric field of the pn-junction towards the outer surface. Electric conductors collect the electron current to an external circuit. If the electric field zone is far away from the surface, the electrons and holes recombine, producing heat. The distance that is needed for them to recombine is called the diffusion length and must be greater than the distance from the surface to the electric field. The longer the diffusion length, the higher the purity of the crystal.

Not every photon releases an electron. There are a few losses:

- Photons that do not have a sufficient threshold energy.
- Reflection losses.
- Transmission losses.
- Electron-hole recombination losses.

The principle of operation of a photovoltaic cell is shown in Fig. 5.

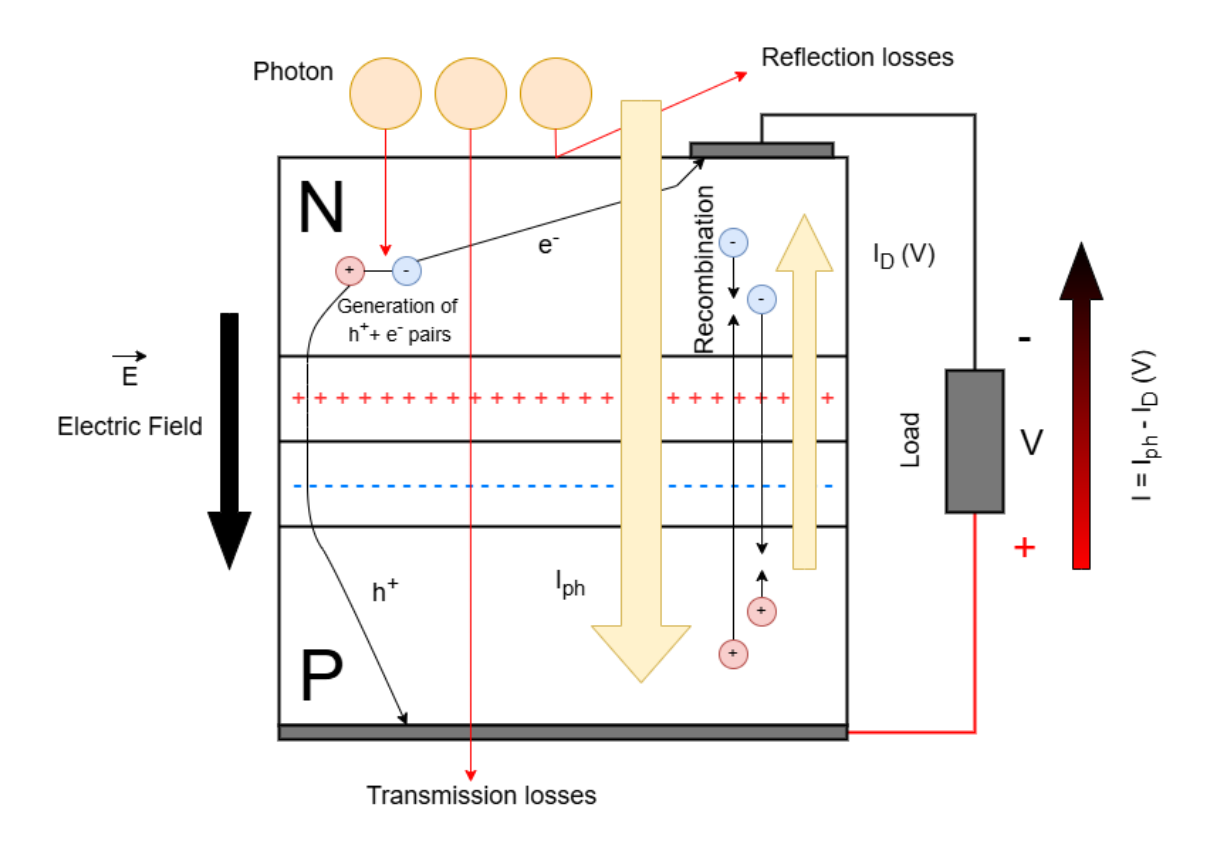


Figure 5. Principle of operation of a photovoltaic cell.

3.1.2 I-V Curves and Electrical Characteristics

The current-voltage (I-V) curve is fundamental to understanding PV panel performance. It shows the relationship between output current and voltage under specific conditions. Key parameters include:

- Short-circuit current (Isc): Maximum current when voltage is zero.
- Open-circuit voltage (Voc): Maximum voltage when current is zero.

• **Fill factor (FF):** It is a value to measure the "shape" of the I-V curve and indicates the quality of the module (Chamarro Camazón, 2023):

$$FF = \frac{I_m * V_m}{I_{SC} * V_{OC}} = \frac{P_m}{I_{SC} * V_{OC}} \tag{18}$$

where:

FF, fill factor,

 I_m , current at the maximum power point (A),

 V_m , voltage at the maximum power point (V),

 I_{SC} , short-circuit current (A),

 V_{OC} , open-circuit voltage (V),

 P_m , power at the maximum power point (W).

FF values higher than 0.7 are considered as acceptable.

• Maximum power point (MPP): The point where power output is maximized.

The current delivered to a load by a solar cell is the net result of two opposing internal components of current:

- Illumination current I_{ph} : due to the release of electrons that produces the light.
- Dark current I_D: due to the recombination of carriers which produces the external voltage necessary to be able to deliver energy to the load.

Photovoltaic panel I-V characteristic derivation can be seen in Fig. 6.

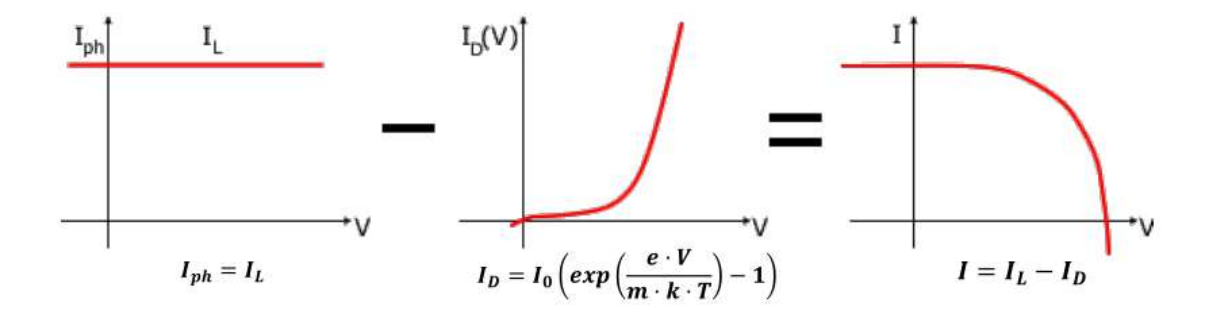


Figure 6. Photovoltaic panel I-V characteristic derivation. Source: (Chamarro Camazón, 2023).

The MPP is affected by the values of I_{SC} and V_{OC} , according to the power-voltage curve of the PV panel. The I-V curve of a photovoltaic panel can be seen in Fig. 7.

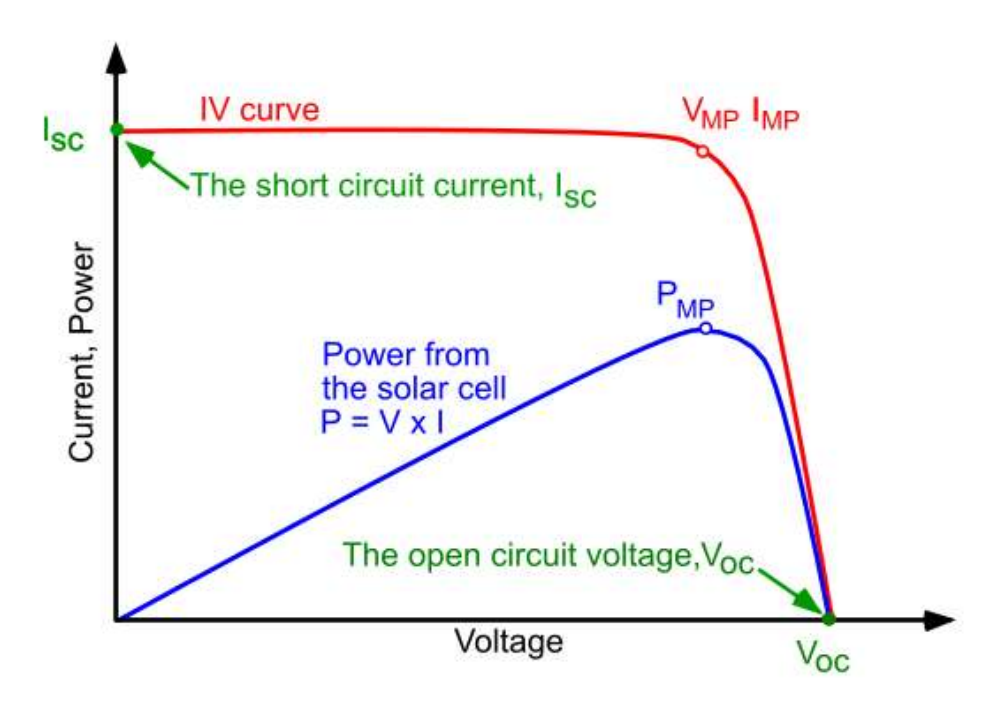


Figure 7. I-V Curve of a photovoltaic panel. Source: (Stuart Bowden & Christiana Honsberg, 2025).

The power-voltage curve's shape is influenced by solar irradiance, cell temperature, and shading conditions. Under standard test conditions (STC: 1000 W/m², 25°C, AM 1.5), manufacturers specify these parameters.

Fig. 8 shows how the I-V curves change according to the factors of change in panel temperature.

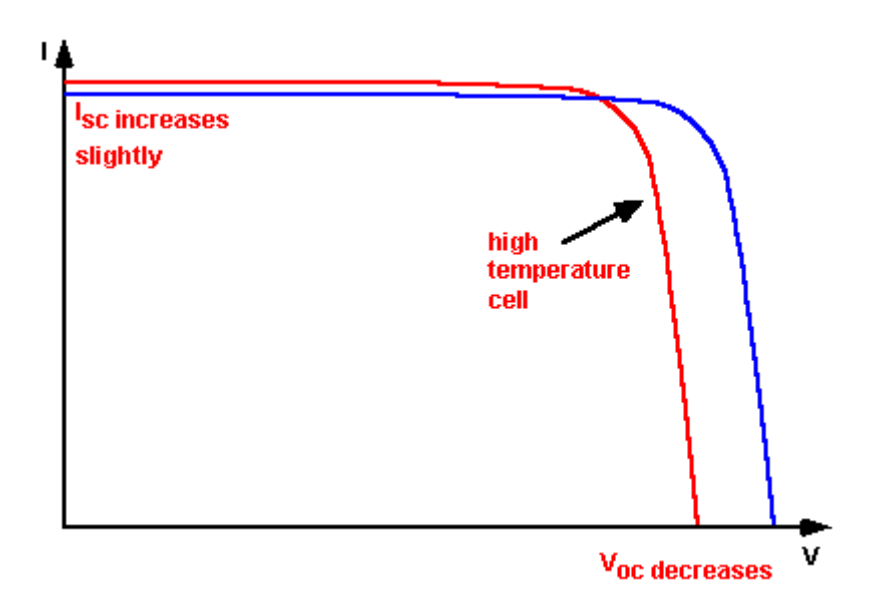


Figure 8. The effect of temperature on the I-V characteristics of a solar cell. Source: (Stuart Bowden & Christiana Honsberg, 2025).

Fig. 9 shows how the I-V curve changes according to the change in received irradiance (at constant temperature).

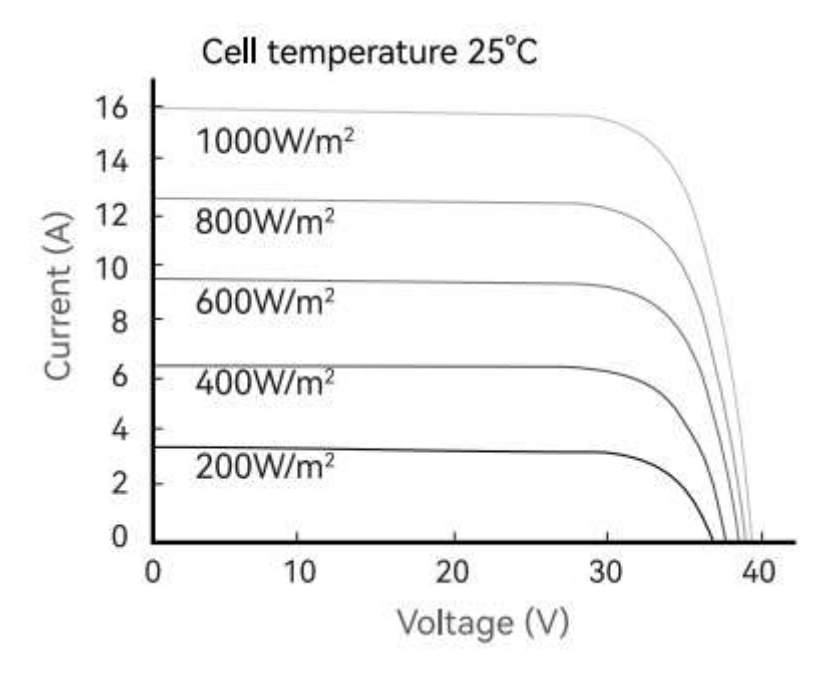


Figure 9. The effect of irradiance on the I-V characteristics of a solar cell. Source: (Stuart Bowden & Christiana Honsberg, 2025).

In general terms, it can be clearly observed that when the panel temperature increases under the same irradiance, the short-circuit current increases slightly while the open-circuit voltage decreases on average. On the other hand, when the panel is kept at a

constant temperature and the irradiance is increased, both parameters show an increase.

There are several factors which affect PV panel performance:

Environmental Factors: Solar irradiance directly affects current output, while temperature inversely affects voltage. Most silicon panels lose about 0.4-0.5% efficiency per degree Celsius above 25°C.

Shading: Even partial shading can dramatically reduce output due to bypass diode activation and current mismatch between cells.

Dust and Soiling: Accumulation of dirt, dust, or other particles can reduce light transmission and decrease efficiency by 5-15%.

Aging and Degradation: PV panels typically degrade at 0.5-0.8% per year, with manufacturers guaranteeing 80% of initial power after 20-25 years.

Spectral Response: Different PV technologies have varying sensitivity to different wavelengths of light, affecting performance under different lighting conditions.

3.1.3 Types of Photovoltaic Panels

Monocrystalline Silicon (c-Si): Made from single crystal silicon wafers, these panels offer the highest efficiency (typically 20-22%) and longest lifespan but are more expensive to manufacture. They're recognizable by their uniform dark appearance and rounded cell edges.

Polycrystalline Silicon (p-Si): Constructed from multiple silicon crystals, these panels are less expensive than monocrystalline but have slightly lower efficiency (15-17%). They appear blue with a crystalline pattern visible on the surface without rounded corners.

Thin-Film Technologies: These include amorphous silicon (a-Si), cadmium telluride (CdTe), and copper indium gallium selenide (CIGS). They are less efficient (10-12%), but

without the need to join several panels. They're flexible, lightweight, and perform better in low-light conditions. They are cheap and with marginal applications.

Bifacial Panels: These can generate electricity from both sides, capturing reflected light from the ground or surrounding surfaces, potentially increasing energy yield by 10-20%.

Perovskites: Family of materials whose crystalline structure is similar to that of calcium titanate CaTiO ₃, offering yields > 25 %. They are made from economically viable and abundant materials, although their lifetime remains limited for the time being.

3.1.4 Connection Systems

The electrical connections in solar panels play a critical role in ensuring the efficiency, safety, and reliability of the entire photovoltaic (PV) system. Proper connections between individual solar cells, between panels (modules), and with the broader electrical system are essential for minimizing energy losses, preventing overheating or electrical faults, and ensuring that power is delivered efficiently to the load or storage system. Poor or faulty connections can lead to reduced performance, hot spots, and even system failures. Therefore, careful design, installation, and maintenance of all electrical connections are key to maximizing the lifespan and energy output of a solar energy system.

Series Connection: Panels connected in series increase voltage while maintaining current. The total voltage equals the sum of individual panel voltages, but current is limited by the weakest panel. Fig. 10 shows the performance I-V curves for two identical solar cells connected in series.

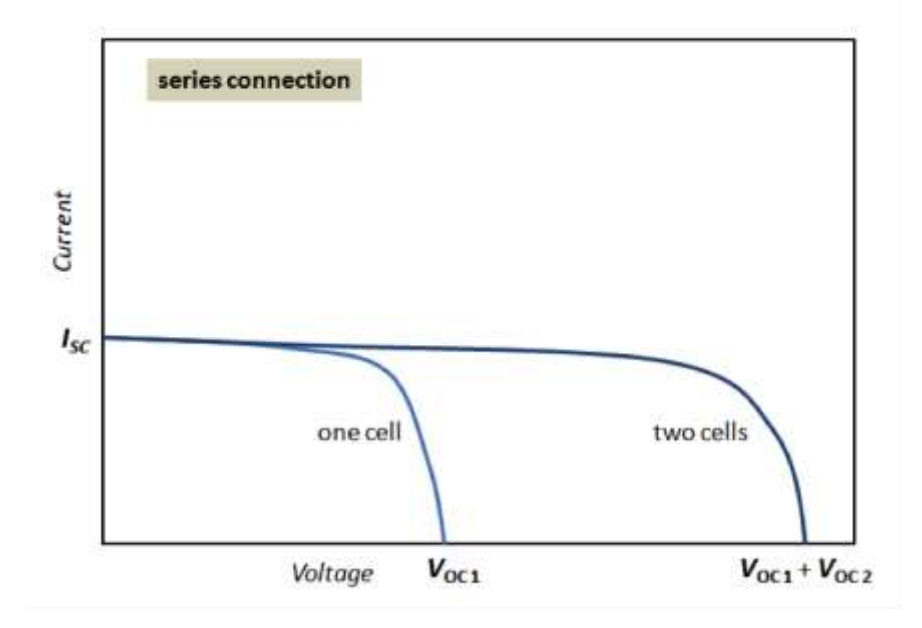


Figure 10. Performance I-V curves for two identical solar cells connected in series.

Source: (Fedkin, 2025).

Parallel Connection: Panels connected in parallel increase current while maintaining voltage. Total current equals the sum of individual currents, providing better performance under partial shading. Fig. 11 shows the performance I-V curves for two identical solar cells connected in parallel.

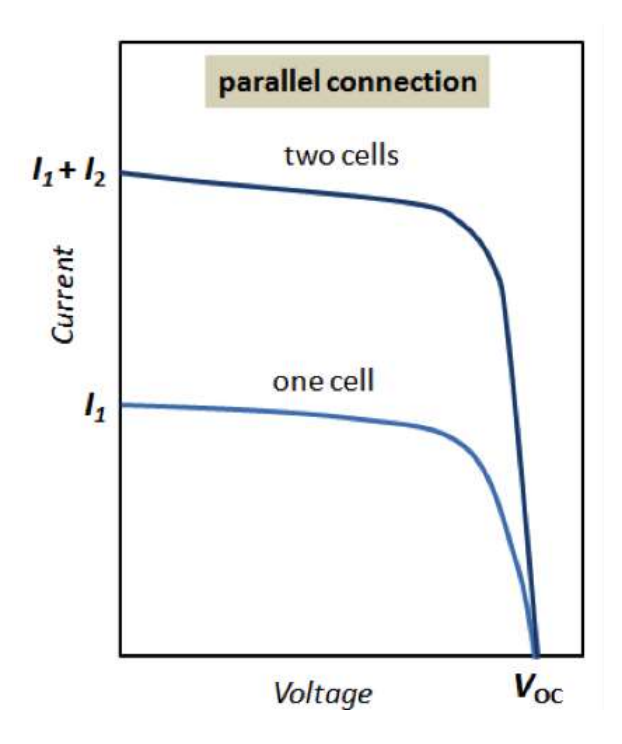


Figure 11. Performance I-V curves for two identical solar cells connected in parallel.

Source: (Fedkin, 2025).

To avoid imbalances, the numbers of PV modules connected in series in each string, should be equal. In addition, they should be exposed to the same conditions: temperature, wind, irradiance, etc. Whether in series or in parallel, the total output power of the PV array is the sum of the power of each PV module.

Series-Parallel Combination: Large PV arrays typically use both configurations to achieve the desired voltage and current levels while optimizing performance.

DC/AC converter (Inverter): it is a device that converts direct current (DC) electricity produced by solar panels into alternating current (AC) electricity, which is what most household appliances and the electrical grid use. It operates by using electronic components like transistors and switches to rapidly turn the DC current on and off, creating pulses that are then shaped into a smooth sine wave, closely matching the standard AC waveform. The output is AC electricity at the proper voltage and frequency (such as 120V/60Hz in the U.S. or 230V/50Hz in Europe), making it ready for use in homes or for feeding into the grid. As can be expected, the conversion from direct current to alternating current is not ideal and that is why it is needed to generate more electricity than really needed because of these losses in transforming the energy.

Fig. 12 shows the type of inverters output waveforms.

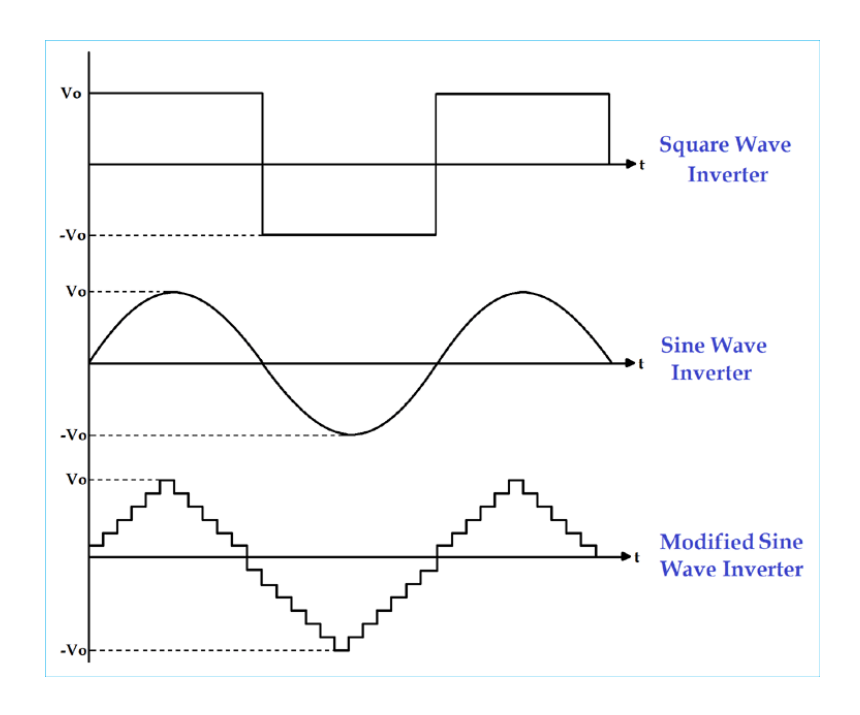


Figure 12. Types of inverters output waveforms. Source: (Kansagara, 2025).

In addition to series and parallel mounting, the mounting of solar panels in terms of how they are positioned with respect to sunlight is categorized as follows:

- Fixed (inclined or horizontal).
- Single-axis tracker (polar, azimuthal, or horizontal) can be seen in Fig. 13.

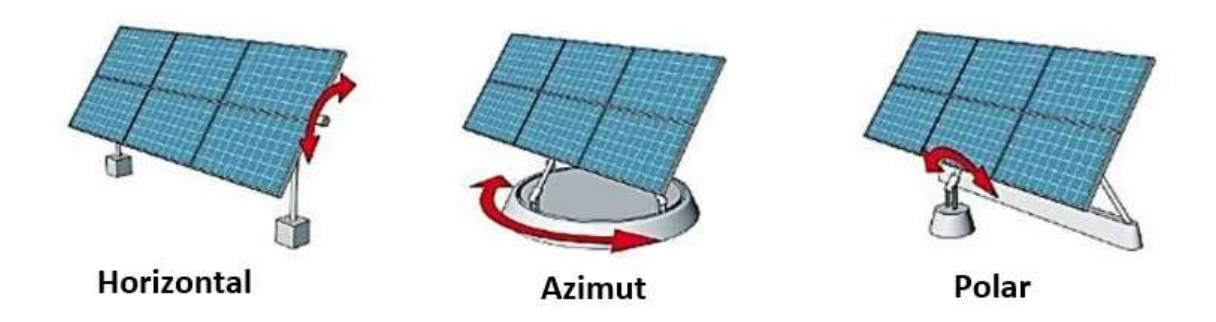


Figure 13. Types of single-axis solar tracking. Source: (Gestor, 2025).

- Dual-axis tracker (monopole, or carousel).

Putting solar panels into context, the expressions used to characterize them in the program are presented. The power generation is defined as the product of the irradiance received by the PV panel, the surface area, and the conversion efficiency:

$$P_{real} = A * I * \eta \tag{19}$$

where:

 P_{real} , real power generated by the solar panels (Wh),

A, surface of the solar panel (m^2),

I, irradiance (W/m²),

 η , efficiency of the solar panel.

Where the efficiency η is defined as follows:

$$\eta = \eta_{ref} * (1 - \beta * (T_c - T_{ref}))$$
 (20)

where:

 η_{ref} , reference efficiency of the solar panel,

 β , temperature coefficient (1/°C),

 T_c , temperature of the solar panel (°C),

 T_{ref} , reference temperature (°C).

The temperature of the PV panel is determined by the following expression:

$$T_c = T_{env} + (\frac{NOCT - 20}{800} * I) \tag{21}$$

where:

 T_c , temperature of the solar panel (°C),

 T_{env} , ambient temperature (°C),

NOCT, nominal operating cell temperature (°C),

I, irradiance (W/m²).

3.2 Battery Energy Storage

Battery energy storage systems are crucial components in residential photovoltaic installations aimed at maximizing self-consumption. They store excess solar energy generated during peak production hours for use during periods of low or no solar generation, reducing dependence on the electrical grid and increasing energy autonomy. This is particularly valuable given the time mismatch between solar generation (typically peak at midday) and residential consumption patterns (often highest in morning and evening).

Batteries store and release electrical energy through reversible electrochemical reactions. They consist of three main components.

3.2.1 Components of batteries

Anode (Negative Electrode): Where oxidation occurs during discharge, releasing electrons to the external circuit. During charging, it accepts electrons and undergoes reduction.

Cathode (Positive Electrode): Where reduction occurs during discharge, accepting electrons from the external circuit. During charging, it releases electrons and undergoes oxidation.

Electrolyte: An ionic conductor that allows the movement of ions between electrodes while preventing direct electron flow, which would cause internal short-circuiting.

The parts of a Lithium-ion battery are shown in Fig. 14, with their corresponding chemical reactions, as this is the most commonly used type of battery for self-consumption. The charging and discharging processes are also shown.

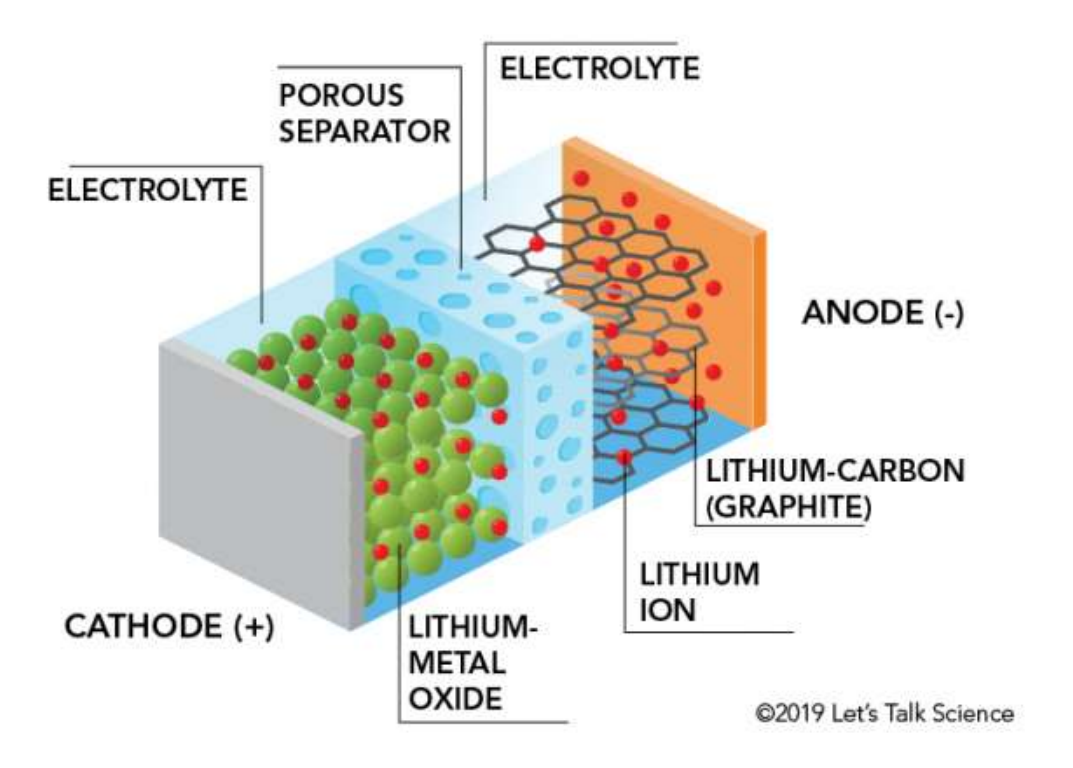


Figure 14. Parts of a lithium-ion battery. Source: (Chapman, 2025).

3.2.2 Redox reactions

Two reactions take place inside lithium-ion batteries (Chapman, 2025):

- **Reduction** takes place at the cathode. There, cobalt oxide combines with lithium ions to form lithium-cobalt oxide (LiCoO2). The half-reaction is:

$$CoO_2 + Li^+ + e^- \rightarrow LiCoO_2$$

- **Oxidation** takes place at the anode. There, the graphite intercalation compound LiC6 forms graphite (C6) and lithium ions. The half-reaction is:

$$LiC_6 \rightarrow C_6 + Li^+ + e^-$$

The full reaction (left to right is discharging, right to left is charging) is the following:

$$LiC_6 + CoO_2 \rightleftarrows C_6 + LiCoO_2$$

Discharge refers to electricity production, which occurs through spontaneous oxidation and reduction reactions. The discharging process can be seen in Fig. 15.

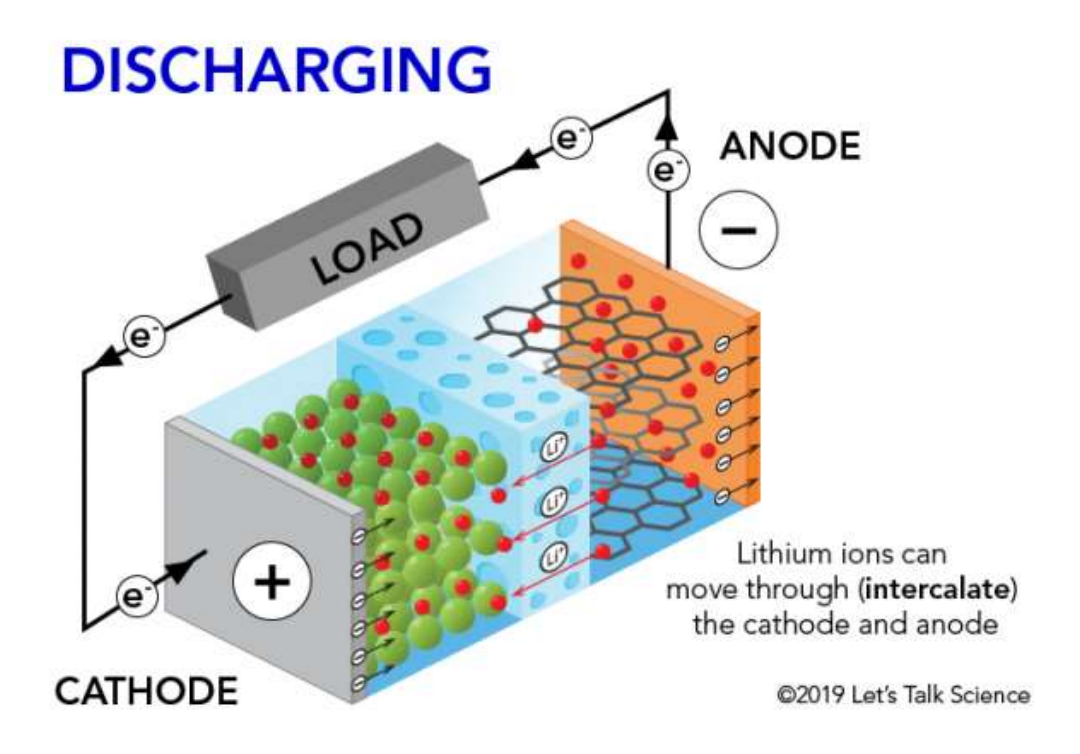


Figure 15. Discharge of a lithium-ion battery. Source: (Chapman, 2025).

During discharging, the battery provides energy, while a spontaneous redox reaction occurs:

- Oxidation at the anode → the anode material loses electrons.
- Reduction at the cathode → the cathode material gains electrons.

During discharging, electrons flow from anode to cathode through the external circuit (this is the electric current which powers the electric devices), while ions move through the electrolyte to maintain charge neutrality.

Charging refers to the process of storing energy by using an external power source to drive oxidation and reduction reactions. The charging process is shown in Fig. 16.

CHARGING POWER SOURCE ANODE CATHODE ©2019 Let's Talk Science

Figure 16. Charge of a lithium-ion battery. Source: (Chapman, 2025).

During charging, the battery receives energy (from an external source, like solar panels or the grid), and the external power source reverses the process:

- Reduction at the anode → now it gains electrons.
- Oxidation at the cathode → now it loses electrons.

The key operating parameters of batteries are the following:

- Capacity and Energy: Measured in kilowatt-hours (kWh), representing the total energy storage capability. Usable capacity is typically 80-95% of nominal capacity to prevent deep discharge and extend battery life.
- Power Rating: Maximum instantaneous power output (kW), determining how many appliances can be powered simultaneously during battery discharge.
- Depth of Discharge (DoD): Percentage of battery capacity that can be safely used. Lithium-ion batteries typically allow 80-95% DoD, while lead-acid systems are limited to 50-60%. It's important to respect the DoD because if not the lifespan of the battery can be dramatically decreased. This is because:

- Deep discharge of batteries leads to several damaging effects on the materials and performance. Structural stress occurs when electrode materials undergo significant volume changes as lithium ions are extracted and inserted during deep discharge. This mechanical stress can result in particle cracking and the loss of electrical contact, which ultimately degrades the battery's efficiency. Additionally, at very low voltages, the electrolyte can decompose, forming a solid electrolyte interface layer. This layer consumes active lithium and increases the internal resistance, further reducing the battery's performance. Over time, deep cycling can also cause active material to become disconnected from the current collector, permanently diminishing the battery's capacity.
- As the depth of discharge (DoD) increases, the battery's voltage drops non-linearly. At high DoD levels, the voltage can decrease rapidly, potentially falling below the minimum required for the connected equipment to operate effectively. This reduction in voltage is accompanied by an increase in internal resistance, which reduces the overall efficiency of the battery. In multi-cell battery packs, there is an increased risk of cell reversal, which can lead to permanent damage. Therefore, managing the depth of discharge is crucial to maintaining battery health and ensuring reliable performance.
- **Round-Trip Efficiency:** Energy output as a percentage of energy input, typically 85-95% for lithium-ion systems and 70-85% for lead-acid.
- Cycle Life: Number of charge-discharge cycles before capacity degrades to 80% of original value. This directly impacts the economic viability of the system.

3.2.3 Battery types for Residential Applications

The types of batteries most commonly used at the residential level are described in the following.

Lithium-ion Batteries: The most commonly used in residential applications due to their high energy density (150-250 Wh/kg), long cycle life (3000-8000 cycles), and decreasing costs. Lithium iron phosphate (LiFePO4) variants are preferred for residential use due to

their thermal stability and safety characteristics, while lithium nickel manganese cobalt oxide (NMC) offers higher energy density.

Lead-Acid Batteries: Traditional technology still used in some applications, particularly flooded lead-acid and valve-regulated lead-acid (VRLA) types. While less expensive initially, they have lower depth of discharge (50-60%), shorter lifespan (500-1500 cycles), and require more maintenance.

Emerging Technologies: Sodium-ion and flow batteries are gaining attention for stationary applications, offering potential advantages in safety, cost, and resource availability, though they're not yet widely commercialized for residential use.

3.2.4 Battery Management Systems (BMS)

The BMS is critical for safe and optimal battery operation, performing several key functions:

Cell Monitoring: Continuously monitors voltage, current, and temperature of individual cells or cell groups to ensure operation within safe parameters.

State of Charge (SoC) Estimation: Uses algorithms combining coulomb counting, voltage measurement, and impedance analysis to accurately determine remaining capacity.

Thermal Management: Controls cooling or heating systems to maintain optimal operating temperatures, as battery performance and lifespan are highly temperature dependent.

Safety Protection: Implements over-voltage, under-voltage, over-current, and over-temperature protection to prevent dangerous conditions.

Cell Balancing: Ensures uniform charging across all cells, preventing capacity degradation due to cell imbalances.

3.2.5 Integration with PV Systems

Batteries play a key role in the integration of photovoltaic (PV) systems by storing excess solar energy and ensuring a stable power supply during periods of low or no solar generation. For this reason, it is essential to understand how to properly combine them with solar panels to maximize efficiency and system reliability.

DC-Coupled Systems: Batteries connect directly to the DC bus, sharing the same inverter with PV panels. This configuration offers higher efficiency for PV-to-battery charging but requires more complex control systems.

AC-Coupled Systems: Batteries have their own inverter and connect to the AC side of the system. This allows easier retrofitting to existing PV installations and simpler control but with slightly lower efficiency due to multiple DC-AC conversions.

Hybrid Inverters: Specialized inverters designed to manage both PV panels and batteries, optimizing energy flows between generation, storage, consumption, and grid interaction.

3.2.6 Control Strategies and Energy Management

Efficient control strategies and energy management are fundamental to ensuring that battery energy storage systems operate optimally, balancing energy flows, extending battery life, and maximizing overall system efficiency.

Self-Consumption Optimization: Algorithms prioritize local consumption, storing excess PV generation when production exceeds demand and releasing stored energy when consumption exceeds generation.

Time-of-Use (ToU) Optimization: In areas with variable electricity pricing, systems can charge batteries during low-rate periods and discharge during high-rate periods, providing additional economic benefits.

Grid Services: Advanced systems can provide ancillary services like frequency regulation or peak shaving, though regulatory frameworks for residential participation vary by location.

Load Prioritization: During outages or limited battery capacity, systems can prioritize critical loads while shedding non-essential consumption.

3.2.7 Performance Factors and Degradation

The performance of battery systems is influenced by various factors such as temperature, charge/discharge rates, and depth of discharge, while degradation mechanisms gradually reduce capacity and efficiency over time, making their understanding essential for reliable system design and operation.

Temperature Effects: Battery capacity and lifespan are significantly affected by operating temperature. High temperatures accelerate chemical degradation, while low temperatures reduce available capacity.

Cycling Patterns: Shallow cycles generally extend battery life compared to deep cycles. Partial state-of-charge operation can be beneficial for some lithium-ion chemistries.

Calendar Aging: Batteries degrade over time even when not in use, with degradation rates typically 2-5% per year depending on storage conditions and chemistry.

Charging Protocols: Proper charging algorithms, including constant current/constant voltage profiles and appropriate end-of-charge criteria, are essential for optimal performance and longevity.

4. Ideal Compression cycle

The vapor-compression refrigeration cycle is the most widely used thermodynamic cycle for cooling and heating applications in residential, commercial, and industrial settings. It is the fundamental operating principle behind air conditioners, refrigerators, and reversible heat pumps. The cycle enables the transfer of thermal energy from one environment to another by using a working fluid, known as a refrigerant, that undergoes phase changes between liquid and vapor.

This process allows heat to be absorbed from a low-temperature space and rejected to a higher-temperature environment, effectively enabling cooling or heating depending on the direction of the cycle. Due to its high efficiency, relatively simple design, and

adaptability to a wide range of applications, the vapor-compression cycle plays a critical role in modern HVAC (Heating, Ventilation, and Air Conditioning) systems.

Understanding the operation and performance of this cycle is essential for the design and optimization of zero-emission buildings, where energy efficiency and environmental impact are central concerns. In the context of this project, the vapor-compression cycle is used in a reversible heat pump system, with the refrigerant R-410A, to meet both heating and cooling demands of a residential building.

The basic components of a standard compression cycle are shown in Fig. 17. This cycle uses a refrigerant, a working fluid that undergoes phase changes (liquid \leftrightarrow vapor) to absorb and release heat. The refrigerant flows in a closed loop through the four components.

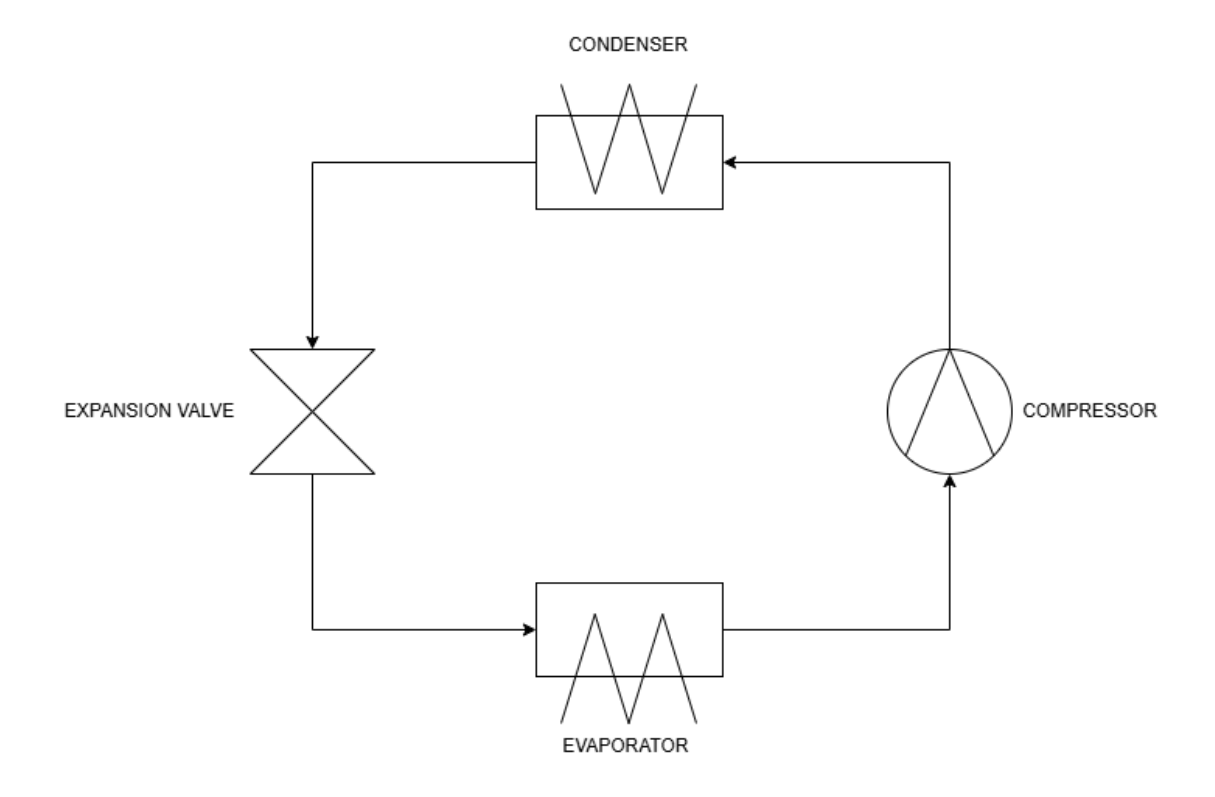


Figure 17. Block diagram of the Compression Cycle.

The cycle is commonly represented on a pressure–enthalpy (P–h) diagram, which is shown in Fig. 18.

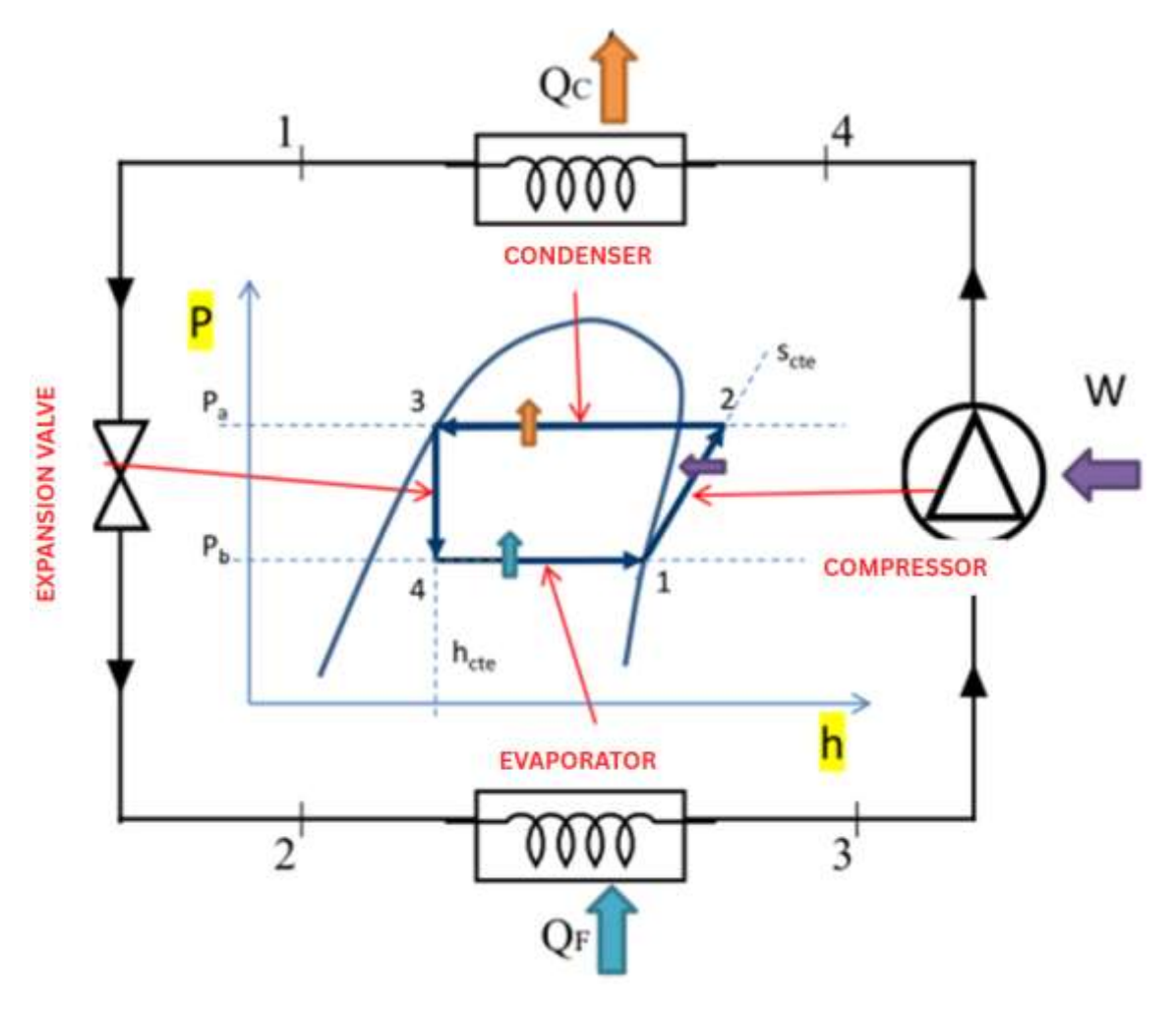


Figure 18. Ideal Compression Cycle. Source: (Tejero González, 2024).

- **1 Evaporation- Evaporator.** Line nearly horizontal where the refrigerant goes from liquid at low pressure and temperature to vapor at low pressure and temperature. The heat is absorbed from the air of the space to be cooled, changing the state of the refrigerant at constant pressure from liquid to vapor. In the real cycle, it's convenient to overheat the refrigerant to ensure that there isn't any drop in the gas to prevent the compressor of any malfunction.
- **2 Compression Compressor.** Line upward diagonal. The compressor uses energy to increase pressure and temperature of the refrigerant (increasing the enthalpy) so that the refrigerant can release heat in the condenser. The refrigerant goes from a vapor state at low pressure and temperature to a high pressure and temperature state (ideally the evolution in this stage is at constant enthalpy because the compressor is considered ideal and therefore is adiabatic and reversible).

3 Condensation – Condenser. Horizontal line where the refrigerant starts as high pressure and temperature vapor and turns into a high pressure, low/medium temperature liquid. During this condensation process at constant pressure the heat is transferred to the surroundings. In heating mode it is responsible for heating the indoor air.

4 Expansion - Expansion Valve. Refrigerant's pressure drops at constant enthalpy. The refrigerant now in liquid state at high pressure and low/medium temperature, passes through an expansion valve, which reduces its pressure abruptly (at constant enthalpy) making the refrigerant's temperature to drop. The refrigerant goes from a liquid high pressure and low/medium temperature state to a low pressure and temperature liquid, partially vaporized. This cold refrigerant returns to the evaporator and the cycle starts again.

The difference between the ideal and actual cycle can be seen in Fig. 19.

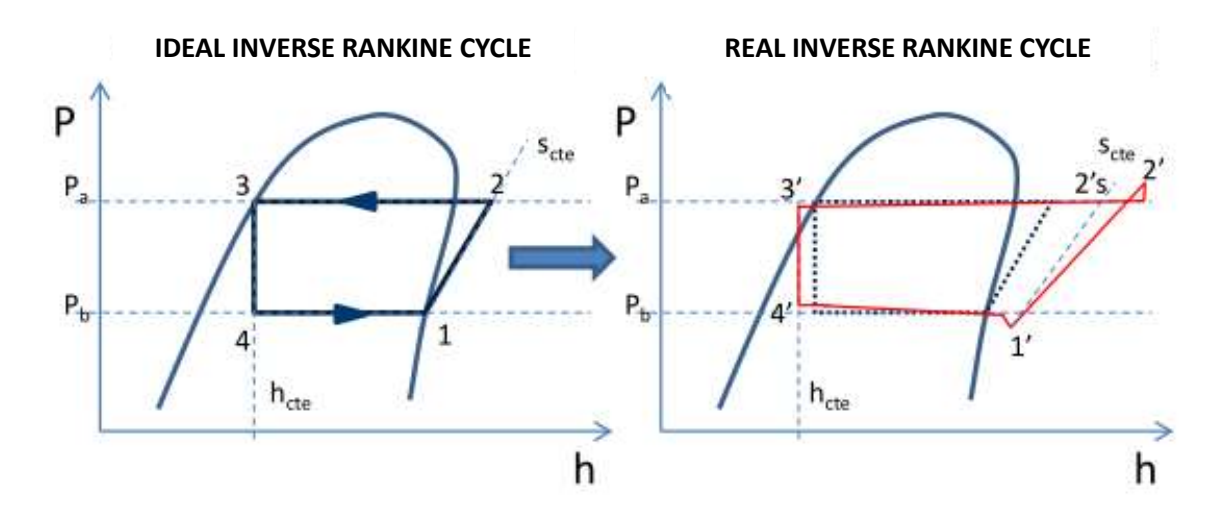


Figure 19. Comparison between the ideal inverse Rankine cycle and the real inverse Rankine cycle.

Additional modifications of the cycle must be considered. On the one hand, there are unavoidable pressure losses of the refrigerant at the exchangers and at the suction and discharge of the compressor. On the other hand, the compressor will not be ideal, and therefore compression will not be reversible. Also, to ensure dry vapour at the outlet of the evaporator, there will be some overheating; and a subcooling at the outlet of the condenser will improve the performance of the cycle.

Disregarding the deviations associated with pressure losses in the various elements, it is possible to work with the approximate Real Inverse Rankine Cycle. Fig. 20 shows the approximated real inverse Rankine cycle.

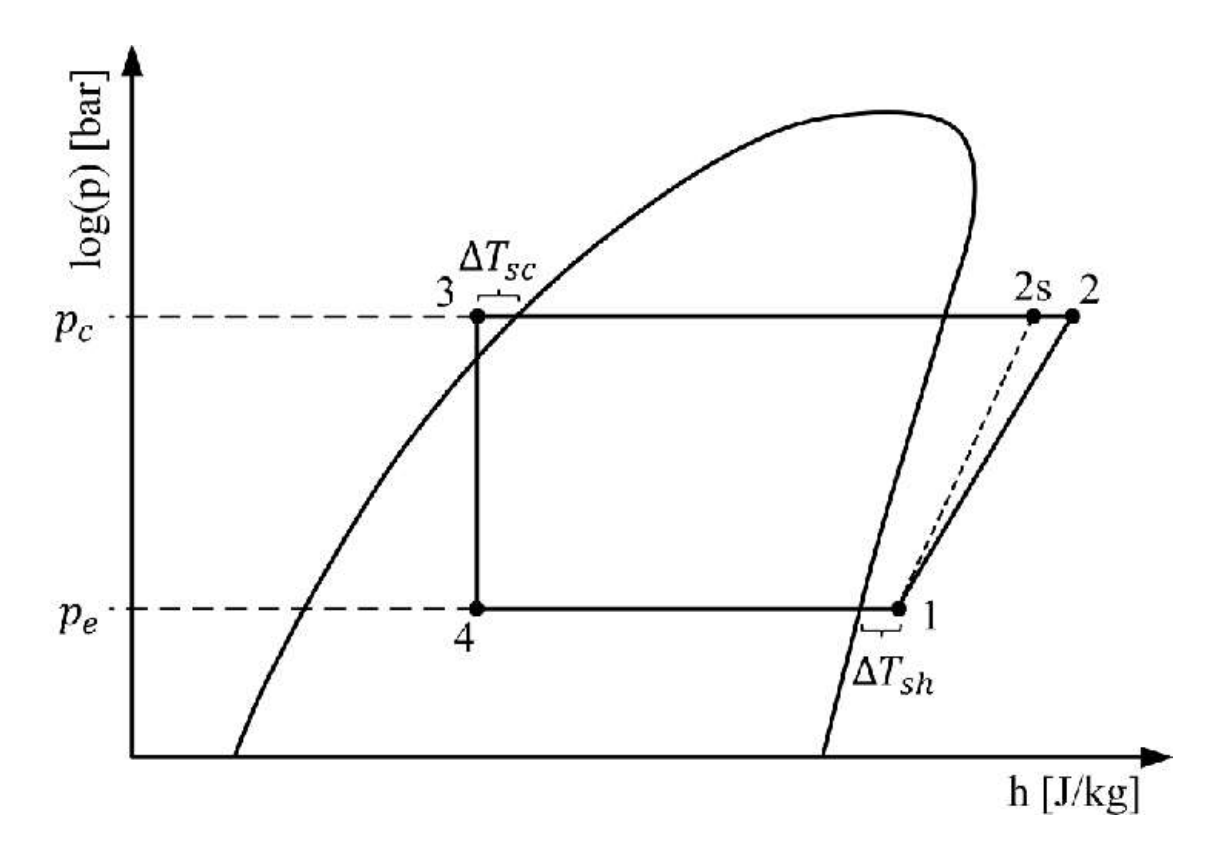


Figure 20. Approximated Real Inverse Rankine Cycle. Source: (Brenner, 2025).

5. Efficient Thermal Systems: Heat Pumps and Four-Way Valves

The reversible heat pumps mode change is enabled by a reversing valve (4-way valve). So basically, the heat exchangers can work as an **evaporator** (**extracts heat**) or a **condenser** (**gives off heat**) indistinctly depending on what is needed, whether heating or cooling the space, as only the direction of flow must be reversed with a 4-way valve whose functioning will be explained next.

At low outdoor temperatures, frost formation may occur on the outdoor coil during heating mode. This triggers automatic defrost cycles, temporarily reversing the refrigerant flow to melt accumulated ice, ensuring continuous and efficient operation.

5.1 Reversible Heat Pumps for Residential Applications

A reversible heat pump is a highly efficient thermal system capable of providing both heating and cooling using a single device. It operates based on the first and second laws of thermodynamics applied to a vapor-compression refrigeration cycle. Heat pumps function by transferring thermal energy from a low-temperature source to a high-temperature source using mechanical work, typically provided by a compressor.

The system consists of four key components: evaporator, compressor, condenser, and expansion valve. By reversing the flow of the refrigerant, the heat pump can switch between heating and cooling modes, making it suitable for year-round climate control. This flexibility, combined with its energy efficiency, makes it particularly advantageous for residential buildings aiming to achieve low energy consumption and zero emissions.

Heat pumps can utilize different heat sources, such as air-to-air, air-to-water, water-to-water, or geothermal sources. In the case of this diploma thesis, the configuration uses air as the external heat source/sink, and heat is exchanged between a two-phase refrigerant (R-410A) and moist air through specialized 2P–MA heat exchangers (e.g., finned-tube coils), located indoors and outdoors. These components are responsible for evaporating or condensing the refrigerant while simultaneously dehumidifying or heating the air, depending on the operating mode. In heating mode, the system absorbs heat from the external environment and delivers it indoors. Conversely, in cooling mode, the cycle is reversed: heat is extracted from the indoor space and rejected to the outside. This flexibility makes reversible heat pumps highly suitable for year-round climate control.

The heat pump's performance is typically evaluated using several key efficiency metrics, including the Coefficient of Performance (COP), which is the ratio of useful thermal energy output to the electrical energy input. For real-world conditions, seasonal performance indicators such as the Seasonal Coefficient of Performance (SCOP) for heating and the Seasonal Energy Efficiency Ratio (SEER) for cooling are used to reflect the variation in efficiency across different temperatures and usage profiles throughout the year. These metrics are influenced by outdoor temperature fluctuations, refrigerant superheating and subcooling, compressor efficiency, and the thermal exchange quality

between refrigerant and air. The operating scheme of a heat pump/ refrigerating machine is shown in Fig. 21.

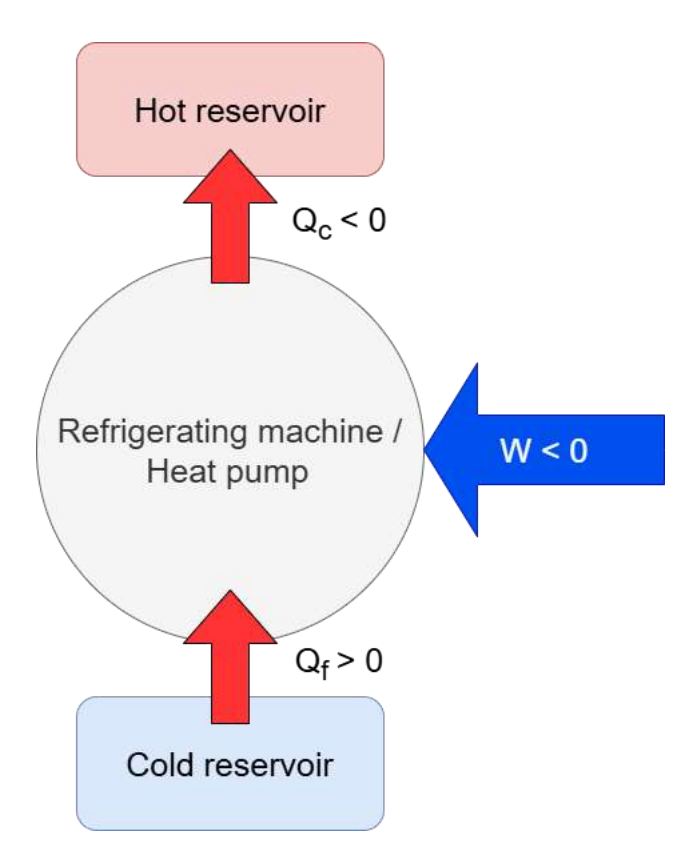


Figure 21. Operating scheme of a heat pump/refrigerating machine.

Once the operating principle of the heat pump has been established, it is essential to analyse its energy performance. This is typically quantified using key indicators such as the efficiency of the cycle:

$$\eta_{cycle_{RF}} = \frac{|\dot{Q_F}|}{W_{Net}} = \frac{|\dot{Q_F}|}{|\dot{Q_C}| - |\dot{Q_F}|}$$
(22)

$$\eta_{cycle_{HP}} = \frac{|\dot{Q_C}|}{W_{Net}} = \frac{|\dot{Q_C}|}{|\dot{Q_C}| - |\dot{Q_F}|} \tag{23}$$

where:

 $\eta_{cycle_{HP}}$, efficiency of the cycle for a heat pump,

 $\eta_{cycle_{RF}}$, efficiency of the cycle for a refrigerating machine,

 $\dot{W_{Net}}$, net work flux (W),

 \vec{Q}_C , heat flux from the hot reservoir (W),

 \dot{Q}_F , heat flux from the cold reservoir (W).

The transformation of the net work to the difference of heat between the reservoirs is possible because of the first law of thermodynamics applied to a closed system, cyclic process, without accumulation of internal energy and negligible kinetic and potential energy changes. So, the expression obtained is the following:

$$\dot{Q}_C + \dot{Q}_F - \dot{W} = 0 \rightarrow |\dot{Q}_C| = |\dot{Q}_F| + |\dot{W}|$$
 (24)

where:

 \dot{Q}_{C} , heat flux from the hot reservoir (W),

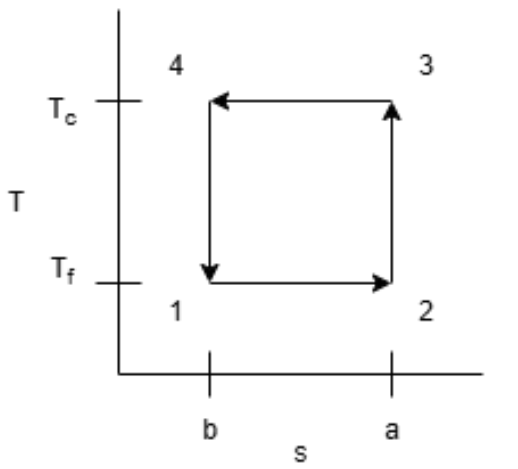
 \dot{Q}_F , heat flux from the cold reservoir (W),

 \dot{W} , work flux (W).

The efficiency of both processes is typically expressed through performance ratios, such as the Energy Efficiency Ratio (EER), for refrigerating machines and the Coefficient of Performance (COP) for heat pumps. In the case of heat pumps used in air conditioning applications, performance is evaluated using the COP in both modes: COP for heating and COP for cooling.

To better understand the theoretical limits of heat pump and refrigeration system performance, it is useful to introduce the inverse Carnot cycle, which serves as an idealized reference for maximum possible efficiency under given temperature conditions. The Fig. 22 shows the inverse Carnot cycle.

INVERSE CARNOT CYCLE



- (1-2) Heat absorption at constant T
- (2-3) Isoentropic compression
- (3-4) Heat transfer at constant T
- (4-1) Isoentropic expansion

Figure 22. Inverse Carnot Cycle.

If the First and Second Law of Thermodynamics are applied, the EER and COP can be expressed as follows:

$$EER = \frac{|\dot{Q_F}|}{\dot{W_{Net}}} = \frac{|\dot{Q_F}|}{|\dot{Q_C}| - |\dot{Q_F}|} = \frac{T_F * \Delta S}{T_C * \Delta S - T_F * \Delta S} = \frac{T_F}{T_C - T_F}$$
(25)

$$COP = \frac{|\dot{Q_C}|}{\dot{W_{Net}}} = \frac{|\dot{Q_C}|}{|\dot{Q_C}| - |\dot{Q_F}|} = \frac{T_C * \Delta S}{T_C * \Delta S - T_F * \Delta S} = \frac{T_C}{T_C - T_F}$$
(26)

where:

EER, Energy Efficiency Ratio,

COP, Coefficient of Performance,

 $\dot{W_{Net}}$, net work flux (W),

 $\dot{Q_{C}}$, heat flux from the hot reservoir (W),

 \dot{Q}_F , heat flux from the cold reservoir (W),

 T_F , temperature of the cold reservoir (°C),

 T_C , temperature of the hot reservoir (°C),

 ΔS , change in entropy (J/K).

While the performance indicators such as COP and EER highlight the inherent efficiency of heat pumps, their true potential emerges when integrated with renewable energy sources. They can be powered by electricity generated from solar photovoltaic (PV) panels or wind turbines, further reducing their environmental impact. Additionally, systems that extract heat from renewable sources such as geothermal energy or ambient air contribute to decarbonization and help meet sustainability goals and operational costs in modern building design.

5.2 Four-Way Valves

These valves allow for the **reversal of the thermal cycle** in heat pumps. By changing the direction of refrigerant flow, they switch the roles of the heat exchangers (evaporator ↔ condenser). They are essential for systems that require both heating and cooling during different seasons.

The system studied in this diploma thesis uses air-refrigerant heat exchangers, where one side of the exchanger circulates R-410A in two-phase flow (evaporation or condensation), and the other side is exposed to moist air from the indoor or outdoor environment.

A four-way reversing valve allows the system to switch between heating and cooling modes by reversing the flow of R-410A through the system:

In heating mode:

- The indoor coil acts as the condenser, and the outdoor coil functions as an evaporator.
- Cold indoor air passes over the warm coil, absorbing sensible heat as the refrigerant condenses.

In cooling mode:

 The indoor coil acts as the evaporator, and the outdoor coil functions as a condenser.

- Warm, moist indoor air passes over the cold coil, transferring sensible heat and condensing moisture, thus also extracting latent heat.
- The refrigerant evaporates, absorbing the heat.

Four-way valves are typically actuated electrically or pneumatically and controlled based on thermostat signals and ambient conditions. The Fig. 23 shows the operating modes of a four-way valve.

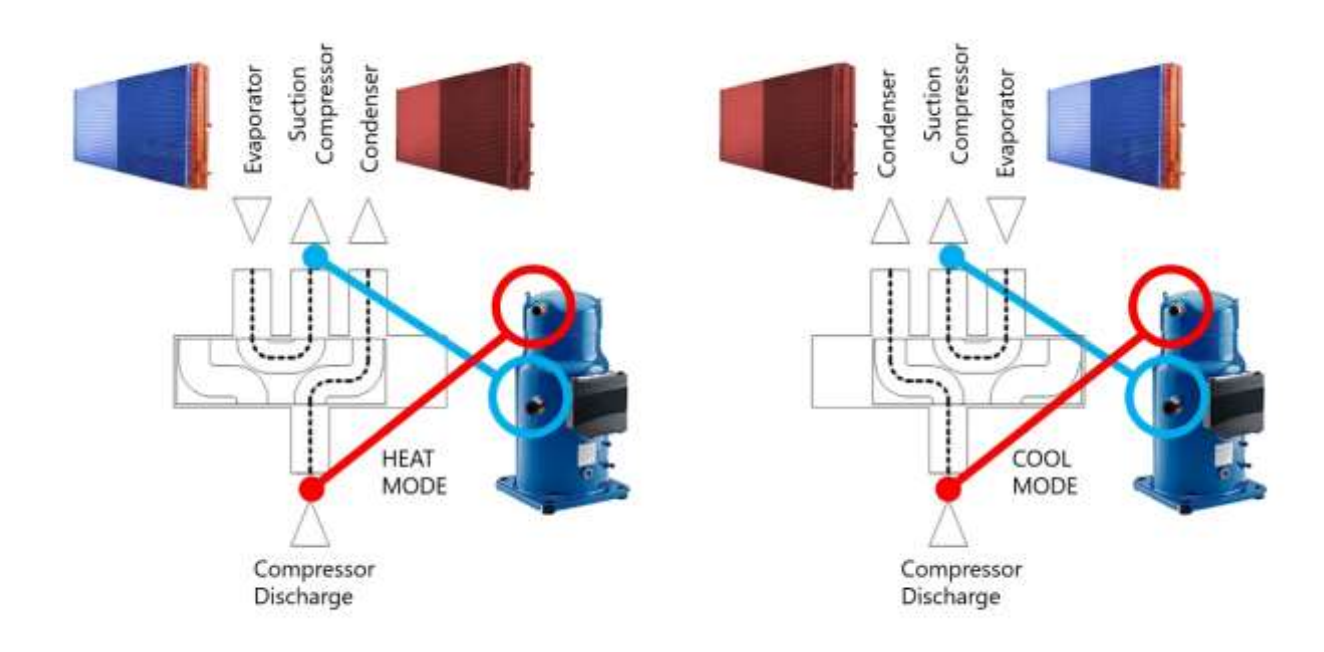


Figure 23. Four-way valve operating modes. Source: (GROUP, 2025).

This exchange enables efficient heat transfer and contributes to indoor comfort by controlling both temperature and humidity.

5.3 Refrigerant: R-410A Properties and Considerations

R-410A is a near-azeotropic ² blend of R-32 and R-125, and it is commonly used in modern residential heat pumps due to its:

² It is a mixture of two or more refrigerants whose physical and chemical properties are very similar to those of an azeotropic refrigerant, but with slight differences in behaviour during evaporation and condensation.

- High heat transfer efficiency.
- Zero ozone depletion potential (ODP = 0).
- Good compatibility with common compressor and heat exchanger designs due
 to its high volumetric capacity and stable thermal behaviour over a wide range
 of operating conditions. R-410A operates at relatively high pressures and
 provides a high volumetric cooling capacity, which makes it ideal for compact
 residential heat pump systems.

However, it does have a relatively high Global Warming Potential (GWP ~2088), which is a consideration in system design and refrigerant leakage prevention and compliance with environmental regulations. The thermodynamic behaviour of R-410A is well understood, with a saturation pressure range suitable for ambient temperatures typically encountered in residential heating and cooling.

6. HVAC Systems and Energy Control

In Zero Emission Buildings (ZEBs), the design and operation of HVAC (Heating, Ventilation, and Air Conditioning) systems must meet stringent efficiency and environmental performance criteria. These systems are not only responsible for ensuring thermal comfort but also play a pivotal role in minimizing energy consumption and operational emissions. Consequently, HVAC systems in ZEBs must be designed with a high degree of efficiency, adaptability, and intelligent control.

One of the foundational elements in energy-efficient HVAC design is the use of mechanical ventilation systems with heat recovery, such as Heat Recovery Ventilators (HRV) and Energy Recovery Ventilators (ERV). These systems, often integrated within controlled mechanical ventilation (VMC) frameworks, significantly reduce ventilation heat losses by recovering thermal energy from the exhaust air and transferring it to the incoming fresh air stream.

Additionally, efficient thermal distribution systems are essential. These may include hydronic networks (water-based heating/cooling loops), fan coil units, radiators, or radiant floor heating systems, depending on the building layout and climatic conditions.

Compared to direct expansion (DX) systems, hydronic systems offer advantages in terms of flexibility, thermal inertia, and integration with low-carbon energy sources.

Advanced zonal temperature control is another critical component, allowing the HVAC system to adjust conditions in different areas of the building based on real-time data. This control often relies on a network of sensors monitoring occupancy, indoor air quality (CO₂ levels), humidity, and ambient temperature to optimize comfort and energy use in each zone individually.

To coordinate all these components effectively, Building Energy Management Systems (BEMS) are deployed. These systems leverage predictive control algorithms, machine learning, and adaptive logic to dynamically manage HVAC operation, energy generation, and storage. By anticipating thermal loads and user behaviour, BEMS enhance overall efficiency while maintaining occupant comfort and reducing unnecessary energy use.

One of the central strategies for achieving near-zero operational emissions involves the integration of a reversible heat pump. This device can operate in both heating and cooling modes, using a vapor-compression refrigeration cycle with a high-efficiency air-to-refrigerant heat exchanger. In the system studied in this diploma thesis, the refrigerant used is R-410A, selected for its favourable thermodynamic properties and compatibility with compact residential applications. While R-410A has a relatively high Global Warming Potential (GWP), it remains widely used due to its thermal performance and established industry infrastructure. However, future improvements may include transitioning to lower-GWP refrigerants.

Ultimately, the combination of smart control, efficient components, and thermodynamically optimized systems forms the backbone of HVAC design in Zero Emission Buildings, supporting both emission reduction goals and high standards of indoor environmental quality.

The success of a zero-emission building does not rely on a single component, but rather on the integrated operation of all systems, working together toward the common goal of minimizing environmental impact and maximizing operational and economic efficiency.

Chapter III: Modelling Setup

This chapter describes the modelling approach used to simulate the energy performance of a residential building. It details the physical characteristics of the building, the components considered in the model (such as HVAC systems, appliances, and PV generation), and the incorporation of real-world data such as temperature and irradiance. The development and implementation of the simulation model in MATLAB and Simulink are also explained, including how the system dynamics and control strategies are represented within the platform.

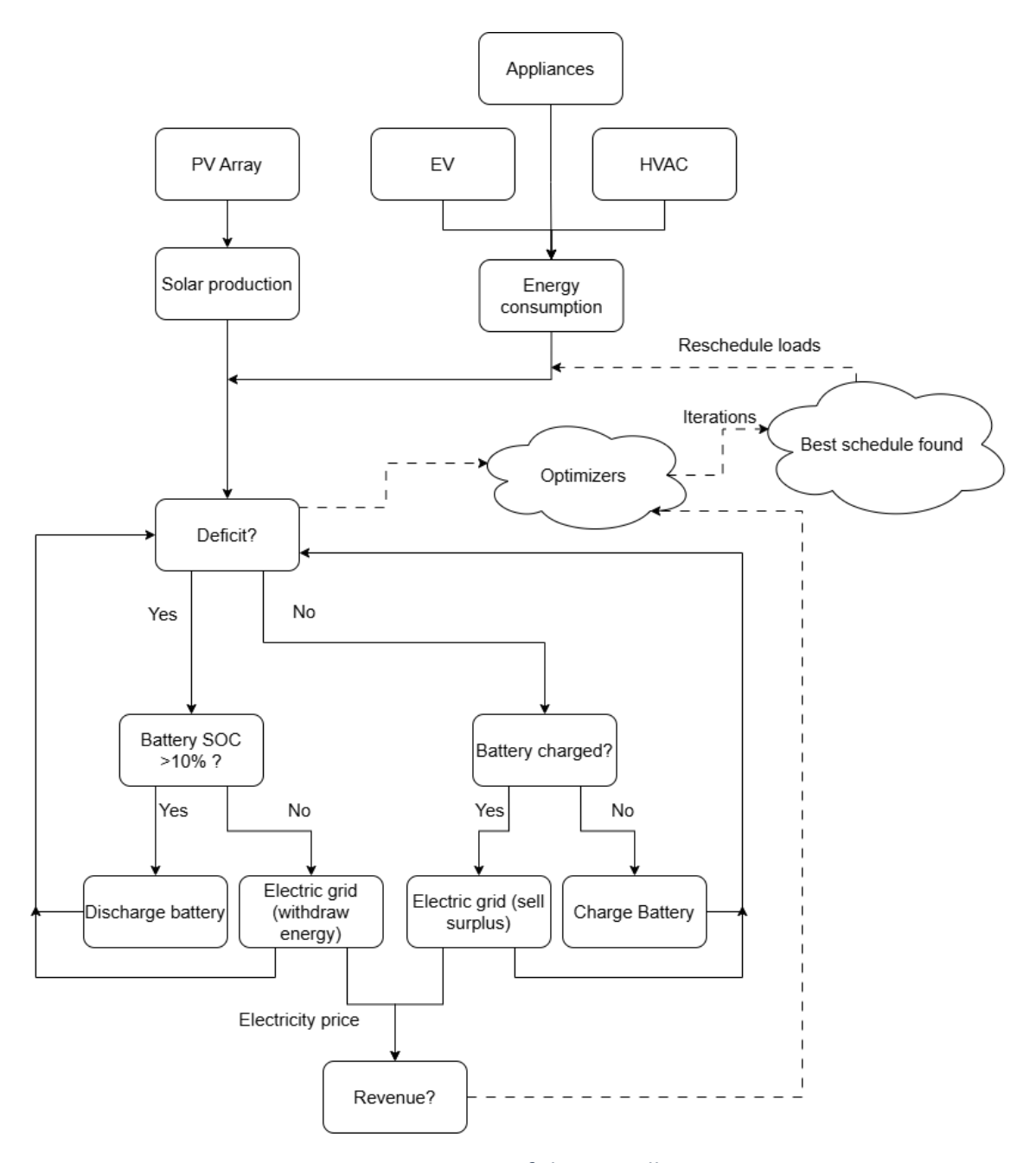


Figure 24. Diagram of the overall system.

A diagram of the operation of the overall system can be seen in Fig. 24. It starts with the PV array which produces energy depending on the temperature and irradiance conditions of the case study. The appliances, EV, and the HVAC system make up energy consumption (loads), then this consumption is compared with the solar production (in AC) to determine if there is a deficit. In the event of a deficit, it will be checked whether the state of the batteries is higher than 10% (they cannot fall below this limit to improve their useful life). When the state of the battery is higher than 10%, it is discharged to compensate for the existing deficit until it reaches the limit of its capacity or there is no

longer a deficit. If energy is needed but the battery is at the limit of its capacity, the amount of energy needed to satisfy the consumption that cannot be covered will be extracted from the electric grid. In the same way as with the battery, energy is extracted from the grid until the situation changes, in this case keeping a record of the price of the energy purchased from the grid.

If solar production exceeds consumption, there is no deficit. Then there are two possible situations, whether the battery is fully charged or not. If the battery is fully charged, the surplus energy is fed into the grid, and a record of the electricity price is kept until the situation changes. If the battery is not fully charged but there is a surplus, it will be charged until the situation changes.

Once the simulation has been completed, the economic benefit of the interaction with the electricity grid (buying/selling of energy) can be determined. Obviously, having to calculate deficits and surpluses during the simulation are also recorded.

The solid lines represent the non-optimized case, while the dash lines represent the optimizers, one seeking to minimize the deficit and the other to maximize the economic benefit. The optimizers perform iterations by changing the load distribution until they find the best possible solution and follow the same logic as in the non-optimized case, comparing the results obtained.

7. Characteristics of the model

The model presented consists of a Simulink model which simulates the thermal behaviour of a house with a HVAC system in response to the environment temperature. The HVAC system can operate in heating and cooling modes to achieve an indoor temperature defined by the user, so that when the temperature outdoors is above the setpoint the HVAC system works in cooling mode until obtaining the desired temperature in the house, similar to what happens when the temperature is below the setpoint but working in heating mode.

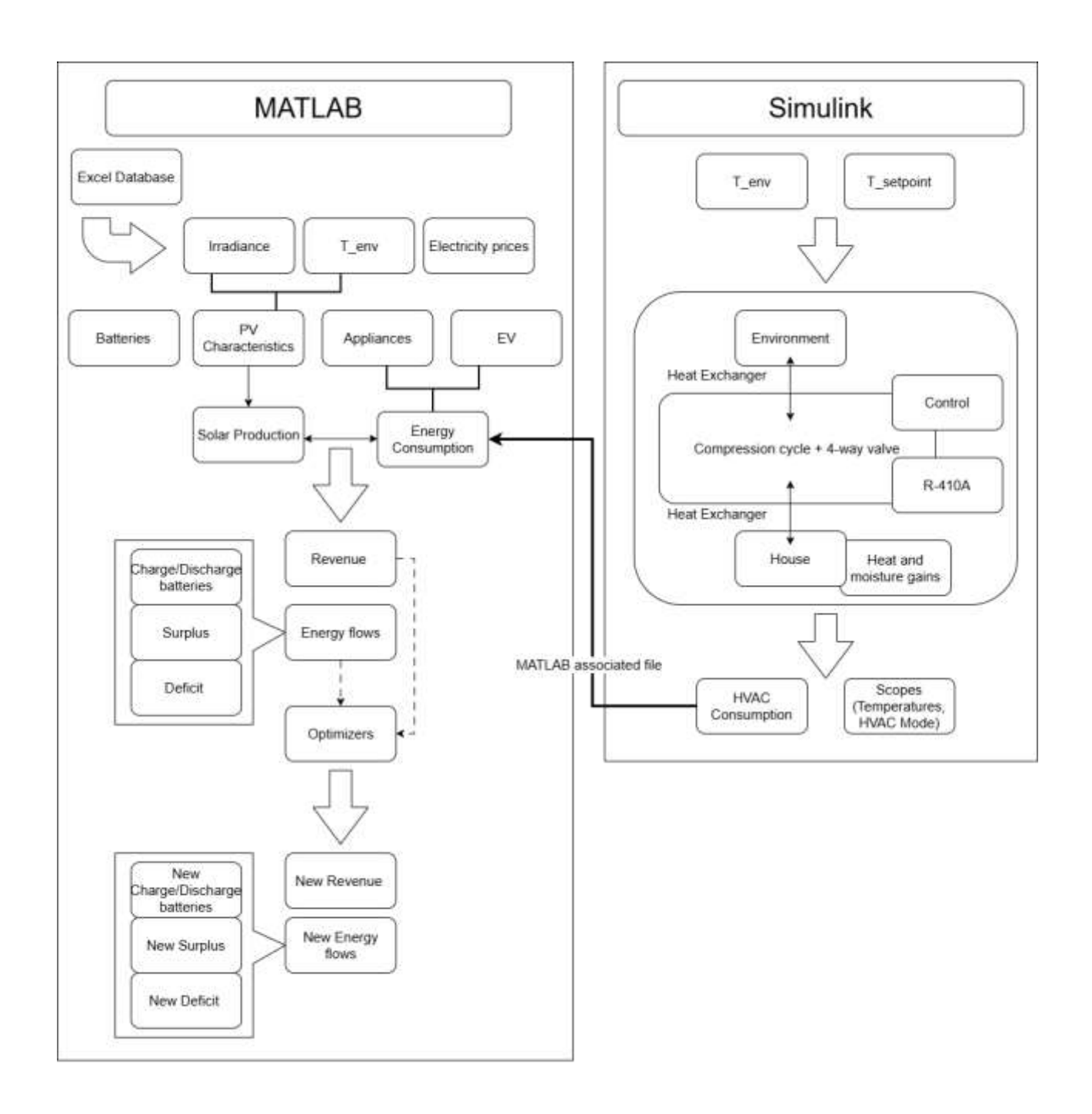


Figure 25. Diagram of the software model.

A diagram of the software model can be seen in Fig. 25. The diagram shows the different components associated with MATLAB and Simulink, as well as how they interact with each other. In the Simulink model section, the blocks will be explained in more detail. The most important inputs of the Simulink model are the external ambient temperature and the setpoint temperature, as they will make the system work in a specific way to obtain the desired thermal comfort. These inputs are analysed by the system which contains a compressor cycle and a 4-way valve that allows cooling and heating modes.

This compressor cycle has associated control blocks that allow it to work in specific and safe ranges. The properties of the working fluid of the cycle are also defined, which is the refrigerant R-410A. The cycle interacts with the environment and the house thanks to two heat exchangers that work as condenser or evaporator depending on the heating or cooling mode.

In the environment block, air properties and operation of a fan for air circulation are defined, while in the house block, air and fan properties as well as thermal and moisture gains due to occupancy and appliances are defined. The thermal characteristics of the building are also defined in this block.

When simulating the Simulink file, the temperature graphs are generated (ambient, indoors and setpoint), while also the Simulink model has associated MATLAB codes from which the consumption of the HVAC system can be extracted and exported to the MATLAB code. This is how both documents are related.

In the MATLAB code, values are imported from an excel file containing data on electricity prices, irradiance and ambient temperature. With this data, the code continues by declaring the variables needed to define the batteries, solar panels, appliances and EV. Once defined, solar production and energy consumption are determined, thanks to the energy exported from the HVAC system. Having the energy production and consumption, the energy flows (deficit, surplus, battery charge/discharge) and the net cost of electricity (bought/sold from the grid) can be determined. This can be done since having a record of the energy flows and the price of energy.

After having calculated the energy flows and the revenue, two optimizers are defined that seek to minimize the deficit and maximize the economic benefit respectively. The optimizers modify the schedule of the energy loads by calculating through iterations the new best values found for the energy flows and net cost.

It is important to note that the ambient temperature used corresponds to the data obtained from the PVGIS database for a location in Valladolid (41.626°, -4.732°). This data provides the air temperature measured two metres above ground level, which is approximated as the ambient temperature for the solar panel. Additionally, the mounting position of the solar panels is fixed at the optimal orientation for the specified location (Slope: 36°, Azimuth: -4°). The environmental temperature data is utilised in both the Simulink and MATLAB models, whereas the irradiance data is used exclusively in the MATLAB model.

8. MATLAB model

This section focuses on the main MATLAB code developed, although there are additional files associated with the Simulink model that are solely used to run the thermal model. A flowchart of the MATLAB code is depicted in Fig. 26.

The main code is used to store all the variables necessary to be able to apply the optimisers and make a better energy management.

The main MATLAB code first executes the selected case study and performs the necessary calculations. Following this, the code receives input parameters such as user-defined restricted charging hours and the type of day on which the analysis is conducted (weekday or weekend/holiday). With these new variables the code will execute two optimisers, the first one tries to find with the imposed constraints, a distribution of the energy loads that allows to diminish the energy deficit. While the second optimiser tries to find a solution to obtain the highest economic benefit, trying to buy energy from the grid at the cheapest times and sell the maximum of surplus energy generated.

Both optimizers aim to improve the management of the energy produced and consumed in the building, taking into account a series of constraints, such as the previously mentioned prohibited charging hours for the electric vehicle. Additionally, the distribution of controllable or programmable appliances is also considered. In this case study, these appliances must operate for at least two consecutive hours and only once

per day. This condition could also be modified for future case studies. Regarding the EV, the code also takes into account the forbidden schedule given by the user.

The only modification to the MATLAB code associated with the Simulink model is to be able to export the energy of the HVAC system on an hourly basis to the main MATLAB code. For this, the energy obtained throughout the simulation is integrated to be able to extract the data on an hourly basis.

The variables that change during the situations to be analysed are ambient temperature and irradiance, but these can be modified by changing the lines that are imported from the excel file where the data of the variables are stored (there is a note for each of the case studies). Similarly, the price can be changed in the excel file in case the tariff is changed in order to study other possible cases.

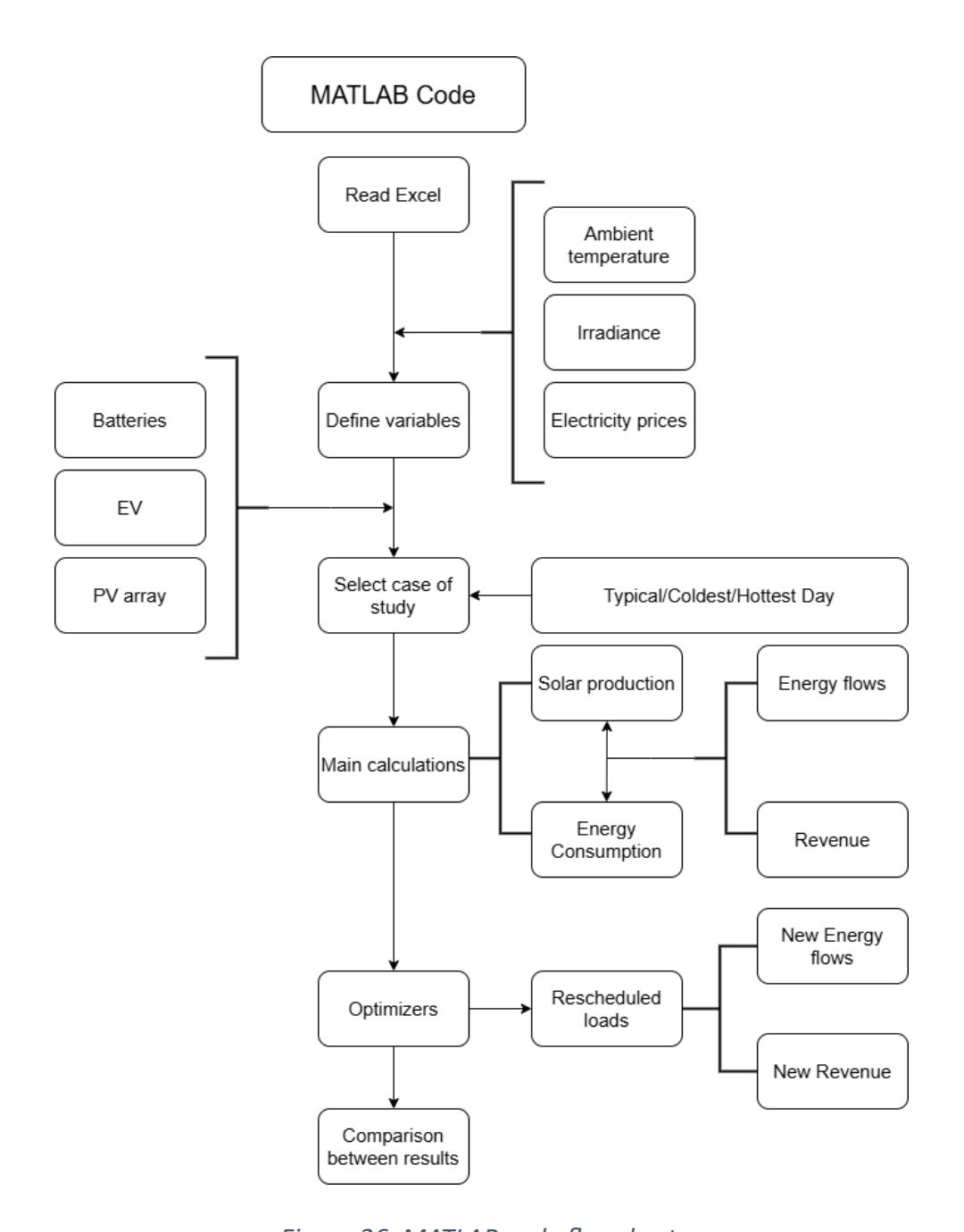


Figure 26. MATLAB code flowchart.

8.1 Original scenario

The code begins importing data from an excel document which contains the environmental temperature, irradiance and the price of buying/selling electricity from the grid on an hourly basis during the whole year. As the environmental temperature and irradiance data change in each of the situations to be studied, only the price of electricity is shown (it remains constant). The rest of the data commented will be shown in the results section as they are used to determine the value of variables needed in the

code such as panel temperature or solar production. The code is prepared to be able to export only the excel data required, only changing the number of rows to be exported.

- Electricity prices are shown in Table 1.

Table 1. Electricity prices.

Hour	Daily €/kWh	Holidays and	Selling prices
		weekend €/kWh	€/kWh
1	0.082334	0.082334	0.07
2	0.082334	0.082334	0.07
3	0.082334	0.082334	0.07
4	0.082334	0.082334	0.07
5	0.082334	0.082334	0.07
6	0.082334	0.082334	0.07
7	0.082334	0.082334	0.07
8	0.082334	0.082334	0.07
9	0.116414	0.082334	0.07
10	0.116414	0.082334	0.07
11	0.185461	0.082334	0.07
12	0.185461	0.082334	0.07
13	0.185461	0.082334	0.07
14	0.185461	0.082334	0.07
15	0.116414	0.082334	0.07
16	0.116414	0.082334	0.07
17	0.116414	0.082334	0.07
18	0.116414	0.082334	0.07
19	0.185461	0.082334	0.07
20	0.185461	0.082334	0.07
21	0.185461	0.082334	0.07
22	0.185461	0.082334	0.07
23	0.116414	0.082334	0.07
24	0.116414	0.082334	0.07

The data for the solar panels are then defined:

- Solar panels:

- $A = 180 \text{ m}^2$
- NOCT = 45°C
- $\beta = -0.0045 \, ^{\circ}\text{C}^{-1}$
- T_{ref} = 25 °C
- $\eta_{ref} = 0.227$

Having such a large surface of solar panels is due to the high consumption of the house due to its large size. This will be seen later but thanks to these dimensions the surface is enough to fit solar panels to cover the energy consumption.

With the above data and the Eq. 19 and Eq. 21, the solar production and the panel temperature, are obtained (hourly throughout the day). Then, the ambient temperature together with the panel temperature are plotted in order to better see the influence of the ambient on the panel temperature. In a similar way, the irradiance and the solar production (in direct current) are plotted. Examples of those plots are shown in Figs. 27-28.

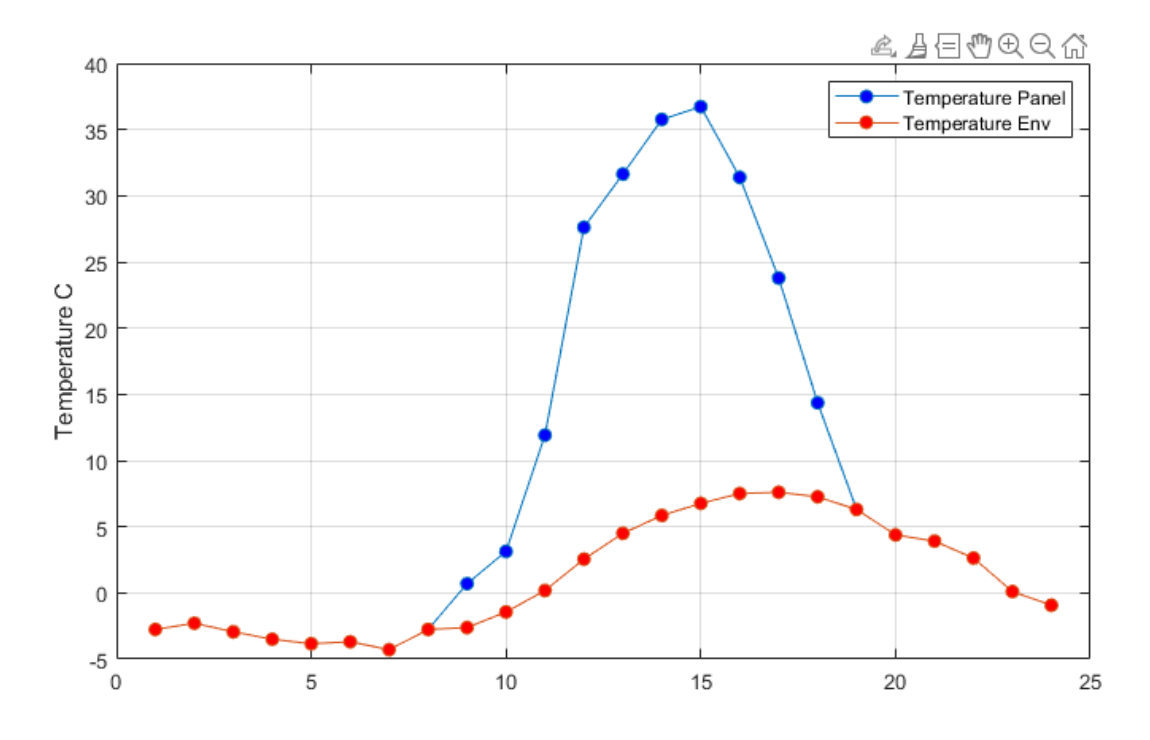


Figure 27. Example of plot with temperature of the panel and ambient temperature.

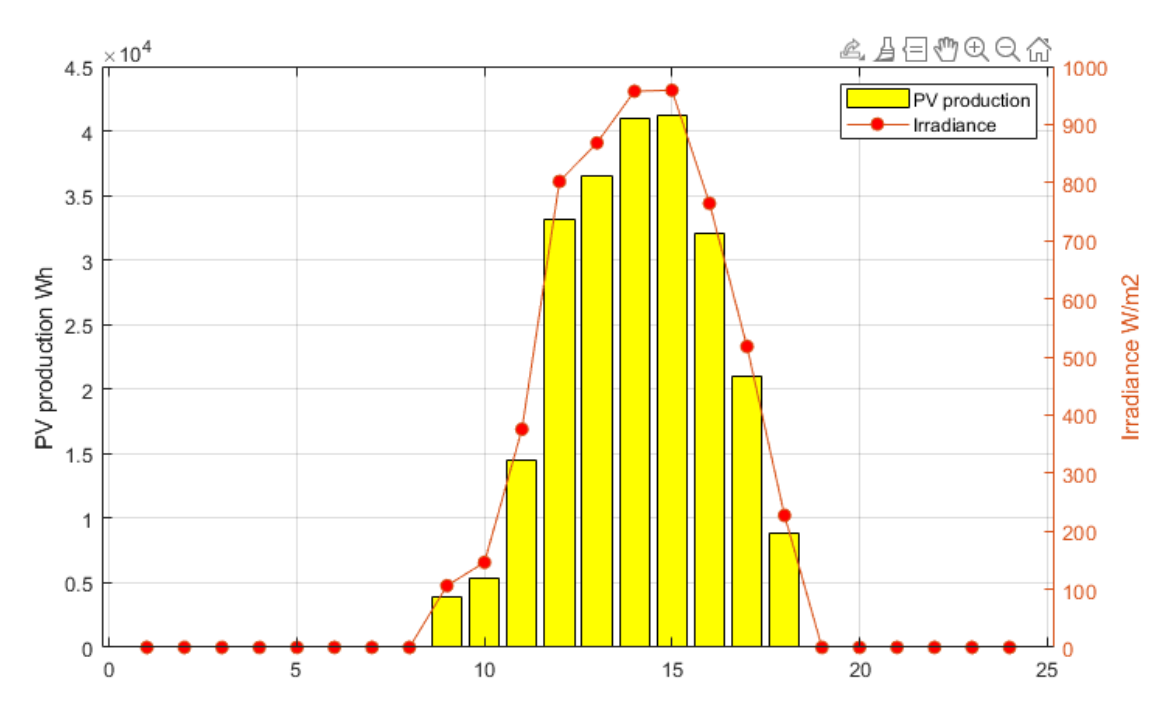


Figure 28. Example of plot with PV production and solar irradiance.

Subsequently, the variables corresponding to the electric vehicle are defined:

Electric vehicle:

- Battery capacity = 77 kWh.
- Charger efficiency = 0.95.
- Initial battery capacity = 10 kWh.
- Charger power = 7.4 kW.
- Original charging schedule: 23-7.
- Forbidden charging hours: 8:00-13:00 and 17:00-21:00.

With the EV variables defined, it is now possible to calculate the consumption, as the power of the charger and the hours it charges are known. The charge supplied to the battery can also be determined thanks to the efficiency of the charger. It is important to note that it also generates a small summary of the battery data such as the initial and final state of the battery, charge made, consumption of that charge, charge to be full (it also generates a text when the EV is fully charged and does not calculate the consumption corresponding to the charge above 100%. The optimisers instead take into account that waste of keeping the EV plugged in while the charge is at 100% — that is why, if it is known that in the base case the EV needs fewer charging hours, the distribution of hours should be adjusted in a better way in the optimisers) and finally the

charging hours, which is important because if the forbidden timetable is very wide and restricts the hours of the non-optimized state, a notification that the same number of hours have not been adjusted will also be displayed.

However, in this study there will not be the situation of having less hours to optimise the charging of the car, as the idea is to plug the EV in during the night and the forbidden hours would correspond to a hypothetical working day shift.

The code also graphs the consumption of the electric vehicle charge throughout the day, as well as the evolution of the state of charge of the battery so a better visualisation of the state of charge when charging is seen is Figs. 29 -30.

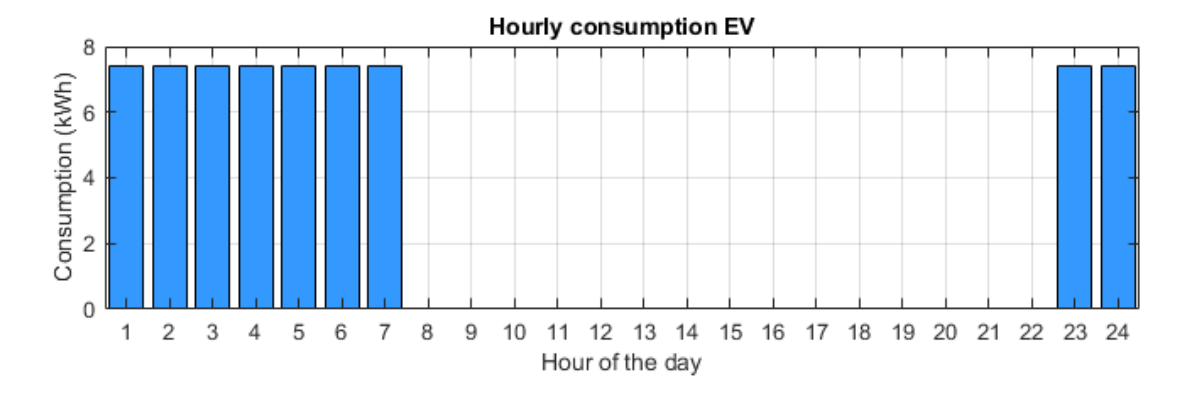


Figure 29. Example plot of EV consumption.

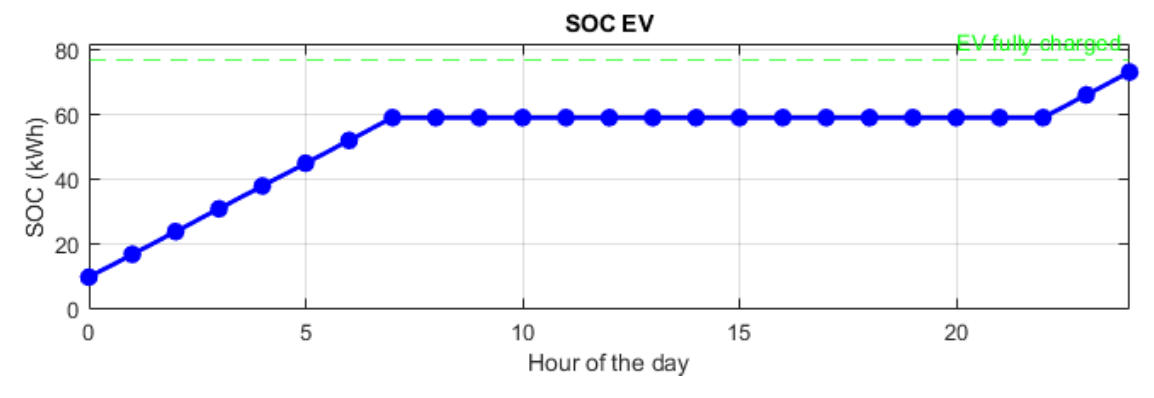


Figure 30. Example plot of EV SOC.

Moving on to the appliances, these will be divided into two groups, controllable and non-controllable, although both groups will have the same usage schedule in the original case, only the controllable ones can change their schedule after applying the optimisers.

The HVAC system is not included in this section because all the variables related to it are on the Simulink model, and also the consumption is not determined by the MATLAB code.

- Appliances:

- Non-controllable appliances power (and schedule).
 - Cooker hub = 3 kW (8:00, 13:00, 19:00).
 - Cooker oven = 3 kW (0:00).
 - Microwave = 1 kW (8:00, 13:00, 19:00).
 - Laptop = 400 W (9:00-12:00, 19:00-24:00).
 - TV = 200 W (19:00-21:00).
 - Refrigerator = 150 W (24h).
- Controllable appliances power (and schedule).
 - Washing machine = 1.2 kW (1:00-2:00).
 - Dishwasher = 2.3 kW (7:00-8:00).

The appliances power consumption and hours of use correspond to a typical power and usage profile. Again, it is important to remember that the controllable appliances in this study should operate for two consecutive hours and only once a day.

Knowing the usage profile and power of all types of appliances, the consumption can be calculated in a disaggregated way (adding the electric vehicle load). Having all these consumptions, the daily energy (without taking into account the HVAC) is determined and a plot is displayed where the total hourly consumption and the elements that form it, are observed.

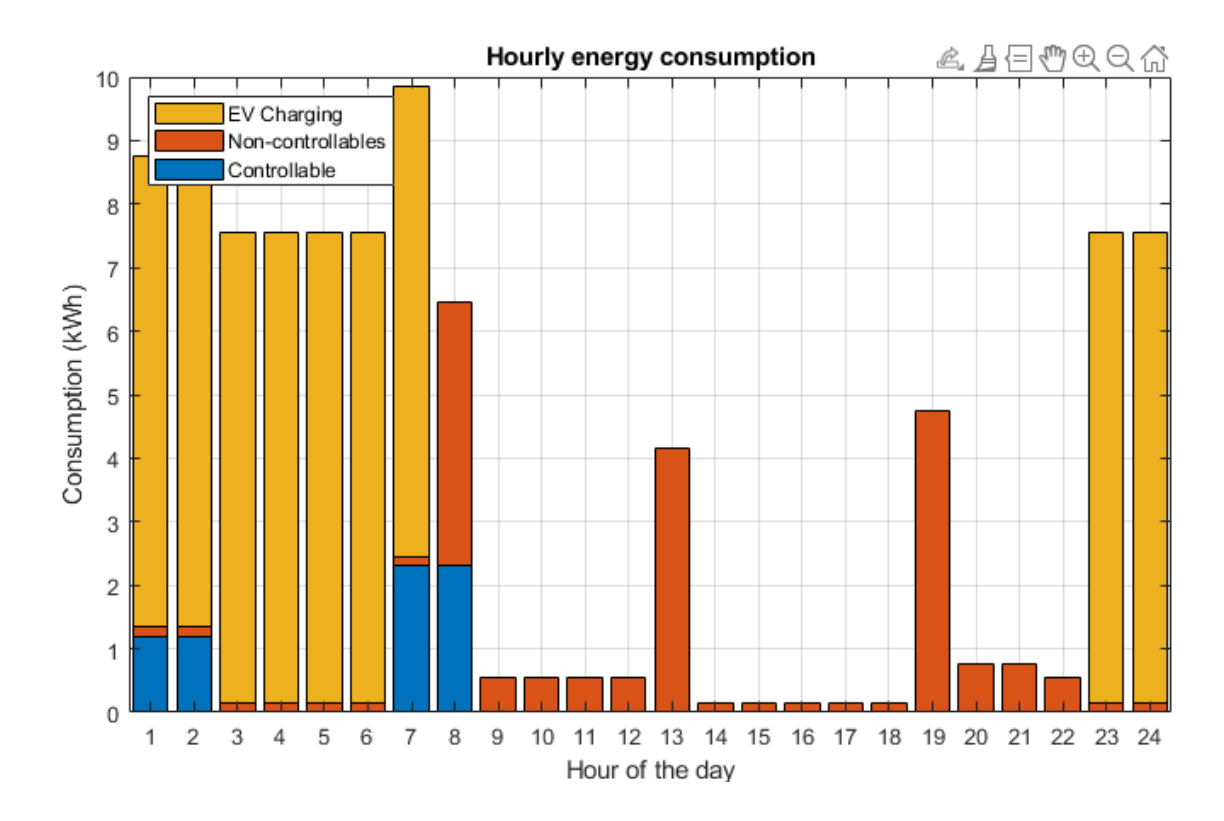


Figure 31. Example plot of hourly energy consumption.

After defining the appliances and determining their consumption, the batteries for selfconsumption are next.

- Batteries:

- Capacity = 100 kWh.
- DOD = 0.9 (minimum charge 10%).
- SOC initial = 50 kWh.
- Inverter efficiency = 0.95.
- Charge efficiency = 0.95.
- Discharge efficiency = 0.95.

As with the rest of the previously defined elements, these battery parameters can be changed, but throughout this study they will remain constant.

As before, some storage variables to make the calculations must be defines, not only for the batteries but also to calculate the load flows, as it is only necessary to export the HVAC system energy from the MATLAB file associated with the Simulink model to have all the consumption variables that are taken into account in this study.

As in the electric vehicle, the variable that stores the state of charge of the battery is forced to start, in this case, at half of the total capacity.

As previously mentioned, the energy of the HVAC system is exported on an hourly basis, and the total hourly consumption and the total consumption throughout the day can be calculated.

To finalise the non-optimised case, a loop is defined so that the energy deficit is calculated, taking into account that, if there is higher energy production than consumption, the batteries are charged until they are fully charged, and then the surplus is fed into the grid. When power generation cannot cover the total demand, energy from the batteries is used until the batteries reach 10% of their capacity (to improve the lifetime of the batteries). The only situation in which energy is drawn from the grid is when there is no energy left in the batteries, and solar production is not sufficient to meet the entire demand.

Once the charge and discharge of the batteries, as well as the energy surplus and deficit, have been determined in the corresponding variables, a graph is displayed comparing energy generation with consumption. The evolution of the state of charge of the batteries is also generated, with delimiting lines that represent 50% of the capacity (initial situation), 100% of the charge, and 10% (minimum charge that the battery can have).

Finally, the energy flows are shown together with a small summary of the batteries (initial, final, charge and discharge status), energy deficit, and energy surplus.

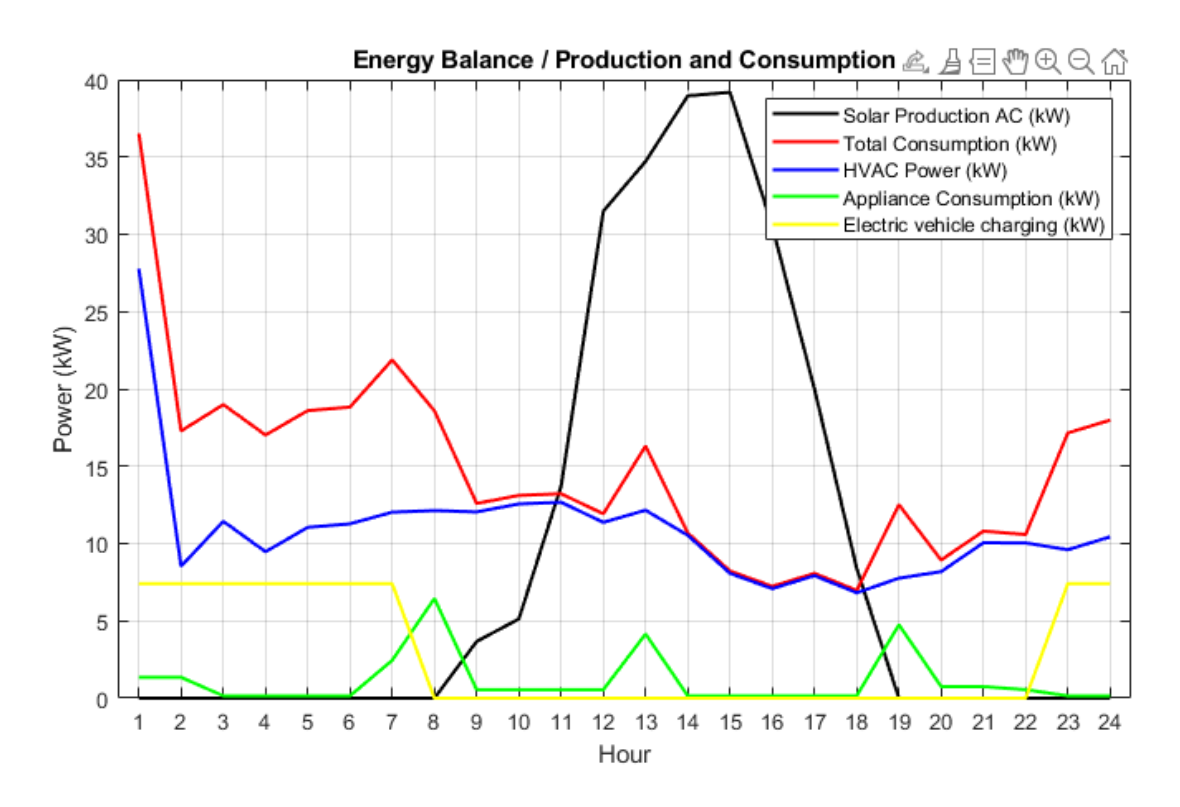


Figure 32. Example plot of energy balance.

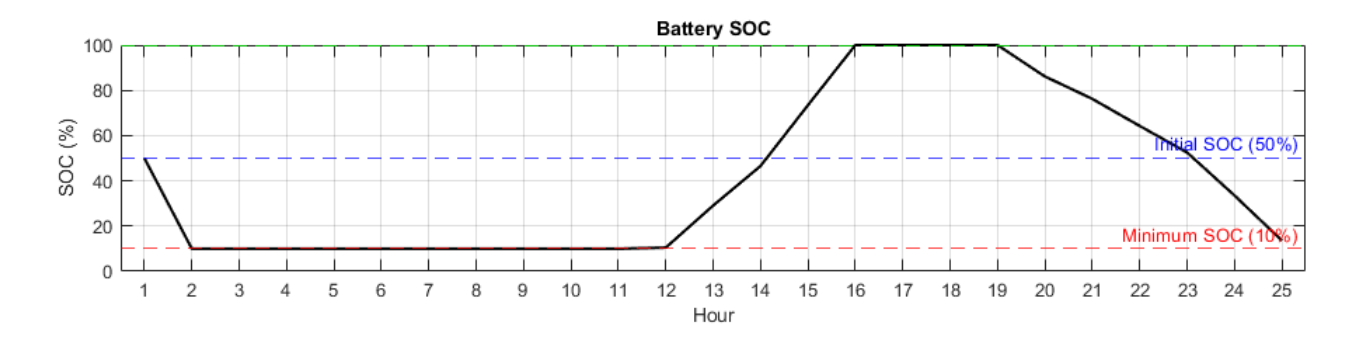


Figure 33. Example plot of battery SOC.

8.2 Consumption optimization

A flowchart of this process is shown in Fig. 34.



Figure 34. Flowchart of the consumption optimization.

This optimizer aims to minimize the daily energy deficit (the energy that cannot be covered by renewable production plus battery storage) within a residential energy system by optimally scheduling the operation of controllable appliances and an electric

vehicle (EV). The system includes photovoltaic (PV) generation, a household battery, and a set of controllable and uncontrollable electrical loads. A multi-variable optimization algorithm based on Particle Swarm Optimization (PSO) is employed to determine the most efficient operating schedule for each element, ensuring that energy consumption aligns as closely as possible with energy availability, particularly from renewable sources. Several operational constraints are taken into account, such as forbidden hours for EV charging, maximum allowable state of charge (SOC) for the EV, the required duration of EV charging, and the efficiency limitations of inverters, chargers, and battery systems. Additionally, the constraint for the controllable appliances is that they must work two hours in a row once a day.

At the beginning of the optimization, the algorithm prompts the user to define specific hours during which the EV must not be charged. The provided input is converted into a vector of prohibited time slots, which are referenced throughout the optimization to enforce charging constraints. In the event that the number of permissible charging hours is insufficient to accommodate the original EV charging plan, the algorithm automatically reduces the charging time, accordingly, displaying a warning with the changes. This adjustment is communicated to the user to ensure transparency and to highlight any compromise in meeting the vehicle's expected energy needs.

The Particle Swarm Optimization algorithm operates by simulating the behaviour of a swarm consisting of 100 individual particles over 250 iterations. Each particle represents a potential scheduling solution, where the position of each particle encodes a proposed set of start times for controllable appliances and designated charging hours for the electric vehicle. The appliances are modelled to operate for two consecutive hours, while the EV must be charged across a specific number of permitted hourly intervals. Each particle updates its position and velocity over time, influenced both by its own historical best solution and by the best-known solution found by the swarm. This dynamic allows the population to converge toward an optimal or near-optimal configuration while exploring a wide solution space. The PSO algorithm parameters (there are two algorithms, one aims to minimize the daily deficit and the other one aims to maximize the economic revenue, but the parameters are the same for both) are the following:

- Number of particles = 100.
- Number of iterations = 250.
- Inertia Weight ³ = 0.7.
- Cognitive component ⁴ = 1.5.
- Social component ⁵ = 1.5.

To evaluate each particle, its encoded variables are converted into binary scheduling matrices that represent the on/off states of controllable appliances and EV charging activities for each hour of the day. The start times of the appliances are translated into two-hour activation periods, while the selected charging hours for the EV are validated to ensure they do not fall within the forbidden range. In cases where a particle includes duplicate or invalid charging times, these are replaced with randomly selected valid hours from the available set. This step guarantees that all solutions considered during optimization are physically and operationally feasible.

8.2.1 Fitness Function and Solution Evaluation

Each scheduling configuration is assessed through a 24-hour energy simulation that incorporates all elements of the residential energy system. The evaluation calculates the total hourly energy consumption, including contributions from controllable and non-controllable appliances, HVAC system, and the EV. It also estimates the AC output from

³ The inertia weight (w) controls the momentum of a particle, balancing exploration and exploitation. Higher values enable broader search space exploration, while lower values promote convergence toward optimal regions.

⁴ Cognitive component (c1) reflects a particle's tendency to return to its personal best position (pbest). A higher value of c1 enhances local search around historically successful solutions found by individual particles.

⁵ The social coefficient (c2) drives a particle toward the global best position (gbest) found by the swarm. A higher value of c2 fosters collective learning and exploration of potentially optimal areas in the search space.

PV generation, accounting for inverter efficiency, and models the state of charge of the household battery while considering both charging and discharging efficiencies. The EV charging behaviour is simulated to ensure that the energy delivered to the vehicle complies with the maximum SOC limit and required energy input. A fitness function is applied to quantify the quality of each solution.

8.2.2 Execution of the PSO Algorithm

Throughout the optimization process, each particle monitors its best previous solution (pbest) and compares it with the global best solution (gbest) found by the swarm. If a better configuration is identified, it replaces the existing best solution. The position and velocity of each particle are then updated using standard PSO rules, ensuring that the solution remains within valid bounds. Specifically, the start hours for appliances must fall between 1 and 23 (they must work two hours in a row), while EV charging times must range from 1 to 24 and exclude prohibited or repeated hours. If duplicates are found in the EV schedule, they are replaced with randomly selected valid times. If no replacements are available, only the non-duplicate times are preserved. This step preserves the integrity of the scheduling solution while ensuring compliance with all constraints.

8.2.3 Optimization Output

Upon completion of the optimization, the algorithm presents the optimal daily schedule for all devices, including the electric vehicle. It also provides visualizations of the EV and battery SOC over time, allowing the user to assess the dynamics of energy storage and usage throughout the day. The total energy deficit is reported both before and after optimization, enabling a quantitative assessment of improvement. Additionally, the algorithm highlights any unused PV energy resulting from the EV reaching its SOC limit, offering insights into system inefficiencies. If the final EV charging schedule deviates from

the original plan, the user is informed accordingly. This ensures that all modifications are explicitly reported, and that system performance can be fully evaluated.

Energy Flow and Performance Comparison

To conclude, a comparative analysis is conducted between the initial (pre-optimization) scenario and the optimized schedule. This comparison highlights reductions in energy deficit, better synchronization between appliance operation and PV energy availability, and improved battery utilization. The results demonstrate that intelligent scheduling through metaheuristic ⁶ optimization techniques like PSO can significantly enhance energy efficiency in smart homes equipped with renewable energy and electric mobility. The methodology proves effective in managing complex operational constraints while maximizing the use of local energy resources.

8.3 Economic optimization

A flowchart of the economic optimization is shown in Fig. 35.

_

⁶ In computer science and mathematical optimization, a metaheuristic is a higher-level procedure or heuristic designed to find, generate, tune, or select a heuristic (partial search algorithm) that may provide a sufficiently good solution to an optimization problem or a machine learning problem, especially with incomplete or imperfect information or limited computation capacity.

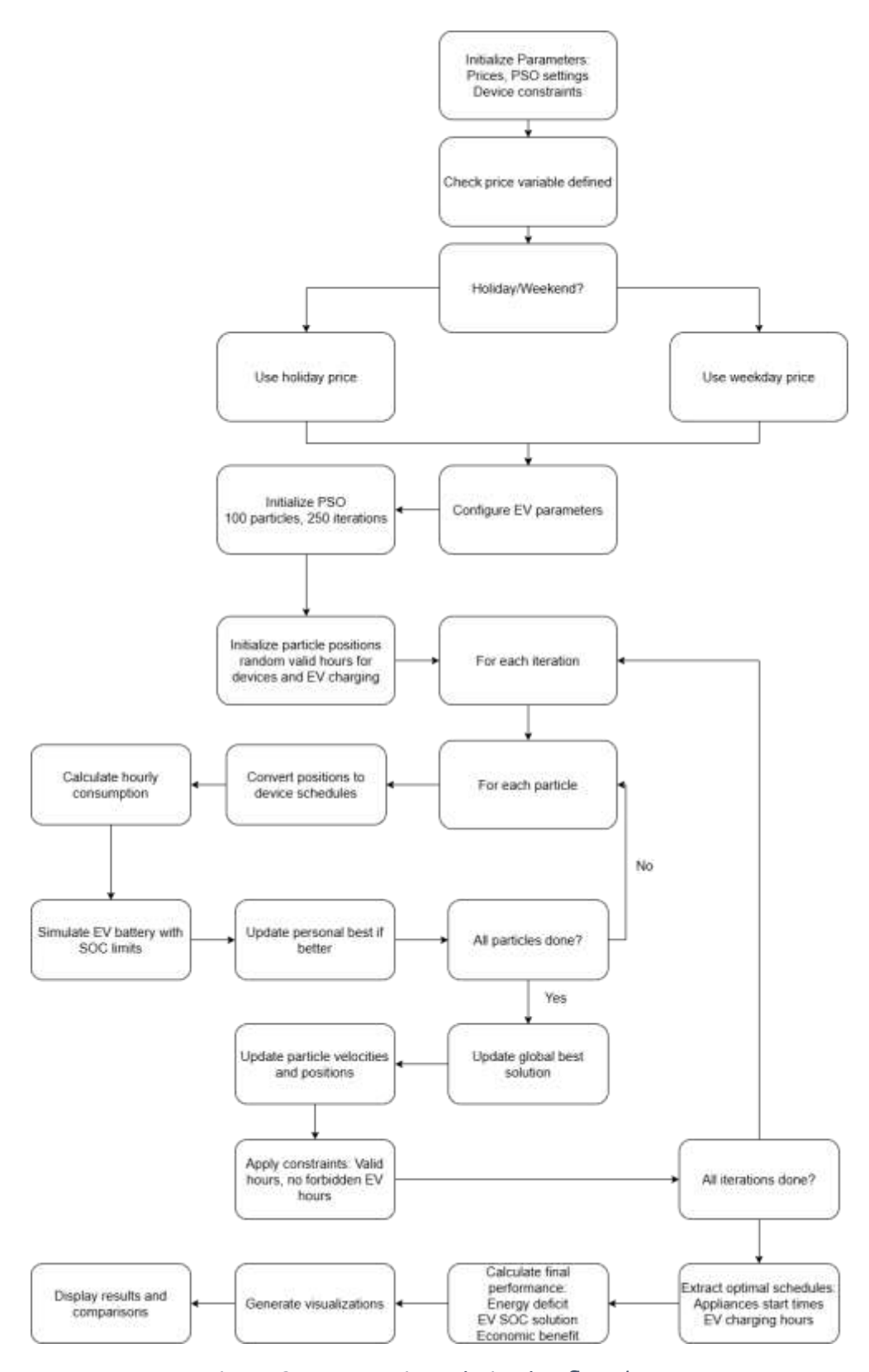


Figure 35. Economic optimization flowchart.

This optimizer also implements a Particle Swarm Optimization (PSO) algorithm to determine the optimal hourly schedule for the operation of household energy assets, specifically electrical appliances, a battery energy storage system, and an electric vehicle (EV). The objective is to maximize the daily net economic benefit derived from energy management while ensuring all physical and operational constraints are respected.

At its core, the optimization process seeks to decide, for each hour of the day, when to activate certain controllable appliances and when to charge or discharge the battery and the EV. The net economic benefit is calculated as the total value of the energy exported to the grid minus the cost of energy imported from the grid. The model considers varying electricity prices throughout the day, distinguishing between weekdays and holidays, and applies an efficiency factor to simulate energy losses during conversion.

Each solution (or particle in PSO terminology) represents a unique combination of activation schedules for the appliances and charging slots for the EV. The code ensures that the EV is only allowed to charge during user-defined permitted hours, and that both the EV and the battery do not exceed their storage capacities. The PSO algorithm iteratively evaluates each candidate solution by simulating the household's energy balance over 24 hours, including photovoltaic (PV) generation, consumption, battery and EV charging/discharging, and energy flows to/from the grid.

During the simulation of each particle, the algorithm computes the hourly state of charge (SOC) for both the battery and the EV. It calculates the energy imported from and exported to the grid, prioritizing self-consumption of PV energy whenever possible. Energy that cannot be consumed instantly is either stored or exported, depending on available capacity and system constraints.

The fitness function used in the PSO evaluates each particle based on the resulting profit, considering any violation of system constraints (such as exceeding SOC limits or charging outside allowed hours). Over several iterations, the swarm of particles converges toward the most profitable schedule, continuously updating each particle's personal best and the global best solution found.

After convergence, the code produces a set of detailed visual outputs to help interpret the results. These include time series plots showing the evolution of the state of charge (SOC) of both the battery and the electric vehicle throughout the day, and the power flows associated with each system component. It also displays binary activation schedules of the flexible appliances, indicating at which hours they are scheduled to operate and the charging of the EV. The charts are shown in Figs. 36-39.

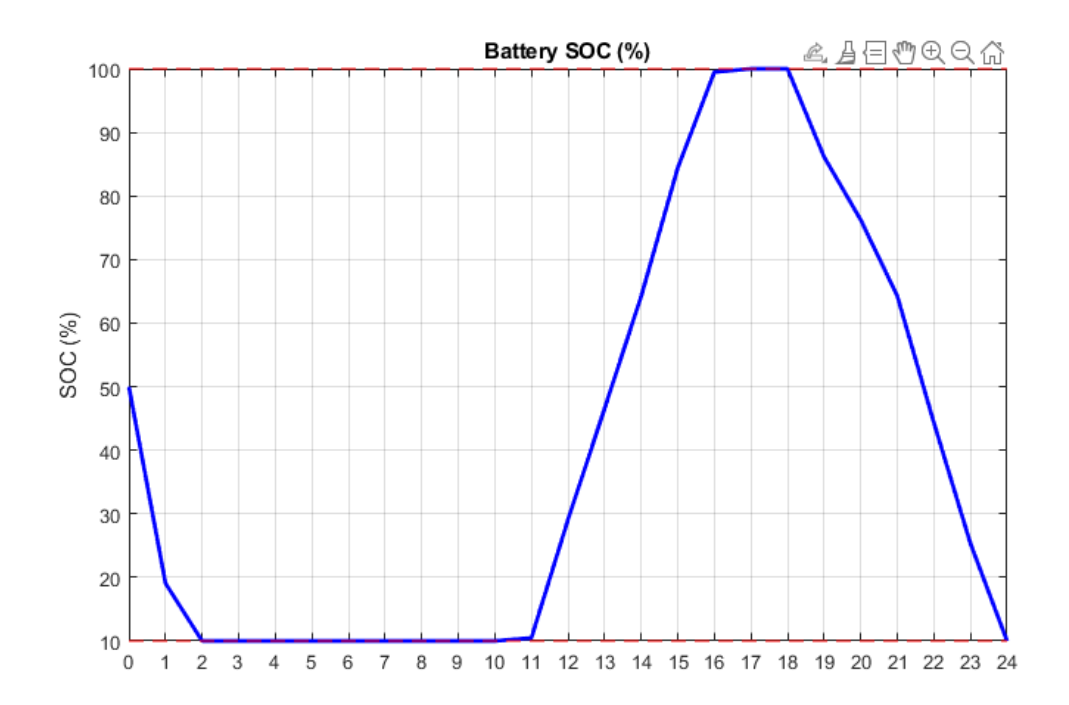


Figure 36. Example plot of battery SOC for economic optimization.

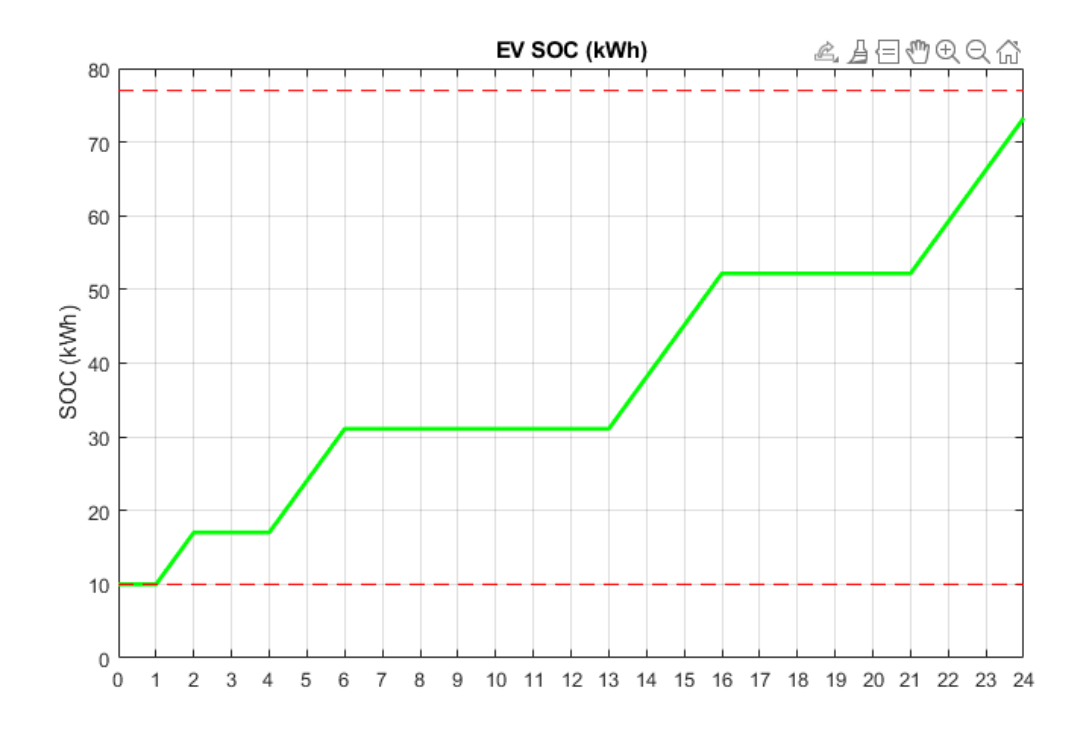


Figure 37. Example plot of EV SOC for economic optimization.

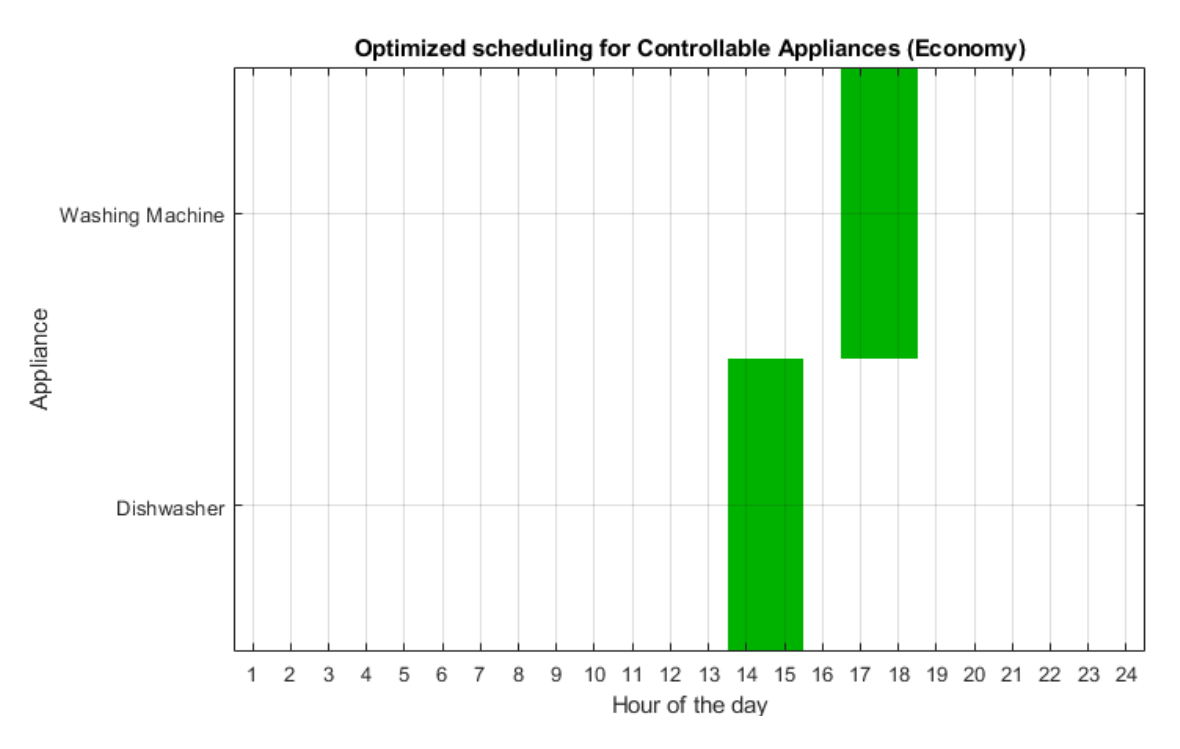


Figure 38. Example of binary activation of appliances for economic optimization.

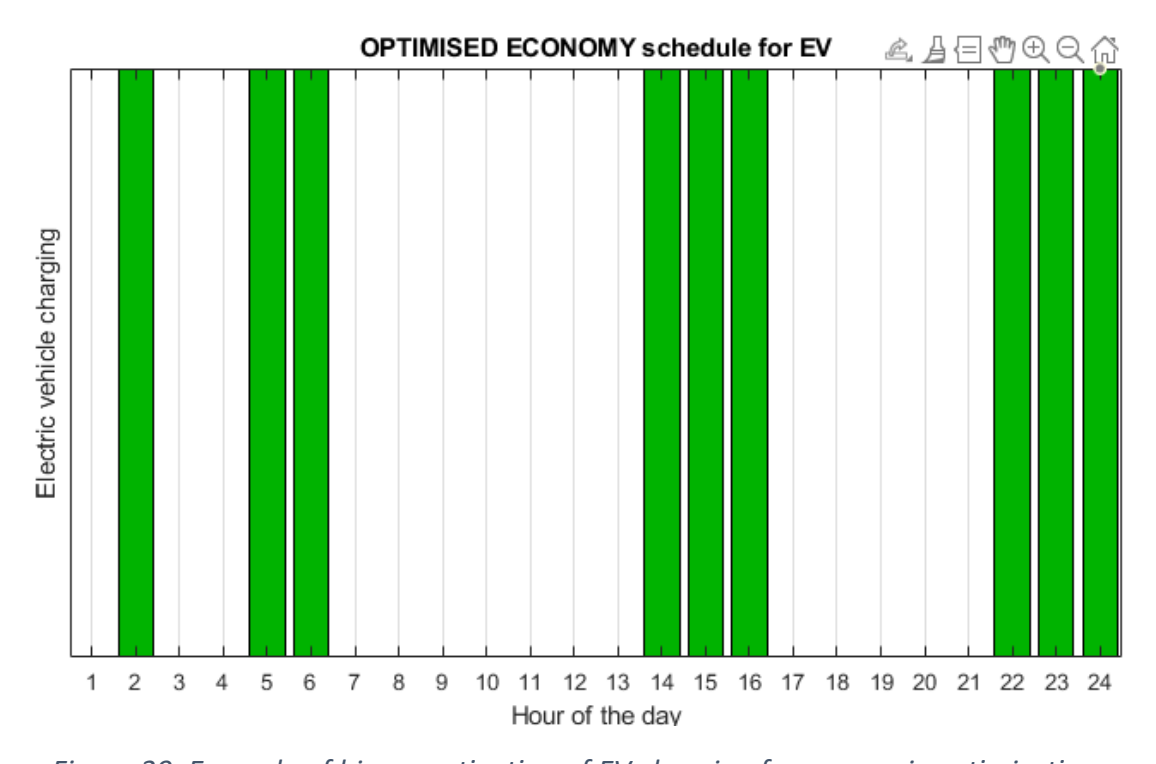


Figure 39. Example of binary activation of EV charging for economic optimization.

8.4 Comparison of results

At the conclusion of the optimizations, a visualization and comparative analysis is executed to evaluate the performance of each optimization strategy. This post-

processing stage is essential for assessing the effectiveness of the proposed solutions and validating the behaviour of all system components—namely, photovoltaic generation, controllable and non-controllable loads, electric vehicle charging, battery storage, and overall economic impact. The energy balance can be shown in Figs. 40-42.

The module begins by displaying the total photovoltaic (PV) energy generated throughout the 24-hour period, in AC, offering a first measure of the renewable potential available for system self-sufficiency. Following this, the total energy consumption is computed for the baseline (non-optimized) scenario, disaggregated into controllable devices, non-controllable loads, HVAC consumption, and the electric vehicle (EV). Then these values are presented in a stacked bar graph that allows the user to understand the relative contributions of each load category across all hours of the day. The stacked bar graphs with the energy consumption can be seen in Figs. 43-45.

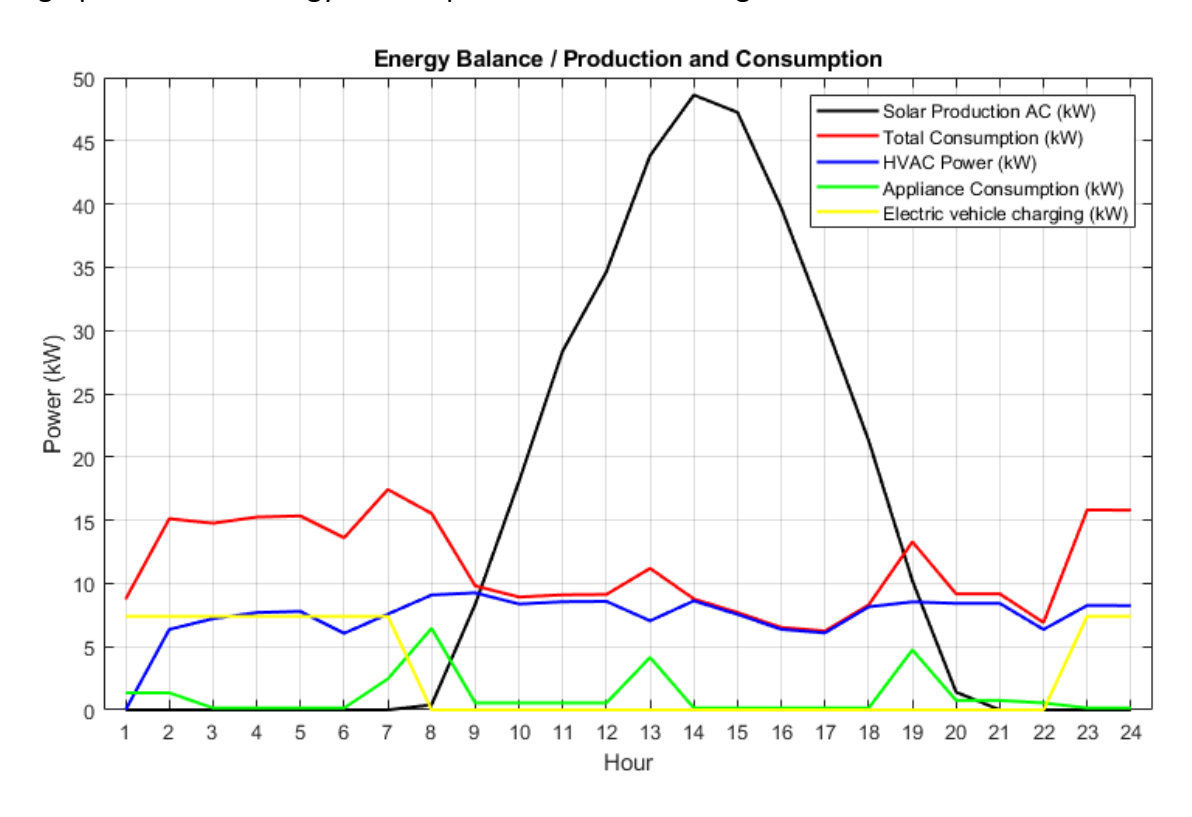


Figure 40. Example of original Energy balance.

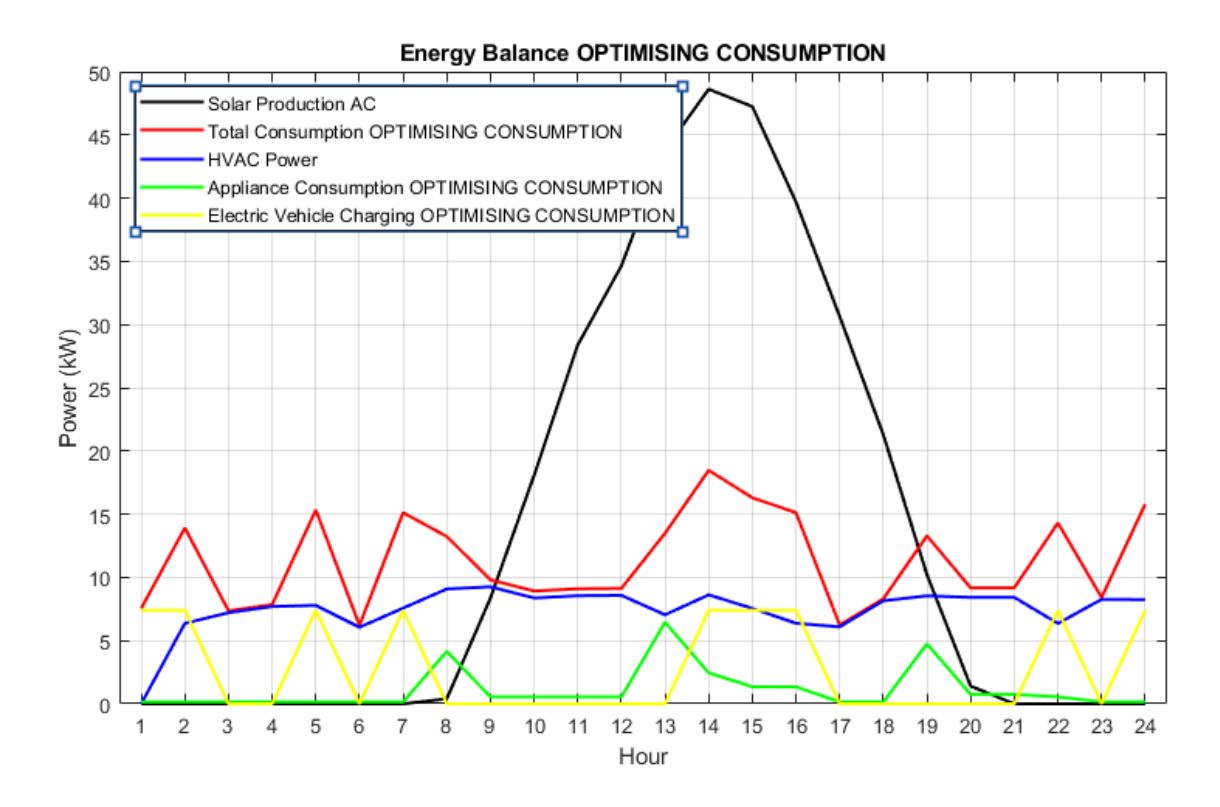


Figure 41.Example plot of energy balance for optimization for minimum consumption.

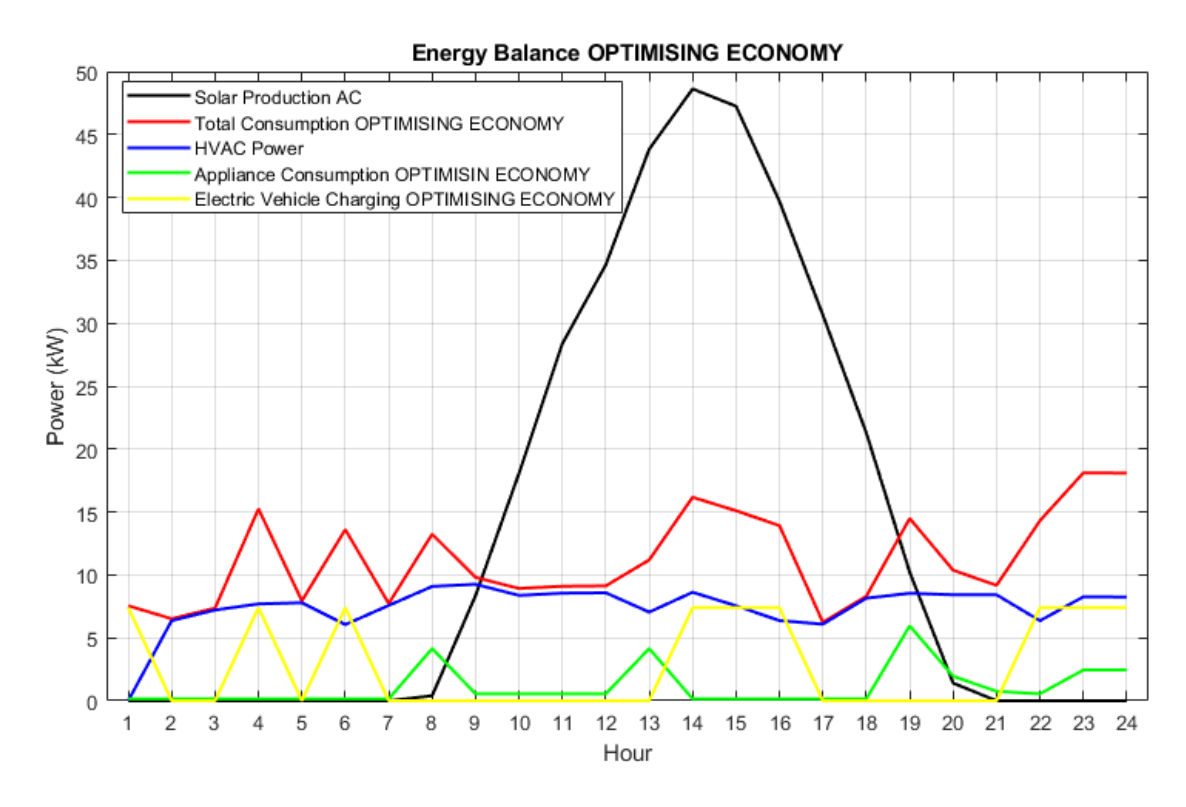


Figure 42. Example plot of energy balance comparison for optimization for maximum net economic benefit.

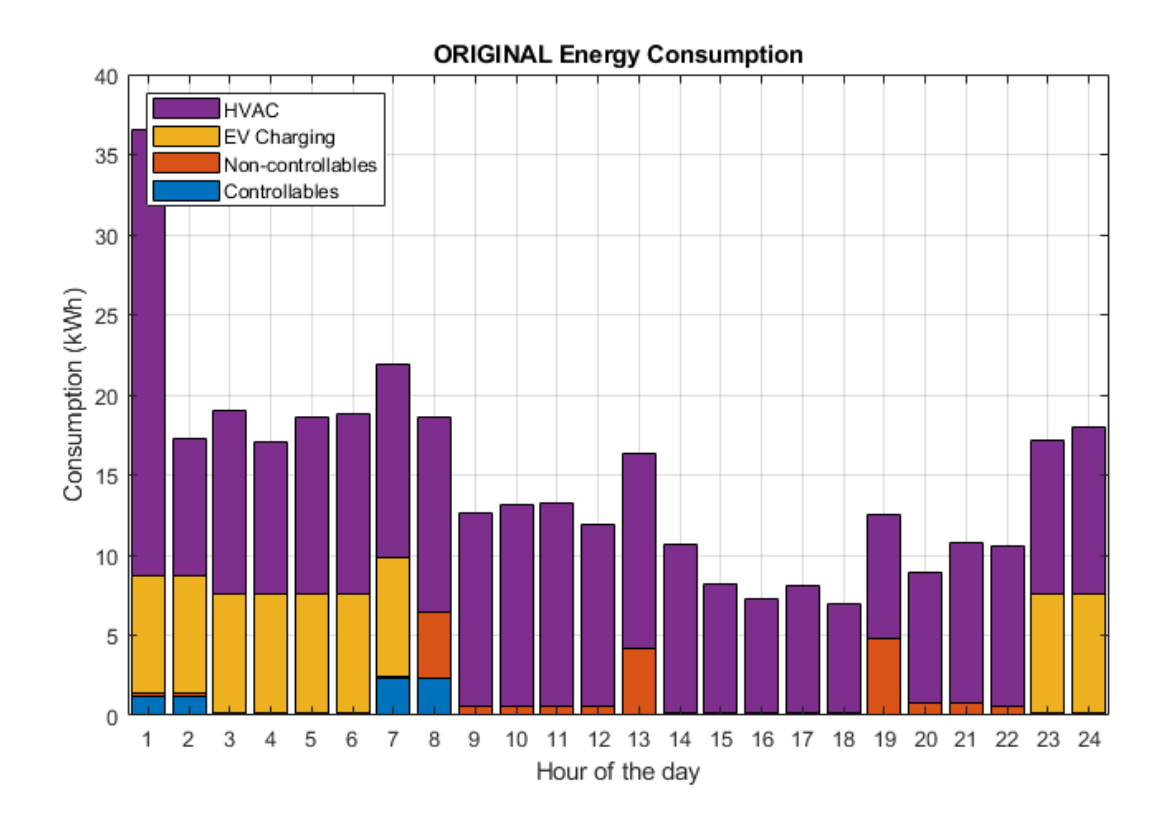


Figure 43. Example plot of original energy consumption.

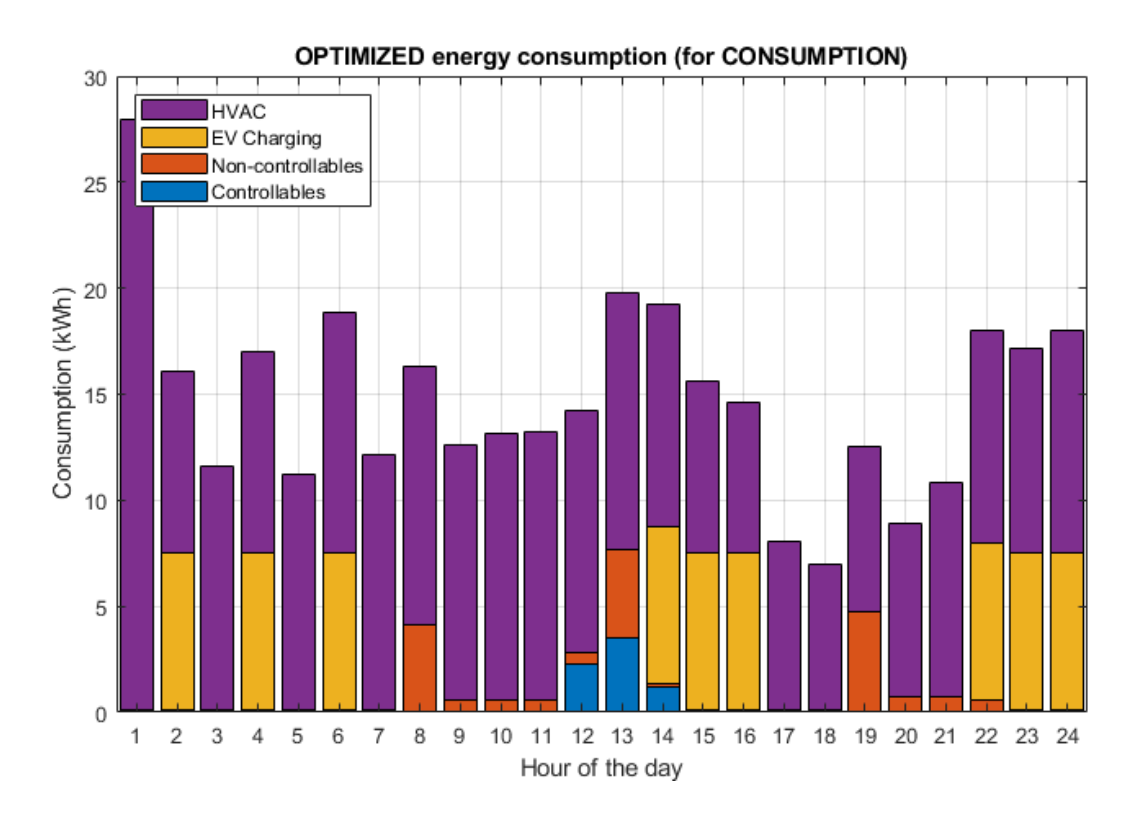


Figure 44. Example plot of energy consumption for optimization for minimum consumption.

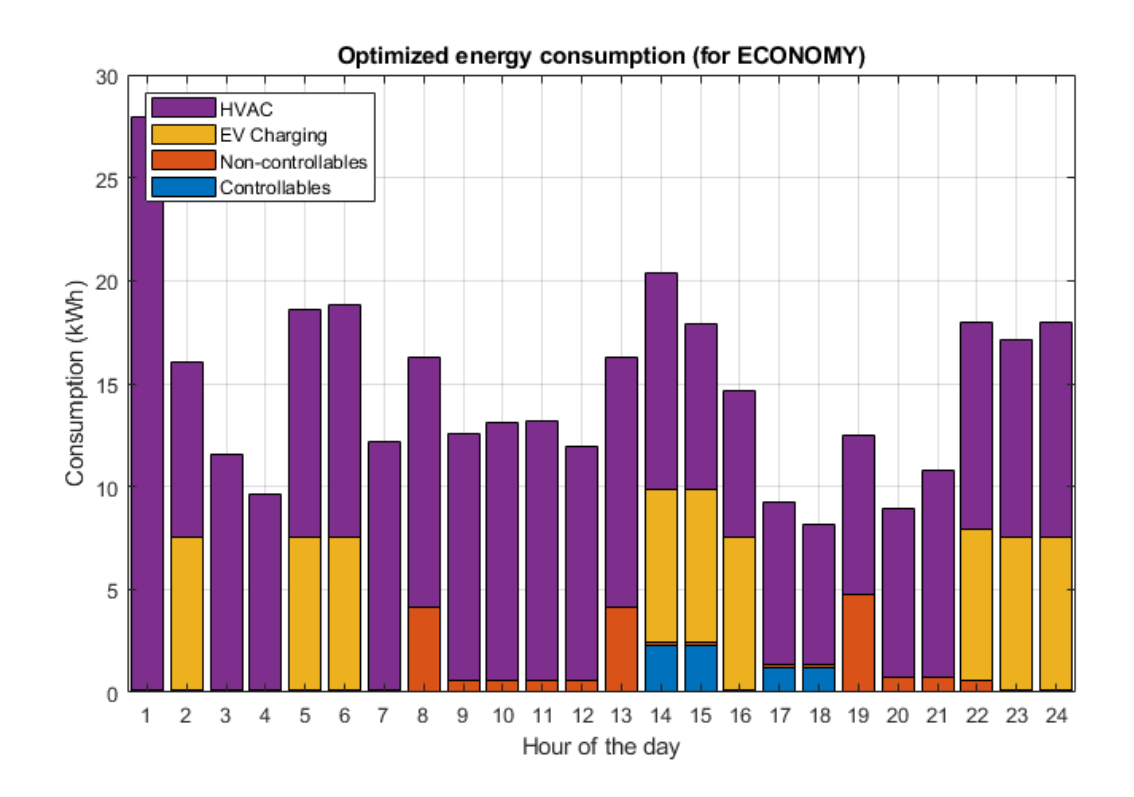


Figure 45. Example plot of energy consumption for optimization for maximum net economic benefit.

A key part of the visualization stage is the comparison of appliance schedules. The original operation plan is contrasted with two optimized scenarios—one focused on minimizing energy deficit (consumption optimization), and another focused on reducing economic costs (economic optimization). This is visualized using binary scheduling matrices, where each row represents a device and each column an hour of the day. These figures make it possible to observe shifts in appliance usage introduced by the optimization algorithms. The different schedules for the appliances are shown in Figs. 46-48.

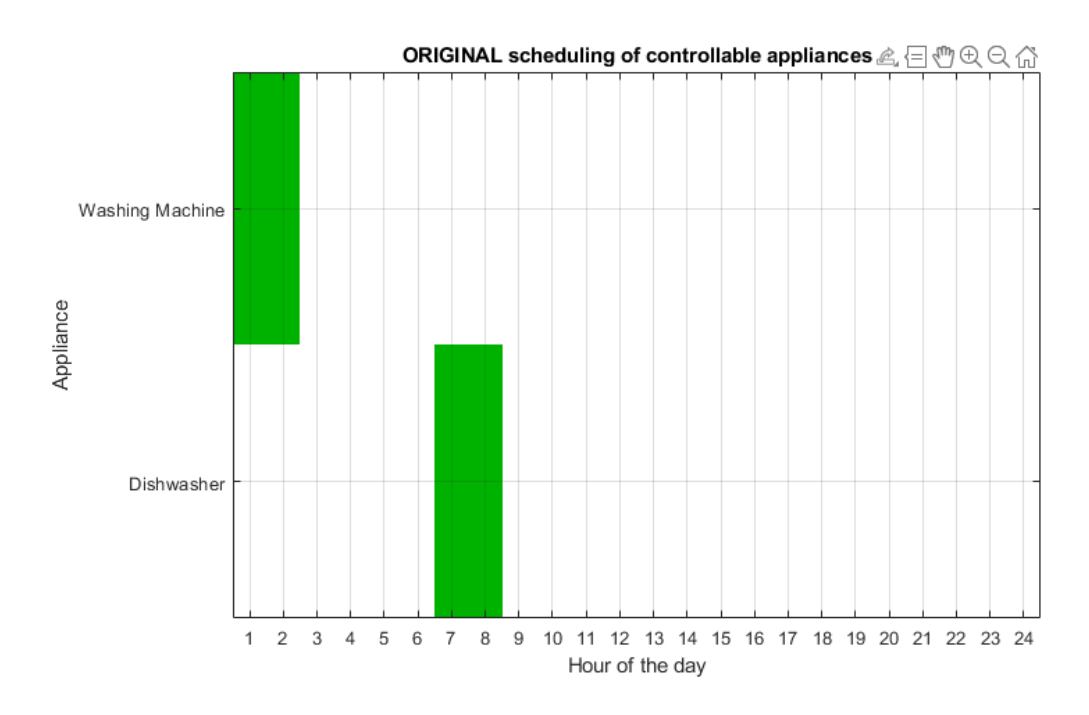


Figure 46. Example of original appliances binary activation.

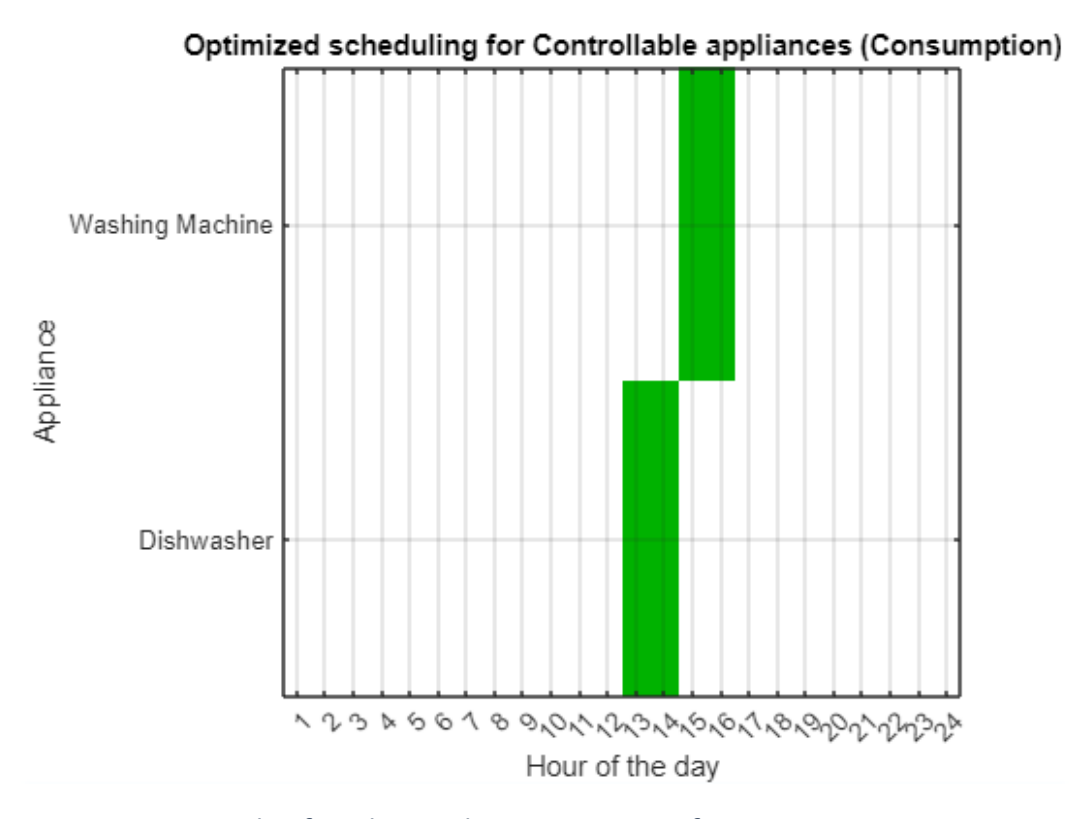


Figure 47. Example of appliances binary activation for minimum energy consumption.

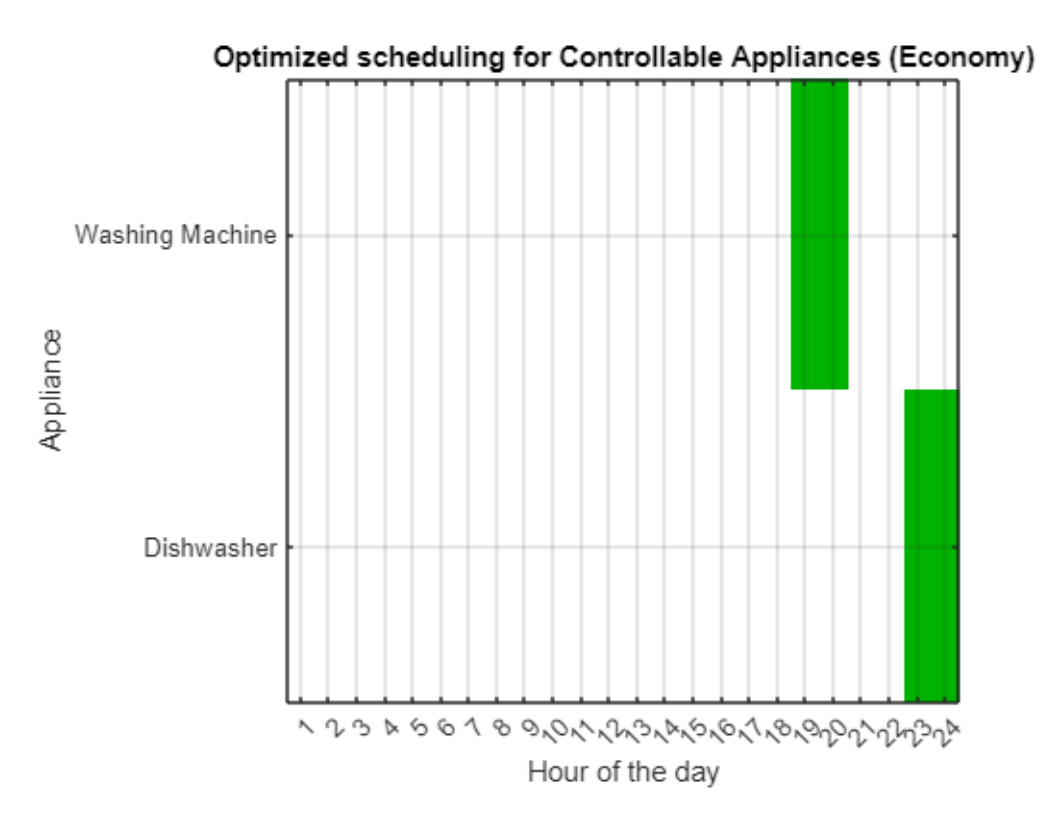


Figure 48. Example of appliance binary activation for maximum net economic benefit.

The energy profiles corresponding to each optimization strategy are then compared sideby-side using a set of stacked bar plots. The Figs. 49-51 display how the overall profiles changes when the appliances and EV charging are rescheduled, enabling a direct comparison between the original system behaviour and that resulting from the application of intelligent scheduling.

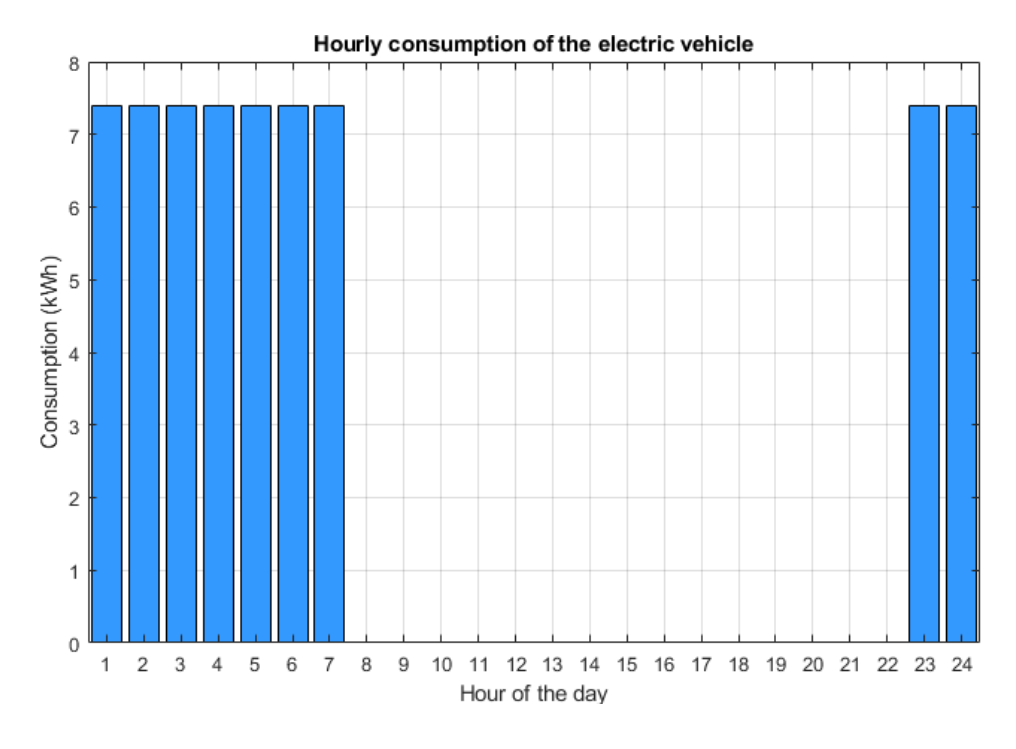


Figure 49. Example of original consumption and schedule of the EV.

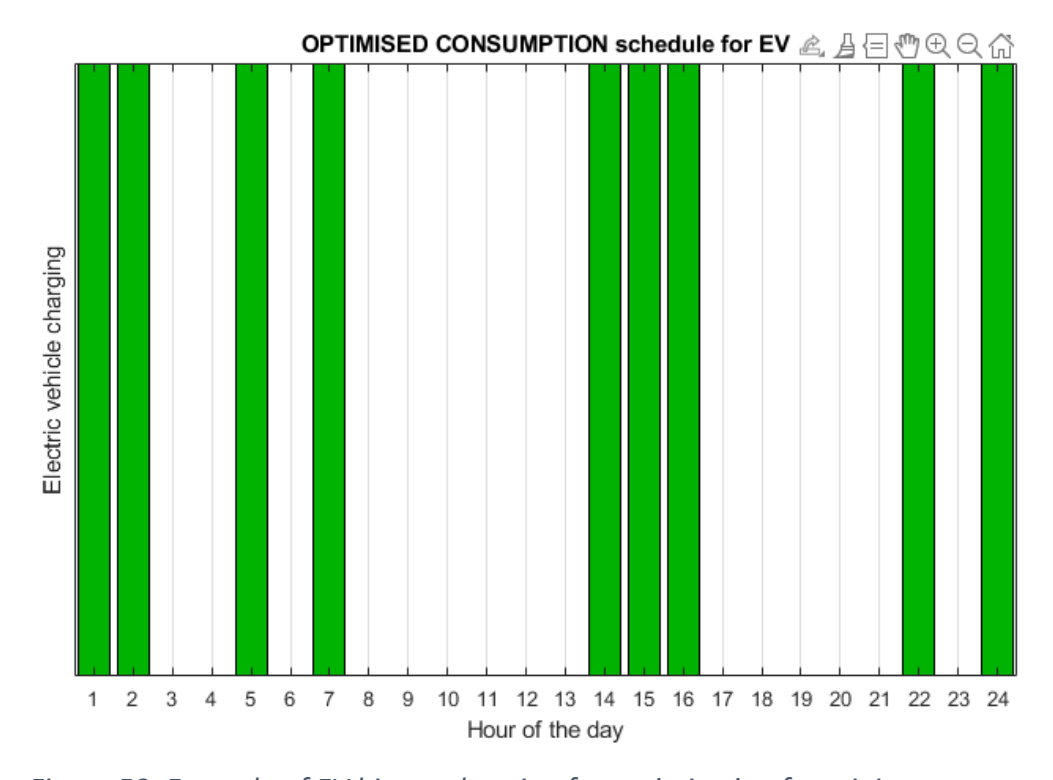


Figure 50. Example of EV binary charging for optimization for minimum energy consumption.

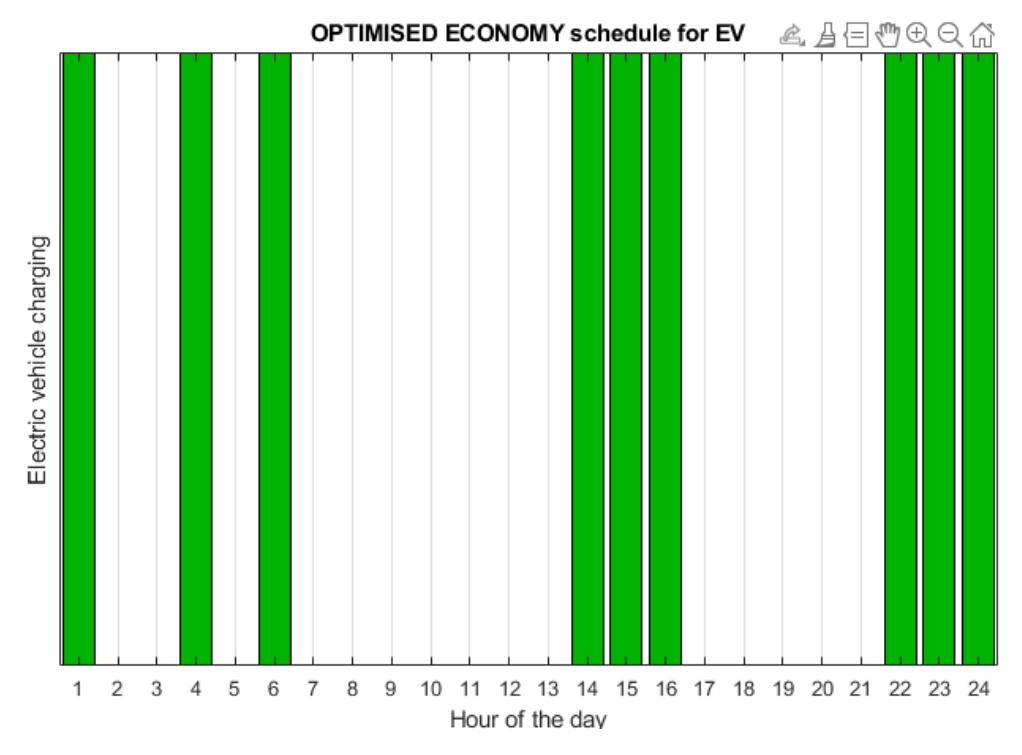


Figure 51. Example of EV binary charging for optimization for maximum net economic benefit.

For the electric vehicle, a dedicated analysis is performed on its state-of-charge (SOC) evolution, number of charging hours, and total energy intake. The optimized charging schedules are validated against user-defined restrictions (such as forbidden hours), and the achievement of the SOC target is verified. Plots of the hourly charging profile and SOC evolution are generated for all three scenarios, along with flags that indicate any violations—such as unmet charging requirements or energy waste due to exceeding the vehicle's storage capacity. The EV SOC comparison can be seen in Fig. 52.

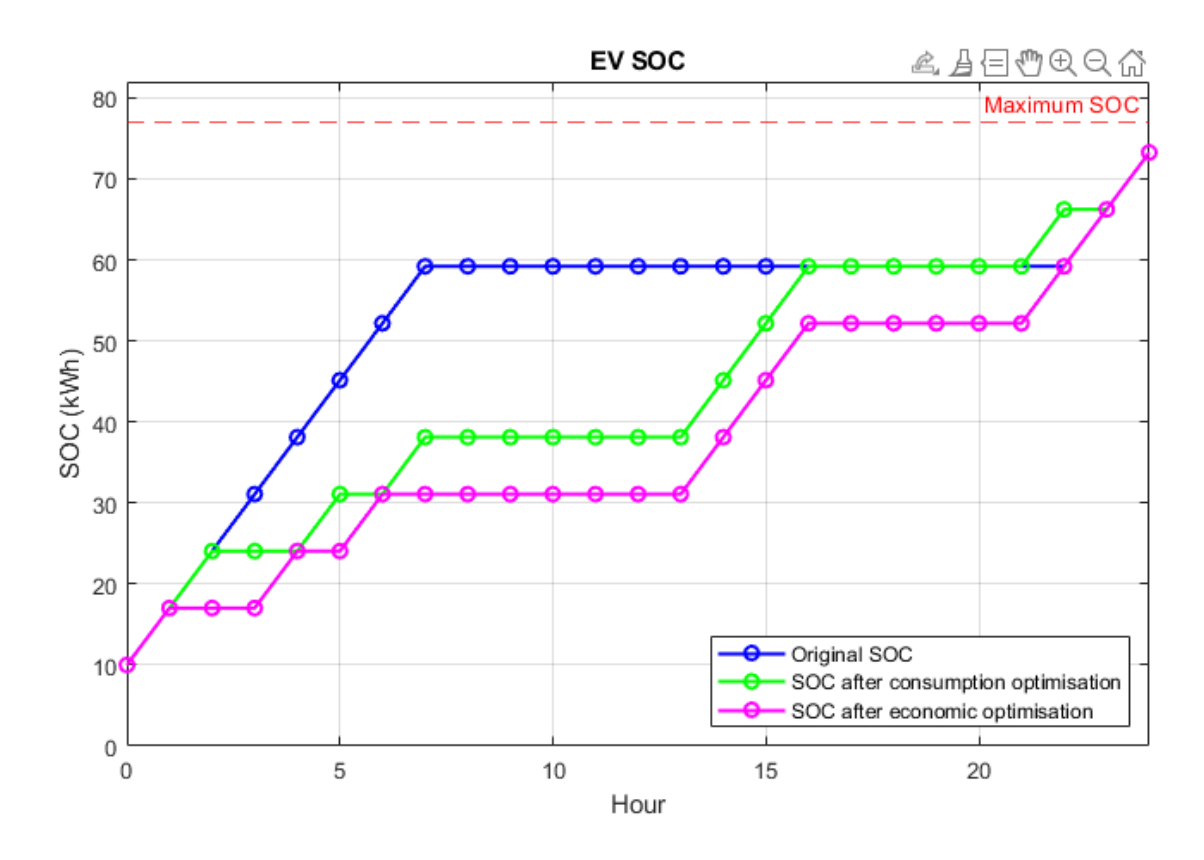


Figure 52. Example of EV SOC comparison.

A similar analysis is performed for the domestic battery. The SOC evolution over 24 hours is plotted, showing the battery's behaviour under each optimization strategy. The figures also report key battery metrics, including the total energy charged and discharged, the initial and final SOC, and the battery utilization range. Reference lines for minimum and maximum allowed SOC levels are included to help assess whether operational limits were respected. The battery SOC comparison is shown in Fig. 53.

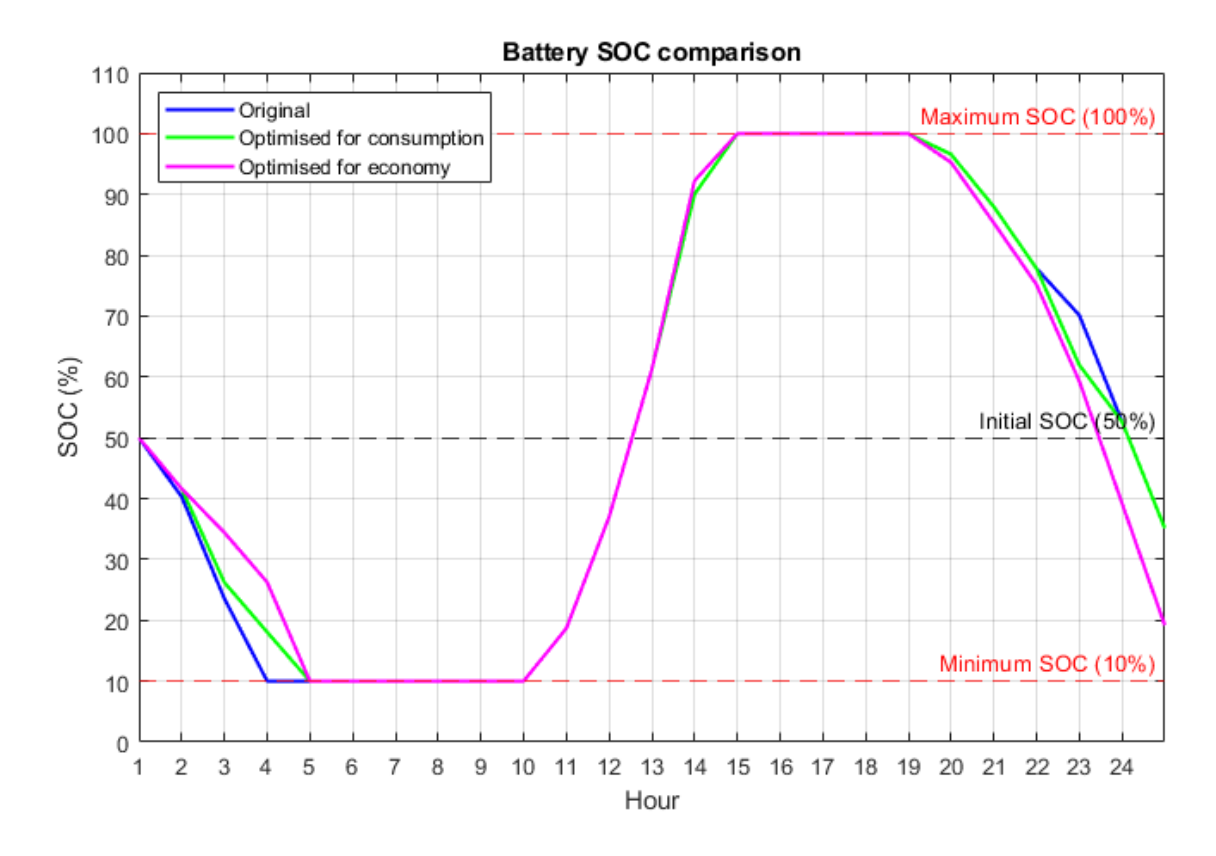


Figure 53. Example of battery SOC comparison.

The economic evaluation follows, comparing net energy costs across the original and optimized scenarios for both weekdays and holidays. This includes the total energy purchased from the grid, energy sold back to it, and the resulting net cost. The economic impact of each optimization strategy is then calculated in absolute and relative terms, quantifying savings in Euros and as a percentage of the original cost. Hourly cost curves are plotted to illustrate the timing and magnitude of expenditures and revenues. Figs. 54-55 show the hourly net cost comparison.

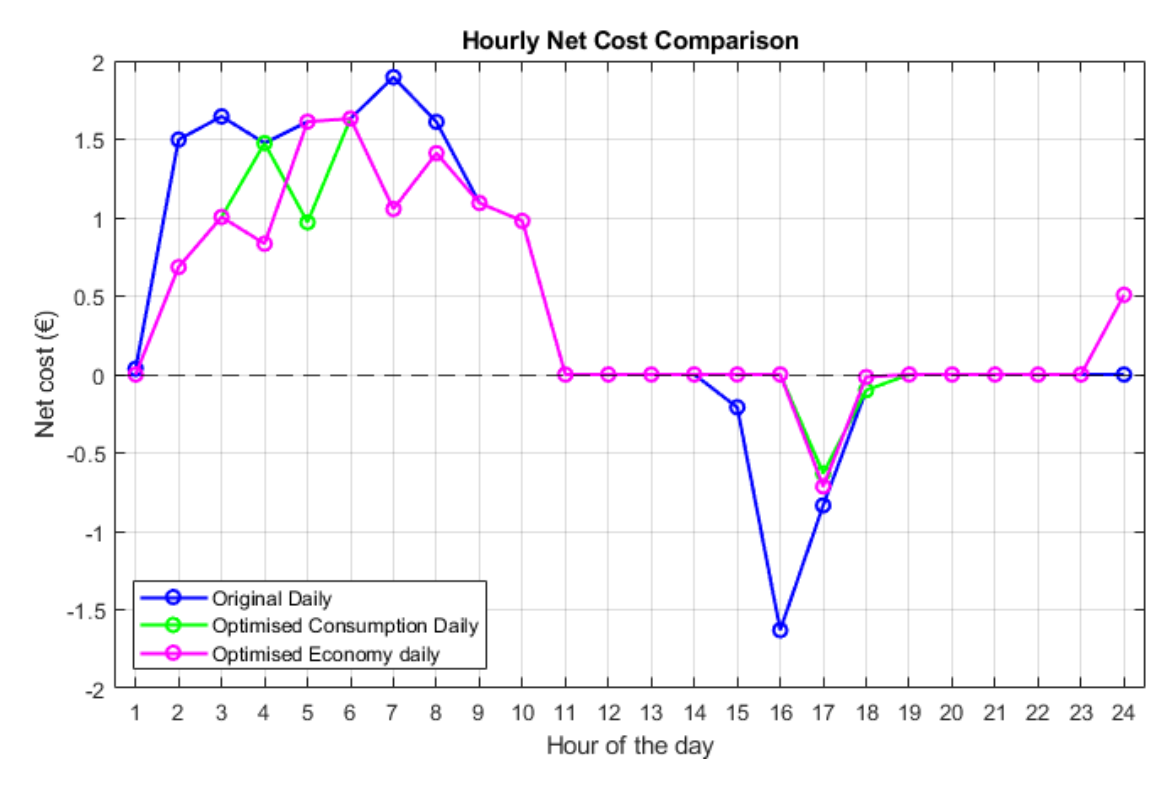


Figure 54. Example of hourly net cost for weekdays comparison.

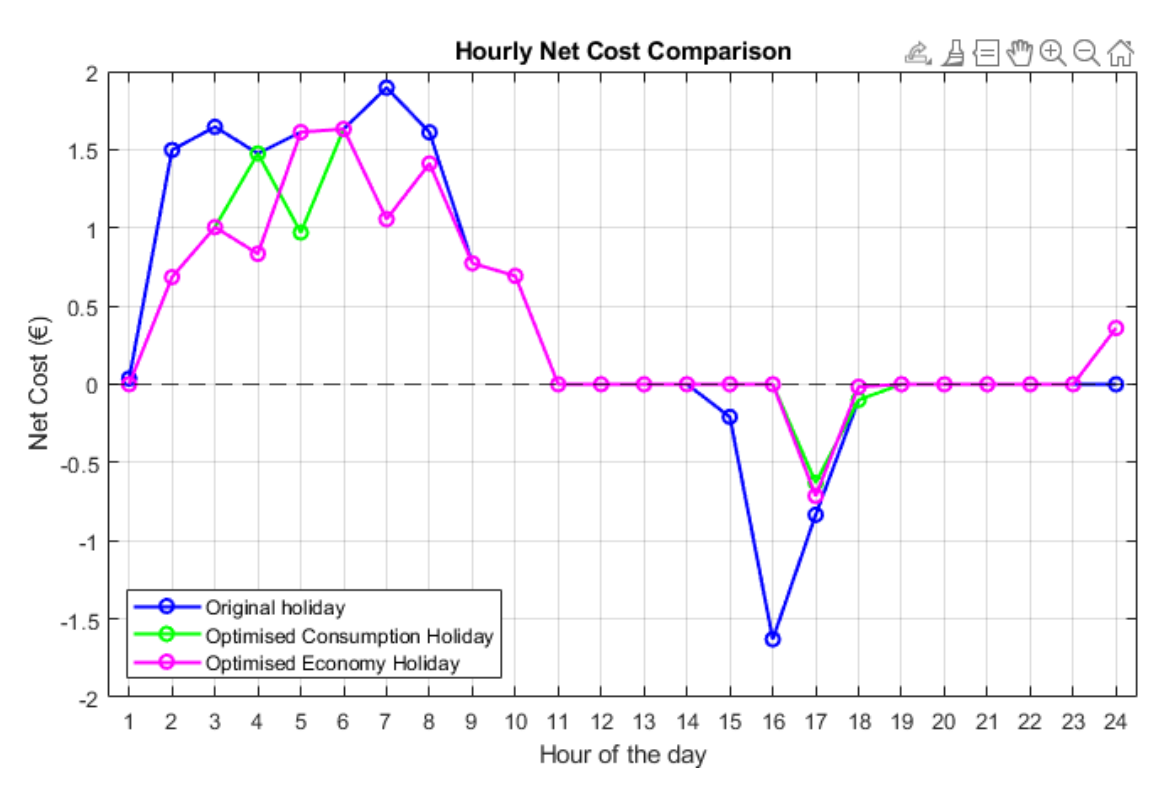


Figure 55. Example of hourly net cost for holidays comparison.

Finally, an energy flow analysis is conducted to examine the dynamics of supply and demand within the system. This includes the use of PV production, battery charge/discharge behaviour, the extent of energy surplus (i.e., unused PV energy), and the residual deficit (i.e., unmet demand from local sources). These are plotted both as time series and as stacked bar charts, providing a clear depiction of how well the system is balanced under each strategy. This step is crucial in confirming that the optimizations do not only shift consumption in time but also make more efficient use of renewable energy and storage assets.

The energy flows can be seen in Figs. 56-58.

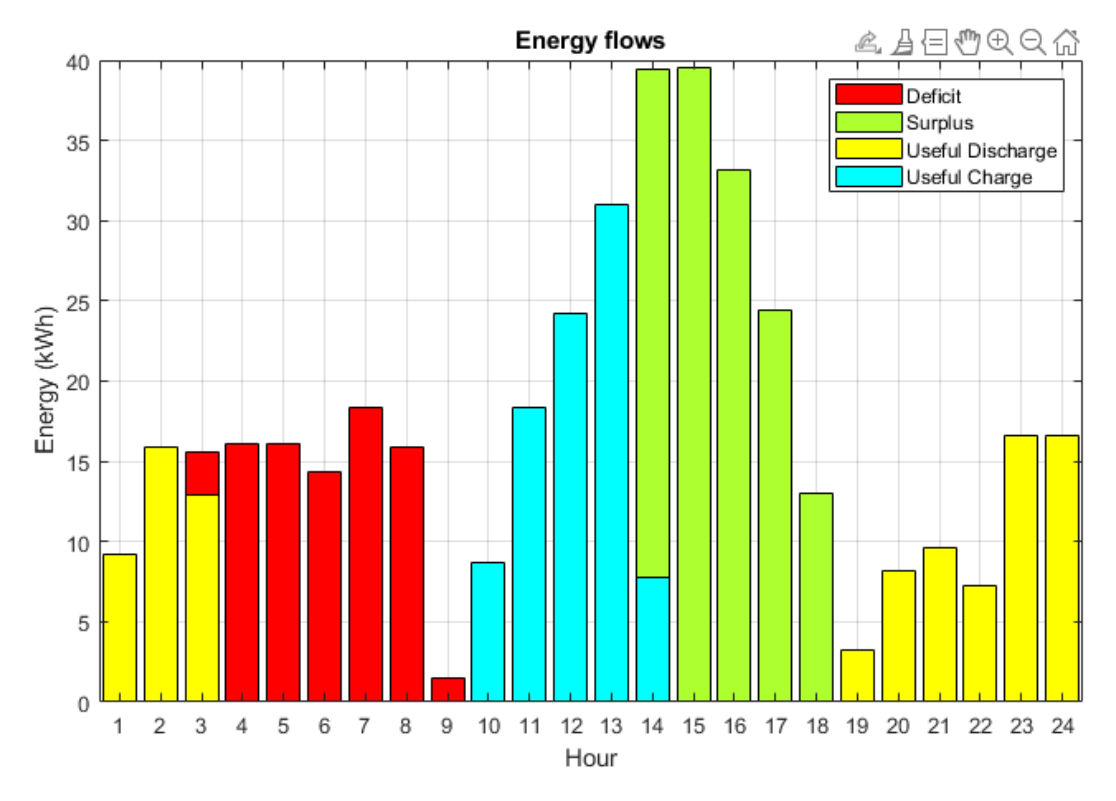


Figure 56. Example of original energy flows.

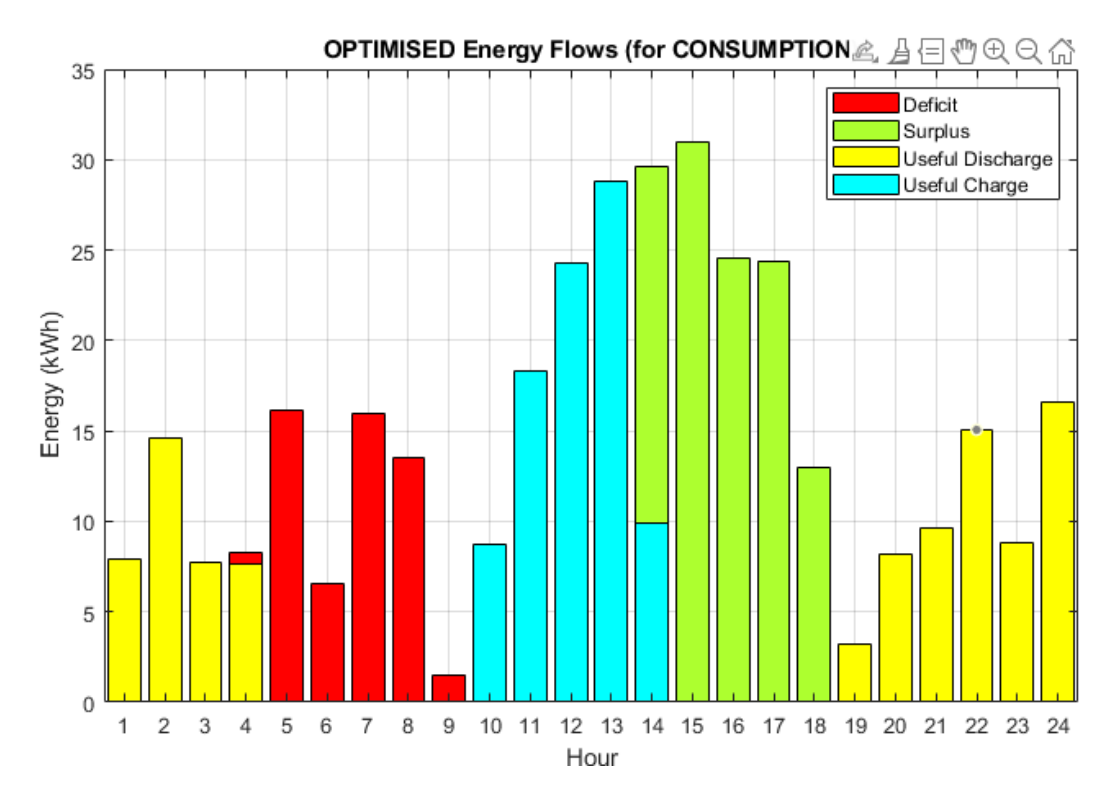


Figure 57. Example of energy flows for optimization for minimum consumption.

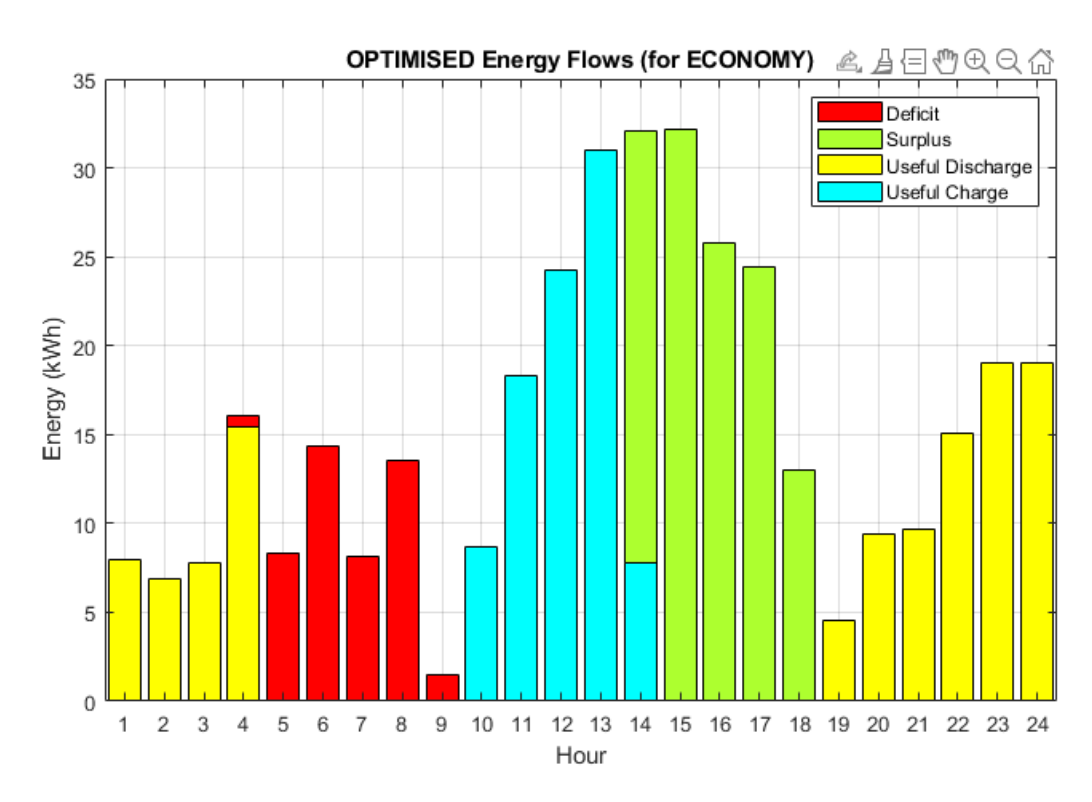


Figure 58. Example of energy flows for optimization for maximum net economic benefit.

This visual and numerical post-analysis module provides a holistic perspective on the effectiveness of the proposed optimization routines. It reveals not only improvements in energy performance but also substantial economic benefits, demonstrating the practical

value of intelligent energy scheduling in residential microgrid systems that include renewables, storage, and electric mobility.

9. Simulink model

The Simulink model is in charge of simulating the thermal behaviour of the building, as well as its interaction with the environment, giving as a result Fig. 61 where the energy consumed by the HVAC is shown as well as Figs. 59-60 where it can be observed how the different temperatures (setpoint, ambient and indoors) evolve and the change of mode between cooling and heating of the system throughout the simulation.

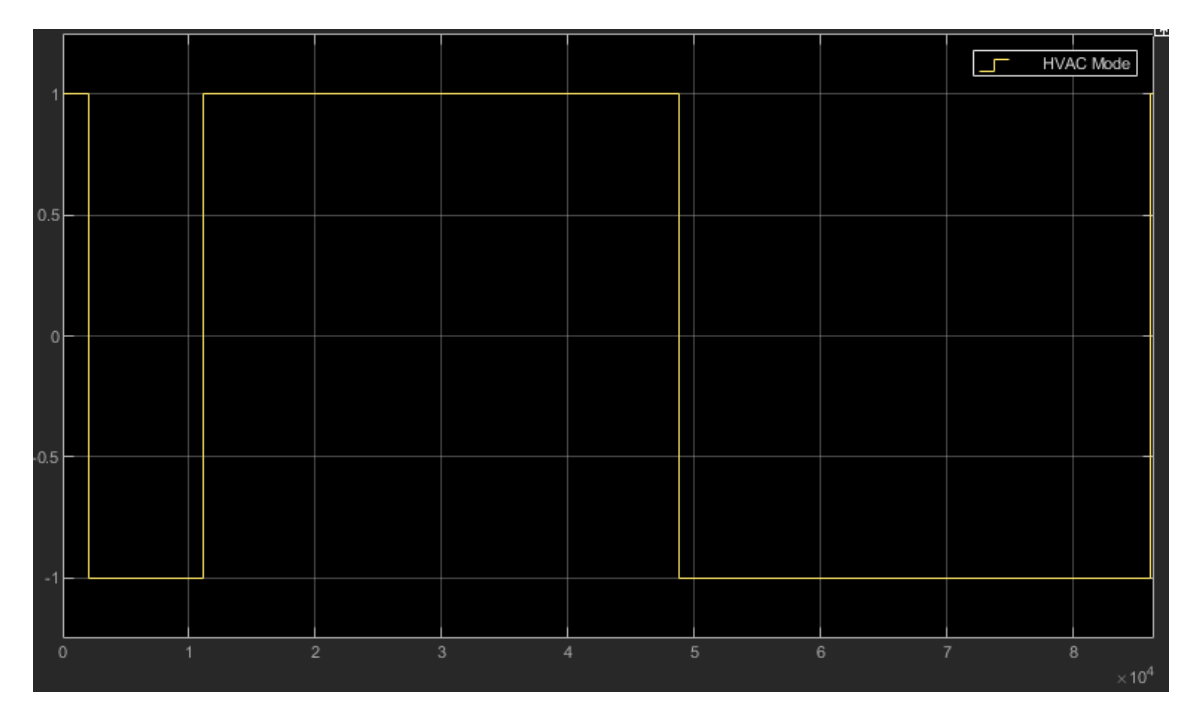


Figure 59. Example plot of HVAC mode switching.

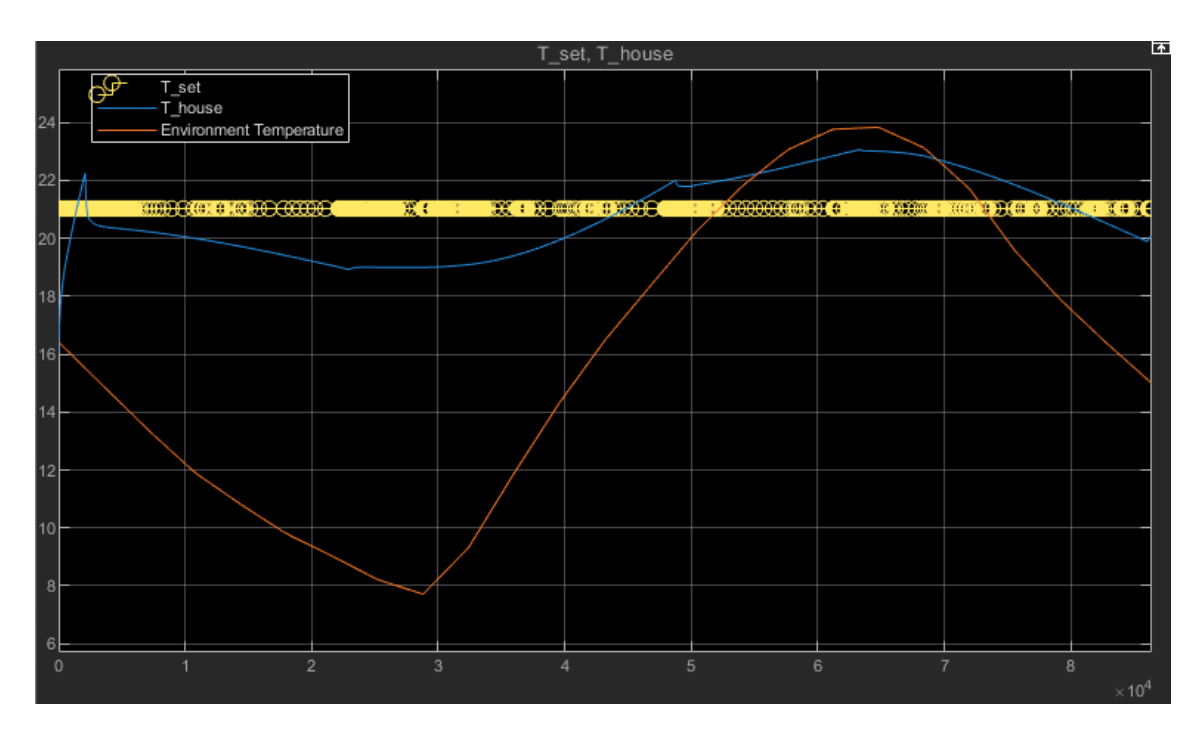


Figure 60. Example plot of setpoint temperature, temperature indoors and ambient temperature.

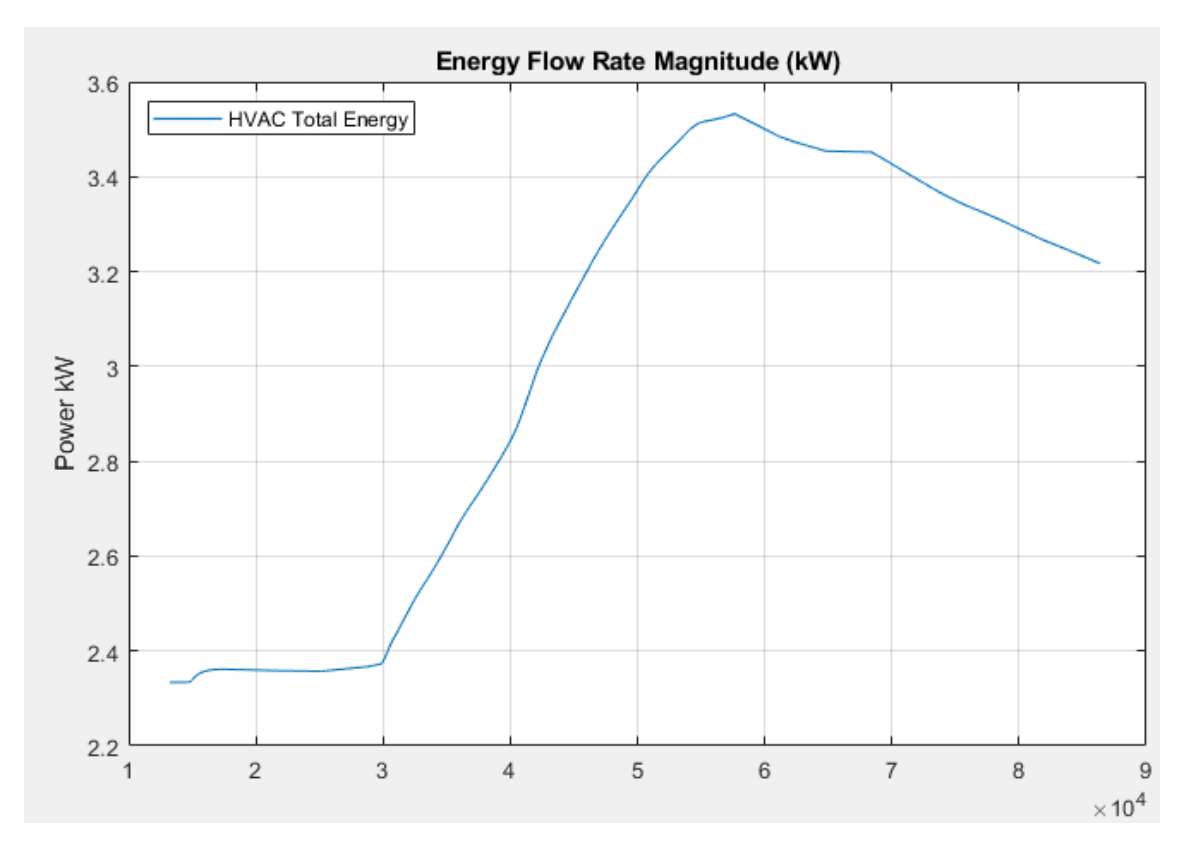


Figure 61. Example plot of HVAC energy consumption.

In order to simulate the model in the different case studies, the input variables to be changed are the ambient temperature, the initial ambient and house temperature levels,

and the target temperature. The model also allows changing other variables such as humidity and temperature gain due to occupancy or appliances; however, these variables will remain constant during the case studies.

Remember that as mentioned before, the HVAC system energy is given by the file associated to the Simulink model and after running both models the HVAC system energy is obtained in a timetable way to be able to use it in the main MATLAB code. However, since this value is not on an hourly basis, it is necessary to integrate the energy variable over each hour of the day in order to obtain the energy on an hourly basis, which is the required format.

The Simulink model which simulates the thermal behaviour of the building is shown in Fig. 62. This model was taken from MATLABWorks, 2025, and some modifications were made to adapt it to the needs of this diploma thesis.

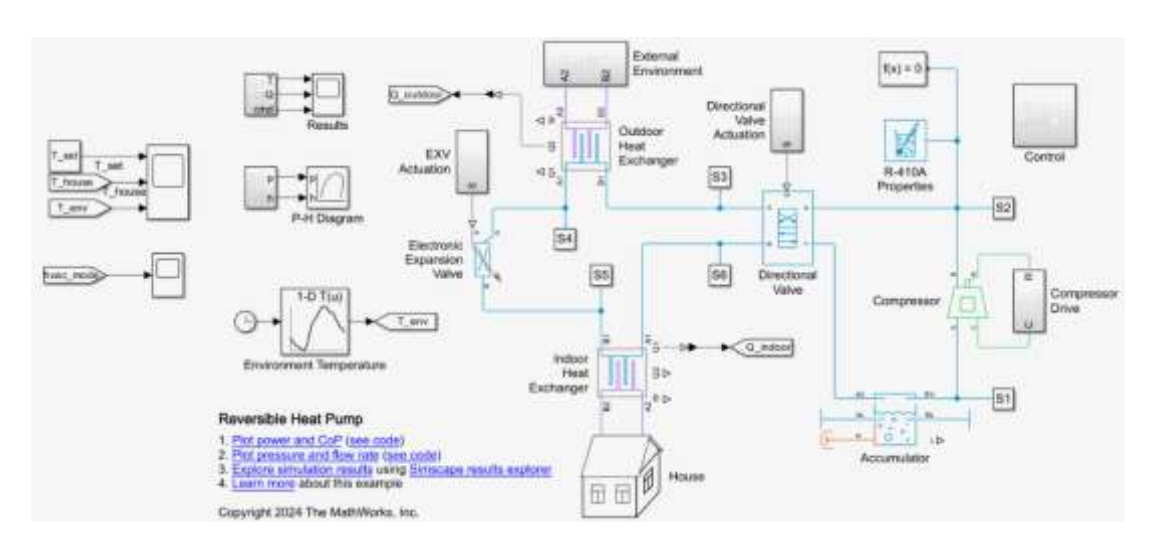


Figure 62. Simulink Reversible heat pump model. Source: (MATLABWorks, 2025).

9.1 System Architecture and Overview

The Simulink model represents a comprehensive reversible heat pump system designed for residential climate control applications. This system operates on the vapor compression refrigeration cycle using R-410A refrigerant, which is evident from the dedicated R-410A Properties block integrated into the model. The heat pump is classified as "reversible" because it can operate in both heating and cooling modes by reversing the direction of refrigerant flow through the system, allowing it to either extract heat

from the outdoor environment to warm the indoor space or remove heat from the indoor space to cool it.

The model architecture follows a closed-loop control strategy where the system continuously monitors environmental conditions and adjusts its operation to maintain the desired indoor temperature. The control system receives three primary temperature inputs: the temperature setpoint (T_set), the current house temperature (T_house), and the external environment temperature (T_env). These inputs are processed through a control algorithm that determines the optimal operating parameters for the various system components.

9.1.1 House block

The internal structure of the house block is shown in Fig. 63.

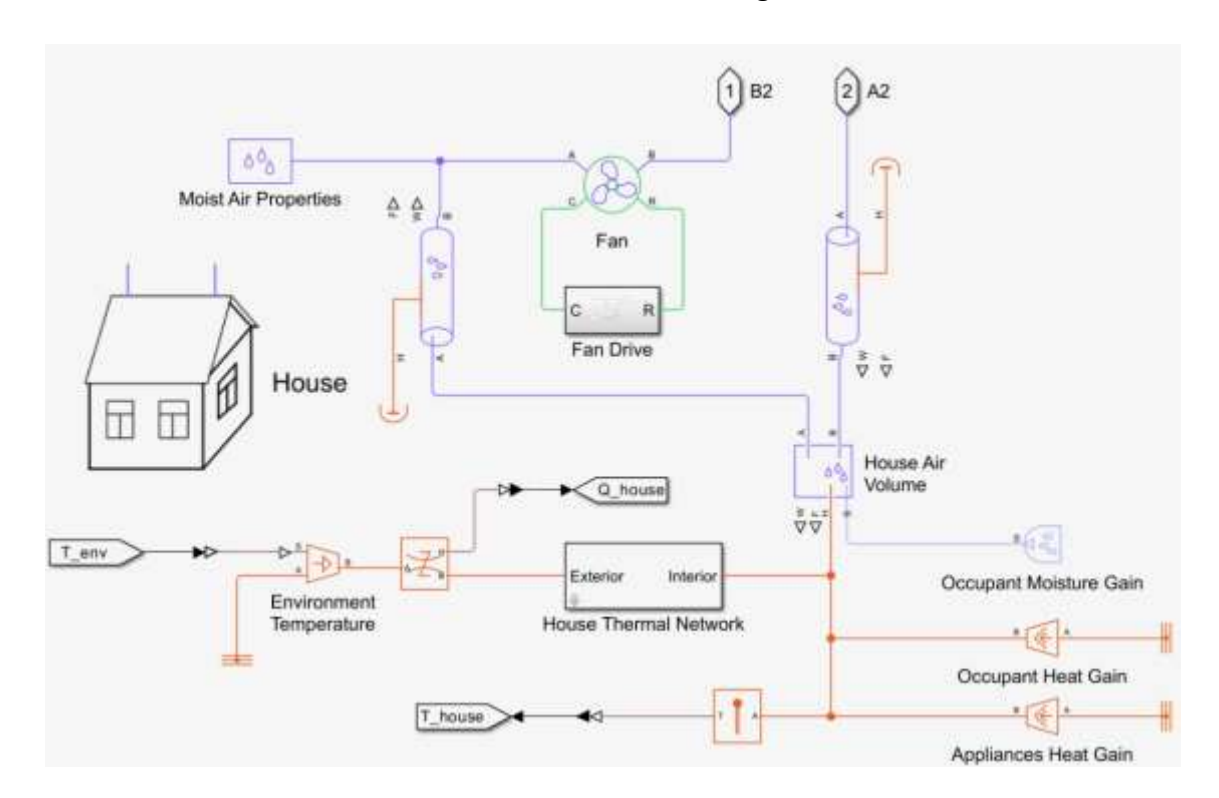


Figure 63. Simulink house block.

The building thermal model represents a comprehensive simulation of the indoor environment and its thermal dynamics, incorporating multiple heat sources and environmental factors that influence the overall thermal load. This subsystem is critical

for accurately predicting the heat pump's performance and energy consumption under realistic operating conditions. The model accounts for the complex thermal interactions between the building envelope, occupants, appliances, and external weather conditions.

The House Thermal Network forms the core of the building model, implementing a thermal network approach that represents the building's thermal mass, insulation properties, and heat transfer characteristics. This network models the heat flow between the exterior and interior environments, considering factors such as wall thermal resistance, window properties, and infiltration rates. The thermal network receives inputs from the Environment Temperature block and provides the house temperature (T_house) as feedback to the control system.

The thermal characteristics of the roof are shown in Table 2.

Table 2. Thermal Characteristics of the roof.

	Roof
Total area (m ²)	261
Thickness (m)	0.2
Density (kg/m³)	32
Specific heat (J/kg K)	835
Conductivity (W/m K)	0.038
Interior heat transfer coefficient (W/ m ² K)	12
Exterior heat transfer coefficient (W/ m ² K)	38

It can be seen in the variable that the house is big, 1200m³ (20x10x6m), so that is making the consumption high, however having this much space allow us to build a surface of solar panels enough to cover the consumption, because the power consumption is large.

The thermal characteristics of the exterior walls, interior walls and windows are shown in Tables 3-5 respectively.

Table 3. Thermal characteristics of the exterior walls.

	Exterior walls
Total area (m ²)	360
Thickness (m)	0.2
Density (kg/m³)	1920
Specific heat (J/kg K)	835
Conductivity (W/m K)	0.038
Interior heat transfer coefficient (W/ m ² K)	24
Exterior heat transfer coefficient (W/ m ² K)	34

The interior walls refer to interior partitions' walls inside the building, that's why there is only an interior heat transfer coefficient.

Table 4. Thermal characteristics of the interior walls.

	Interior walls
Total area (m²)	640
Thickness (m)	0.15
Density (kg/m³)	10
Specific heat (J/kg K)	1000
Conductivity (W/m K)	0.2
Interior heat transfer coefficient (W/ m ² K)	24

Table 5. Thermal characteristics of the windows.

	Windows
Total area (m²)	12
Thickness (m)	0.01
Density (kg/m³)	277
Specific heat (J/kg K)	840
Conductivity (W/m K)	0.78
Interior heat transfer coefficient (W/ m ² K)	25

Exterior heat transfer coefficient (W/ m ² K)	32
--	----

The building model includes detailed representation of internal heat gains from three primary sources: occupant heat gain, appliances heat gain, and occupant moisture gain. The occupant heat gain component models the sensible heat generated by five occupants in the building, accounting for their metabolic heat production which varies based on activity levels and time of day. This heat source represents a significant portion of the internal thermal load and must be accurately modelled to predict the building's cooling requirements, particularly during summer months when occupant heat gain contributes to the overall cooling load. For this case of study, the occupants heat gain is 5 p * 70 W/p = 350 W and moisture gain is 5 p * 0.04 g/p s = 0.2 g/s.

The appliances heat gain block simulates the thermal contribution from various electrical and electronic devices within the building, including lighting, computers, kitchen appliances, and other household equipment. This component is essential for realistic thermal load calculations as appliances can contribute substantial heat gains that affect the HVAC system's operation. The heat gain from appliances typically follows daily usage patterns and varies seasonally based on occupant behaviour and equipment utilization. For this case the appliances heat gain is 500 W.

The moisture dynamics within the building are captured through the occupant moisture gain component and the moist air properties block. The occupant moisture's gain models the water vapor production from the five occupants through respiration and perspiration, which affects the indoor humidity levels. The House Air Volume block represents the building's internal air mass and its thermal and moisture storage capacity. The moist air properties component calculates the thermodynamic properties of the indoor air, including humidity ratio, enthalpy, and density, which are essential for accurate HVAC system modelling and energy calculations.

The fan and fan drive components within the building model represent the air circulation system that distributes conditioned air throughout the indoor space. The fan system is crucial for maintaining uniform temperature distribution and ensuring effective heat transfer between the HVAC system and the building's thermal mass. The fan drive controls the air circulation rate based on system requirements and operating conditions,

with the ability to modulate airflow to optimize comfort and energy efficiency. The fan operation is coordinated with the heat pump system to ensure proper air circulation during both heating and cooling modes, maintaining consistent indoor environmental conditions throughout the building.

9.2 Control System Architecture and Logic

The control system architecture and logic blocks are shown in Fig. 64.

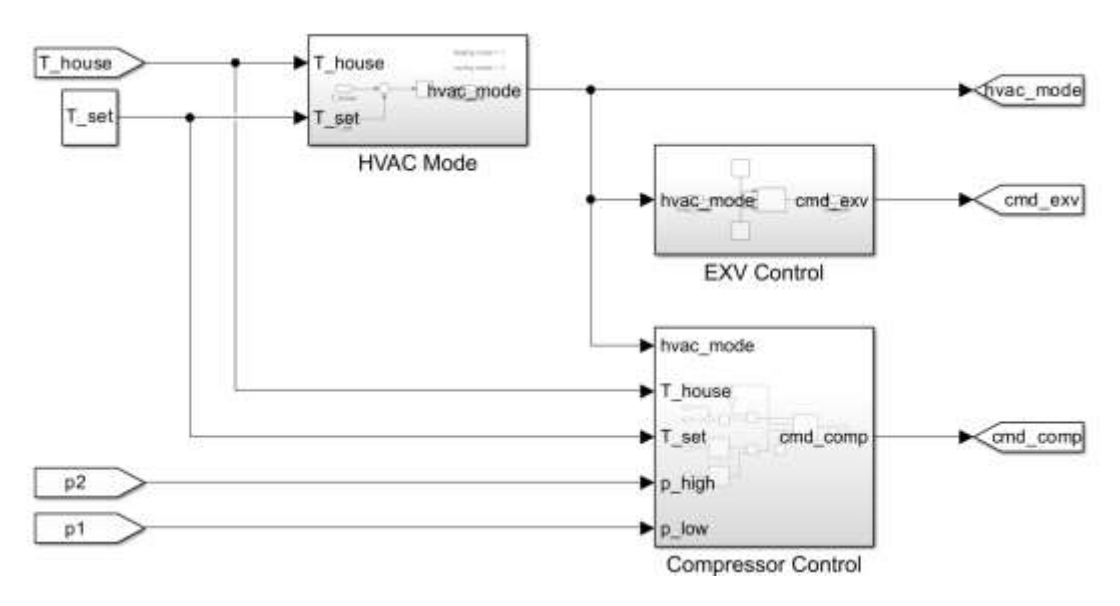


Figure 64. Simulink system architecture and logic blocks.

The control system for this reversible heat pump model implements a hierarchical control architecture consisting of three primary control blocks: HVAC Mode determination, EXV (Electronic Expansion Valve) Control, and Compressor Control. This multi-layered approach enables sophisticated system management by separating high-level operational decisions from component-specific control algorithms.

9.2.1 HVAC mode block

The HVAC mode block selection is shown in Fig. 65.

heating mode = 1

cooling mode = -1

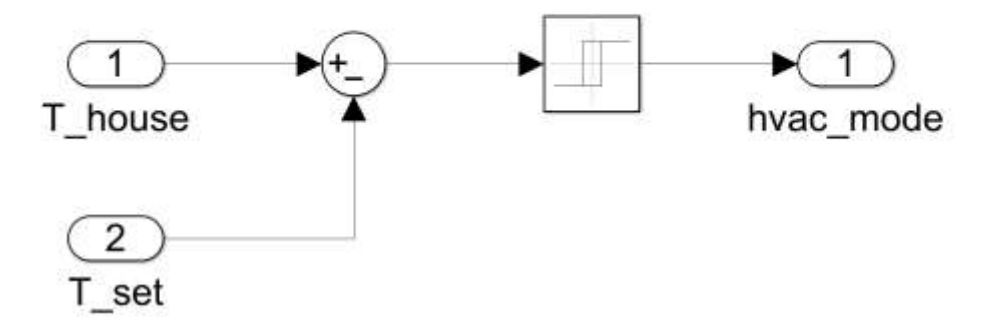


Figure 65. Simulink HVAC mode block.

The HVAC Mode block serves as the master controller that determines the fundamental operating mode of the system based on the temperature setpoint (T_set) and the current house temperature (T_house). This block implements the decision logic that compares the actual indoor temperature with the desired setpoint to determine whether the system should operate in heating mode (hvac_mode = 1) or cooling mode (hvac_mode = -1). The mode determination is critical because it affects the operation of all downstream components, including valve positioning, compressor operation, and heat exchanger roles. The block incorporates hysteresis control to prevent frequent mode switching when the house temperature oscillates around the setpoint, which would otherwise cause system instability and reduced efficiency.

9.2.2 EXV Control block

The EXV control block is shown in Fig. 66.

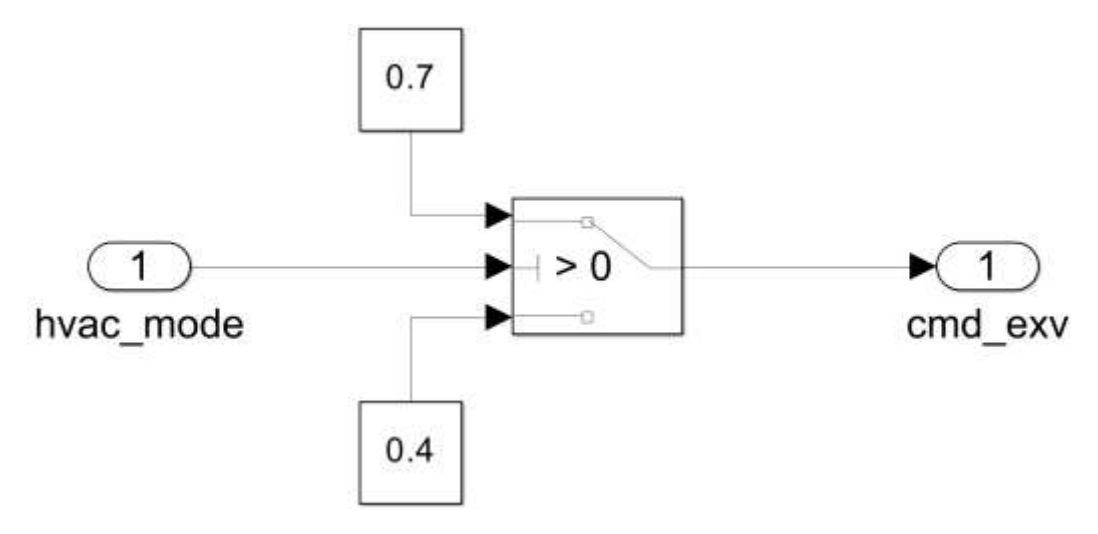


Figure 66. Simulink EXV Control block.

The EXV Control block receives the HVAC mode signal and generates appropriate command signals (cmd_exv) for the electronic expansion valve. This control block manages the refrigerant flow rate and superheat control by modulating the valve opening based on the operating mode and system conditions. In heating mode, the expansion valve controls the refrigerant flow entering the outdoor heat exchanger (acting as evaporator), while in cooling mode, it controls flow to the indoor heat exchanger (acting as evaporator). Precise control of refrigerant flow is essential for maintaining optimal superheat levels, which directly impacts system efficiency and component protection.

9.2.3 The compressor control block

The compressor control block is displayed in Fig. 67.

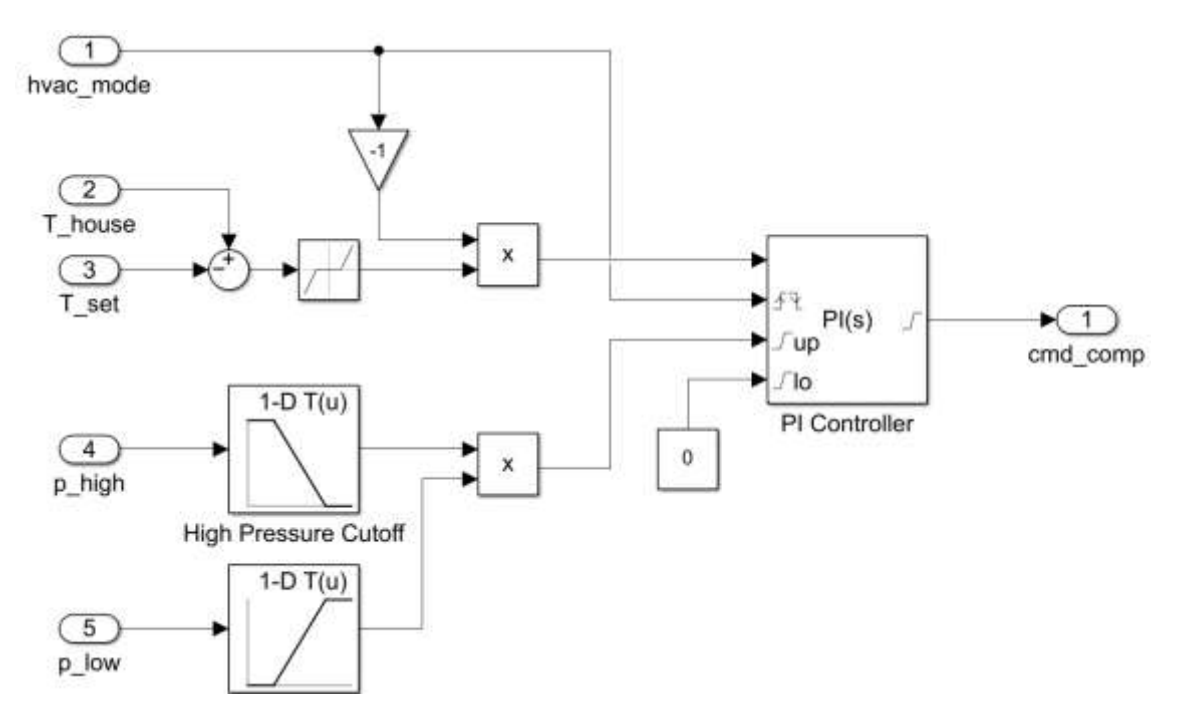


Figure 67. Simulink Compressor control block.

The Compressor Control block represents the most complex control subsystem, incorporating multiple feedback signals including the HVAC mode, house temperature (T_house), temperature setpoint (T_set), high-side pressure (p_high), and low-side pressure (p_low). This comprehensive input set enables the controller to implement sophisticated control strategies such as capacity modulation, pressure ratio optimization, and protective shutdown procedures. The compressor control algorithm generates the cmd_comp signal that regulates compressor speed or cycling to match the system capacity with the thermal load while maintaining safe operating pressures and temperatures, making for example the compressor works only in the temperatures inside the dead band (setpoint ± dead band).

9.3 Heat Exchanger Subsystems

The model incorporates two primary heat exchangers that form the core of the heat pump's thermal management system. The outdoor heat exchanger serves as the interface between the refrigerant circuit and the external environment, facilitating heat transfer with the ambient air. This component's performance is heavily influenced by outdoor conditions, including temperature, humidity, and air flow rates. The heat exchanger's effectiveness directly impacts the system's overall coefficient of

performance (CoP) and determines how efficiently the system can extract or reject heat to the environment.

The indoor heat exchanger operates as the terminal unit within the conditioned space, transferring heat between the refrigerant and the indoor air. This component is responsible for delivering the heating or cooling effect to maintain the desired indoor temperature. The heat transfer rate and capacity of this exchanger are critical parameters that determine the system's ability to meet the thermal load requirements of the building. Both heat exchangers are modelled with appropriate thermal dynamics to capture the transient behaviour of heat transfer processes.

9.4 Refrigerant Circuit and Flow Control

The refrigerant circuit forms the backbone of the heat pump system, with R-410A serving as the working fluid. This refrigerant was chosen for its favourable thermodynamic properties and environmental characteristics. The circuit includes several critical flow control components that regulate refrigerant movement and system operation. The Electronic Expansion Valve (EXV) plays a crucial role in controlling the refrigerant flow rate and creating the necessary pressure drop between the high and low-pressure sides of the system. This valve's modulation directly affects the system's capacity and efficiency by controlling the amount of refrigerant entering the evaporator.

The directional valves in the system enable the reversible operation characteristic of heat pumps. These valves can redirect refrigerant flow to switch between heating and cooling modes without requiring physical reconfiguration of the system. In heating mode, the indoor heat exchanger operates as the condenser while the outdoor unit functions as the evaporator. In cooling mode, these roles are reversed. The seamless transition between these modes is accomplished through precise control of the directional valves based on the system's operational requirements.

9.5 Compressor System and Mechanical Components

The compressor represents the heart of the heat pump system, providing the mechanical energy necessary to circulate the refrigerant and maintain the pressure differential

required for effective heat transfer. The model includes both the compressor unit and its associated drive system, which controls the compressor's operation based on system demands. The compressor's performance characteristics, that influence the overall system performance and energy consumption are displayed in Fig. 68.

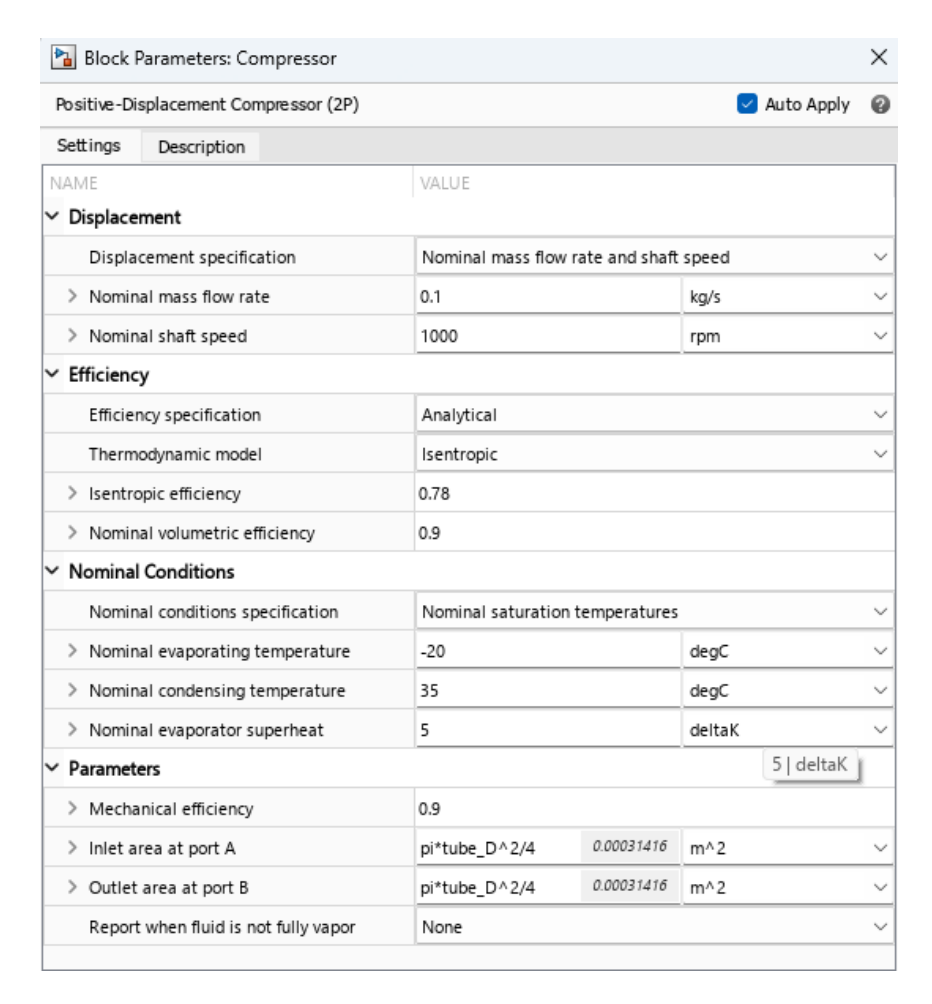


Figure 68. Simulink compressor parameters.

The accumulator serves as a protective component for the compressor while also providing system stability. It stores excess refrigerant during low load conditions and prevents liquid refrigerant from entering the compressor, which could cause mechanical damage. The accumulator also helps maintain proper refrigerant distribution throughout the system and compensates for variations in refrigerant charge due to operating conditions and ambient temperature changes.

9.6 Control System Integration and Operation

The control system orchestrates the operation of all system components to maintain optimal performance and achieve the desired indoor temperature. The controller processes the temperature inputs and generates appropriate control signals for the various actuators, including the compressor drive, expansion valve, and directional valves. The control algorithm incorporates proportional-integral-derivative (PID) control logic to minimize temperature deviations and optimize energy consumption.

The ambient temperature block can be seen in Fig. 69.

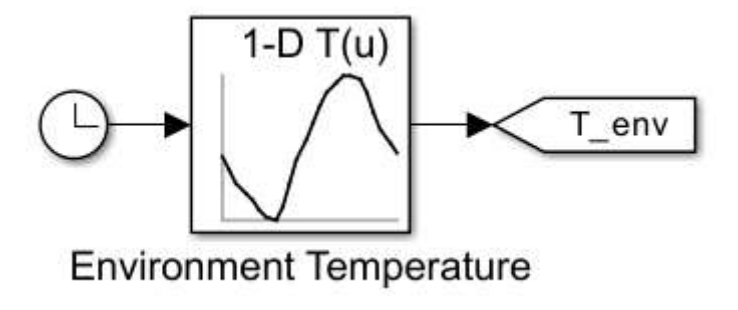


Figure 69. Simulink Ambient temperature block.

The system's response to environmental conditions is managed through the Environment Temperature block, which simulates external temperature variations using a 1-D lookup table with data imported from PVGIS. This allows the model to evaluate system performance under different ambient conditions and seasonal variations. The control system must account for these external factors when determining the optimal operating strategy, as outdoor temperature significantly affects the heat pump's capacity and efficiency.

9.7 Performance Monitoring and Analysis

The model includes comprehensive performance monitoring capabilities that track key system parameters such as power consumption, coefficient of performance (CoP), pressure levels, and flow rates. These metrics are essential for evaluating the system's efficiency and identifying opportunities for optimization. The P-H (Pressure-Enthalpy) diagram block provides thermodynamic analysis capabilities, allowing for detailed

examination of the refrigeration cycle and identification of potential improvements in system design or operation.

The performance data generated by the model serves multiple purposes, including system optimization, fault detection, and energy consumption analysis. By monitoring these parameters continuously, the control system can adapt its operation to maintain optimal performance under varying conditions and detect any deviations from normal operation that might indicate component degradation or system faults.

Chapter IV: Results

In this chapter, the results of the simulations are presented and analysed. The results include the energy performance of the building under baseline conditions, as well as under various optimization scenarios aimed at reducing emissions and improving economic efficiency. Key performance indicators such as net energy demand and cost savings are evaluated. The impact of the energy management algorithm is discussed, and the effectiveness of the different strategies is compared.

To provide a comprehensive assessment of the building's energy performance and the effectiveness of the proposed optimization strategies, three representative days of Valladolid (41.626°, -4.732°) were selected as case studies: a typical day with average temperatures, the coldest day of the year, and the hottest day of the year. These cases were chosen to capture the variability in energy demand and system behaviour under different climatic conditions.

The typical day represents standard operating conditions, offering a baseline for evaluating average energy consumption and identifying patterns that may not be visible during extreme events. In contrast, the coldest and hottest days of the year serve as stress tests for the building's energy systems. These days typically present the highest heating and cooling loads, respectively, and therefore provide critical insights into how well the optimization strategies perform under peak demand scenarios. Analysing these extremes ensures that the proposed solutions are not only effective during typical conditions but also resilient and efficient during the most challenging periods of the year.

It's worth noting that the constraint conditions for each of the cases of study are the same, also variables like the capacity of the batteries, original schedule etc. remain constant during each case.

Regarding the constraint conditions, the optimization searches for a solution where the appliances operate for two hours in a row because the appliances' programs are at least two hours long. Before the optimization process, the user is asked for prohibited hours where the EV is not able to be charged for whatever reason, the **forbidden schedule for**

every case is from 8:00-13:00 and 17:00-21:00 which corresponds to a normal working shift in a job where commuting is needed so the EV is needed to be outside the house, in other words, the EV cannot be charged in the house.

Typical day

Once the common variables for all cases in the present study have been introduced, the specific variables for the current case—namely, the typical day—can be defined, allowing for the execution of the program. First, the variables corresponding to this particular case will be presented, followed by the results and the corresponding tables.

As previously mentioned, the case specific variables will be introduced first.

The **set point temperature** indoors is **21** °C (± **2** °C), also the temperature of the **house initially** is **16** °C. The panel temperature and solar output variables have been determined with Eq. 21 and Eq. 19 respectively. The value of T_env=14.87 is set in the Simulink model to start the simulation. The typical day hourly data can be seen in Fig. 6.

Table 6. Typical day hourly solar data.

Hour	Irradiance	T environment	T panel	PV Production
	(W/m^2)	(°C)	(°C)	DC (kWh)
1	0	14.87	14.87	0
2	0	13.33	13.33	0
3	0	11.9	11.9	0
4	0	10.81	10.81	0
5	0	9.8	9.8	0
6	0	9.03	9.03	0
7	0	8.22	8.22	0
8	11.08	7.71	8.06	0.42
9	224.16	9.32	16.33	8.80
10	462.72	11.89	26.35	19.02
11	696.33	14.33	36.09	29.87
12	827.83	16.49	42.36	36.47

13	1014.74	18.37	50.08	46.14
14	1104.63	20.23	54.75	51.18
15	1071.18	21.79	55.26	49.73
16	913.17	23.05	51.59	41.78
17	720.65	23.76	46.28	32.27
18	513.99	23.83	39.89	22.41
19	256.05	23.12	31.12	10.75
20	36.49	21.7	22.84	1.48
21	0	19.56	19.56	0
22	0	17.87	17.87	0
23	0	16.39	16.39	0
24	0	14.99	14.99	0
		350.31		

The plots of the environmental temperature and temperature of the PV panels are presented in Fig. 70, while the solar irradiance and PV energy production are plotted in Fig. 71.

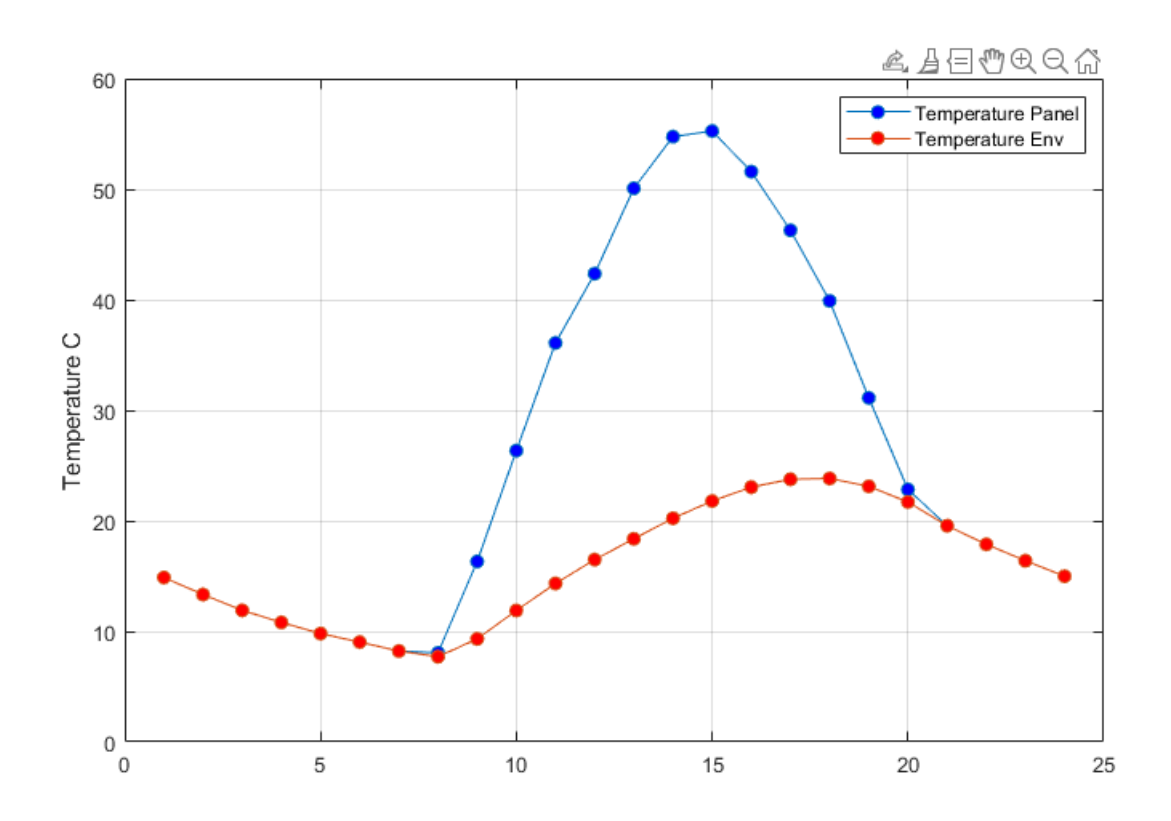


Figure 70. Typical day plot with Temperature of the Panel and Ambient Temperature.

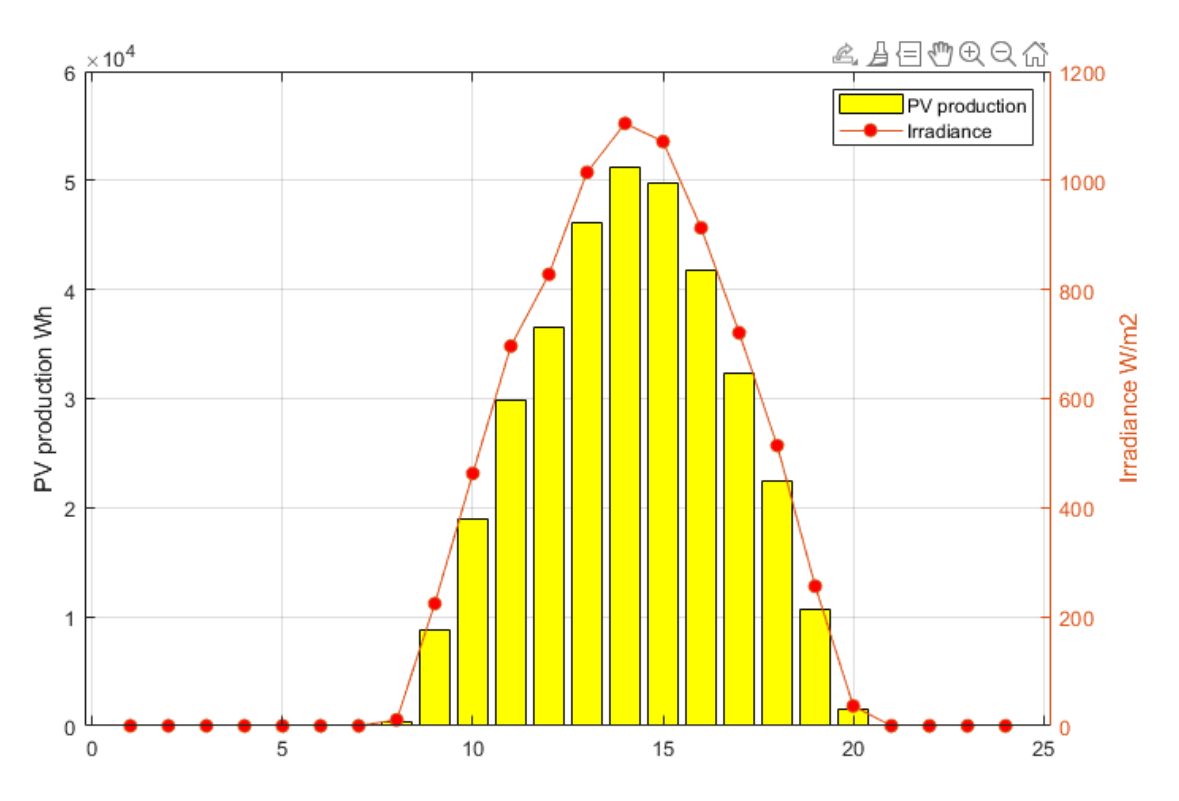


Figure 71. Typical day plot with PV Production and Irradiance.

The distributions of the different loads modelled are shown in Figs. 72-73.

The analysis begins with the controllable appliances, followed by the state of charge of the EV and its corresponding load, in order to clearly observe how the state of charge changes when the EV is plugged in.

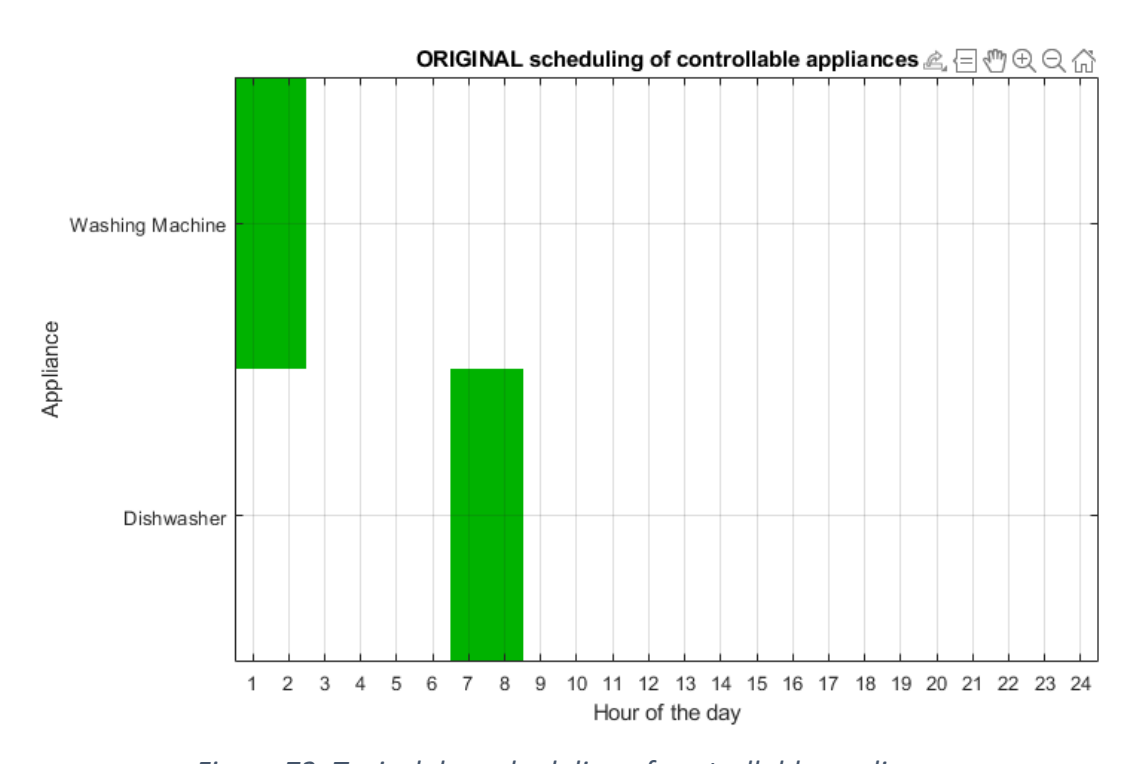


Figure 72. Typical day scheduling of controllable appliances.

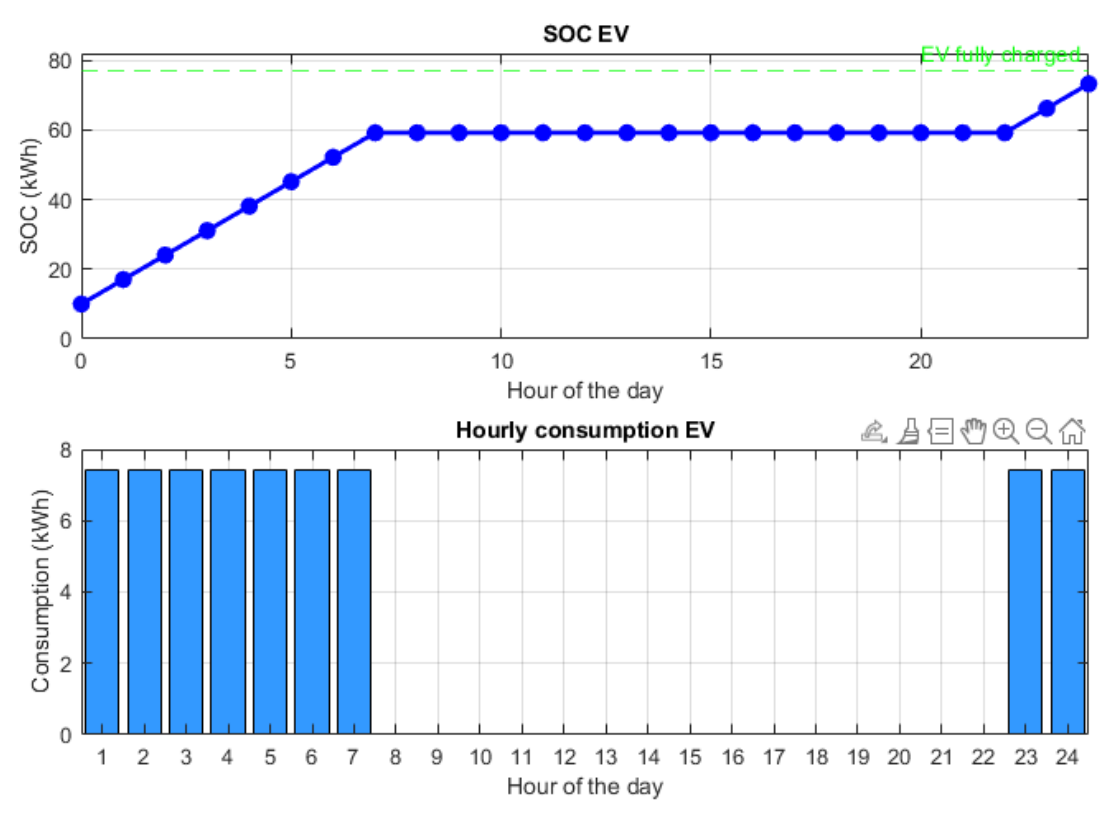


Figure 73. Typical day EV SOC and Consumption.

Fig. 74 shows a graph that combines the energy consumption of all elements, categorized according to their respective energy sources. It should be noted that the HVAC consumption is provided by the simulation of the Simulink model; however, the consumption of all elements will later be presented in relation to the electricity generation.

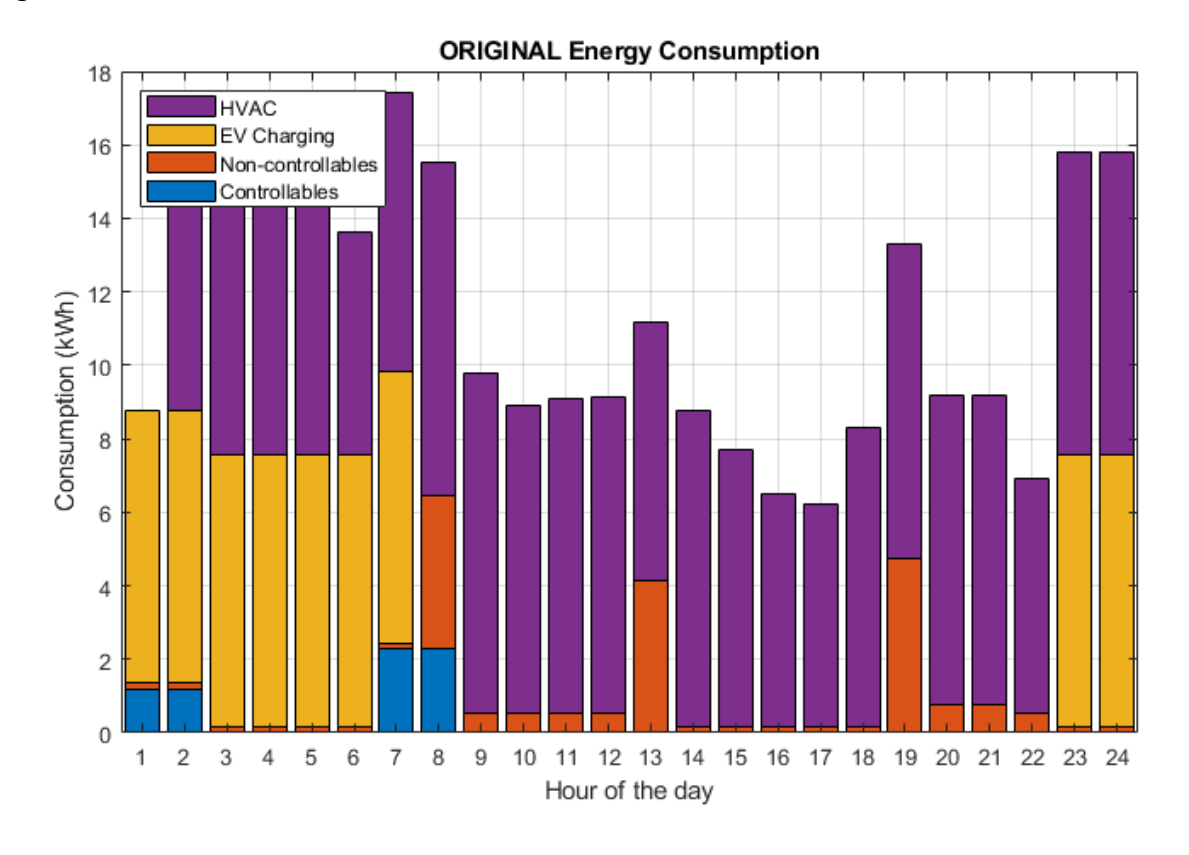


Figure 74. Typical day hourly energy consumption.

For a clearer visualisation of the values for each type of consumption, Table 7 is shown below.

Table 7. Typical day energy consumption.

ENERGY CONSUMPTION (kWh)					
Hour	CA	N-CA	EV	HVAC	TOTAL HOURLY
1	1.2	0.15	7.4	0	8.75
2	1.2	0.15	7.4	6.37	15.121
3	0	0.15	7.4	7.21	14.76
4	0	0.15	7.4	7.70	15.25

5	0	0.15	7.4	7.79	15.34
6	0	0.15	7.4	6.06	13.61
7	2.3	0.15	7.4	7.57	17.42
8	2.3	4.15	0	9.09	15.54
9	0	0.55	0	9.26	9.81
10	0	0.55	0	8.37	8.92
11	0	0.55	0	8.55	9.10
12	0	0.55	0	8.58	9.13
13	0	4.15	0	7.04	11.19
14	0	0.15	0	8.62	8.77
15	0	0.15	0	7.55	7.70
16	0	0.15	0	6.37	6.52
17	0	0.15	0	6.09	6.24
18	0	0.15	0	8.15	8.30
19	0	4.75	0	8.54	13.29
20	0	0.75	0	8.42	9.17
21	0	0.75	0	8.42	9.17
22	0	0.55	0	6.36	6.91
23	0	0.15	7.4	8.26	15.81
24	0	0.15	7.4	8.24	15.79
TOTAL	7	19.4	66.6	178.61	271.61

The Figs. 75-76 are extracted from the Simulink model representing the mode changes between cooling/heating, setpoint temperature vs. temperature of the environment and indoor temperature respectively. It is important to note that the compressor stops running if the indoor temperature is \pm 2 °C the target temperature so it is not running 24 hours a day.

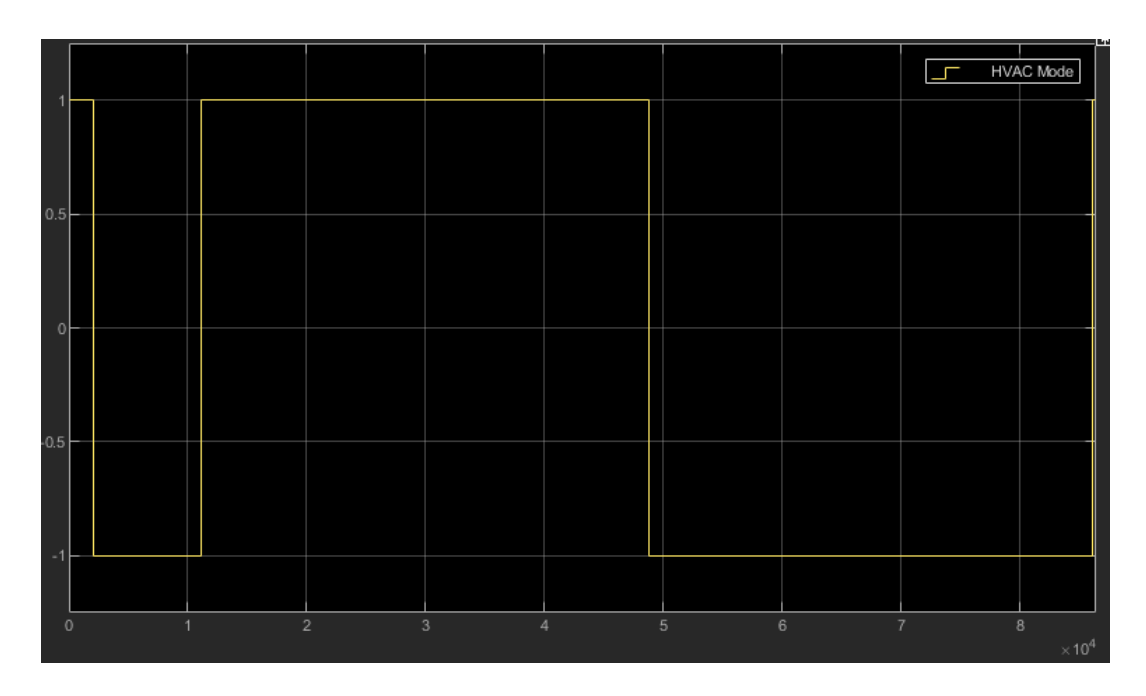


Figure 75. Typical day HVAC mode.

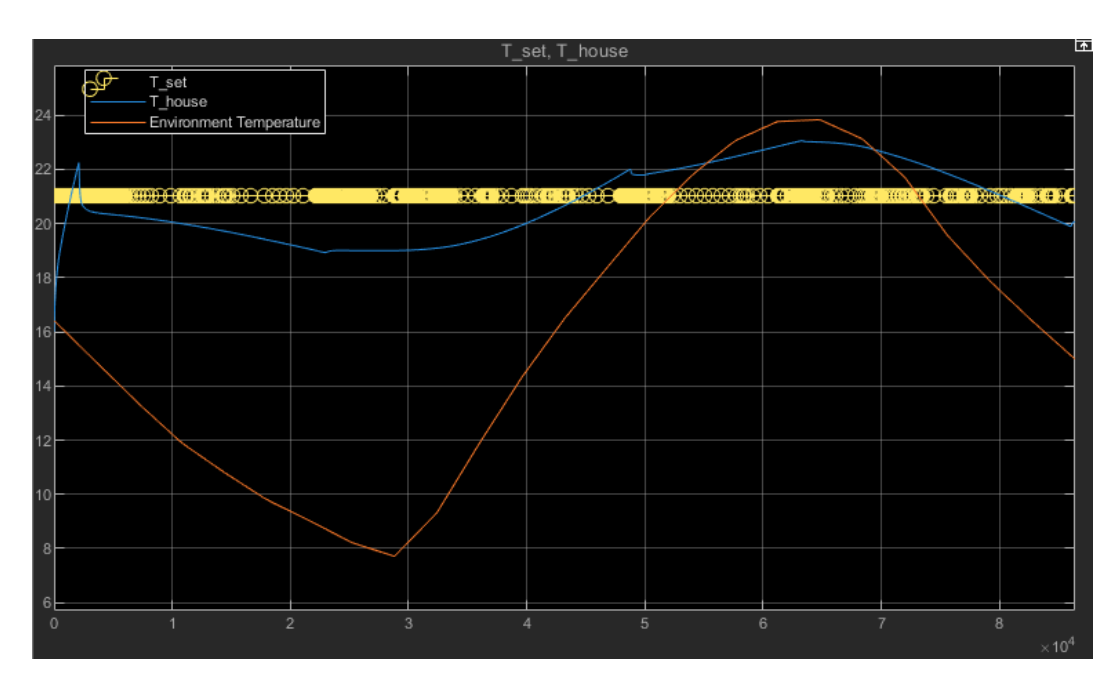


Figure 76 Typical day plot of setpoint temperature, temperature indoors and ambient temperature.

Finally, to conclude the typical day before optimisation, Fig. 77 shows the comparison between energy production and consumption, the state of charge of the house batteries and the state of charge of the batteries in percent, respectively. Fig. 79 shows the energy flows resulting from the simulation.

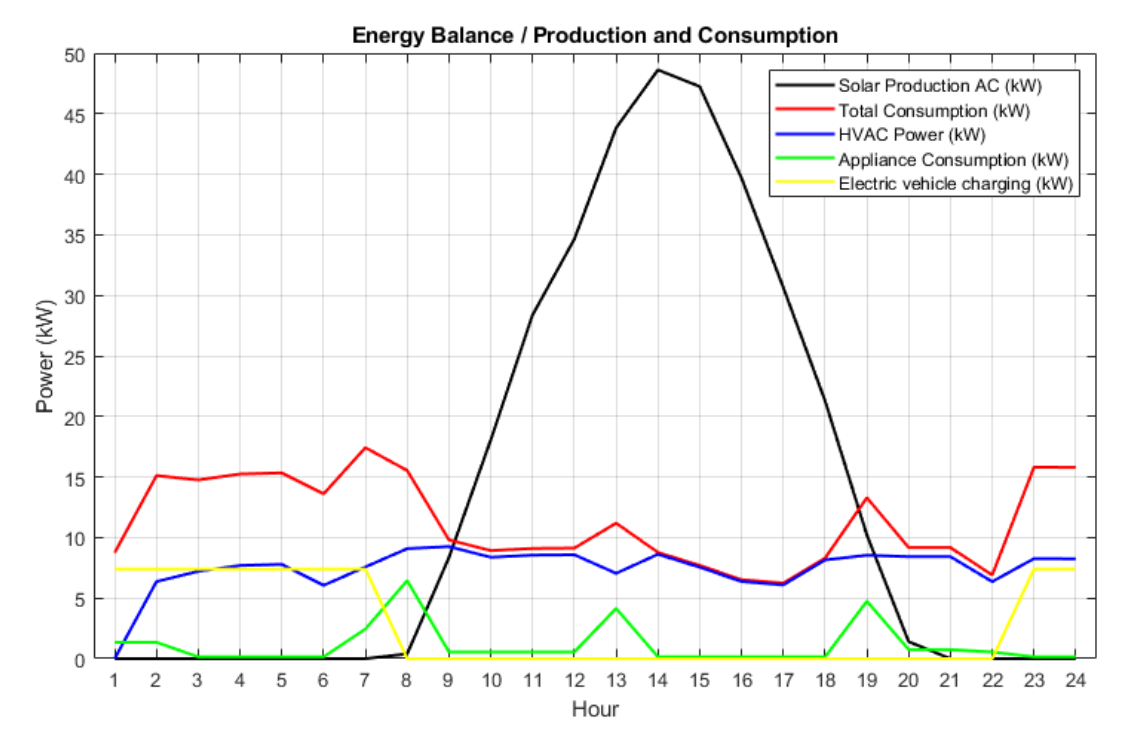


Figure 77. Typical day Energy Balance.

The Typical day battery SOC can be seen in Fig. 78.

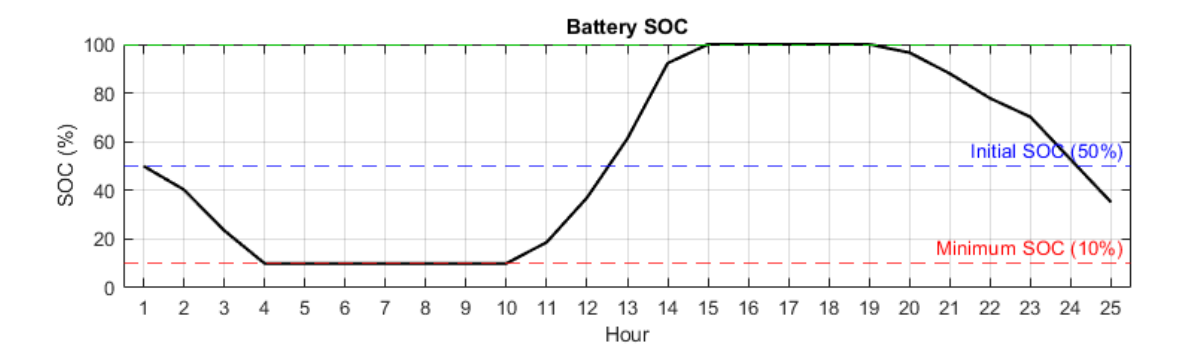


Figure 78. Typical day Battery SOC

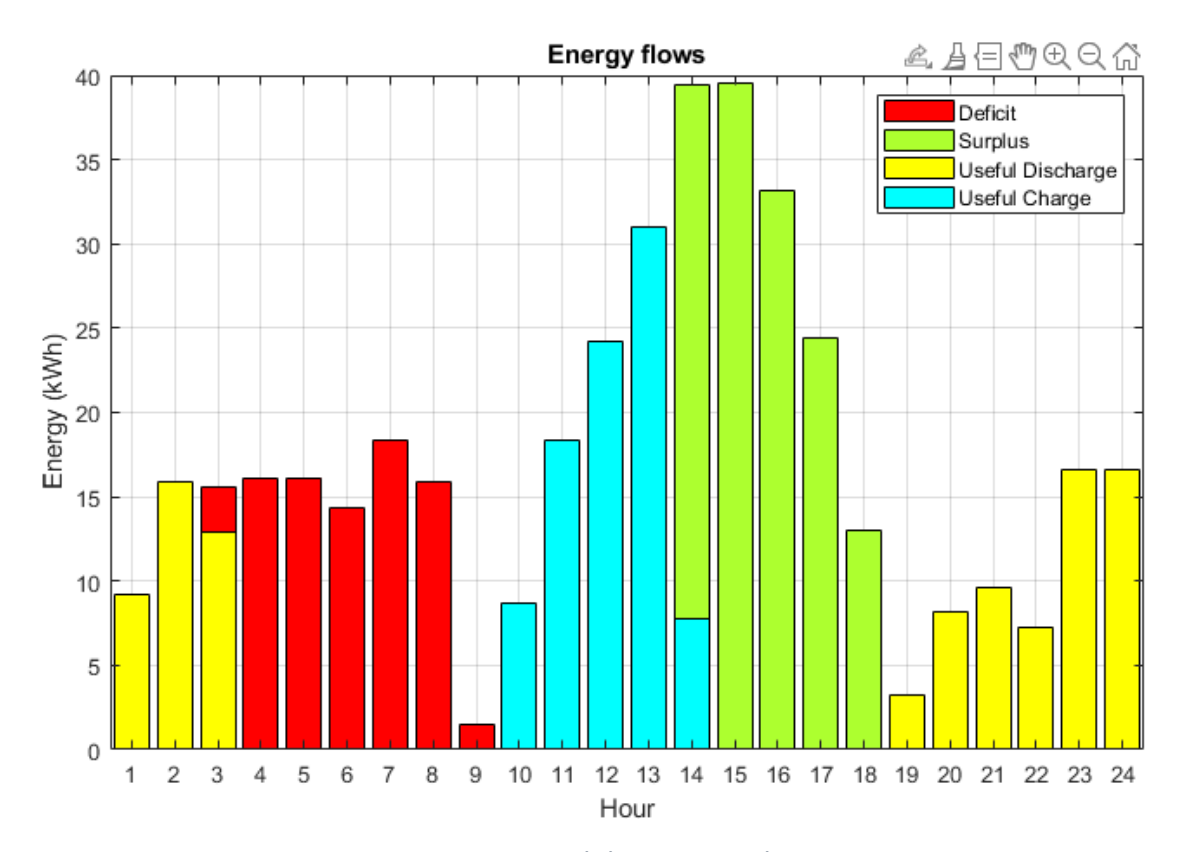


Figure 79. Typical day Energy Flows.

Once the above results have been obtained, the optimisers are applied. It should be remembered that the prohibited charging hours are: 8:00-13:00 and 17:00-21:00. Also, in the economic optimizer Also, in the economic optimizer the type of day can be selected between weekdays and holidays/weekends, as these have different electric tariffs. In this diploma thesis, the type of day chosen is a weekday.

After the optimisation the results depicted in Figs. 80-98 are derived.

Figs. 80-86 provide information on the hours of use of the appliances, EV load and EV state of charge, in both the initial and optimized situations as a tool for comparison.

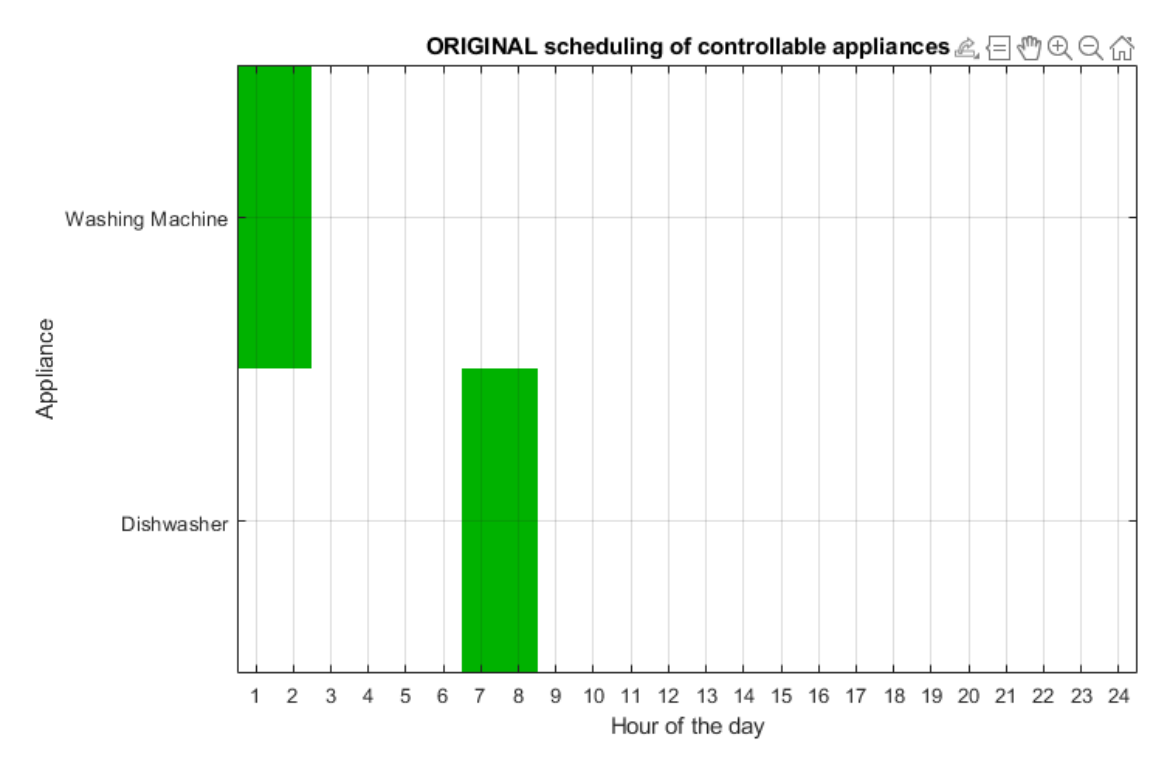


Figure 80. Typical day original scheduling of controllable appliances.

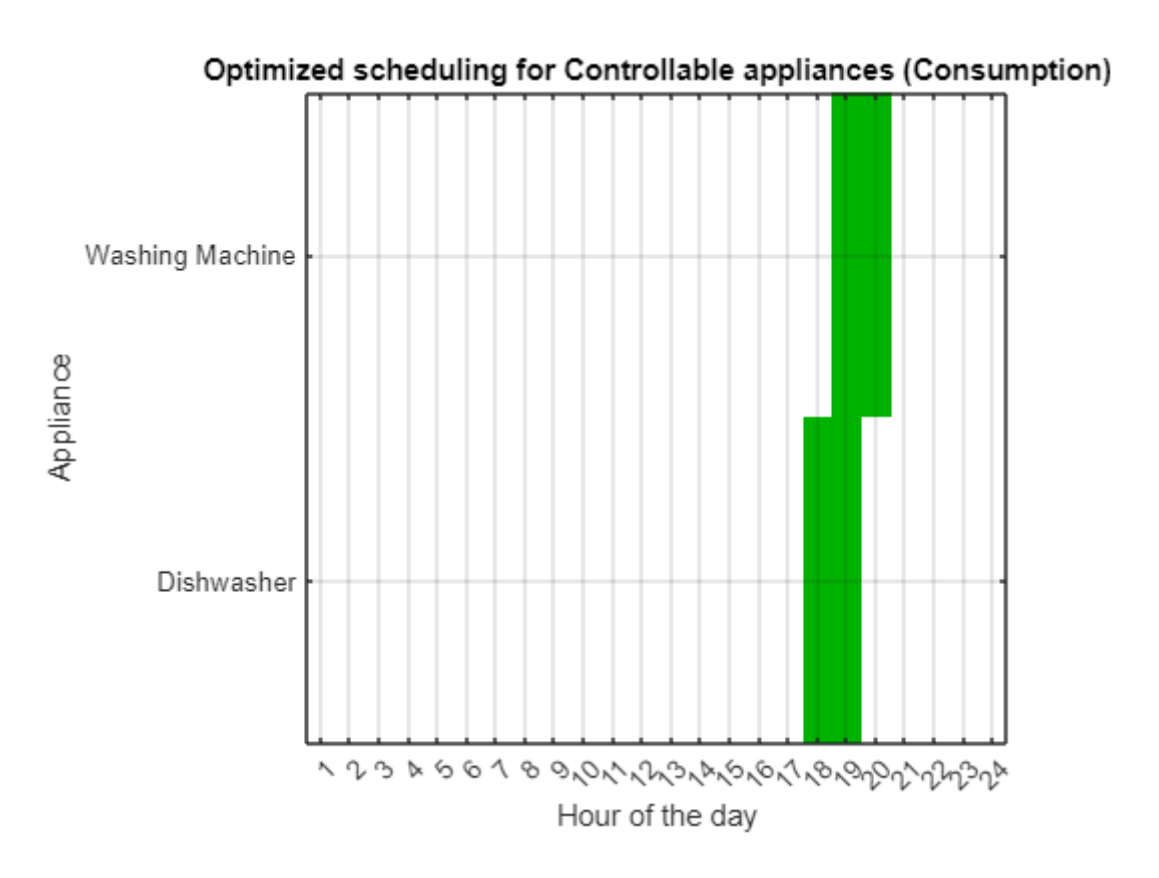


Figure 81. Typical day scheduling of controllable appliances for optimization for minimum consumption.

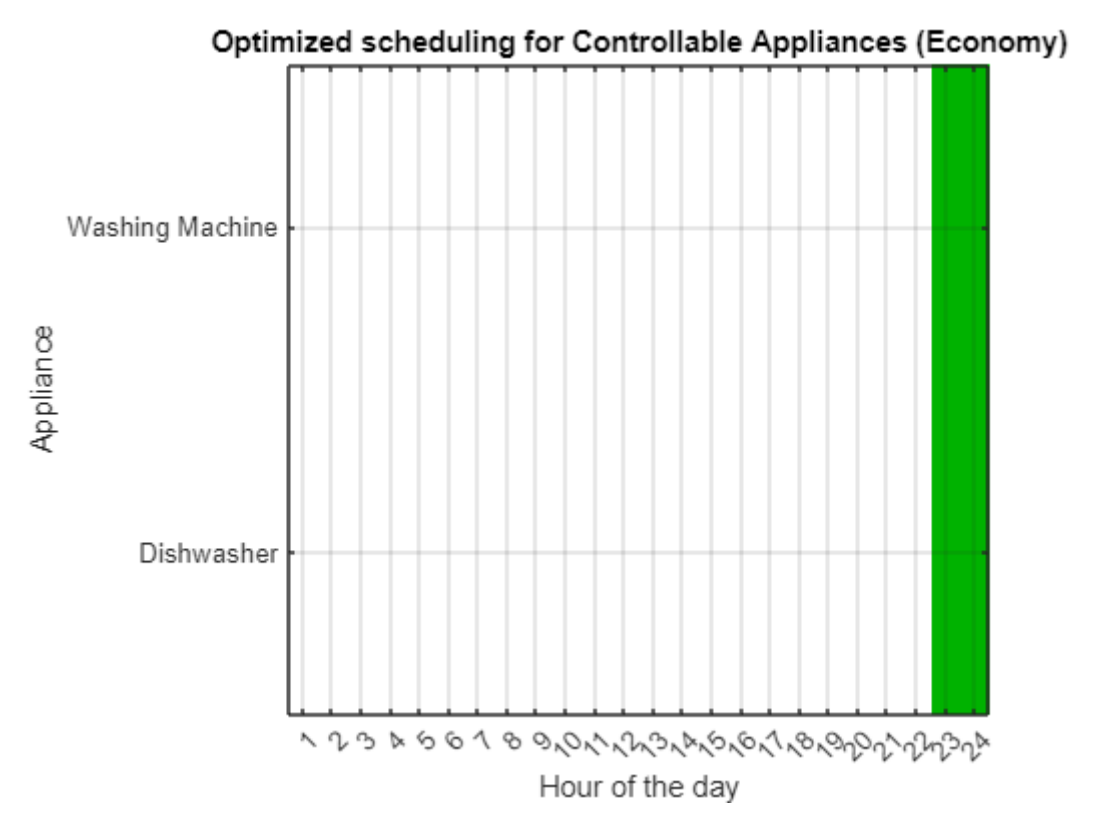


Figure 82. Typical day scheduling of controllable appliances for optimization for maximum net economic benefit.

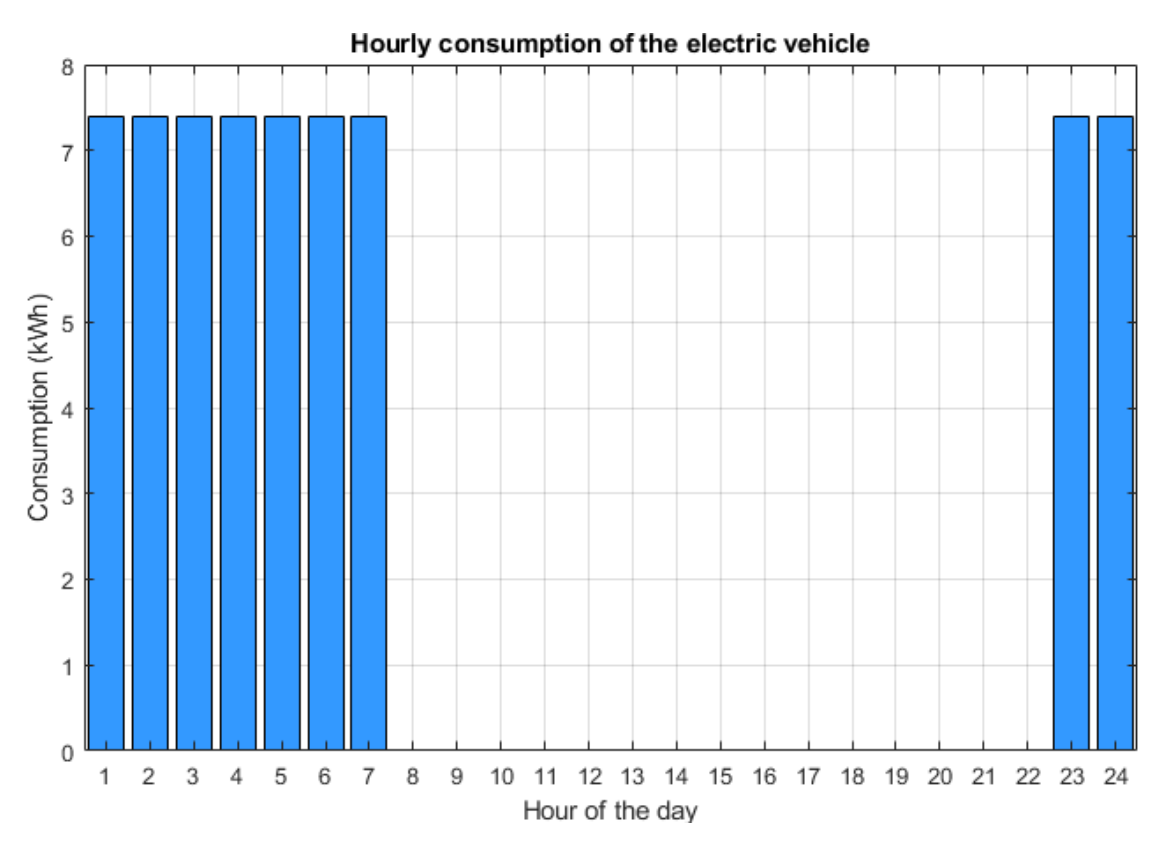


Figure 83. Typical day EV consumption and charging schedule.

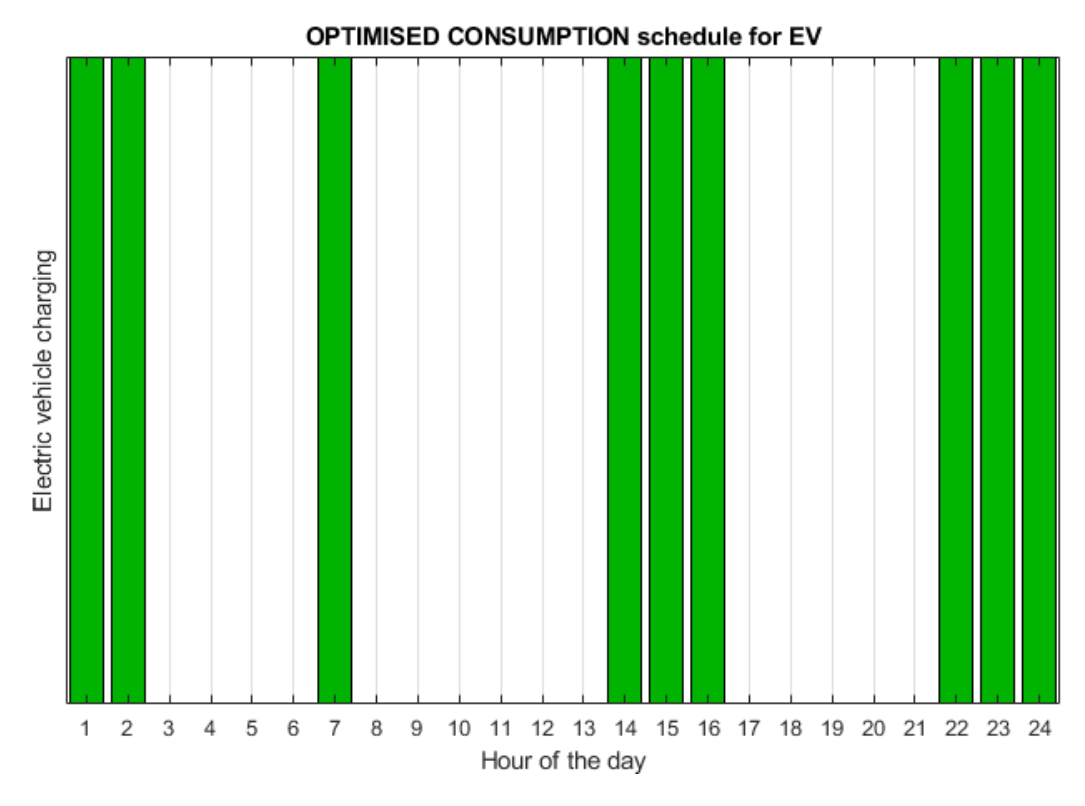


Figure 84. Typical day EV charging schedule for optimization for minimum consumption.

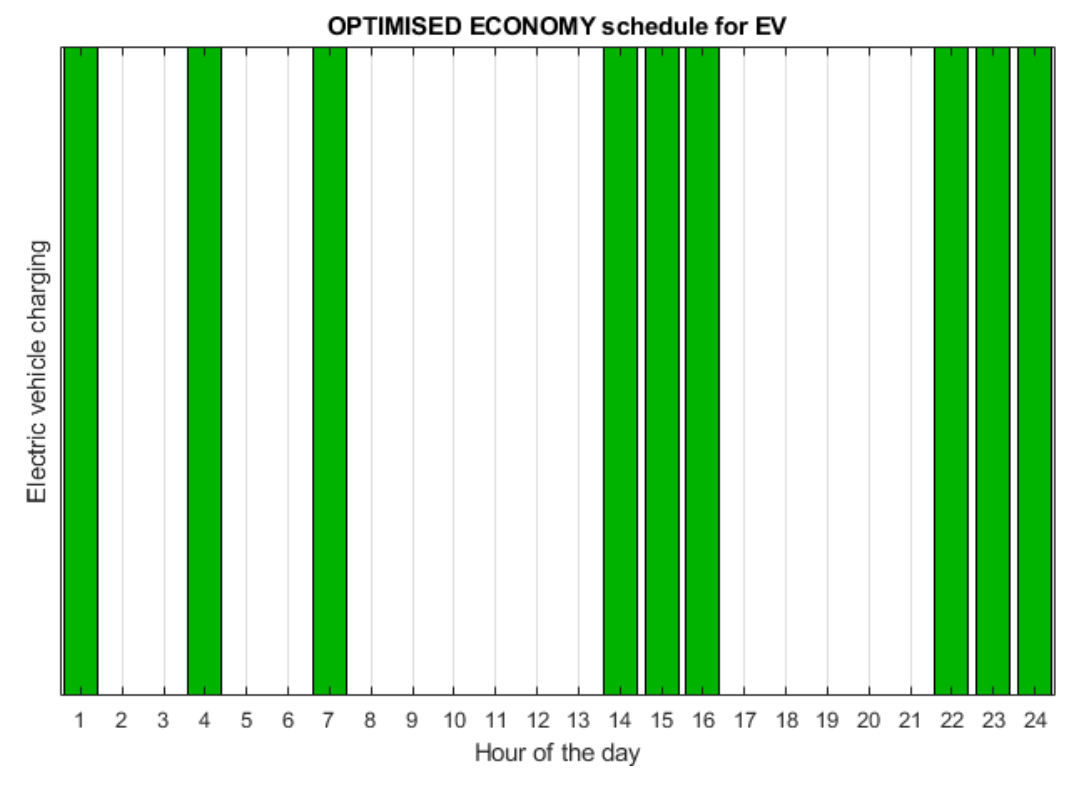


Figure 85. Typical day EV charging schedule for optimization for maximum net economic benefit.

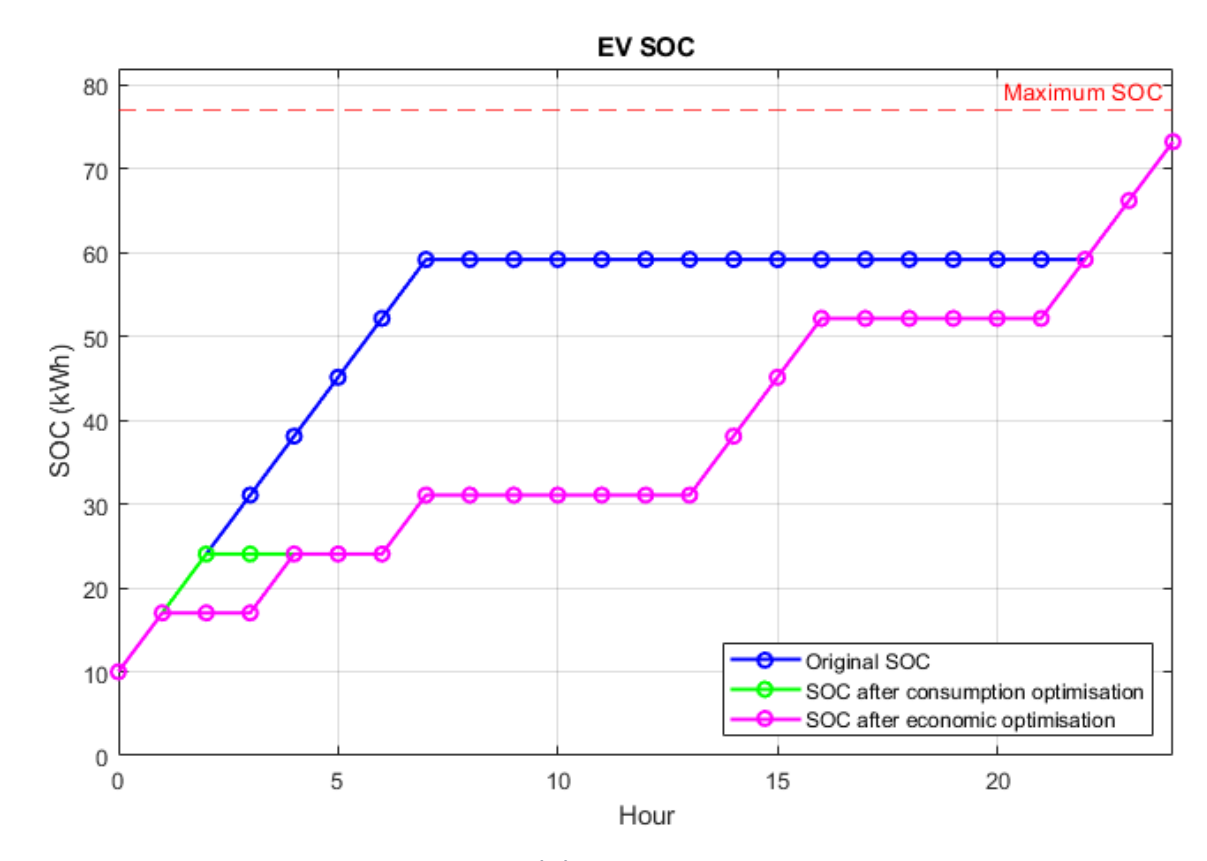


Figure 86. Typical day EV SOC comparison.

The Table 8 presents the parameters of the electric vehicle in the initial and optimised cases. The results for EV charging do not change, as the same prohibited schedule applies for both optimizers.

The possible EV charging hours is higher than the original number of charging hours, so that the EV can be charged for the same number of hours as in the non-optimized situation. This means that the EV battery can be charged to the same extent.

Table 8. Typical day EV parameters.

ELECTRIC VEHICLE	ORIGINAL	OPTIMIZATION FOR	OPTIMIZATION FOR
		MINIMUM	MAXIMUM NET
		CONSUMPTION	ECONOMIC BENEFIT
Initial SOC (kWh)	10	10	10
Final SOC (kWh)	73.27	73.27	73.27
Charging	63.27	63.27	63.27
performed (kWh)			

Charging	66.60	66.60	66.60
consumption			
(kWh)			
Charging hours	9	9	9
Battery missing	3.73	3.73	3.73
(kWh)			

About energy consumption, only the usage time of the controllable appliances and the charging of the electric vehicle can be modified. As a result, the non-controllable appliances remain unchanged despite the application of the optimisations. The same thing happens with the HVAC consumption. The Figs. 87-89 show the different energy consumption for the typical day.

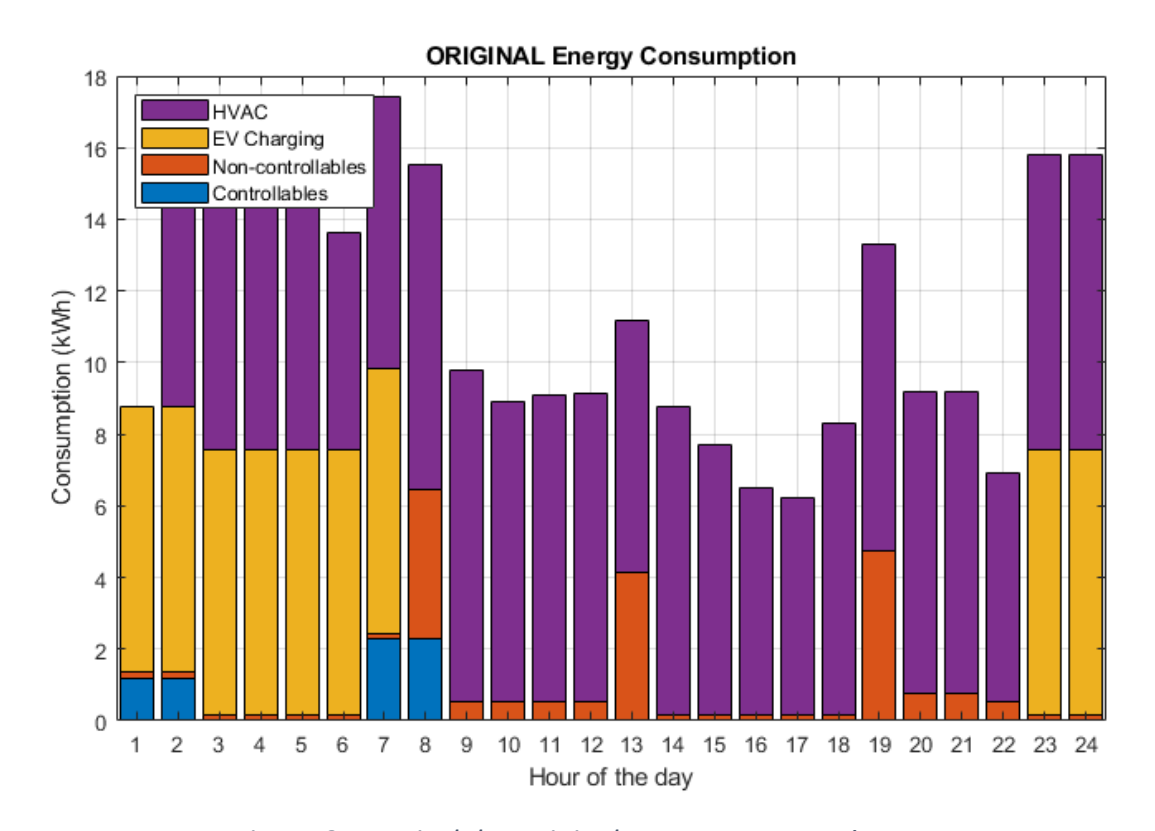


Figure 87. Typical day original energy consumption.

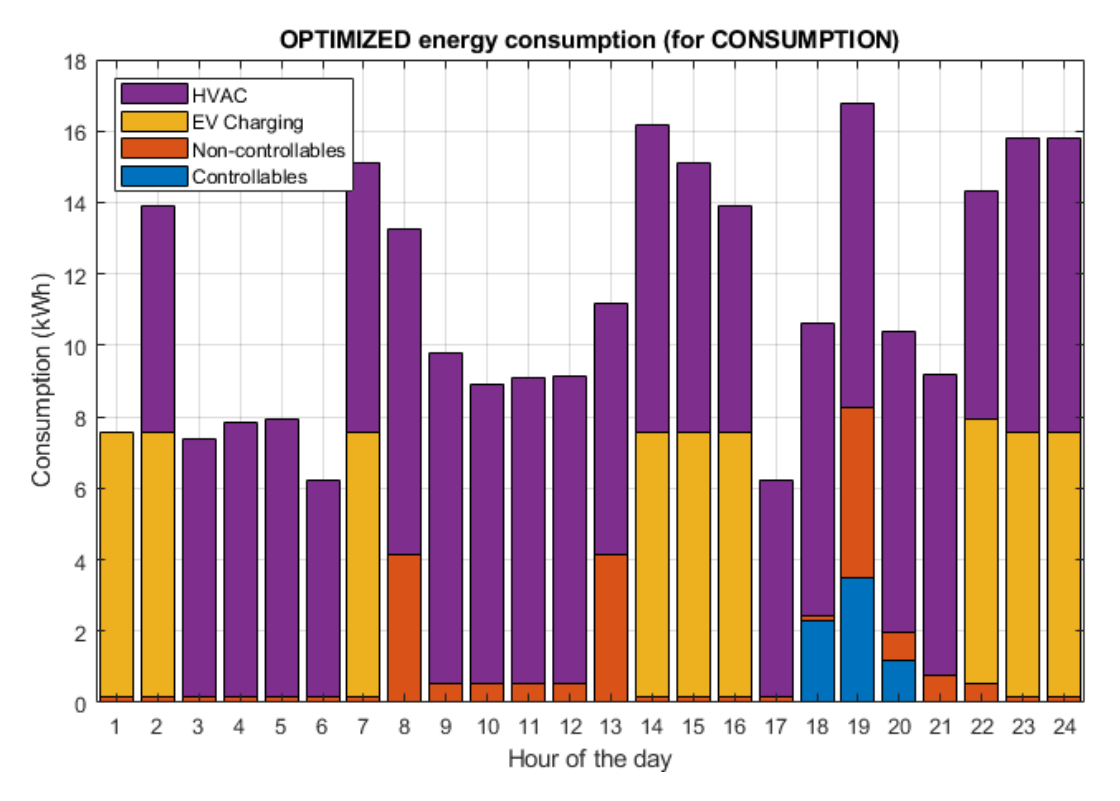


Figure 88. Typical day energy consumption for optimization for minimum energy consumption.

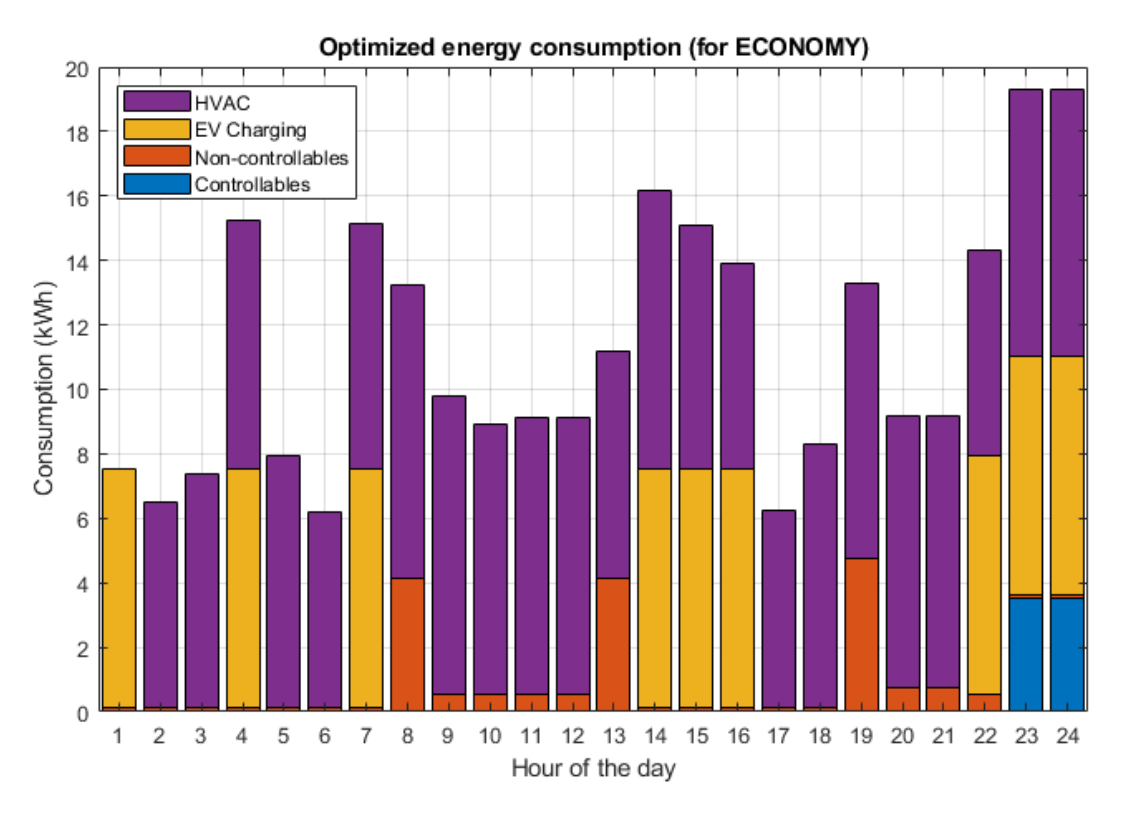


Figure 89. Typical day energy consumption for optimization for maximum net economic benefit.

Below a comparison is presented of the batteries' state of charge before and after the optimiser. Fig. 90 is accompanied by a summary in Table 9 with the battery parameters in the different cases investigated.

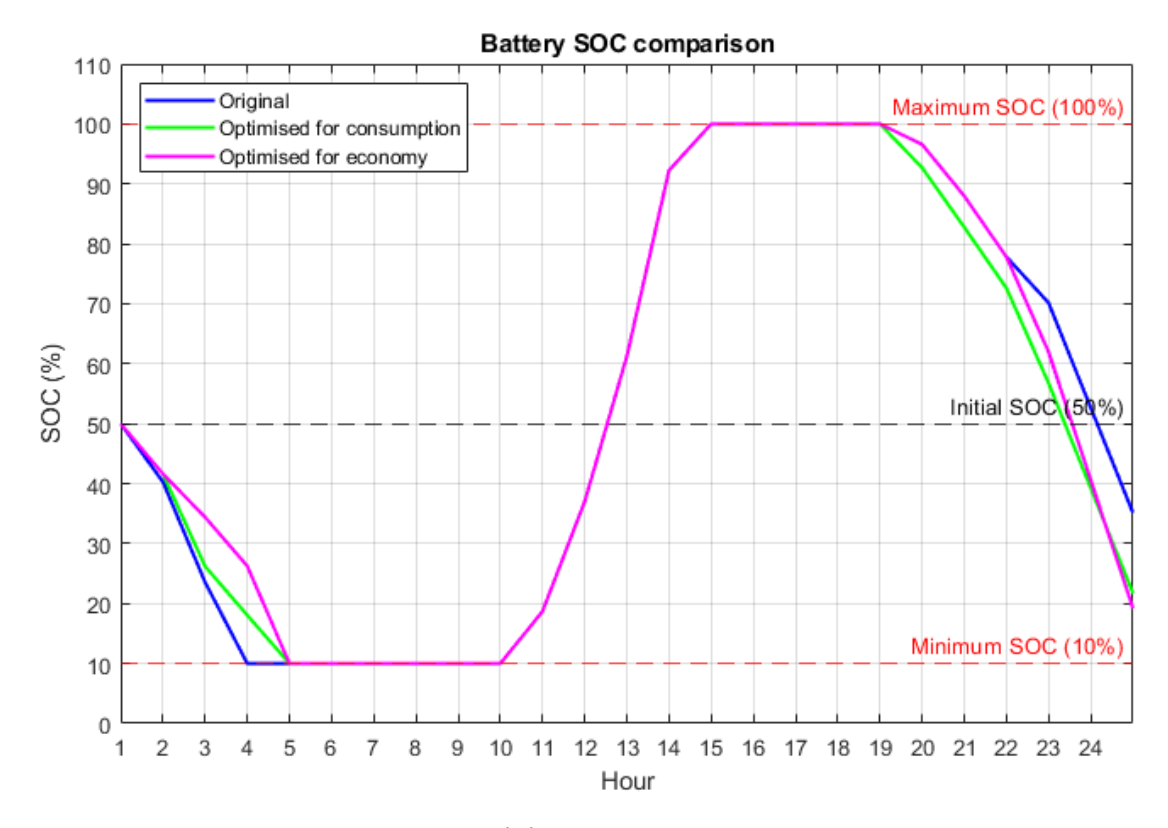


Figure 90. Typical day Battery SOC comparison.

It is important to note that the graph ends at hour 25 because the variable is stored in a vector. When the variable is initialized, its first value is stored at position 1. As a result, the final value corresponds to the end hour, 24, and is stored in position 25, making the graph appear to end at hour 25. This same behaviour will occur in the remaining cases.

Table 9. Typical day batteries parameters summary.

BATTERIES	ORIGINAL	OPTIMIZATION FOR	OPTIMIZATION FOR
		MINIMUM	MAXIMUM NET
		CONSUMPTION	ECONOMIC
			BENEFIT
Initial SOC (kWh)	50	50	50
Final SOC (kWh)	35.14	26.94	19.18

Charging	90	90	90
performed (kWh)			
Discharging	99.62	112.35	114.78
performed (kWh)			

In the economic field, the net hourly cost is calculated for each type of day before and after optimisation. These results can be seen in Figs. 91-92.

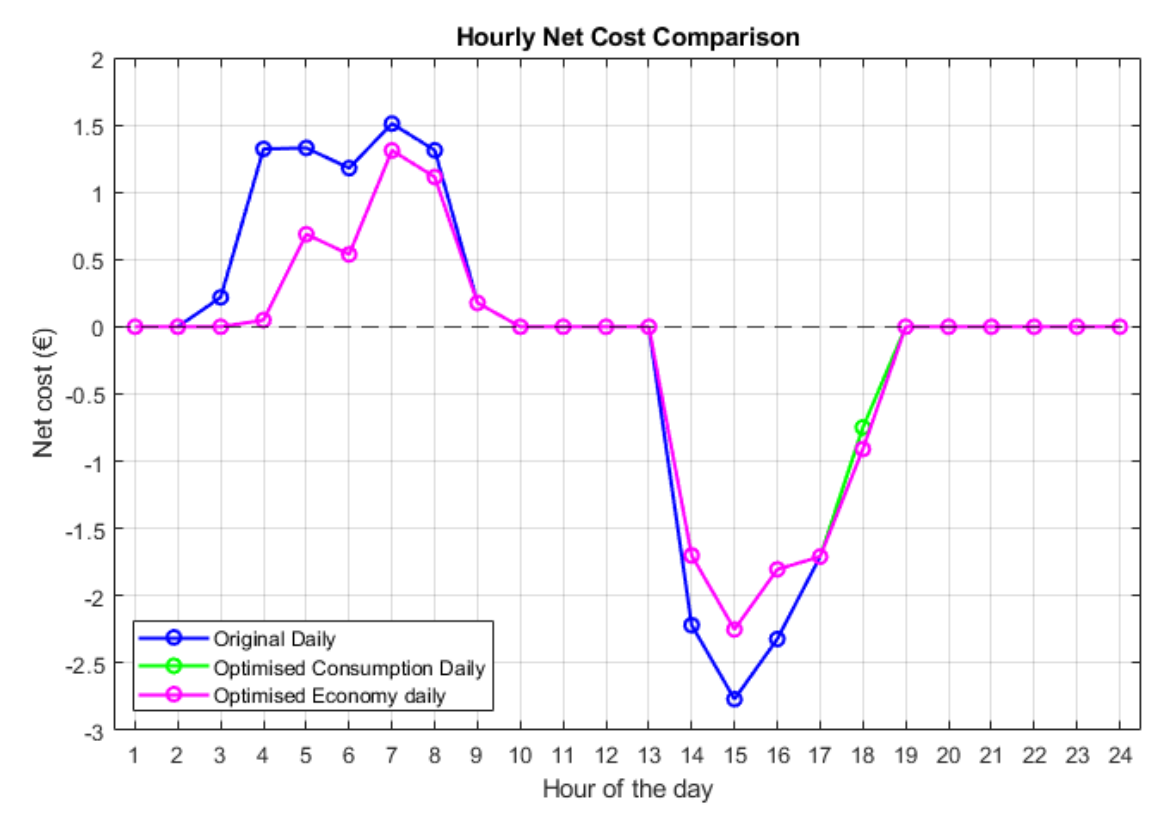


Figure 91. Typical day hourly net cost comparison for weekdays.

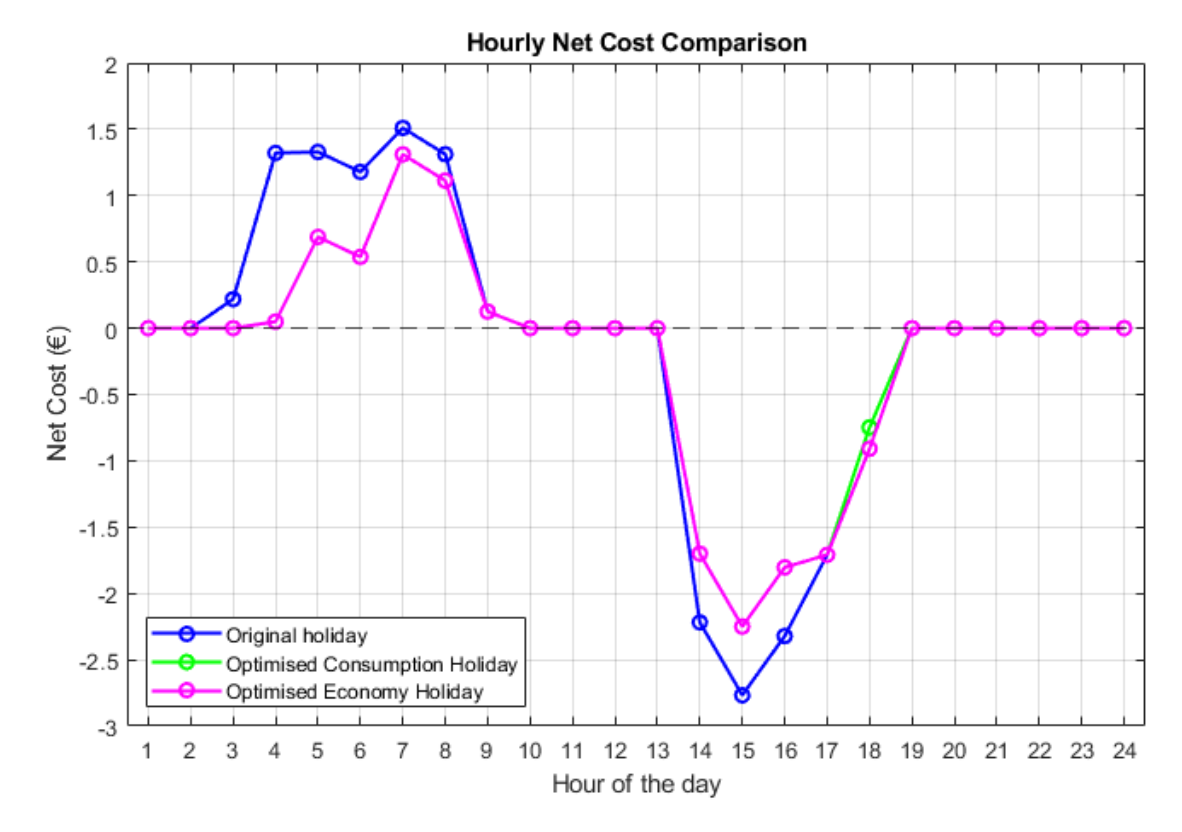


Figure 92. Typical day hourly net cost comparison for holidays.

For a better visualisation and to provide information about the total daily net benefit, Table 10 shows the improvement compared to the initial situation.

Table 10. Typical day economic cost comparison.

ECONOMIC COST				
DAILY				
	ORIGINAL	OPTIMISED FOR CONSUMPTION	OPTIMIZATION FOR	
			MAXIMUM NET ECONOMIC	
			BENEFIT	
Purchase cost (€)	7.05	3.88	3.88	
Selling profit (€)	9.93	8.21	8.37	
Net cost (€)	-2.88	-4.34	-4.50	
Economic saving		1.46 (-50.6%)	1.62 (-56.2%)	
PUBLIC HOLIDAYS AND WEEKENDS				
Purchase cost (€)	7	3.82	3.82	
Selling profit (€)	9.93	8.21	8.37	

Net cost (€)	-2.93	-4.39	-4.55
Economic saving		1.46 (-49.7%)	1.62 (-55.2%)

To conclude with the first day of the study, a breakdown of the original consumption and production versus the modified one is shown in Figs. 93-95 followed by a comparison of the energy flow diagrams shown in Figs. 96-98 of the commented situations and a summary Table 11 of the different cases where the improvement with respect to the initial situation can also be seen.

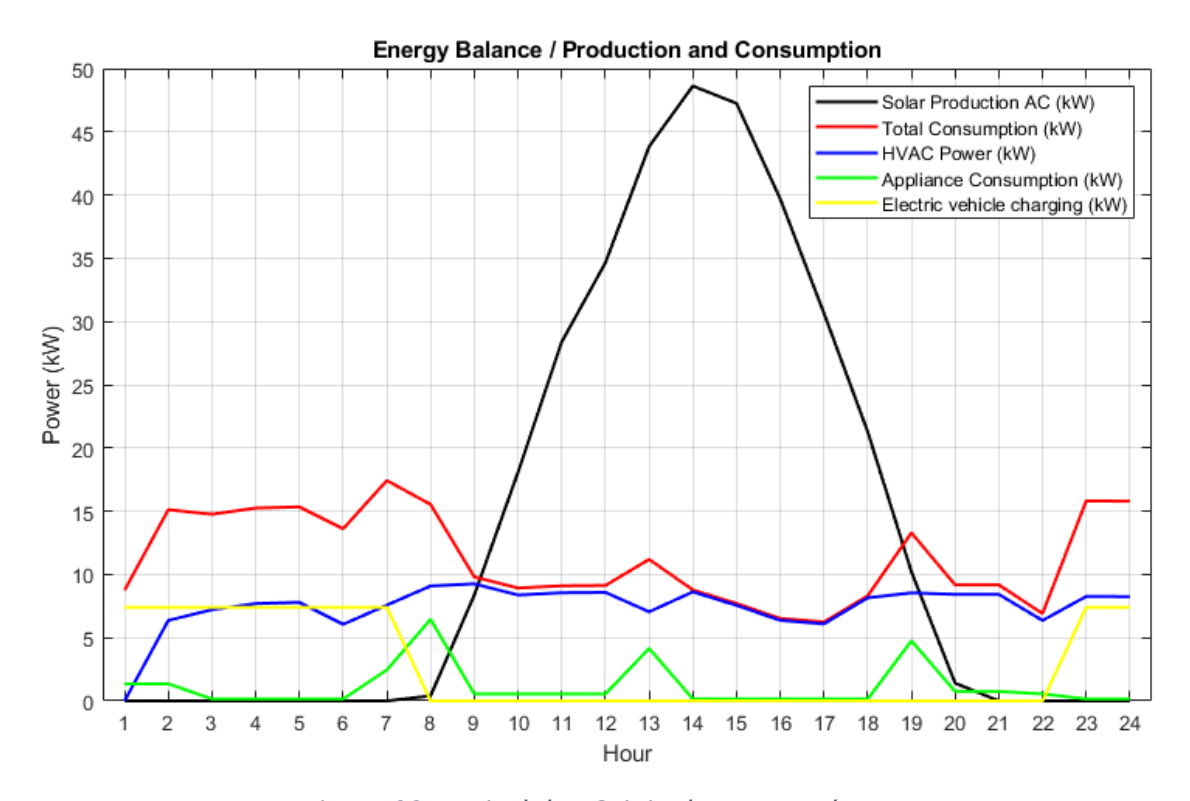


Figure 93. Typical day Original Energy Balance.

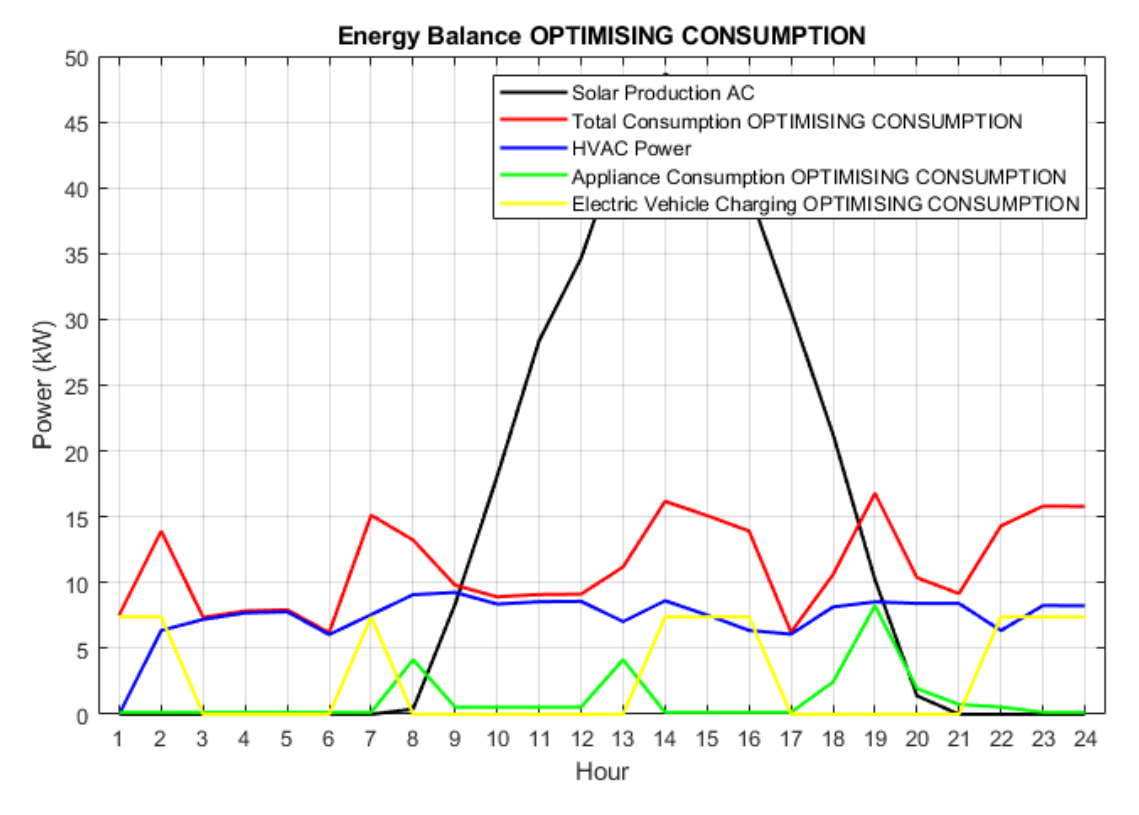


Figure 94. Typical day Energy Balance for optimization for minimum consumption.

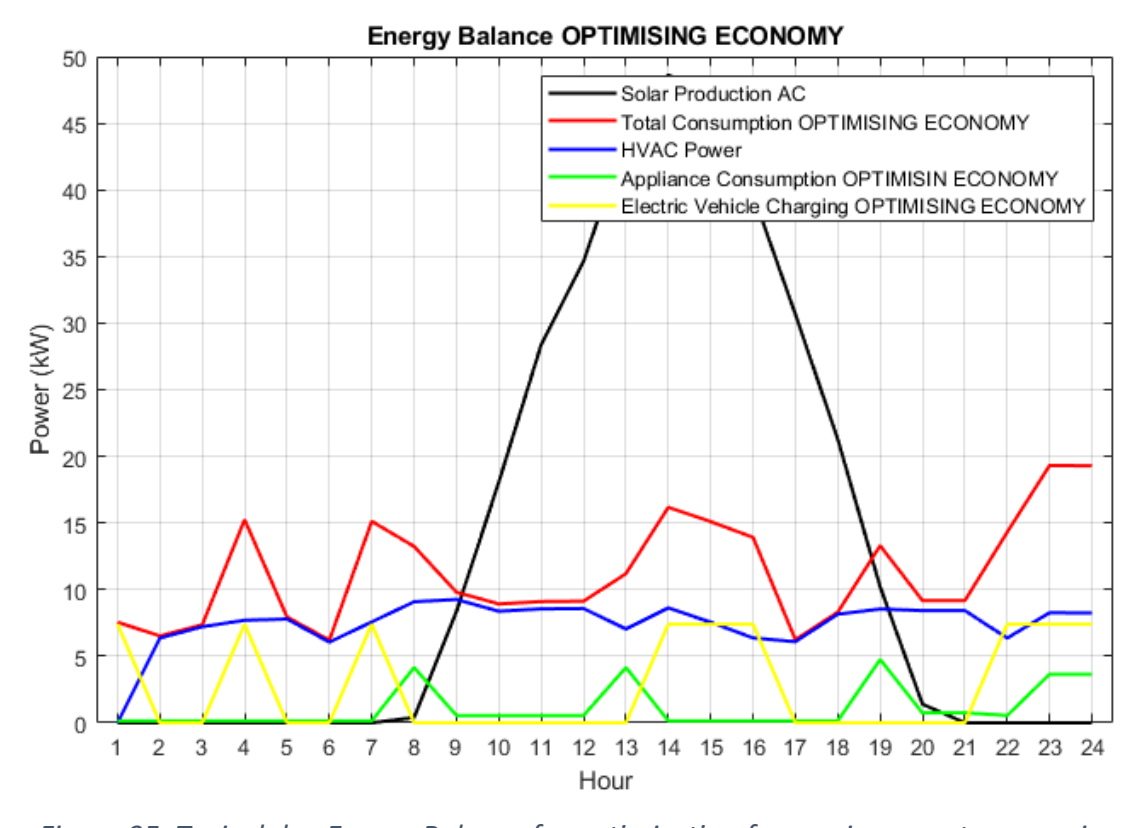


Figure 95, Typical day Energy Balance for optimization for maximum net economic benefit.

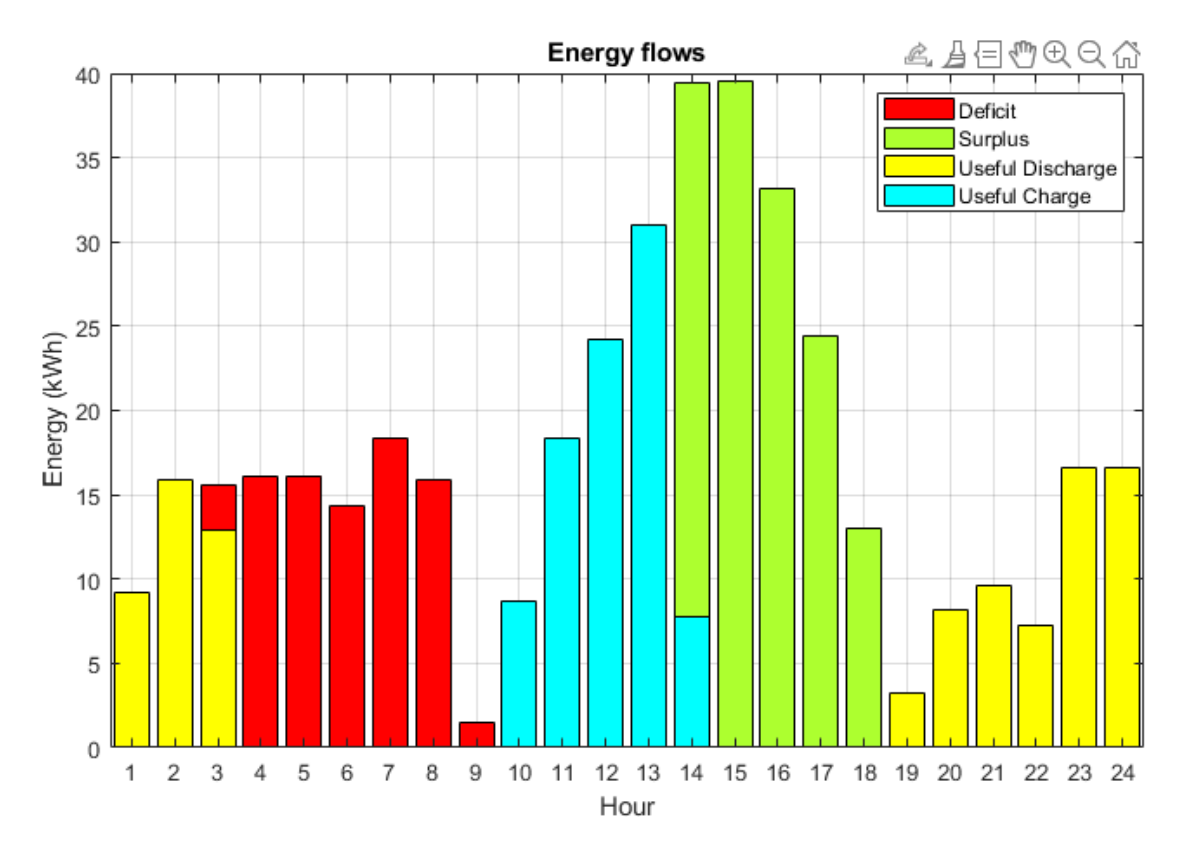


Figure 96. Typical day original Energy Flows.

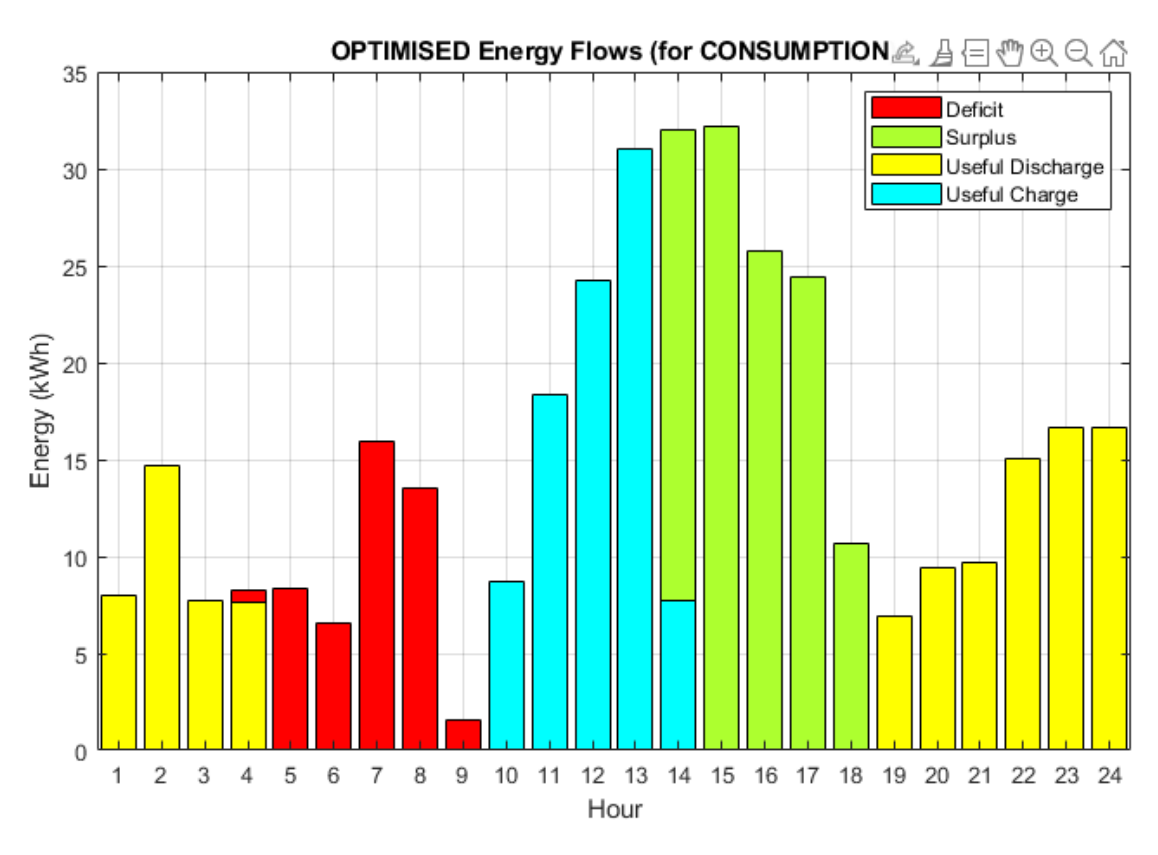


Figure 97. Typical day Energy Flows for optimization for minimum consumption.

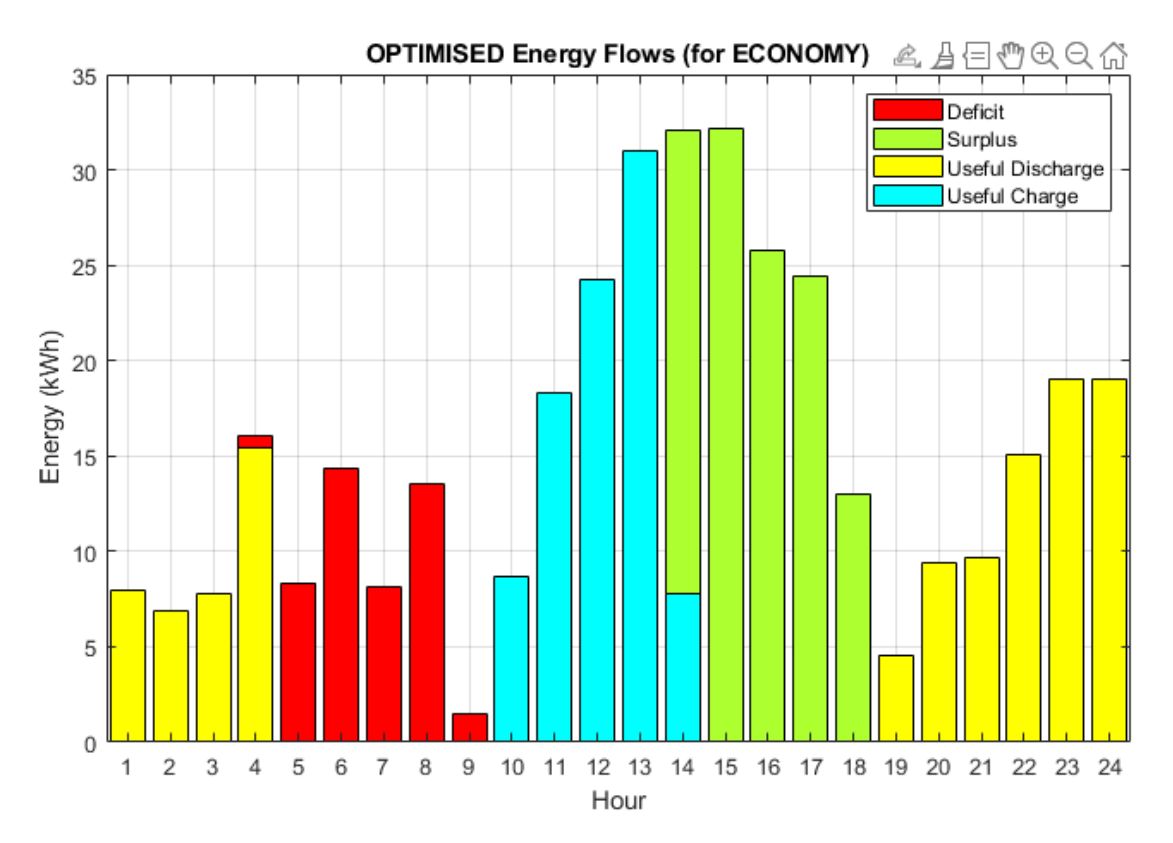


Figure 98. Typical day Energy Flows for optimization for maximum net economic benefit.

Table 11. Typical day Energy Flows summary.

ENERGY	ORIGINAL	OPTIMIZATION FOR	OPTIMIZATION FOR
FLOWS		MINIMUM	MAXIMUM NET
		CONSUMPTION	ECONOMIC BENEFIT
Surplus (kWh)	141.80	117.30	119.60
Deficit (kWh)	84.97	46.45	46.45
Improvement		38.53 (45.3%)	38.53 (45.3%)

The coldest day

The starting variables are the initial indoor temperature and initial environmental temperature, both at 16°C. The setpoint remains the same as before.

The structure followed to present the result is the same as previously, starting this case of study showing a table with the variables which allows us to determine the panel temperature and the PV production (DC) with the Eq. 21 and Eq. 19.

The Table 12 show the coldest day hourly solar data.

Table 12. The coldest day hourly solar data.

Hour	Irradiance	T environment	T panel	PV Production DC
	(W/m²)	(°C)	(°C)	(kWh)
1	0	-2.76	-2.76	0
2	0	-2.29	-2.29	0
3	0	-2.94	-2.94	0
4	0	-3.5	-3.5	0
5	0	-3.84	-3.84	0
6	0	-3.69	-3.69	0
7	0	-4.29	-4.29	0
8	0	-2.76	-2.76	0
9	106.15	-2.62	0.70	3.86
10	146.42	-1.44	3.14	5.39
11	375.53	0.18	11.92	14.44
12	801.99	2.55	27.61	33.15
13	868.36	4.5	31.64	36.54
14	957.2	5.85	35.76	41.01
15	958.88	6.76	36.73	41.25
16	764.23	7.51	31.39	32.12
17	517.97	7.6	23.79	21.05
18	227.17	7.26	14.36	8.84
19	0	6.3	6.30	0

20	0	4.38	4.38	0
21	0	3.91	3.91	0
22	0	2.63	2.63	0
23	0	0.1	0.10	0
24	0	-0.93	-0.93	0
TOTAL kWh:			237.66	

The plots of the environmental temperature and temperature of the PV panels are presented in Fig. 99, while the solar irradiance and PV energy production are plotted in Fig. 100.

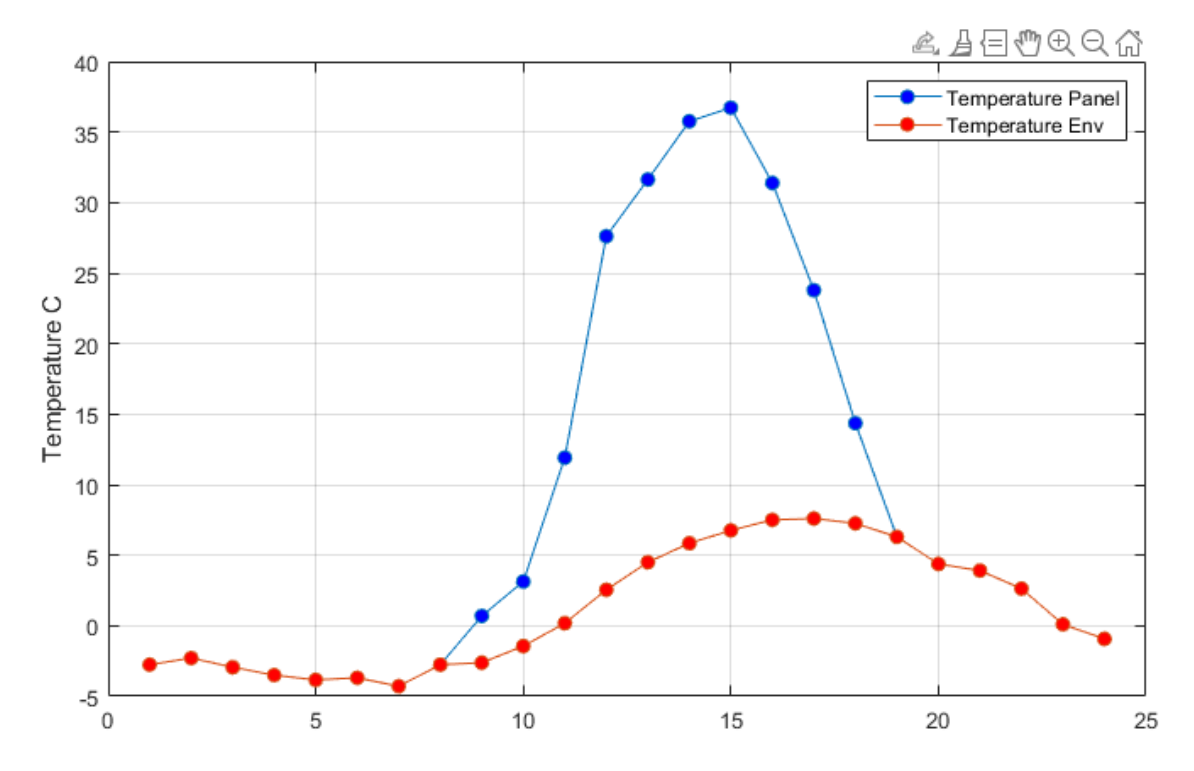


Figure 99. The coldest day plot with Temperature of the Panel and Ambient Temperature.

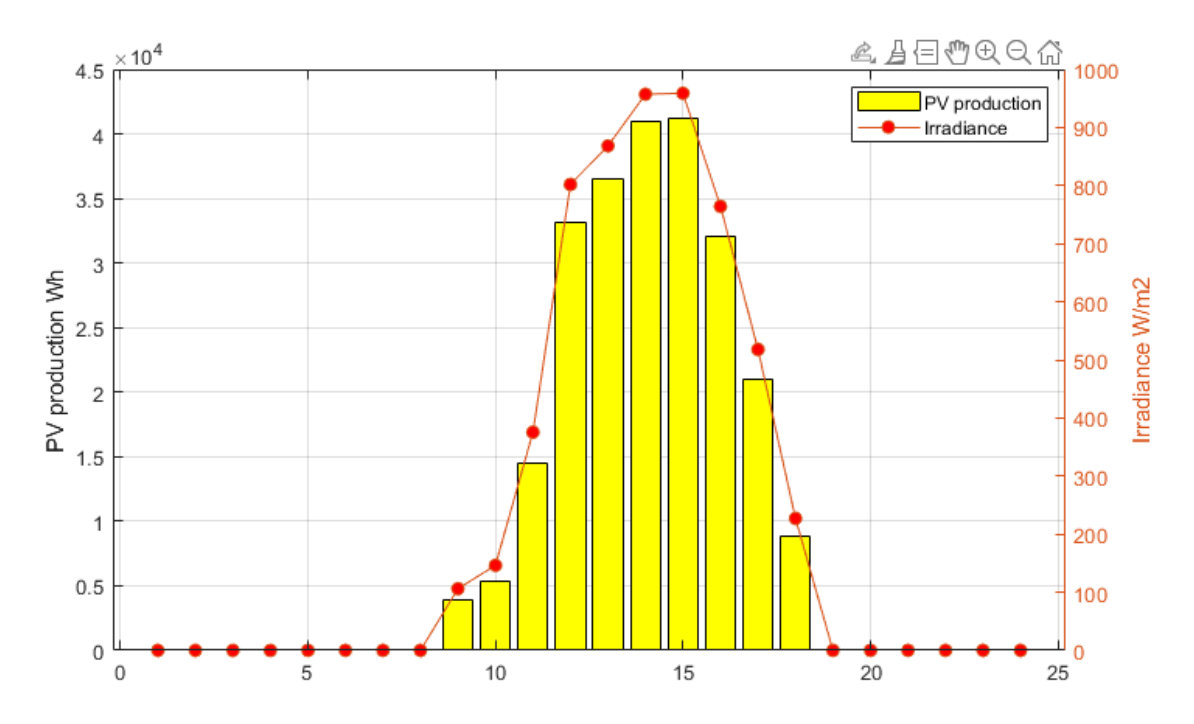


Figure 100. The coldest day plot with PV Production and Irradiance.

In order to establish a more similar baseline for comparison, the schedule of the appliances and the EV charging profile remain the same in the non-optimized scenario of every case.

The coldest day original schedule of controllable appliances and EV charging and battery SOC can be seen in Figs. 101-102.

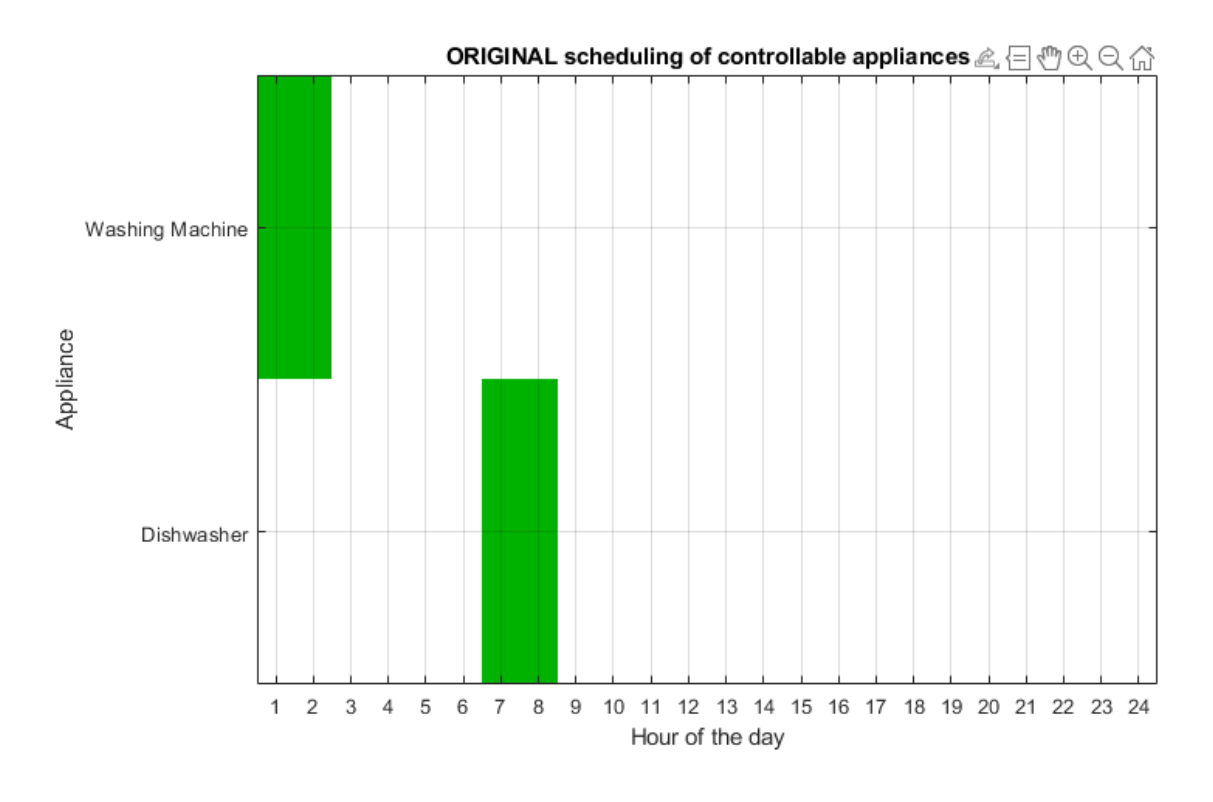


Figure 101. The coldest day scheduling of controllable appliances.

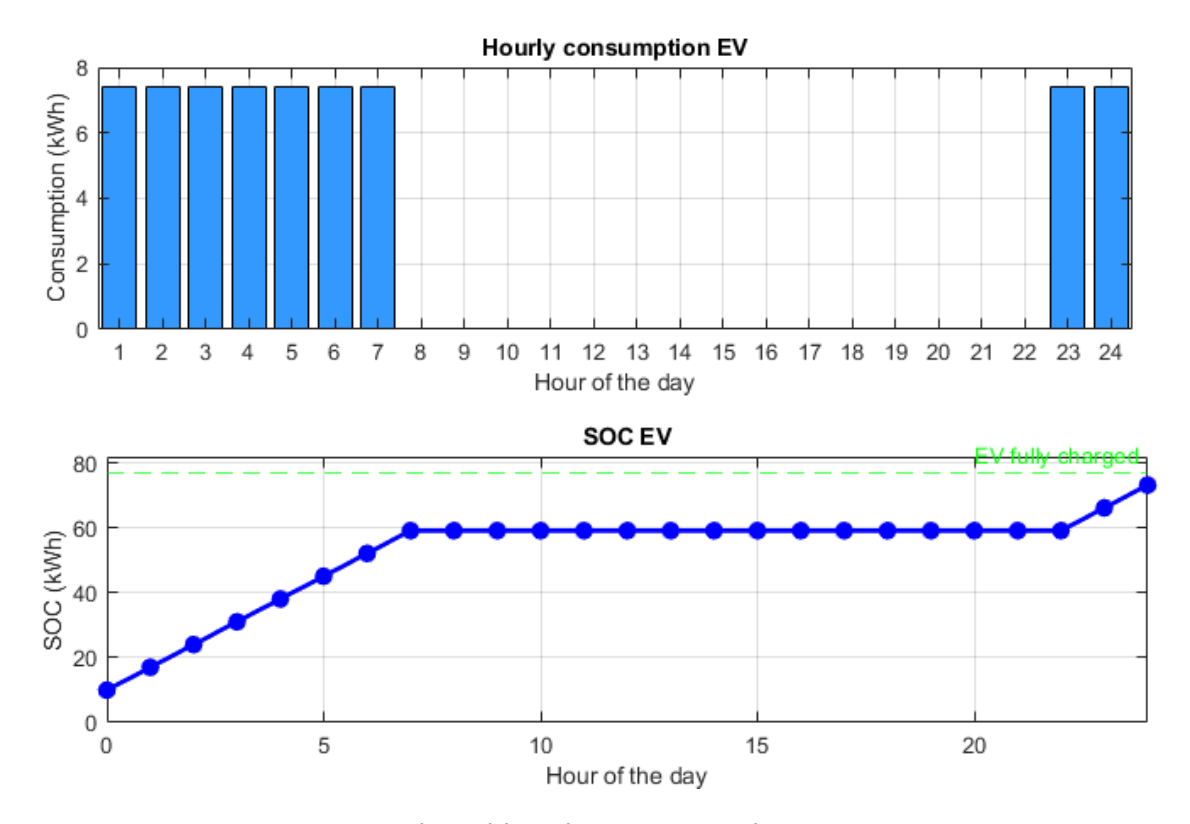


Figure 102. The coldest day EV SOC and Consumption.

The hourly energy consumption is shown in Fig. 103. Also, the Table 13 summarizes the energy consumption and displays the total of each element.

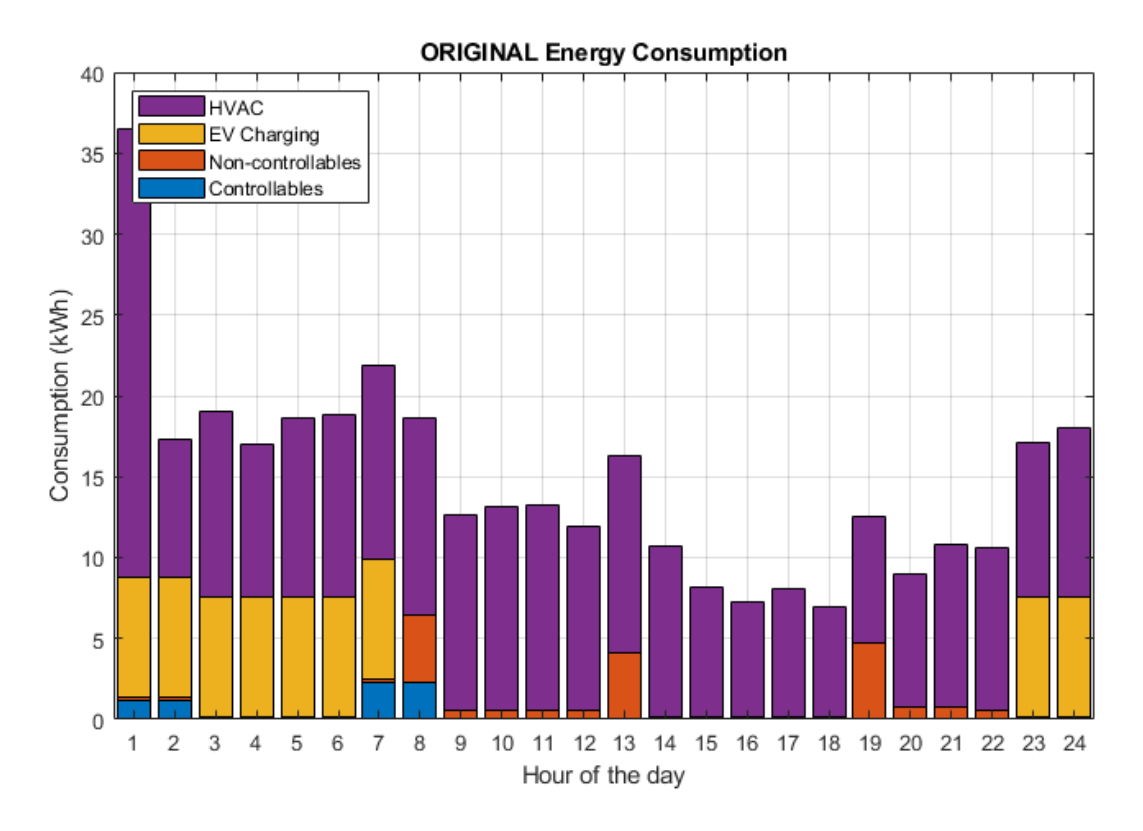


Figure 103. The coldest day hourly energy consumption.

Table 13. The coldest day energy consumption.

ENERGY CONSUMPTION (kWh)						
Hour	CA	N-CA	EV	HVAC	TOTAL HOURLY	
1	1.2	0.15	7.4	27.77	36.52	
2	1.2	0.15	7.4	8.53	17.28	
3	0	0.15	7.4	11.44	18.99	
4	0	0.15	7.4	9.47	17.02	
5	0	0.15	7.4	11.05	18.60	
6	0	0.15	7.4	11.28	18.83	
7	2.3	0.15	7.4	12.03	21.88	
8	2.3	4.15	0	12.13	18.58	
9	0	0.55	0	12.04	12.59	
10	0	0.55	0	12.57	13.12	
11	0	0.55	0	12.67	13.22	
12	0	0.55	0	11.37	11.92	
13	0	4.15	0	12.16	16.31	
14	0	0.15	0	10.53	10.68	
15	0	0.15	0	8.07	8.22	
16	0	0.15	0	7.08	7.23	
17	0	0.15	0	7.92	8.07	
18	0	0.15	0	6.82	6.97	
19	0	4.75	0	7.76	12.51	
20	0	0.75	0	8.19	8.94	
21	0	0.75	0	10.05	10.80	
22	0	0.55	0	10.04	10.59	
23	0	0.15	7.4	9.60	17.15	
24	0	0.15	7.4	10.43	17.98	
TOTAL	7	19.4	66.6	261.01	354.01	

Another thing that changes regarding the previous case is the switch in the cooling/heating mode, as well as the evolution of the temperature indoors during the simulation. This is because the environment is way cooler than before. The HVAC mode and the temperatures for the coldest day are shown in Figs. 104-105.

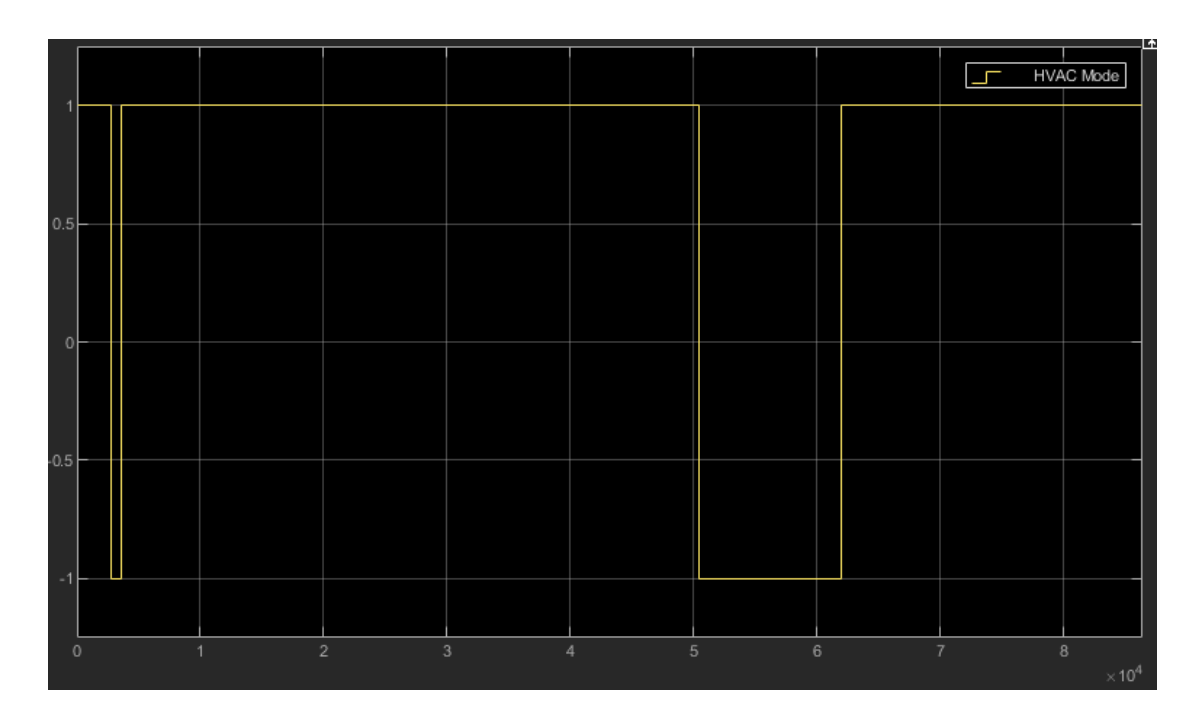


Figure 104. The coldest day HVAC mode.

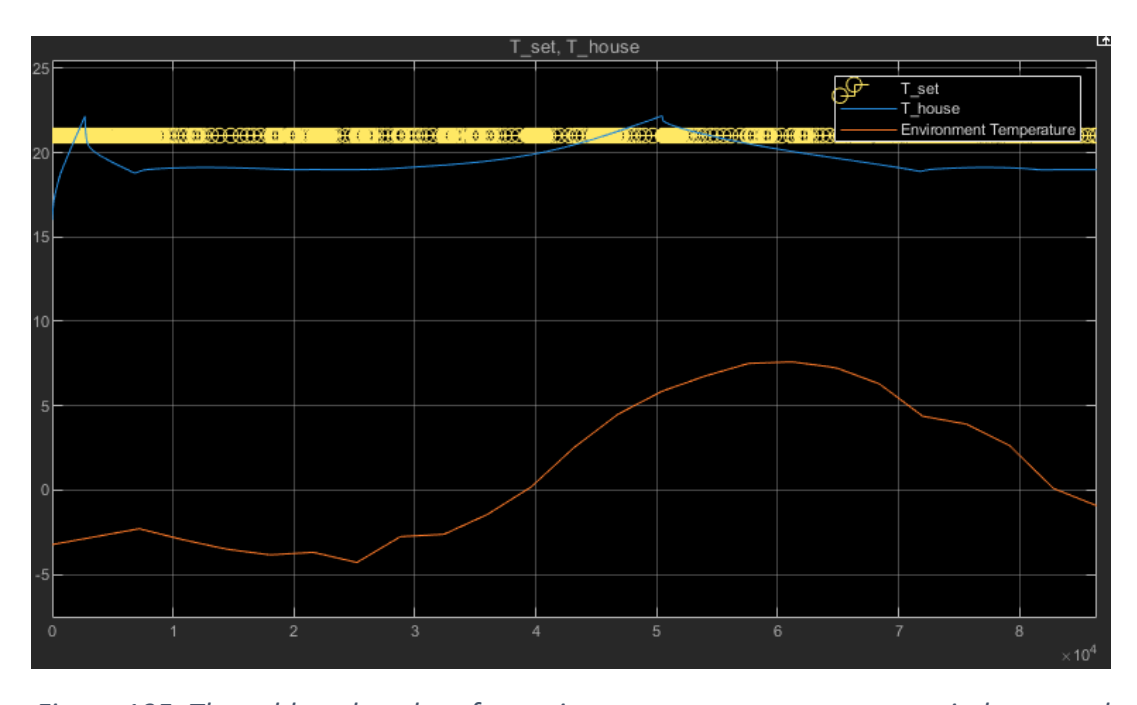


Figure 105. The coldest day plot of setpoint temperature, temperature indoors, and ambient temperature.

As the Fig. 104 shows, the system is operating practically all day in heating mode. There are times when it cools down and this is due to the configuration of the model, as when it works in an hourly mode it heats up above the permitted range, causing the house to have a higher temperature than desired, which is why there are two times when the system makes the decision to cool down. The solution to this would be to have the system make decisions more times over the course of an hour in order to be able to make decisions more accurately than in this case.

Below is a comparison of consumption versus solar production, as well as the evolution of the state of the battery, where in this case it is at 10% of its capacity for a long time (it cannot be discharged more than that), so the energy must be drawn from the electrical grid. This can be seen in the energy flow diagram of Fig. 106, where the large deficit can be observed. This situation is due to the discharge of the battery causing the battery to be at the 10% limit and not being able to discharge more energy. Also, as there is a higher energy consumption than the solar production, the battery cannot be charged.

The battery SOC and the original energy flows for the coldest day are shown in Figs. 107-108.

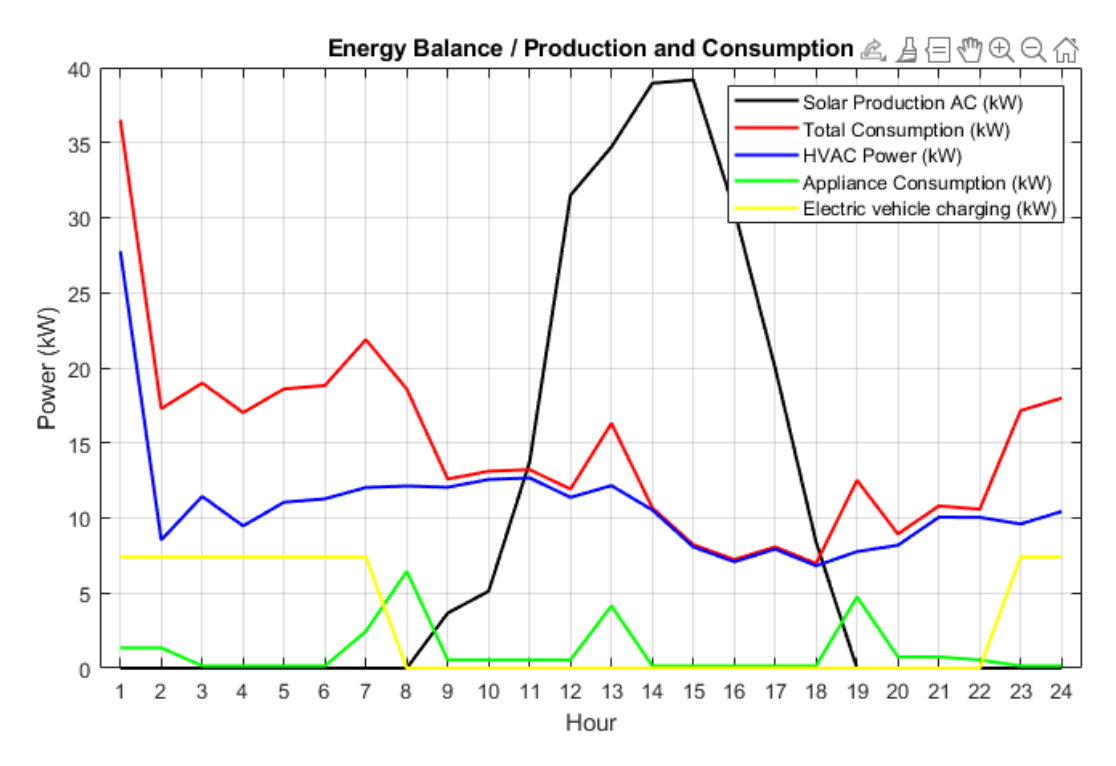


Figure 106. The coldest day Energy Balance.

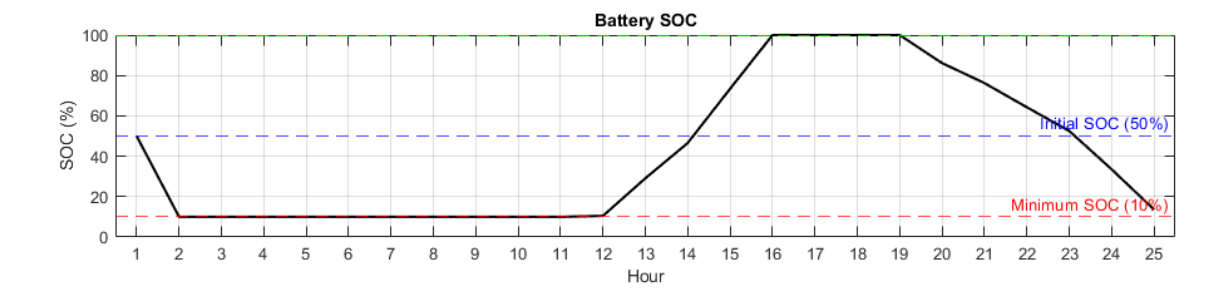


Figure 107. The coldest day Battery SOC.

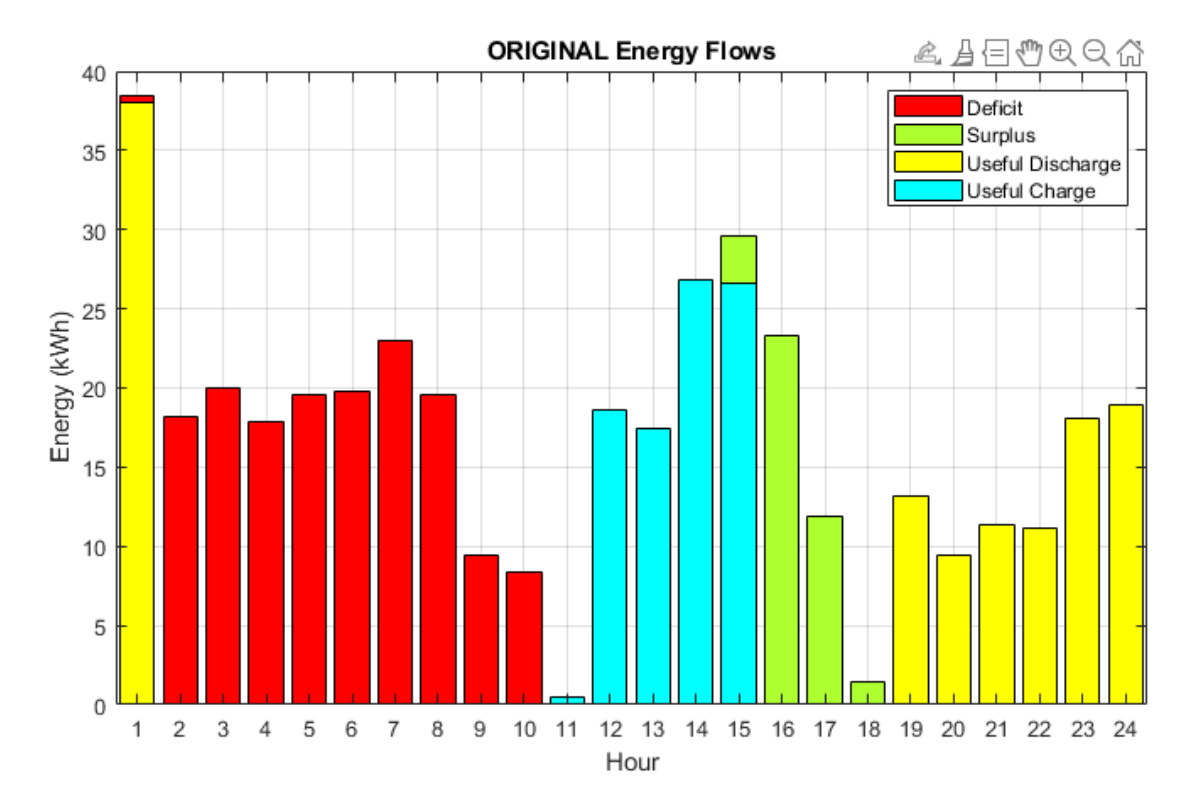


Figure 108. The coldest day Energy Flows.

After applying the optimisers, the following results are presented in Figs. 109-125.

The optimization starts with the reallocation of the hours of use of the loads, in other words, the hours of use of the controllable appliances, as well as the charging of the electric vehicle. As previously mentioned, the timetable of the electrical appliances and the electric vehicle in the original cases will remain constant and that is why it is not shown again in each case.

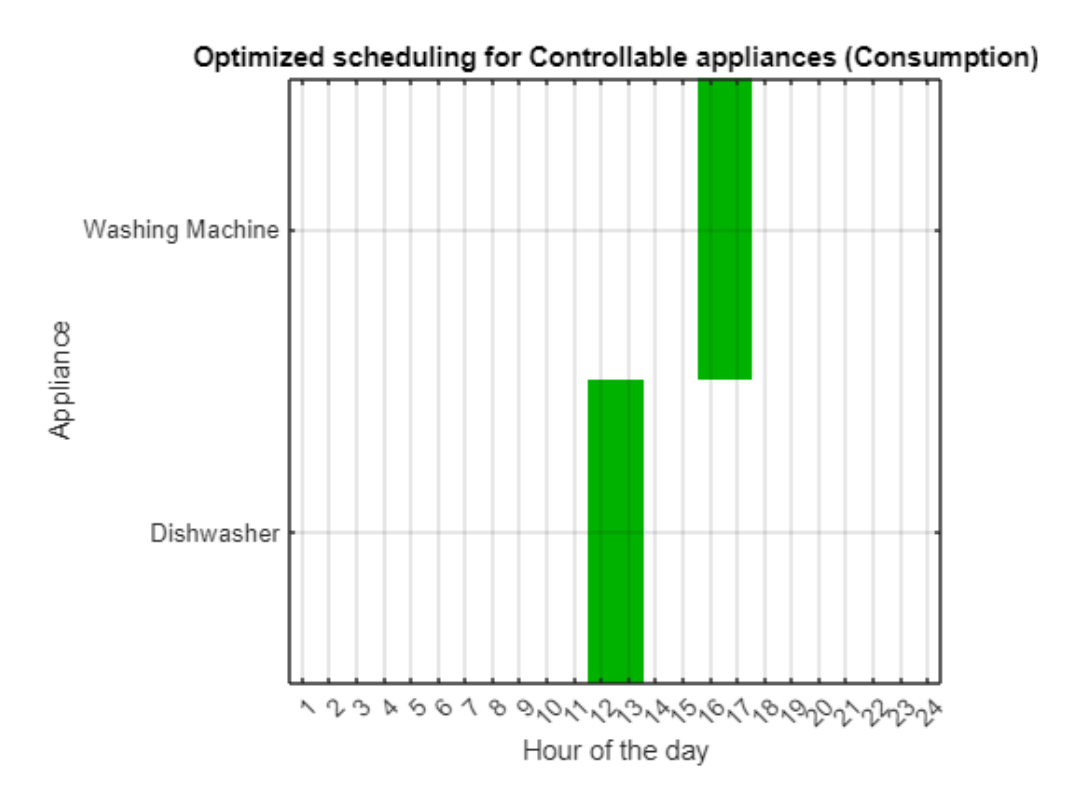


Figure 109. The coldest day scheduling of controllable appliances for optimization for minimum consumption.

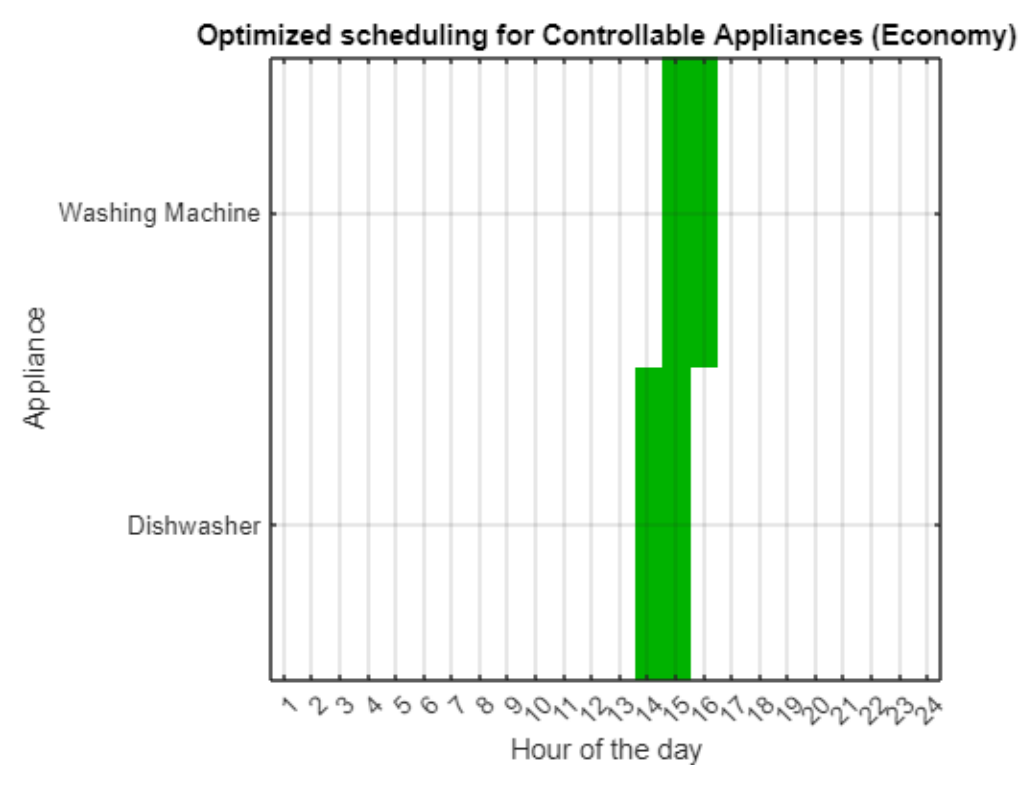


Figure 110. The coldest day scheduling of controllable appliances for optimization for maximum net economic benefit.

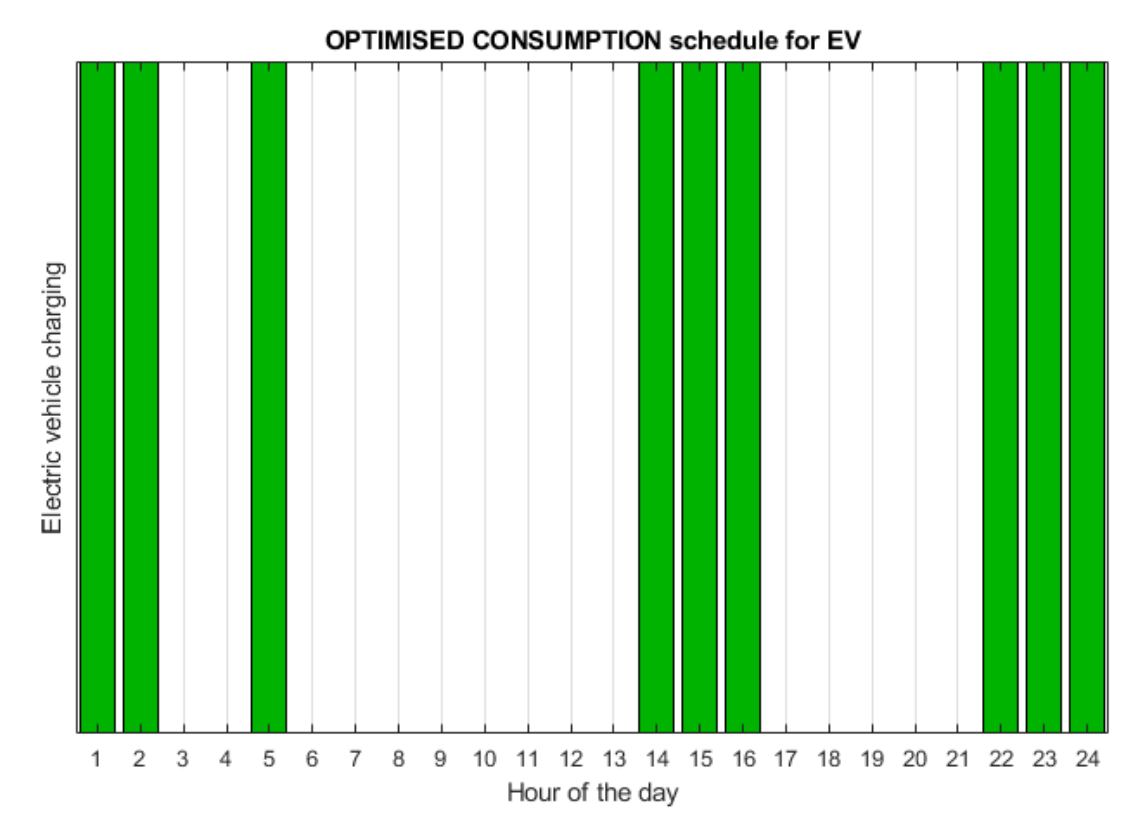


Figure 111. The coldest day EV charging schedule for optimization for minimum consumption.

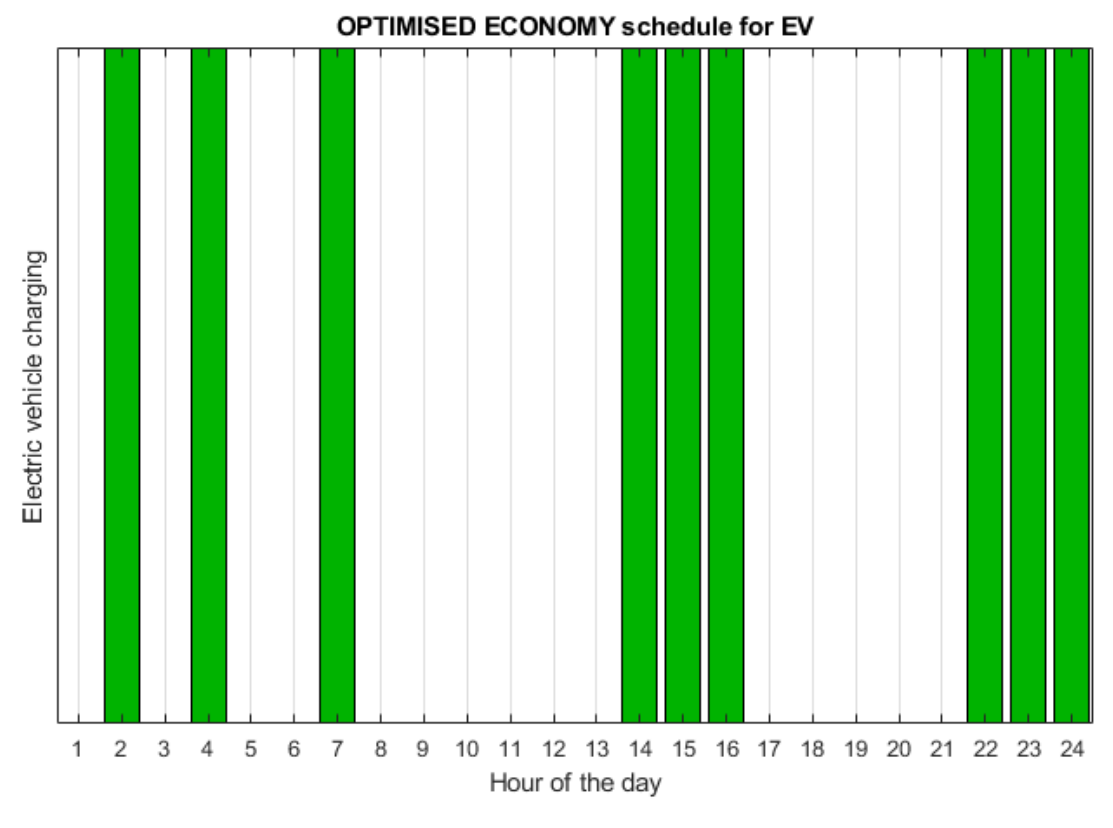


Figure 112. The coldest day EV charging schedule for optimization for maximum net economic benefit.

The optimised schedule for the charging of the electric vehicle makes the EV's battery charge as shown in Fig. 113.

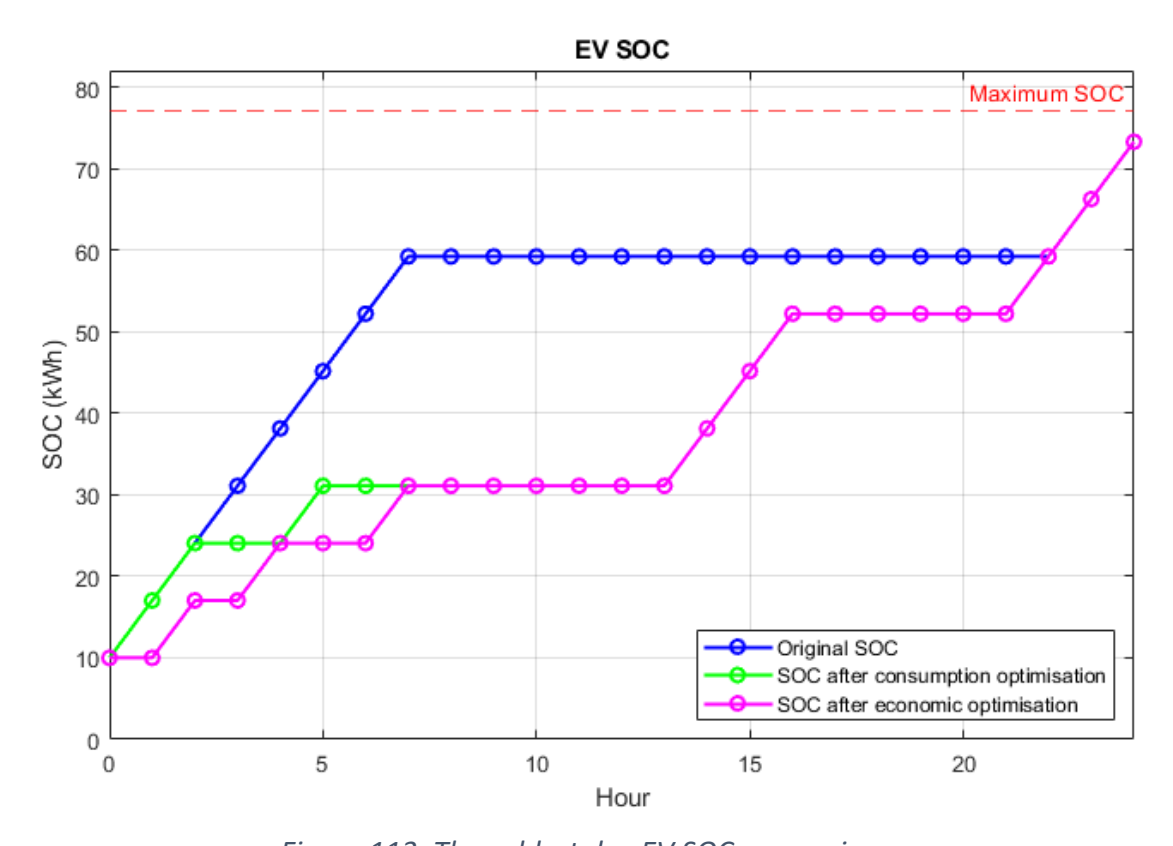


Figure 113. The coldest day EV SOC comparison.

A summary of the EV's batteries performance is shown in Table 14.

Table 14. The coldest day EV parameters.

ELECTRIC VEHICLE	ORIGINAL	OPTIMIZATION FOR	OPTIMIZATION FOR
		MINIMUM	MAXIMUM NET
		CONSUMPTION	ECONOMIC
			BENEFIT
Initial SOC (kWh)	10	10	10
Final SOC (kWh)	73.27	73.27	73.27
Charging	63.27	63.27	63.27
performed (kWh)			
Charging	66.60	66.60	66.60
consumption			
(kWh)			

Charging hours	9	9	9
Battery missing	3.73	3.73	3.73
(kWh)			

As has been done so far, the consumption before optimisation is shown in Fig. 114 and compare it with the results of the two optimizers, shown in Figs. 115-116. Here it can clearly be seen where the load hours are reallocated as they are broken down by colour. Accompanying the consumption, the evolution of the batteries in both the non-optimised and the two optimised cases can be found in Fig. 117.

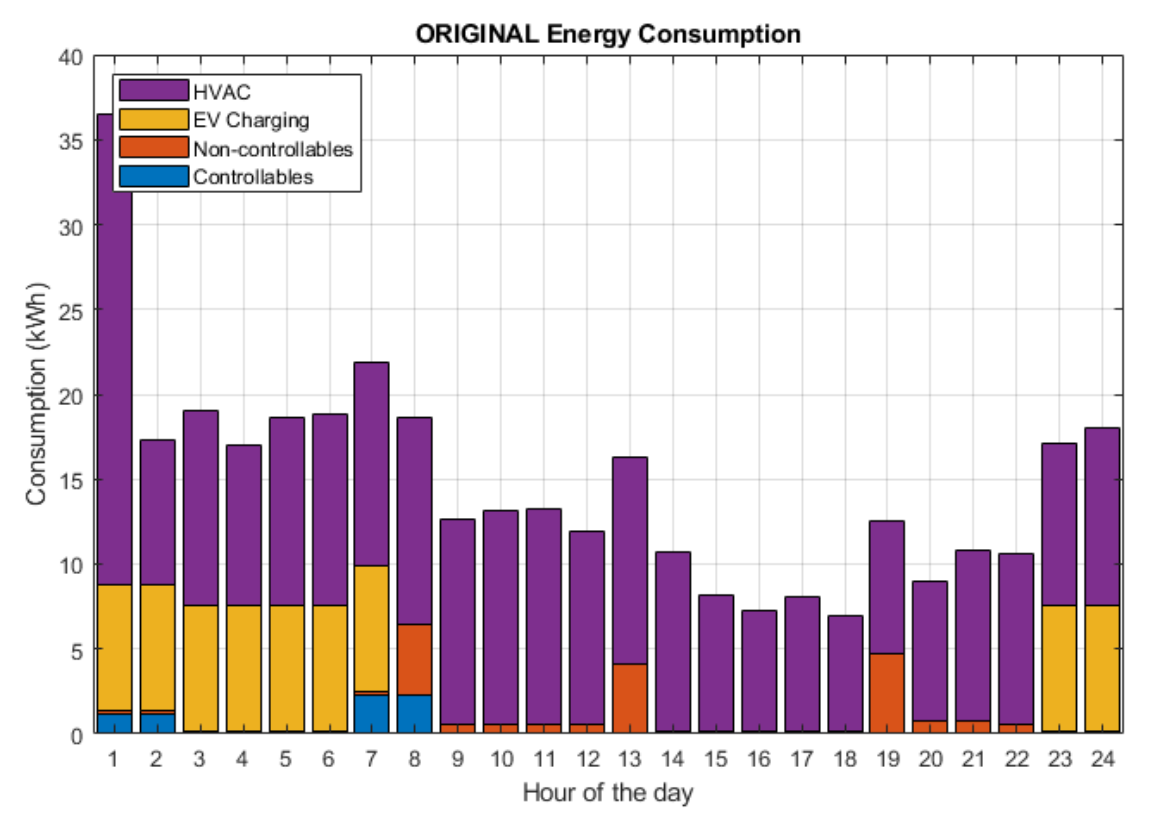


Figure 114. The coldest day original energy consumption.

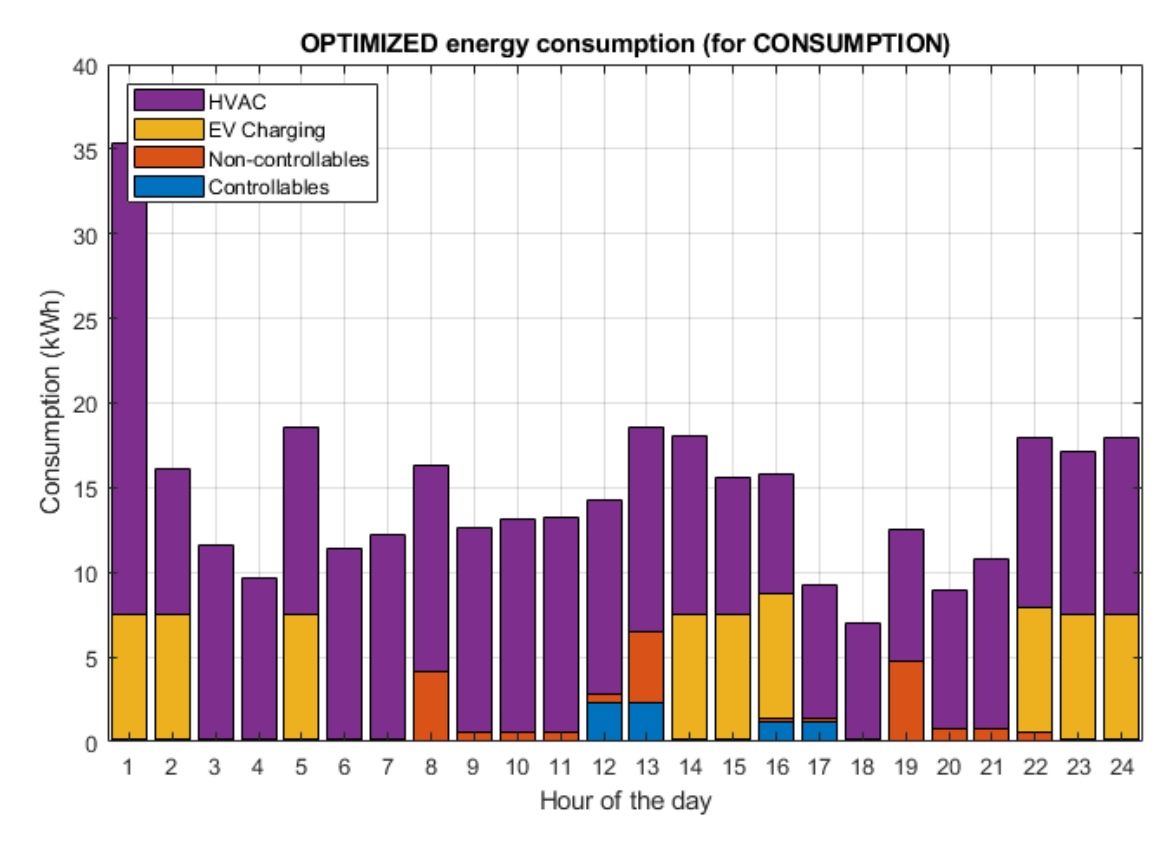


Figure 115. The coldest day energy consumption for optimization for minimum energy consumption.

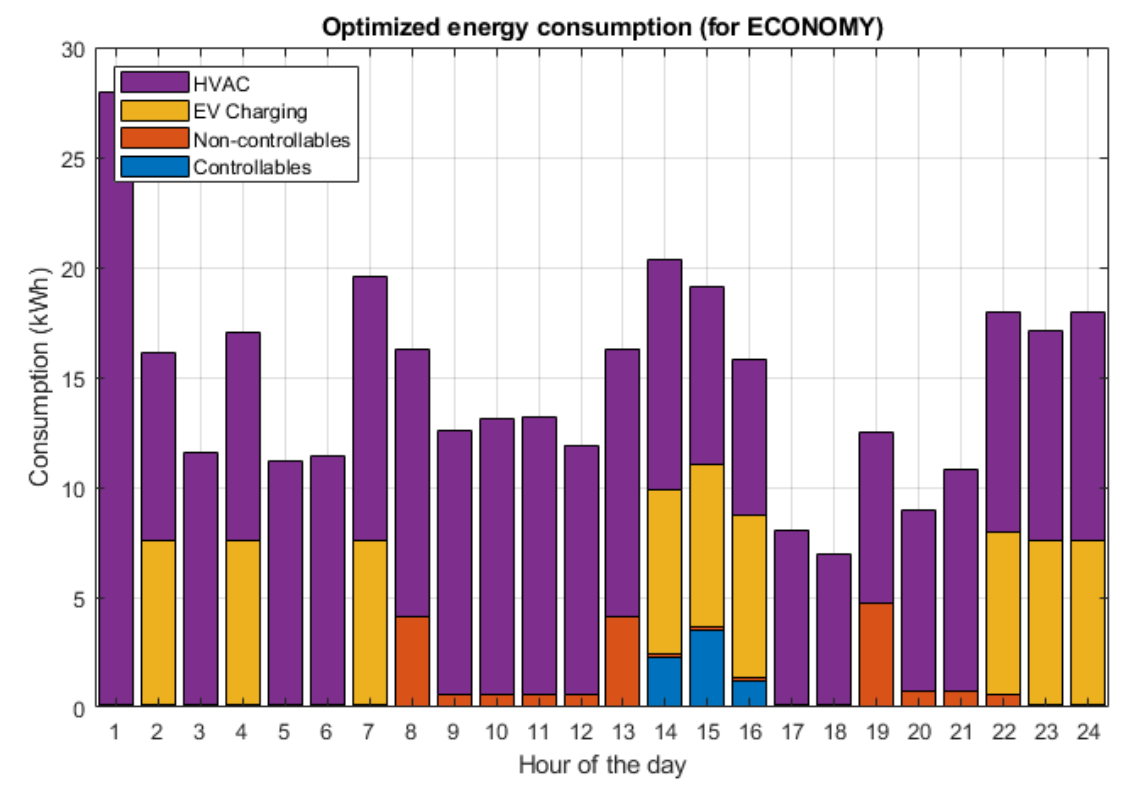


Figure 116. The coldest day energy consumption for optimization for maximum net economic benefit.

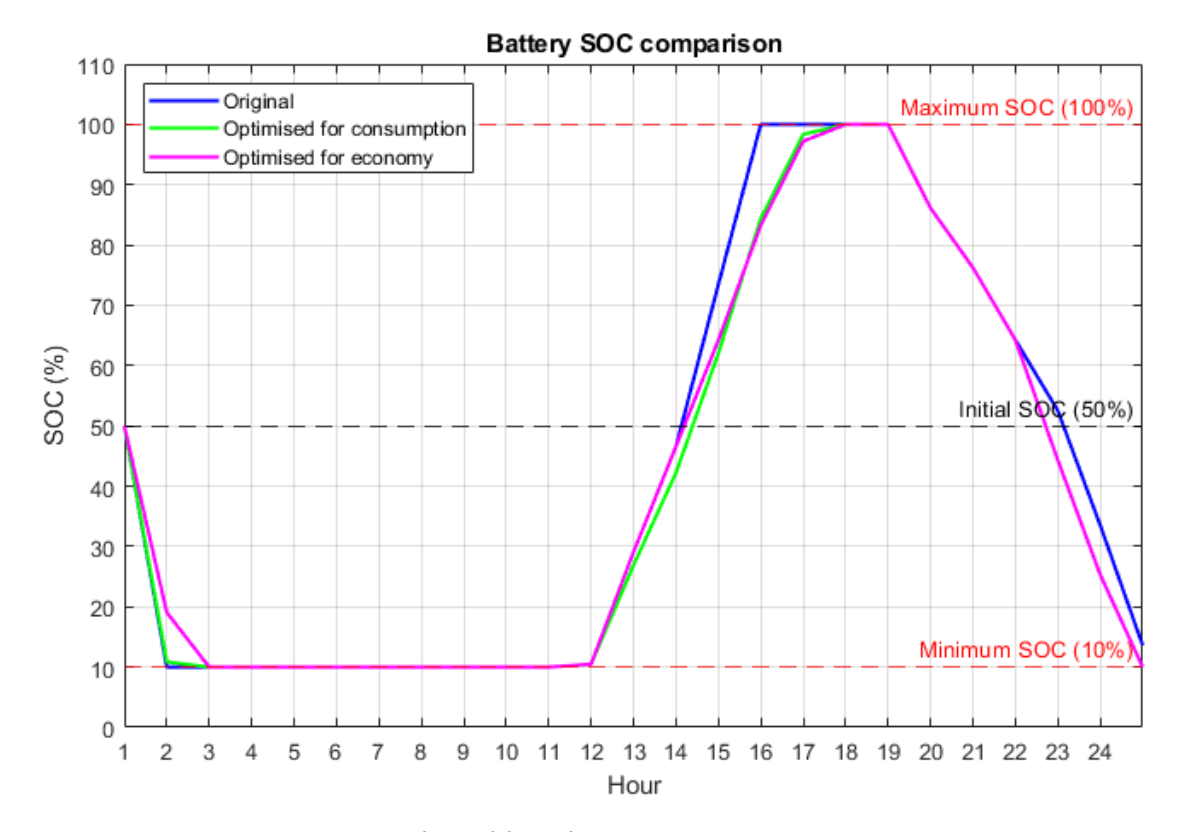


Figure 117. The coldest day Battery SOC comparison.

To get a better overview of the performance of the batteries throughout the simulation, the Table 15 is shown.

The results do not change because the feasible solution space is constrained, leading both optimizers to a very similar optimal point where the there is no difference between the behaviour of the batteries. Also in the coldest day, the temperature conditions are the most demanding, so the system has limited flexibility due to the constraints and severe temperature conditions, leading to fewer viable optimal solutions.

Table 15. The coldest day batteries parameters summary.

BATTERIES	ORIGINAL	OPTIMIZATION FOR	OPTIMIZATION FOR
		MINIMUM	MAXIMUM NET
		CONSUMPTION	ECONOMIC
			BENEFIT
Initial SOC (kWh)	50	50	50
Final SOC (kWh)	13.60	10	10

Charged performed	90	90	90
(kWh)			
Discharge	120.08	123.50	123.50
performed (kWh)			

Moving on to the economic study, the graphs presented in Figs. 118-119 inform us of the purchase/sale of energy in the non-optimised and optimised cases, while also the Table 16 is generated as a summary to present the total amount of energy bought and sold in order to be able to easily determine the benefit, as well as the improvement compared to the original case.

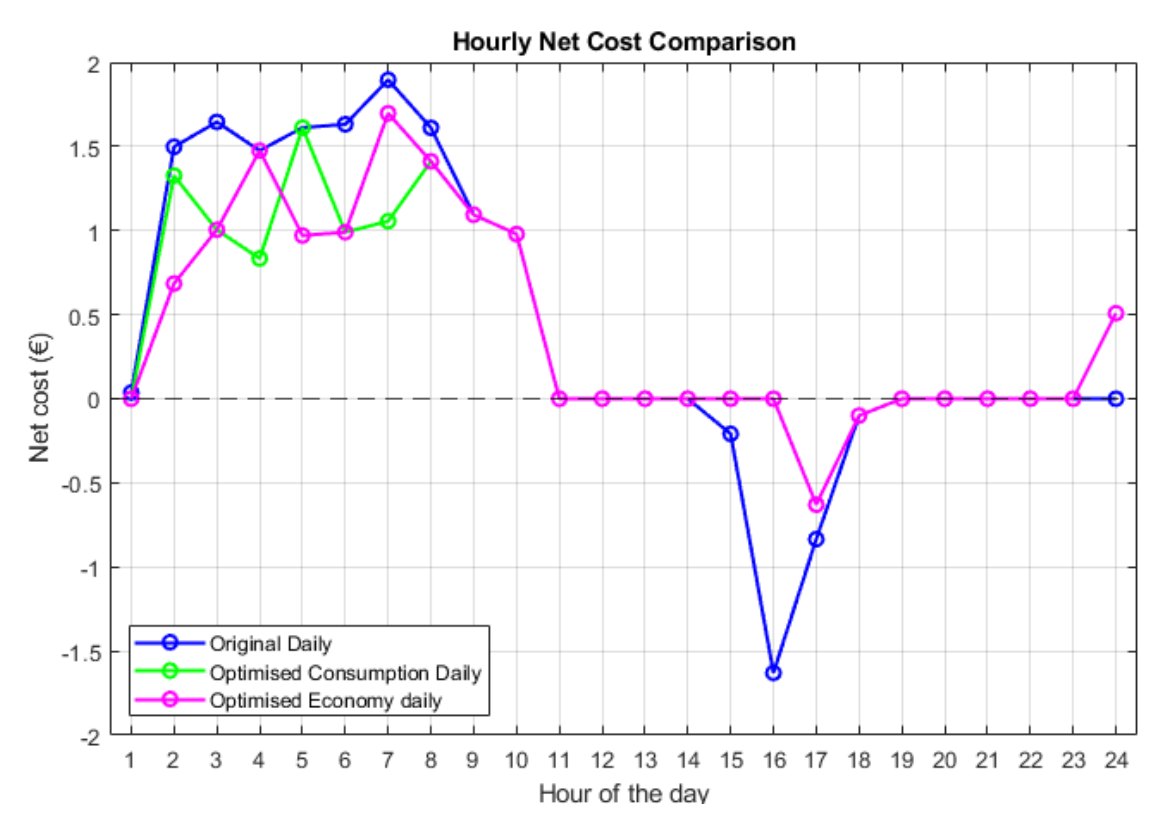


Figure 118. The coldest day hourly net cost comparison for weekdays.

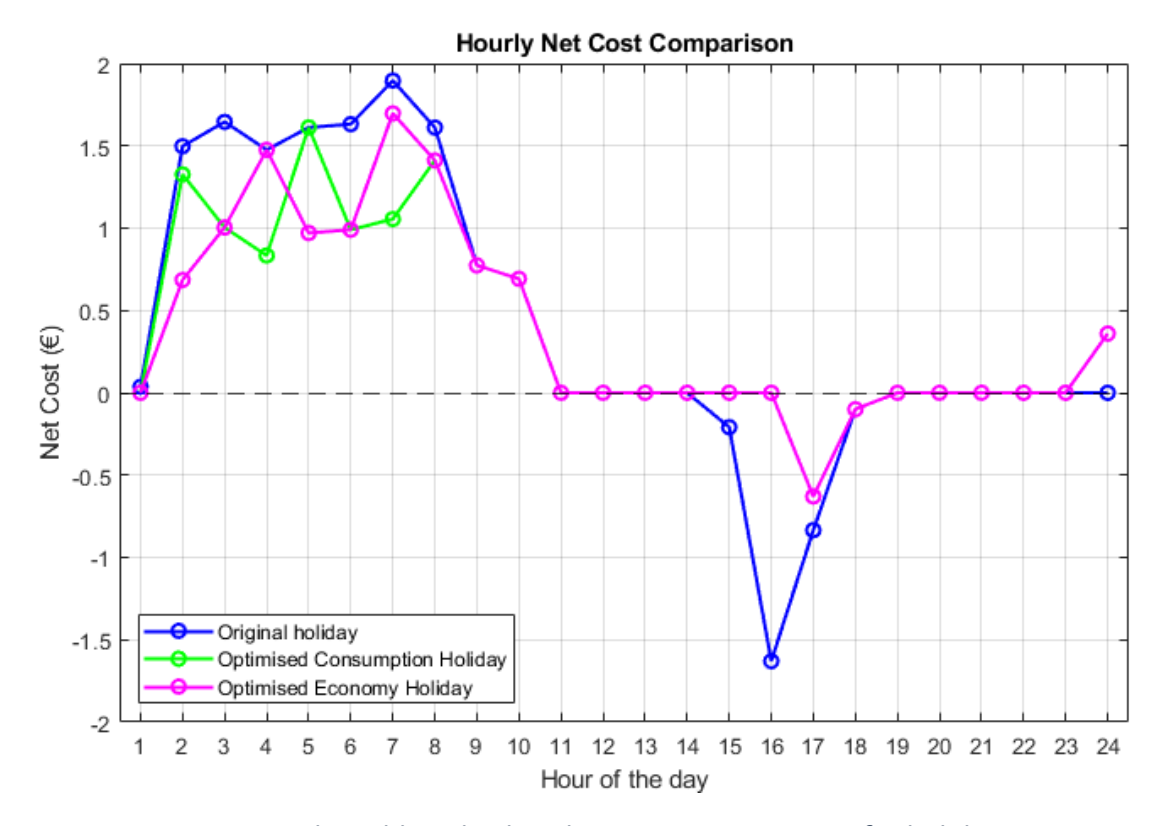


Figure 119. The coldest day hourly net cost comparison for holidays.

Table 16 shows consistent results because the restricted solution space causes both optimization methods to arrive at nearly identical outcomes, yielding the same economic cost. On the coldest day, the system faces the most challenging temperature demands, which further restrict its operational flexibility. As a result, the combination of tight constraints and extreme weather significantly narrows the range of acceptable optimal solutions.

Table 16. The coldest day economic cost comparison.

ECONOMIC COST						
	DAILY					
	ORIGINAL	OPTIMISED FOR CONSUMPTION	OPTIMIZATION FOR MAXIMUM			
	NET ECONOMIC BENEFIT					
Purchase cost (€)	13.48	10.81	10.81			
Selling profit (€)	2.77	0.73	0.73			
Net cost (€)	10.70	10.09	10.09			
Economic saving		0.62 (5.8%)	0.62 (5.8%)			

PUBLIC HOLIDAYS AND WEEKENDS					
Purchase cost (€)	12.87	10.06	10.06		
Selling profit (€)	2.77	0.73	0.73		
Net cost (€)	10.10	9.33	9.33		
Economic saving		0.77 (7.6%)	0.77 (7.6%)		

To conclude the case of the coldest day of the year, the summary of energy consumption and generation before and after optimization is shown in Figs. 120-122. In addition to the energy flows with their summary table, as in previous cases, the improvement compared to the base case is calculated and the total quantities of the parameters relevant to this study are shown in Figs. 123-125 and Table 17.

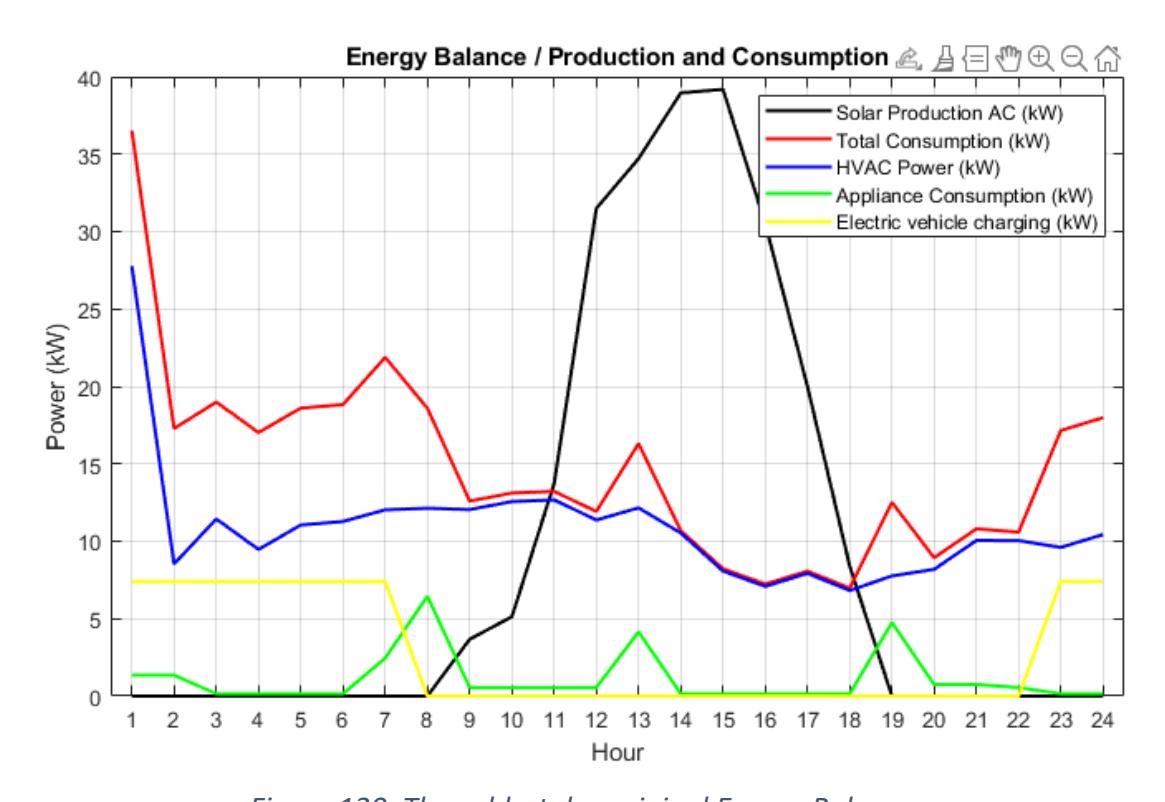


Figure 120. The coldest day original Energy Balance.

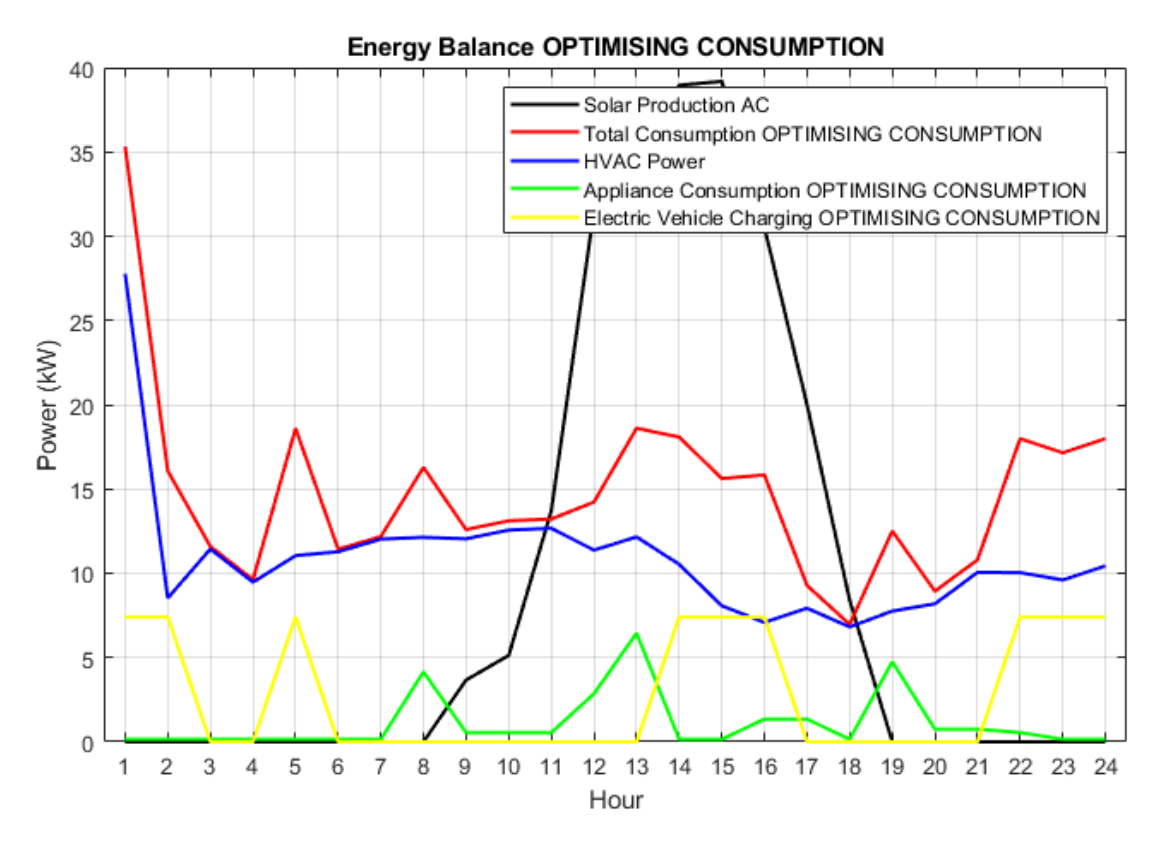


Figure 121. The coldest day Energy Balance for optimization for minimum consumption.

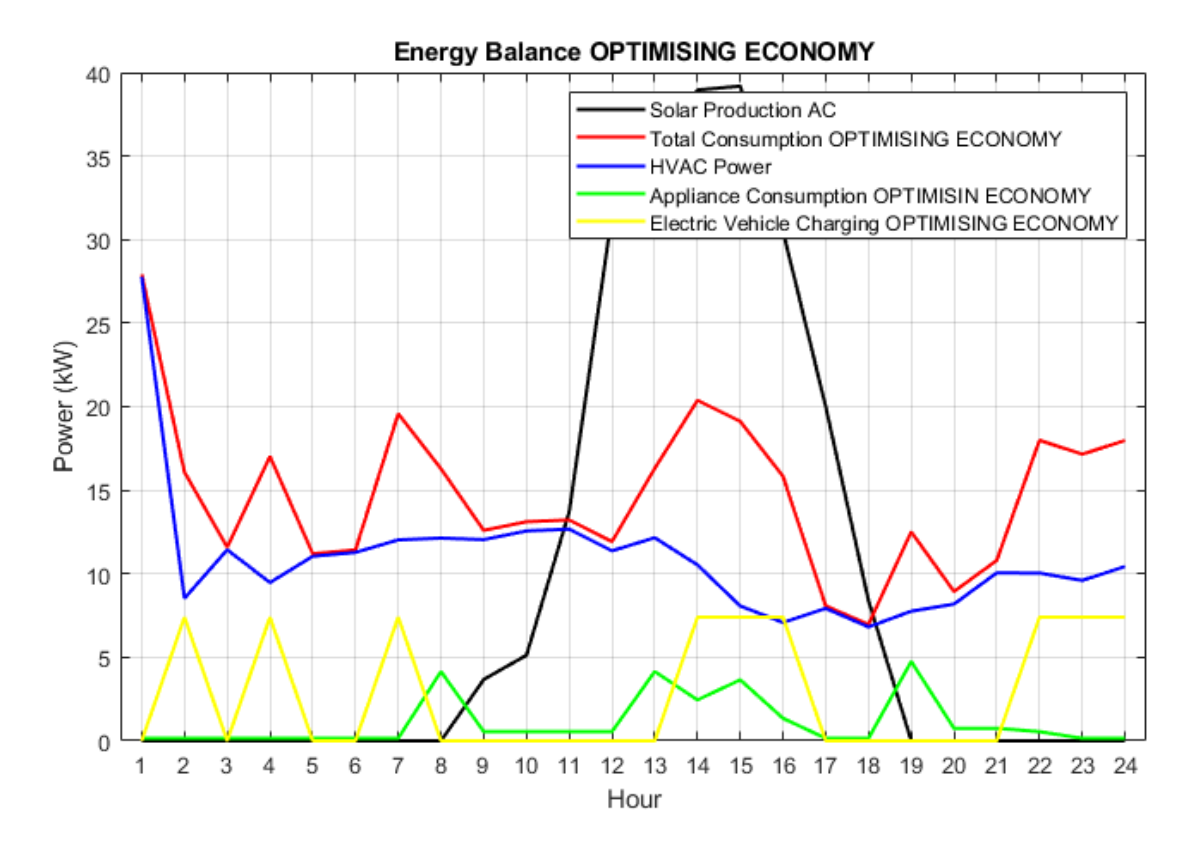


Figure 122. The coldest day Energy Balance for optimization for maximum net economic benefit.

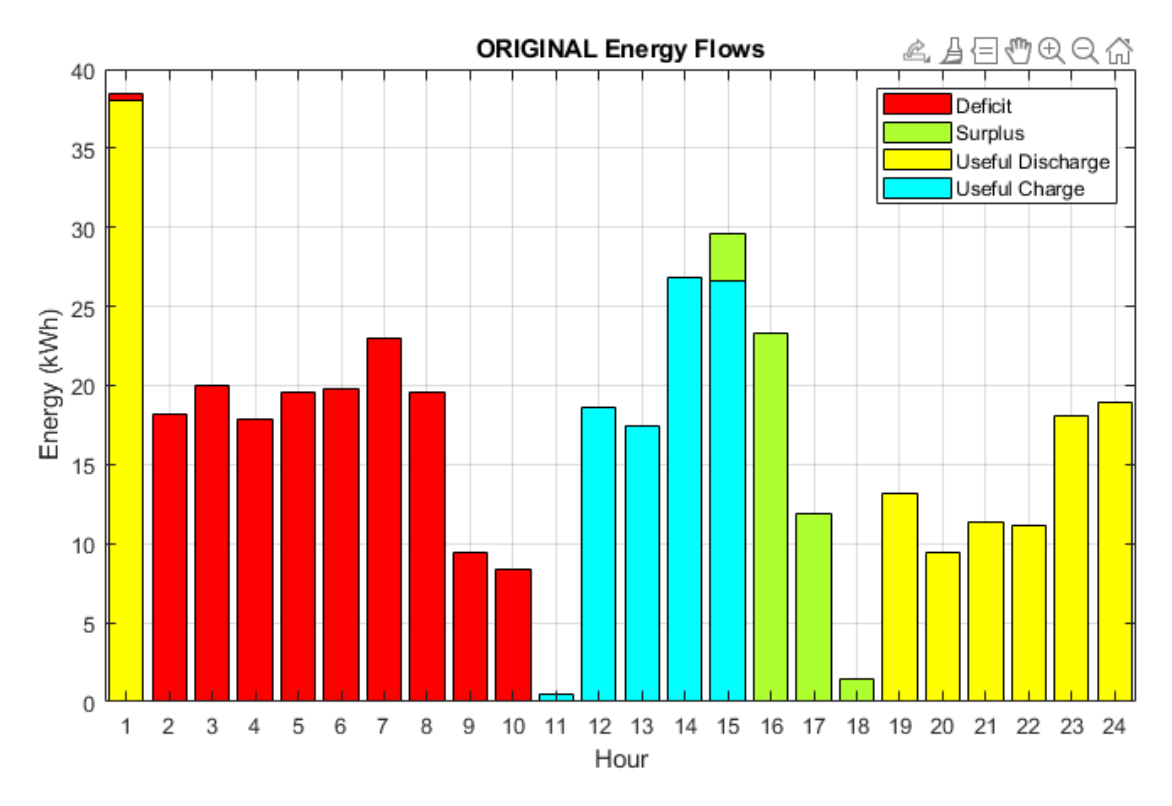


Figure 123. The coldest day original Energy Flows.

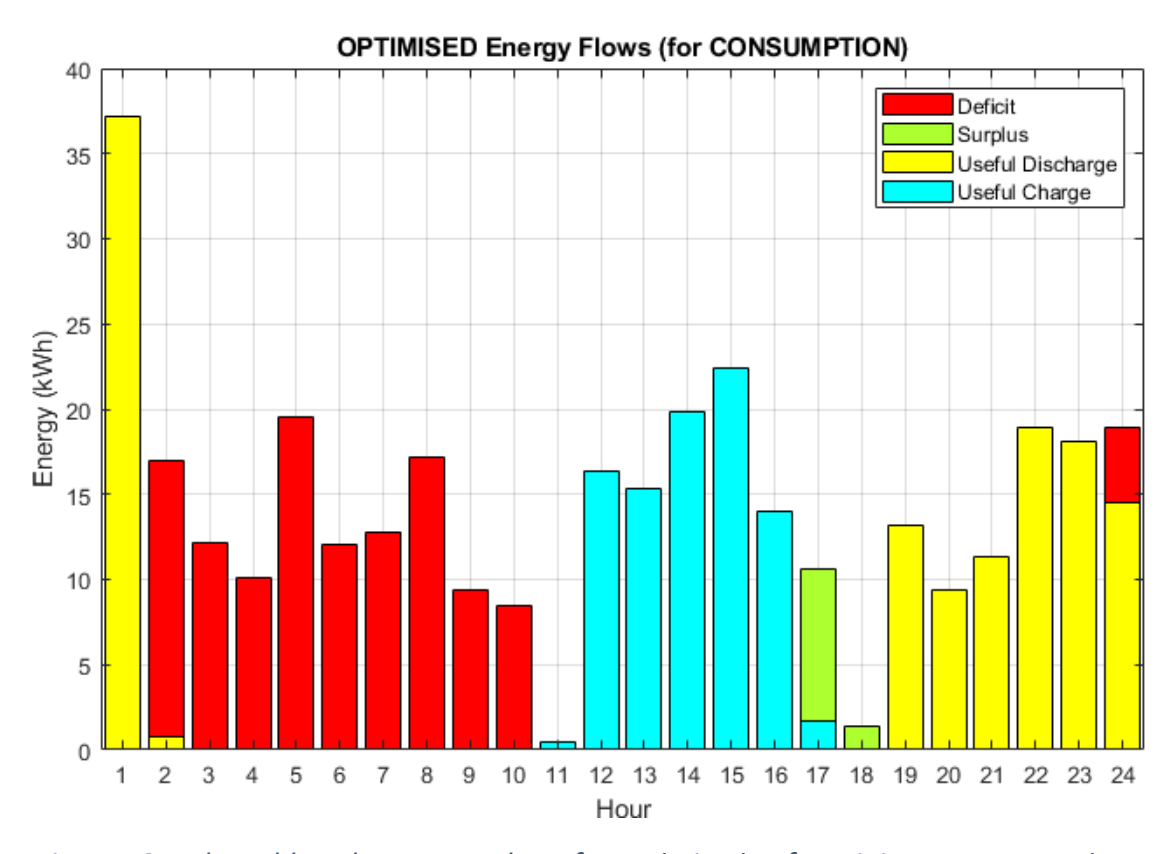


Figure 124. The coldest day Energy Flows for optimization for minimum consumption.

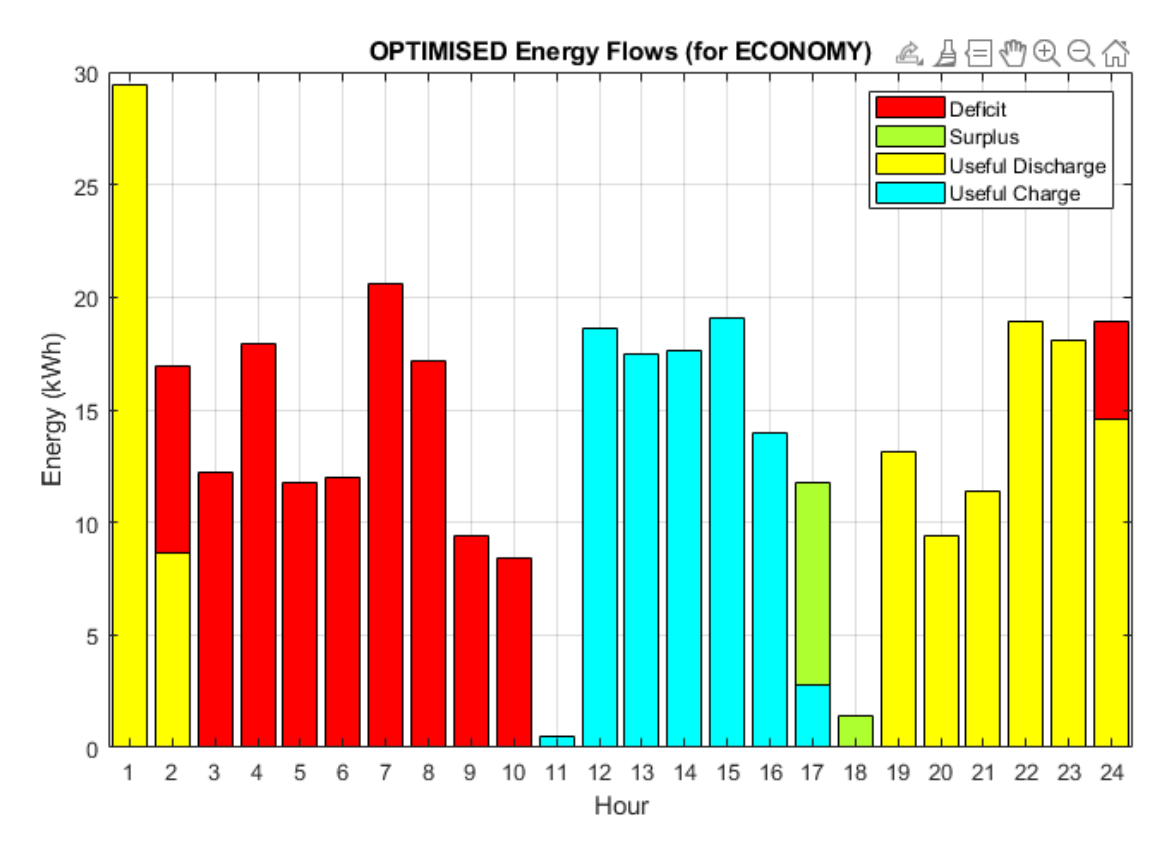


Figure 125. The coldest day Energy Flows for optimization for maximum net economic benefit.

Due to the severe temperatures and constraints, the system has limited flexibility to achieve different solutions. The extreme environmental conditions significantly narrow the feasible operating range forcing both optimizers to converge toward the same energy flows. Under these demanding conditions, the battery system's operational parameters become heavily restricted, leaving little room for alternative solutions.

Table 17. The coldest day Energy Flows summary.

ENERGY	ORIGINAL	OPTIMIZATION FOR	OPTIMIZATION FOR
FLOWS		MINIMUM	MAXIMUM NET
		CONSUMPTION	ECONOMIC BENEFIT
Surplus (kWh)	39.62	10.42	10.42
Deficit (kWh)	156.33	122.17	122.17
Improvement		34.16 (21.9%)	34.16 (21.9%)

The hottest day

As has been done so far, the case without optimization is presented, commenting only on what has changed with respect to the previous cases, following the same structure as before. Subsequently, the comparative results of the original case with respect to the optimised ones are presented.

In this case the temperature indoors, environment and setpoint initially change compared to the previous cases. In order to have a more realistic approach, the setpoint is 22 (±2) °C, the initial temperature indoors is going to be 25°C and the environmental temperature at 26°C.

The hottest day hourly solar data is shown in Table 18.

Table 18. The hottest day hourly solar data.

Hour	Irradiance	T environment	T panel	PV Production DC
	(W/m²)	(°C)	(°C)	(kWh)
1	0	25.44	25.44	0
2	0	24.14	24.14	0
3	0	22.7	22.70	0
4	0	21.6	21.60	0
5	0	21.02	21.02	0
6	0	20.36	20.36	0
7	44.93	19.97	21.37	1.81
8	214.8	22.54	29.25	8.95
9	432.87	27.22	40.75	18.94
10	662.83	30.7	51.41	30.30
11	824.72	33.05	58.82	38.83
12	949.75	34.86	64.54	45.72
13	1000.53	36.56	67.83	48.76
14	906.52	38.04	66.37	43.94
15	561.84	39.03	56.59	26.22
16	491.48	39.36	54.72	22.77

17	309.76	37.72	47.40	13.93
18	185.13	36.65	42.44	8.16
19	27.7	36.56	37.423	1.20
20	9.55	34.47	34.77	0.41
21	0	32.5	32.50	0
22	0	30.89	30.89	0
23	0	29.37	29.37	0
24	0	27.8	27.80	0
		309.91		

The plots of the environmental temperature and temperature of the PV panels are presented in Fig. 126, while the solar irradiance and PV energy production are plotted in Fig. 127.

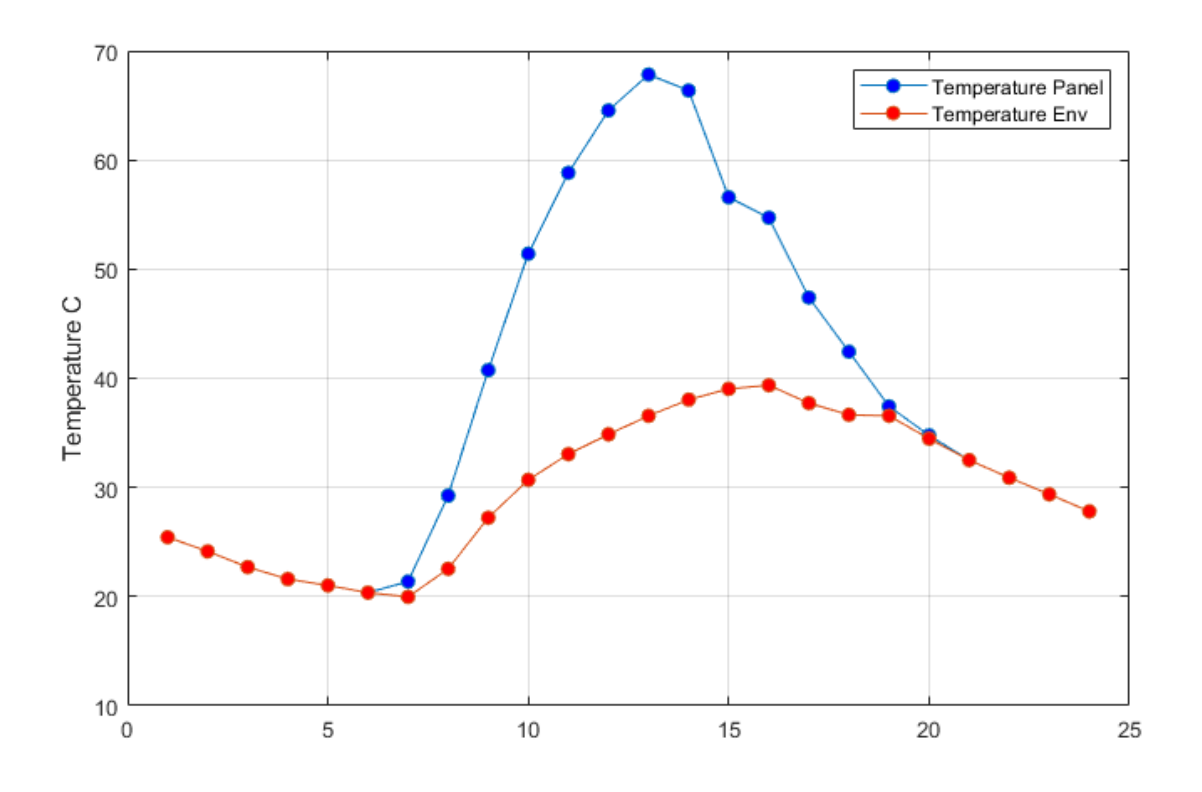


Figure 126. The hottest day plot with Temperature of the Panel and Ambient Temperature.

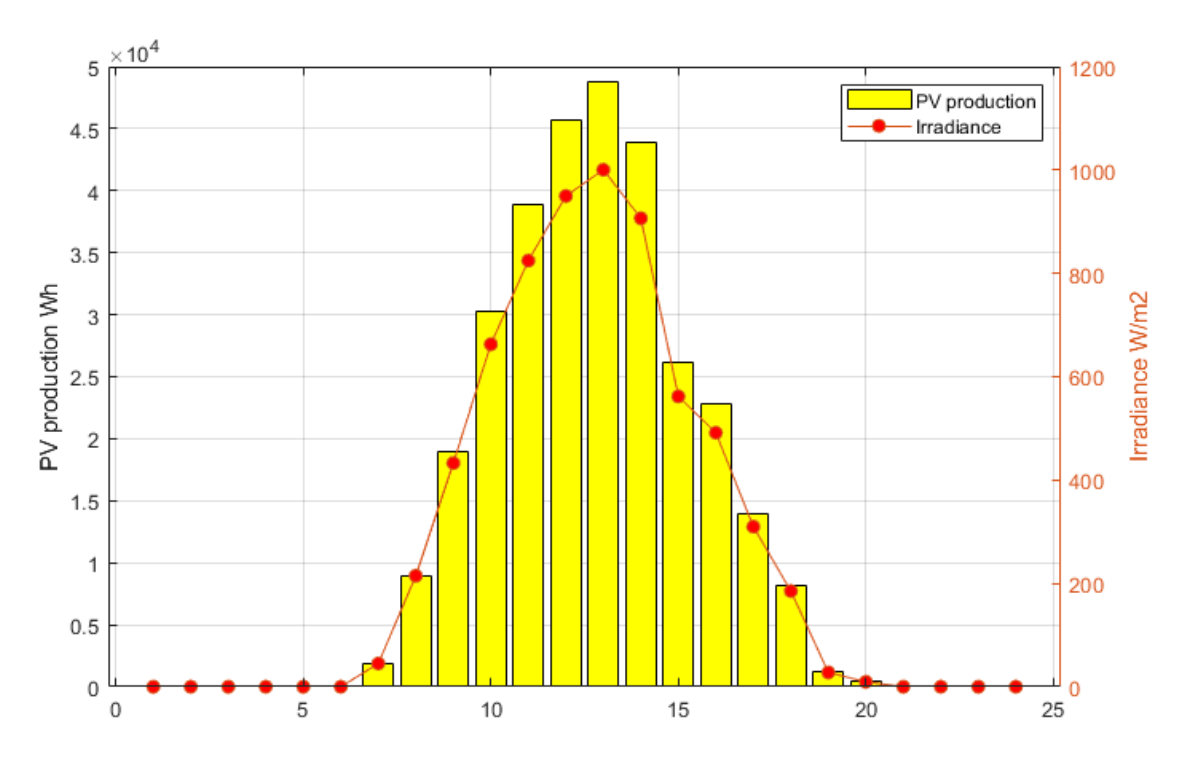


Figure 127. The hottest day plot with PV Production and Irradiance.

The original schedule of the loads remains constant during the different cases of study.

The hottest day original schedule of controllable appliances and EV charging and consumption and SOC of the EV are shown in Figs. 128-129.

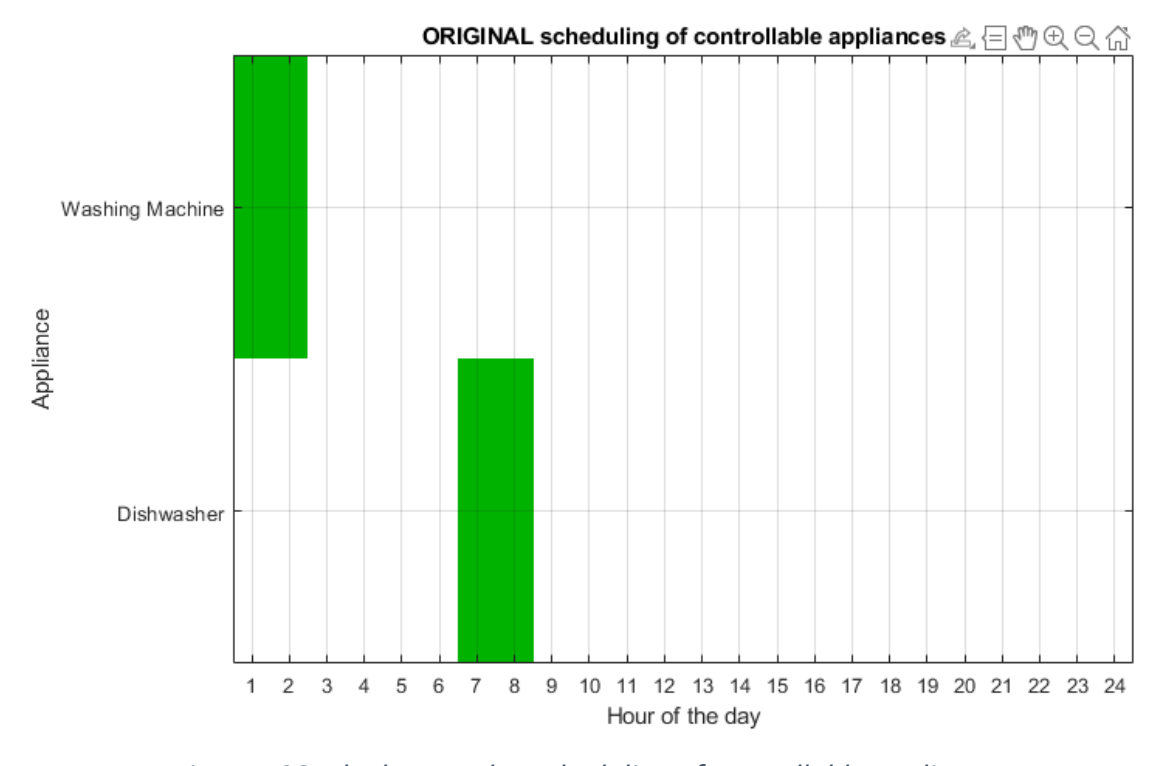


Figure 128. The hottest day scheduling of controllable appliances.

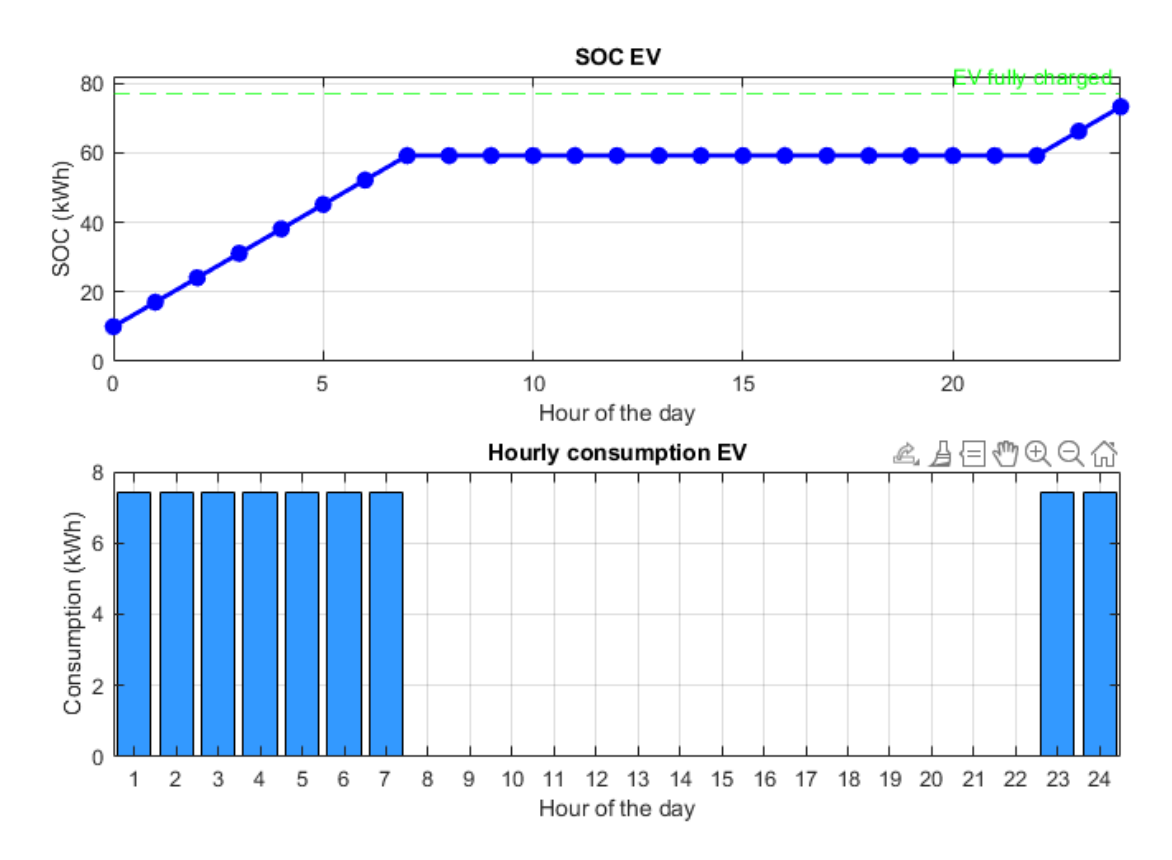


Figure 129. The hottest day EV SOC and Consumption.

In the same way, the consumption without including the HVAC remains the same, because none of the loads varies due to temperature, unlike the HVAC consumption which depends on the outside and target temperature levels, respectively. The hottest day hourly energy consumption can be seen in Fig. 130 and the Table 19 shows a summary of the hourly energy consumption.

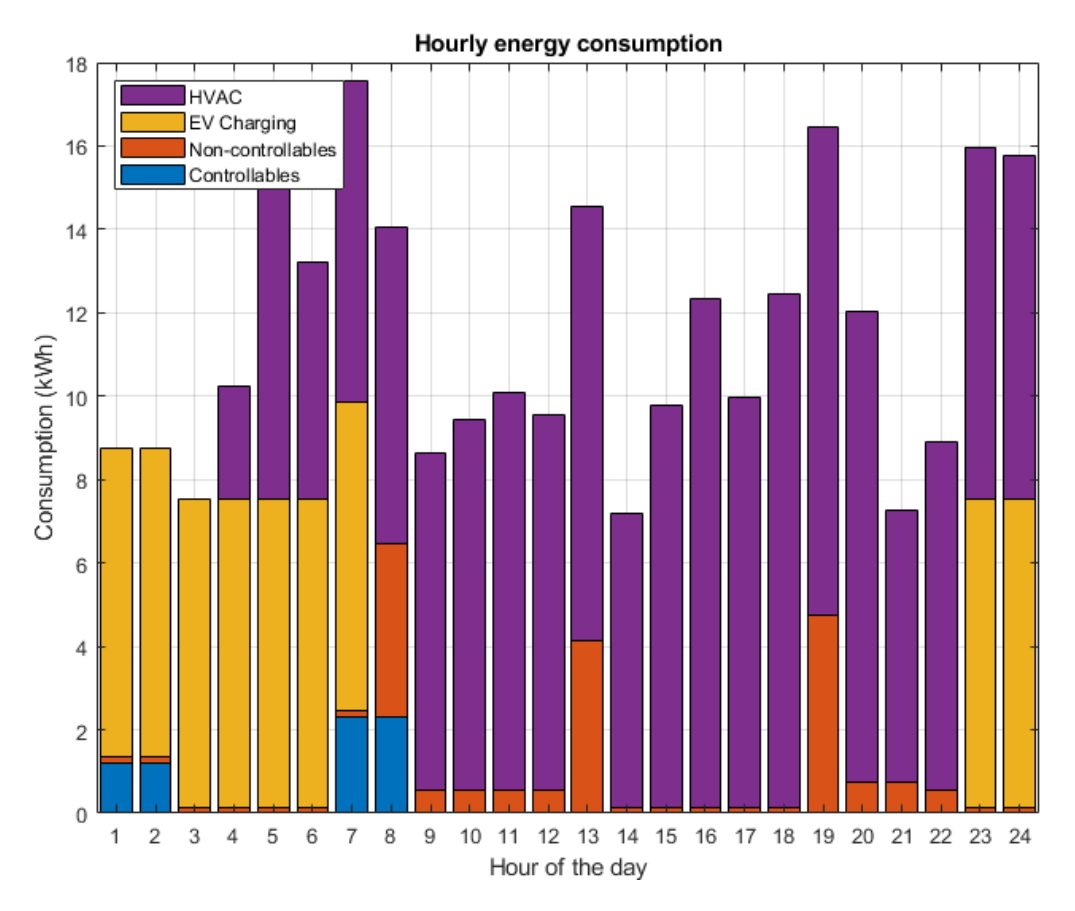


Figure 130. The hottest day hourly energy consumption.

Table 19. The hottest day energy consumption.

	ENERGY CONSUMPTION (kWh)						
					TOTAL		
Hour	CA	N-CA	EV	HVAC	HOURLY		
1	1.2	0.15	7.4	0	8.75		
2	1.2	0.15	7.4	0	8.75		
3	0	0.15	7.4	0	7.55		
4	0	0.15	7.4	2.70	10.25		
5	0	0.15	7.4	8.32	15.87		
6	0	0.15	7.4	5.67	13.22		
7	2.3	0.15	7.4	7.72	17.57		
8	2.3	4.15	0	7.61	14.06		
9	0	0.55	0	8.08	8.63		
10	0	0.55	0	8.89	9.44		

11	0	0.55	0	9.53	10.08
12	0	0.55	0	8.99	9.54
13	0	4.15	0	10.40	14.55
14	0	0.15	0	7.05	7.20
15	0	0.15	0	9.62	9.77
16	0	0.15	0	12.19	12.34
17	0	0.15	0	9.83	9.98
18	0	0.15	0	12.31	12.46
19	0	4.75	0	11.70	16.45
20	0	0.75	0	11.27	12.02
21	0	0.75	0	6.51	7.26
22	0	0.55	0	8.34	8.89
23	0	0.15	7.4	8.43	15.98
24	0	0.15	7.4	8.22	15.77
TOTAL	7	19.4	66.6	183.40	276.40

The results which are different so far is the irradiance, the environmental temperature, the temperature of the PV panels, as well as the solar production and the HVAC consumption.

The HVAC mode and the relevant temperatures are shown in Figs. 131-132 respectively.

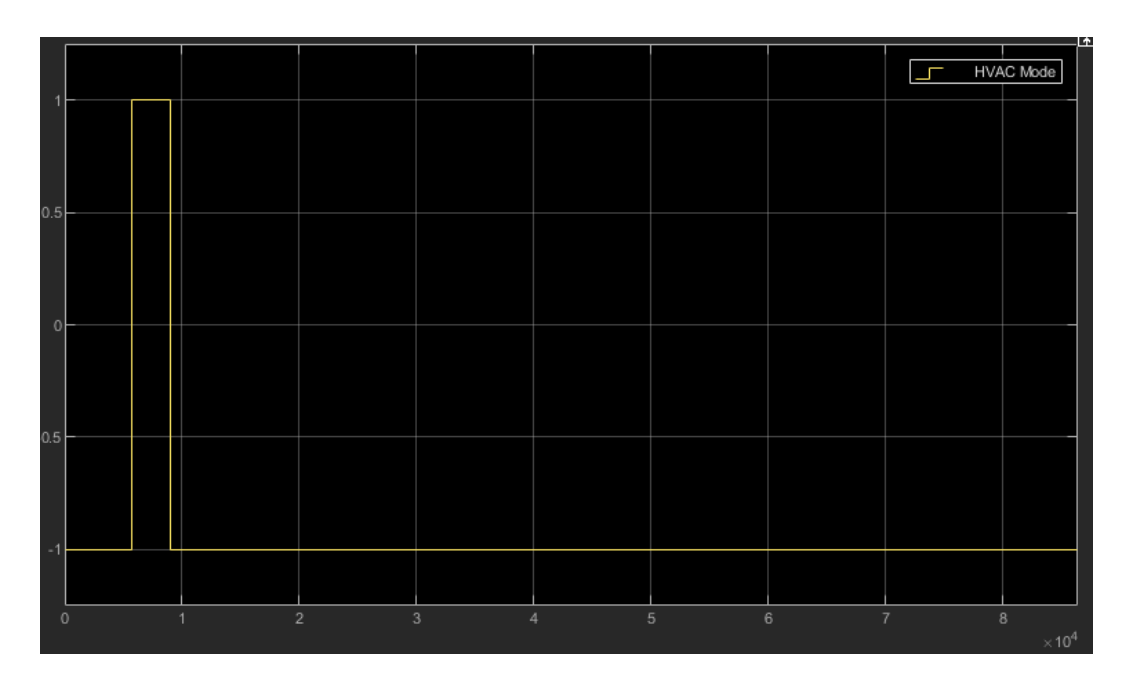


Figure 131. The hottest day HVAC mode.

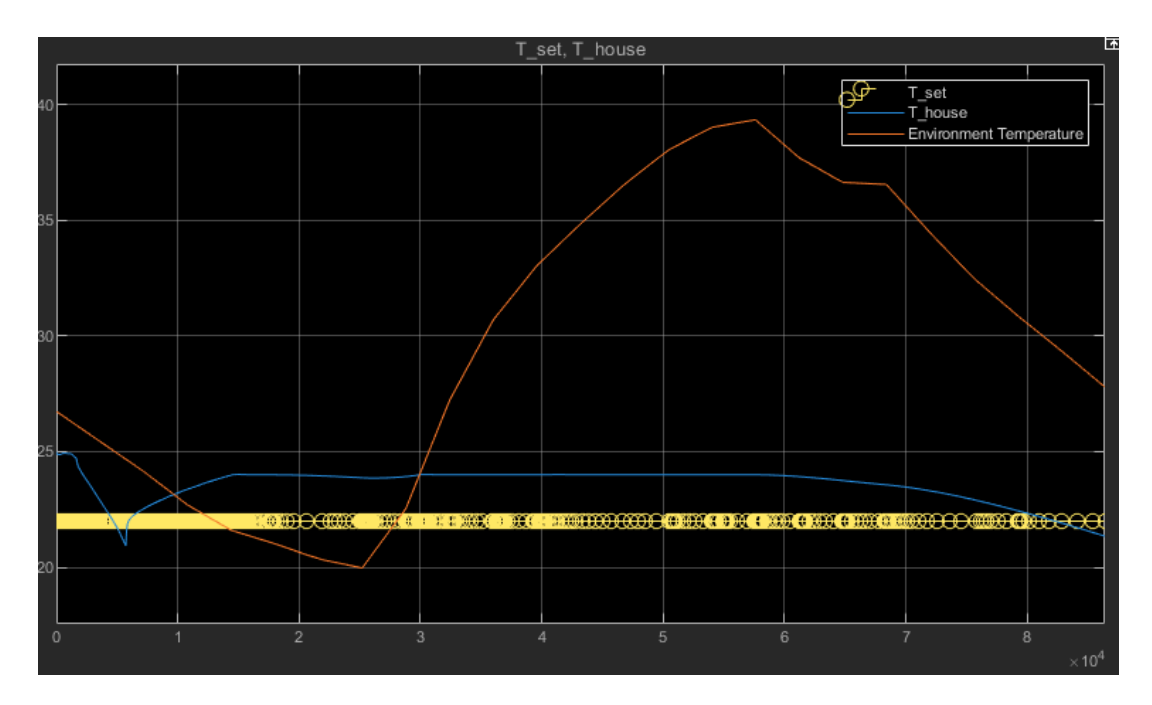


Figure 132. The hottest day plot of setpoint temperature, temperature indoors and ambient temperature.

The switching in the heating/cooling mode is explained exactly in the same way as in the previous case, however, now it's working in cooling mode instead of heating. Figs. 133-135 show the original energy balance for the hottest day, the battery SOC and the original energy flows respectively.

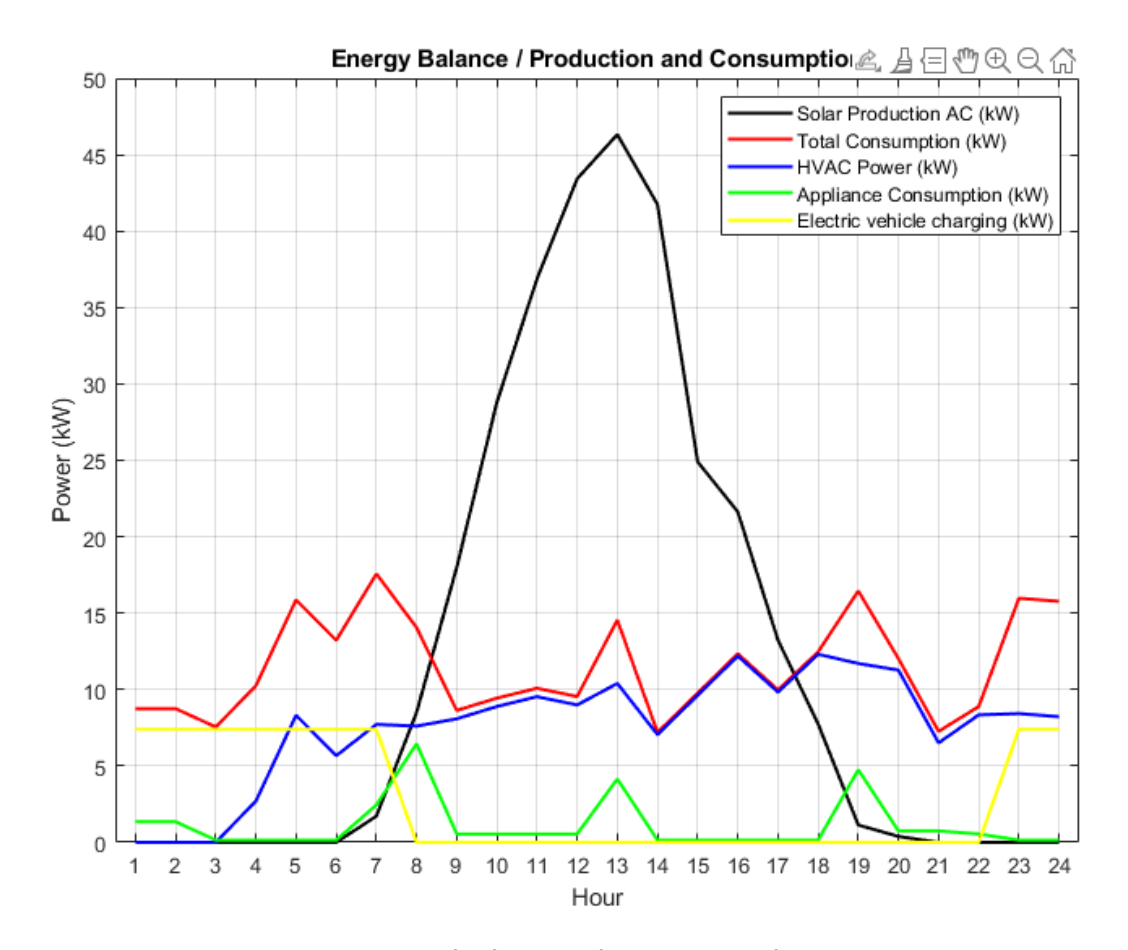


Figure 133. The hottest day Energy Balance.

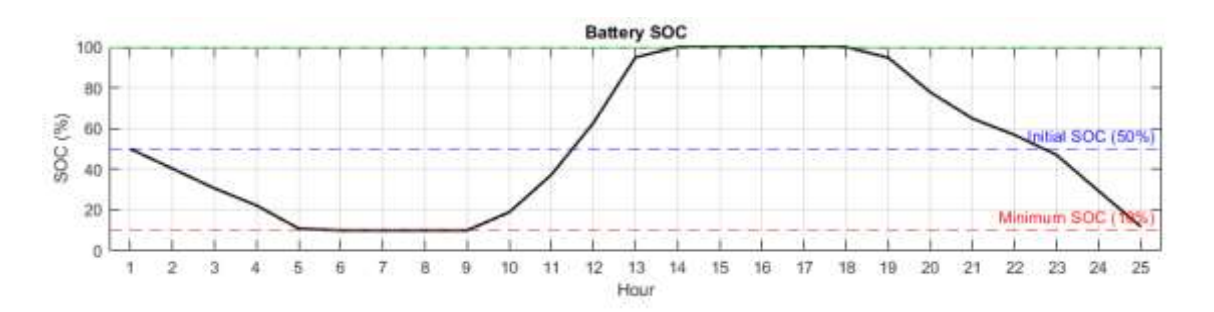


Figure 134. The hottest day Battery SOC.

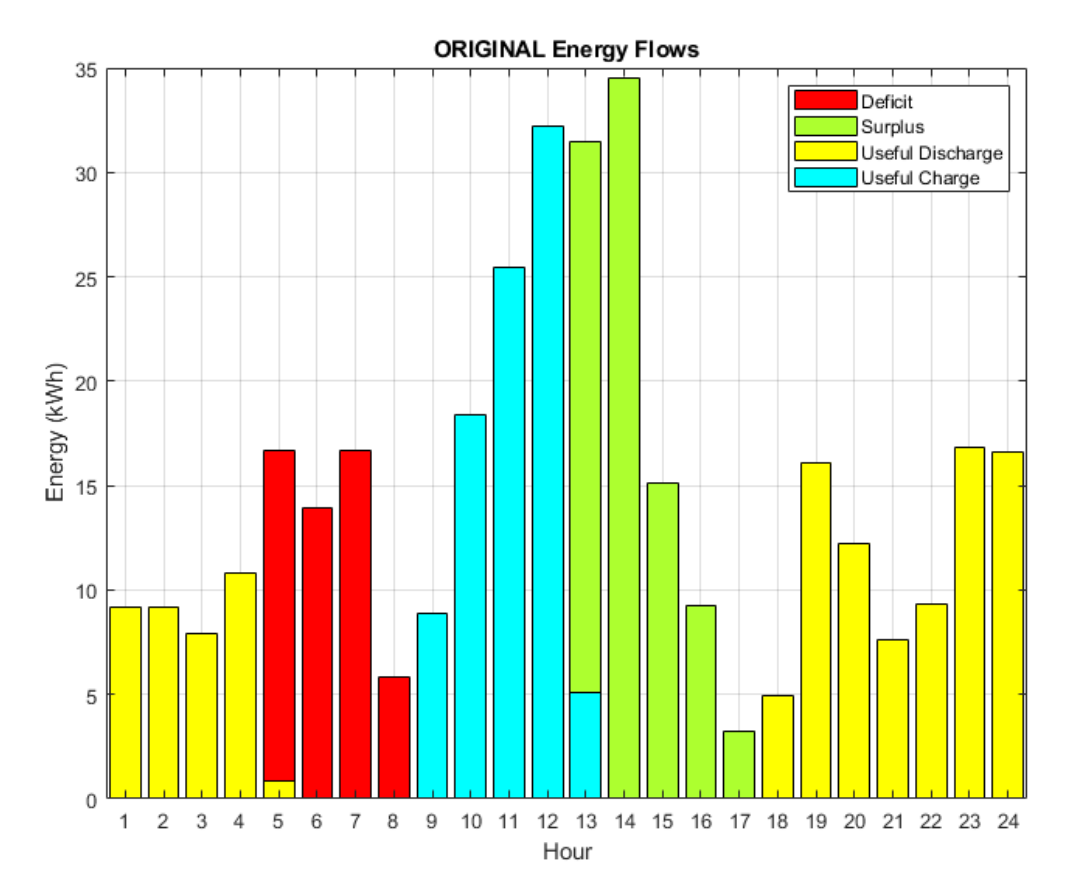


Figure 135. The hottest day Energy Flows.

Although the temperatures are still severe, their proximity to the comfort temperature grants the system additional operational flexibility compared to the coldest day. The unchanged functional restrictions, combined with the smaller temperature gap (between the setpoint temperature and the ambient temperature), create a moderately expanded feasible region that still leads both optimizers to comparable solutions.

This can be observed in controllable appliances, that after optimization the time of use is when there is more solar production than energy consumption, making the energy surplus vary slightly. This results in a higher surplus in the optimizer that seeks to maximize the economic benefit and therefore a higher profit. On the other hand, the optimizer that seeks to minimize energy consumption does not aim to discharge the greatest amount of energy to the grid, but to reduce the deficit, which is why it has a slightly lower surplus, as the difference is due to the consumption of the controllable appliances, which does not account for a large percentage of energy consumption. In addition, the energy consumption of the HVAC and the EV load remain the same in both

optimizers. The optimised schedules of the loads are shown in Figs. 136-139, while Fig. 140 shows the EV SOC comparison for the hottest day.

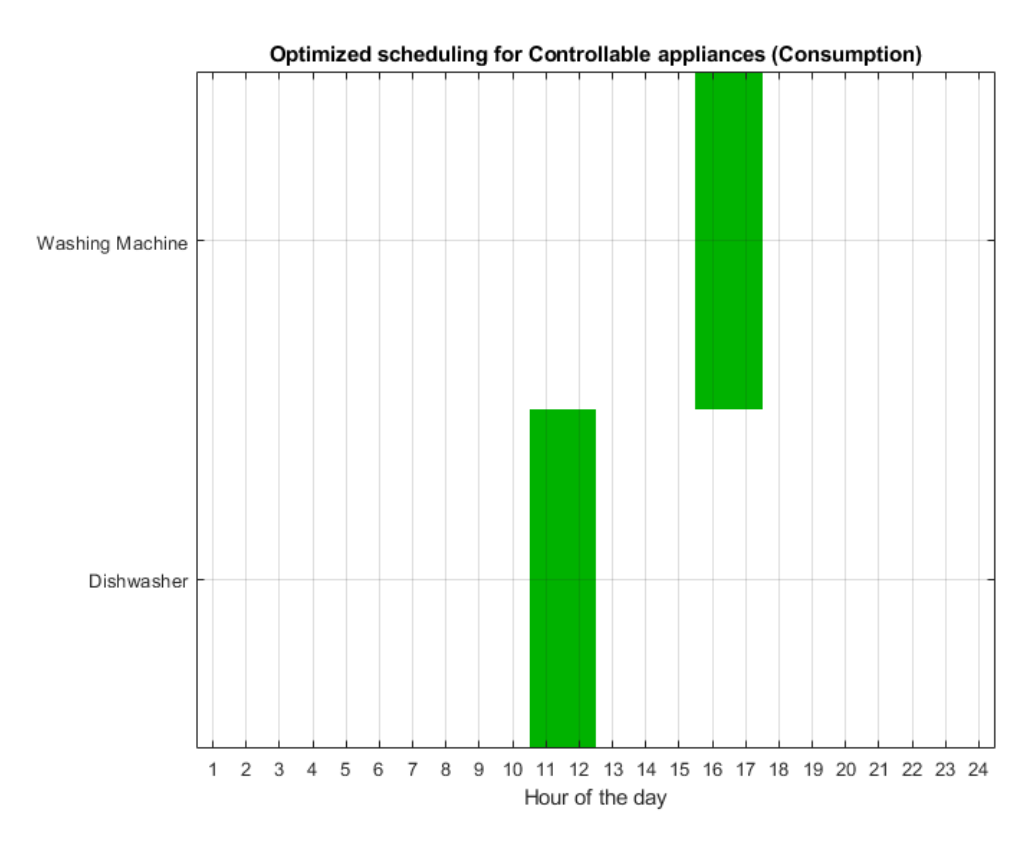


Figure 136. The hottest day scheduling of controllable appliances for optimization for minimum consumption.

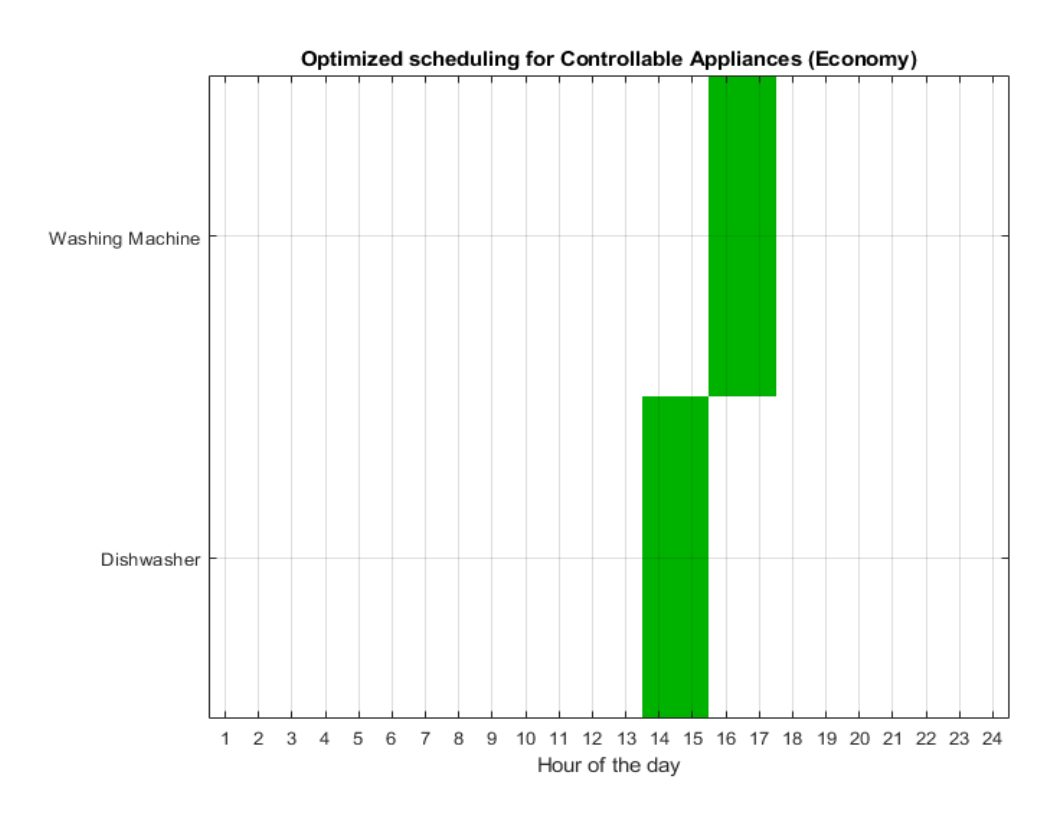


Figure 137. The hottest day scheduling of controllable appliances for optimization for maximum net economic benefit.

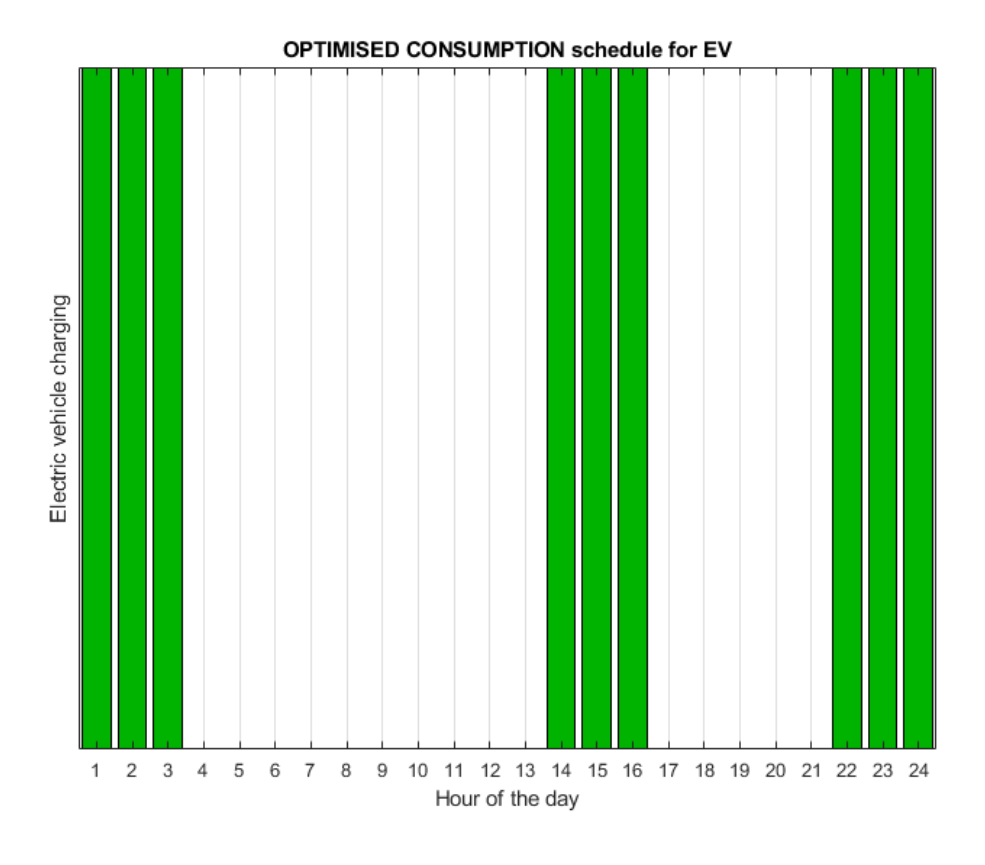


Figure 138. The hottest day EV charging schedule for optimization for minimum consumption.

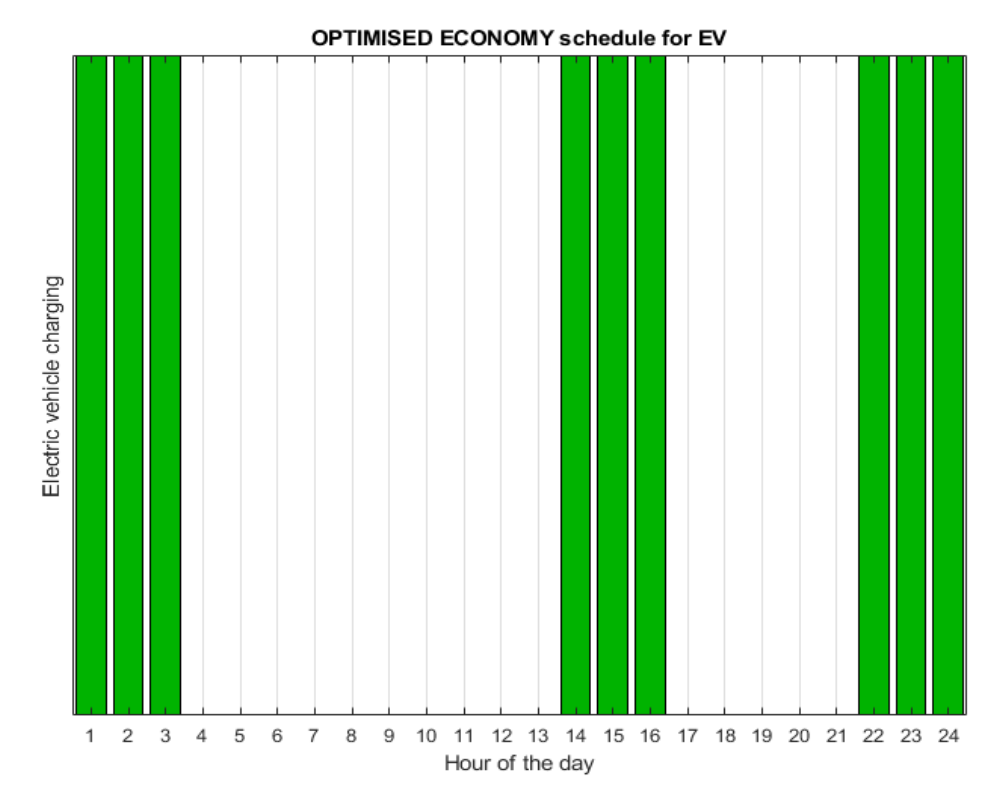


Figure 139. The hottest day EV charging schedule for optimization for maximum net economic benefit.

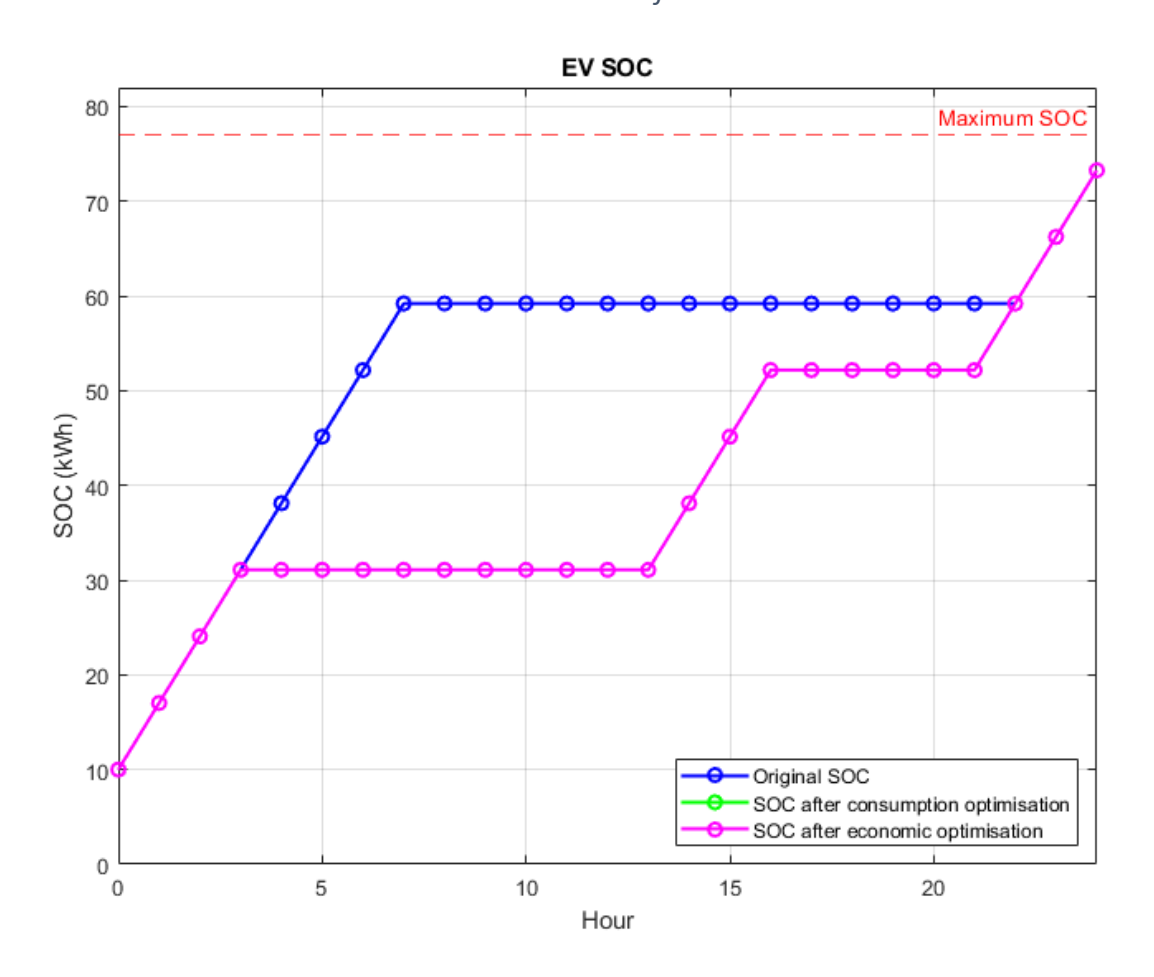


Figure 140. The hottest day EV SOC comparison.

As previously mentioned, the solution is practically the same because the only slight difference lies in the distribution of the appliances, which do not represent a significant energy consumption. Additionally, the EV has the same charging schedule in both solutions. This is why the functions overlap in most of the graphs. The summary of the EV parameters is shown in Table 20.

In Figs. 142-143 the energy consumption of both optimizers is shown, while Fig. 141 shows the original energy consumption for the hottest day. The difference is that the dishwasher in the optimizer that minimizes consumption starts running at 11:00 while in the optimizer that seeks to maximize net economic benefit it starts at 14:00, this has a power of 2.3kW and runs for two hours at a time. In both optimizers the batteries start to charge at 9:00 as there is more solar production than energy consumption and the batteries are fully charged at 13:00 having a surplus. In the optimizer that minimizes consumption it is indifferent to run the dishwasher at that time because it would not reduce the deficit, however the optimizer that maximizes the economic benefit plugs in the dishwasher at 14:00 to generate more surplus because the energy consumption of the HVAC is lower at that time. This makes the optimizers have different but similar solutions as the factor that is different is the time of dishwasher use, as the EV load and the energy consumption of the HVAC system remains the same.

The hottest day battery SOC comparison can be observed in Fig. 144.

Table 20. The hottest day EV parameters.

ELECTRIC VEHICLE	ORIGINAL	OPTIMIZATION FOR	OPTIMISIN
		MINIMUM	ECONOMY
		CONSUMPTION	
Initial SOC (kWh)	10	10	10
Final SOC (kWh)	73.27	73.27	73.27
Charging	63.27	63.27	63.27
performed (kWh)			

Charging	66.60	66.60	66.60
consumption			
(kWh)			
Charging hours	9	9	9
Battery missing	3.27	3.27	3.27
(kWh)			

The same happens with the batteries and the power flows, which are practically identical and only vary slightly due to the appliances consumption.

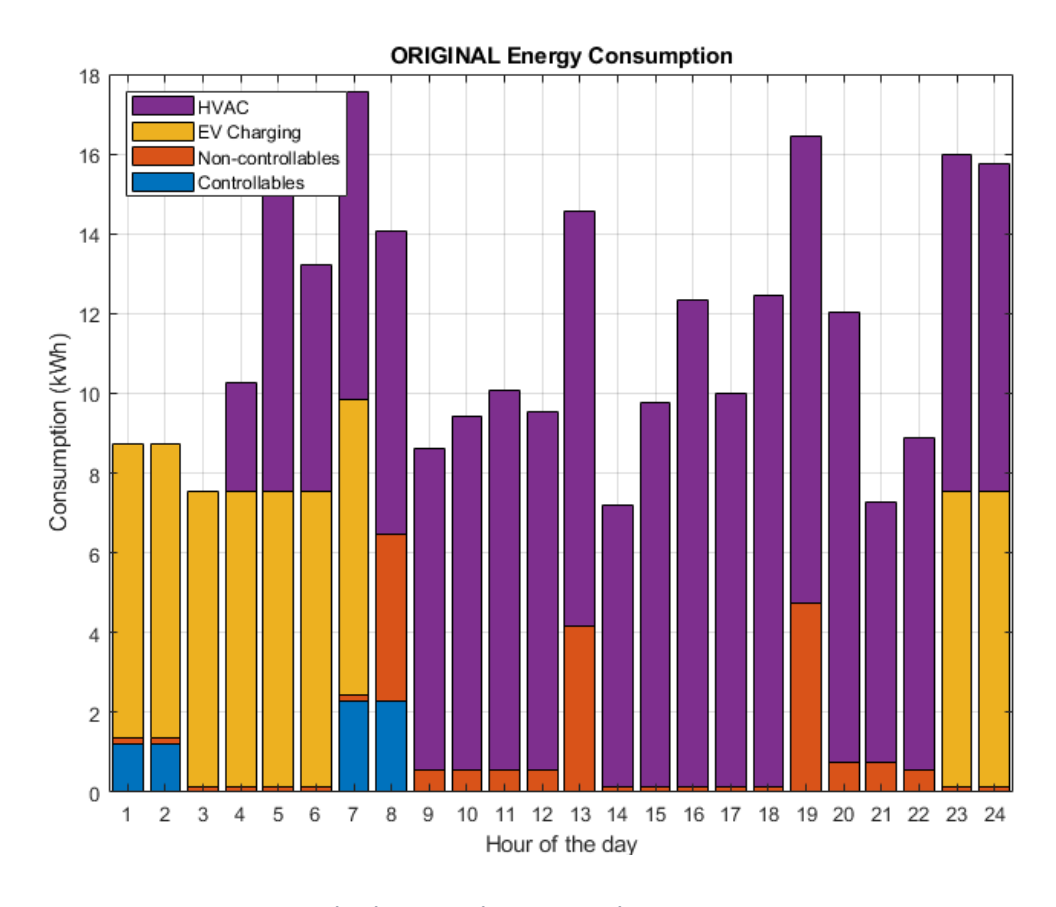


Figure 141. The hottest day original energy consumption.

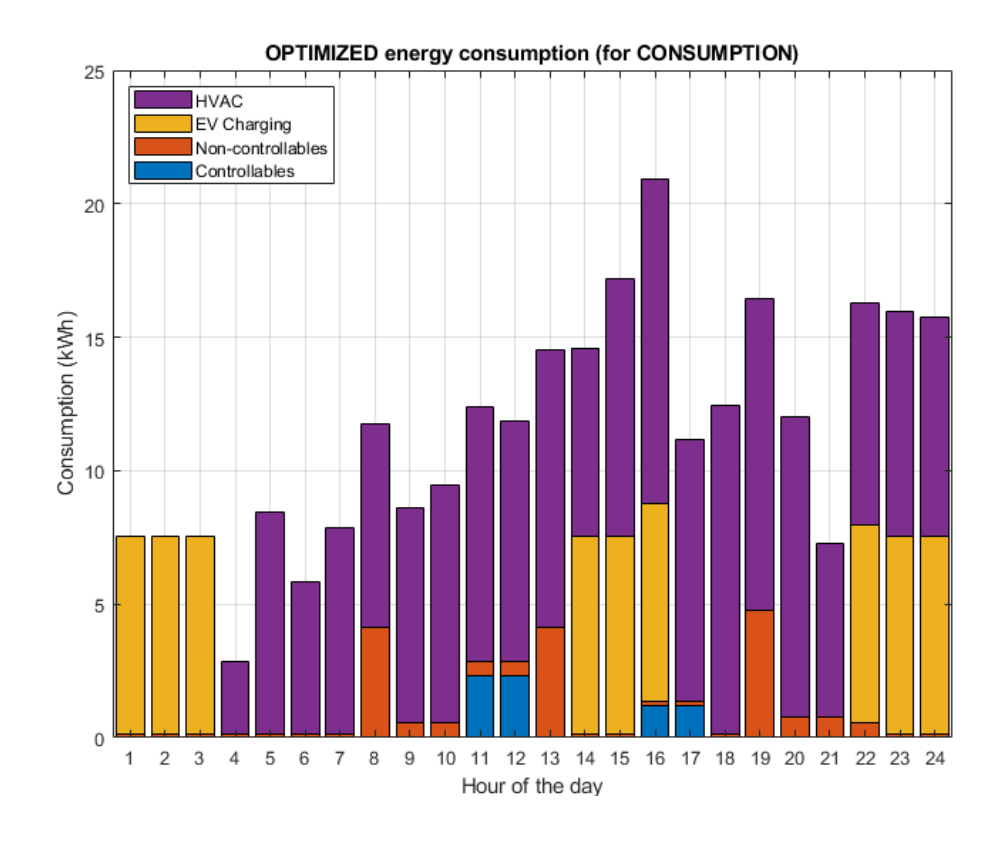


Figure 142. The hottest day energy consumption for optimization for minimum energy consumption.

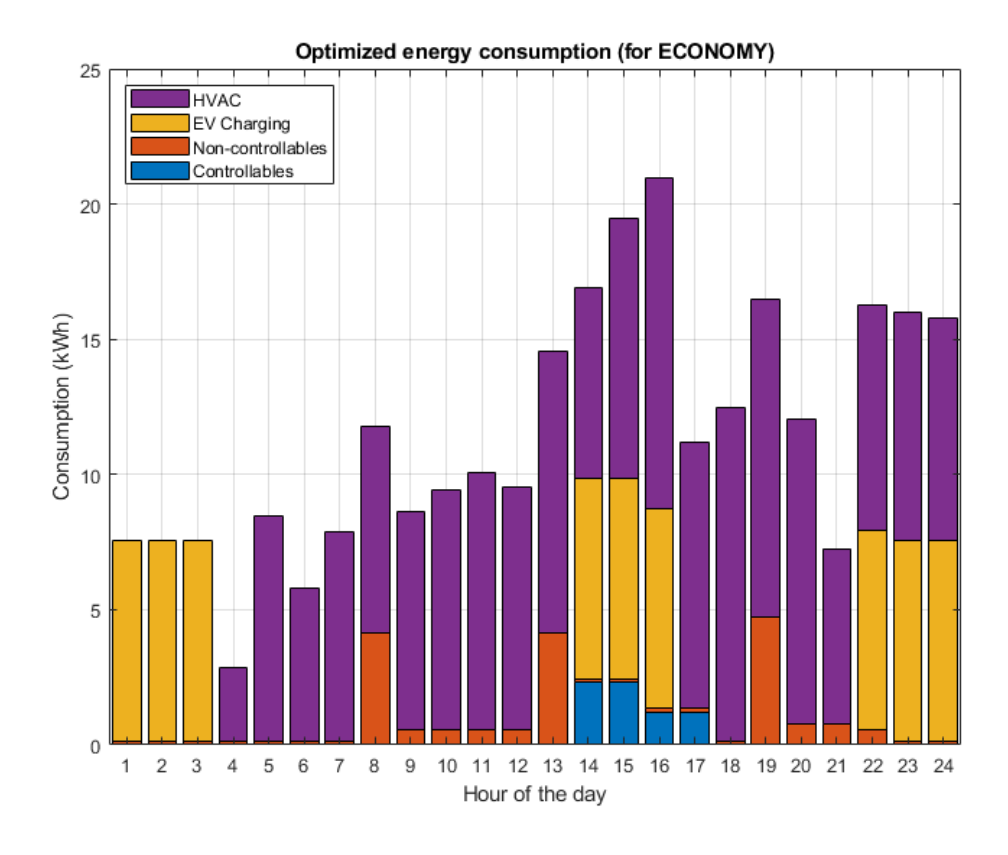


Figure 143. The hottest day energy consumption for optimization for maximum net economic benefit.

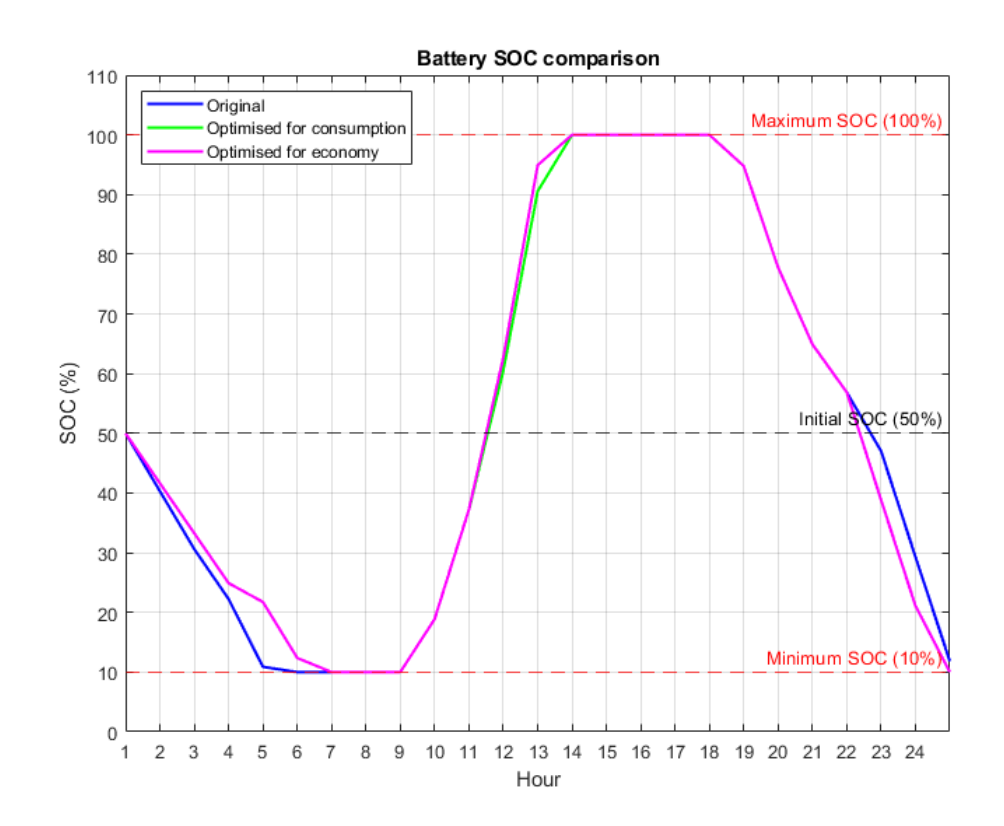


Figure 144. The hottest day Battery SOC comparison.

Table 21. The hottest day batteries parameter summary.

BATTERIES	ORIGINAL	OPTIMIZATION FOR	OPTIMIZATION FOR
		MINIMUM	MAXIMUM NET
		CONSUMPTION	ECONOMIC
			BENEFIT
Initial SOC (kWh)	50	50	50
Final SOC (kWh)	11.84	10	10
Charged performed	90	90.46	90
(kWh)			
Discharge	121.76	121.94	123.50
performed (kWh)			

These small variations in consumption are not significant enough for the economic solution to provide noticeable changes. This can also be seen in Figs. 145-146 where the consumption/production diagrams and energy flow charts are shown. The Table 22

shows that the percentage improvement is the same in both cases, as the results are so similar that they do not represent any appreciable change.

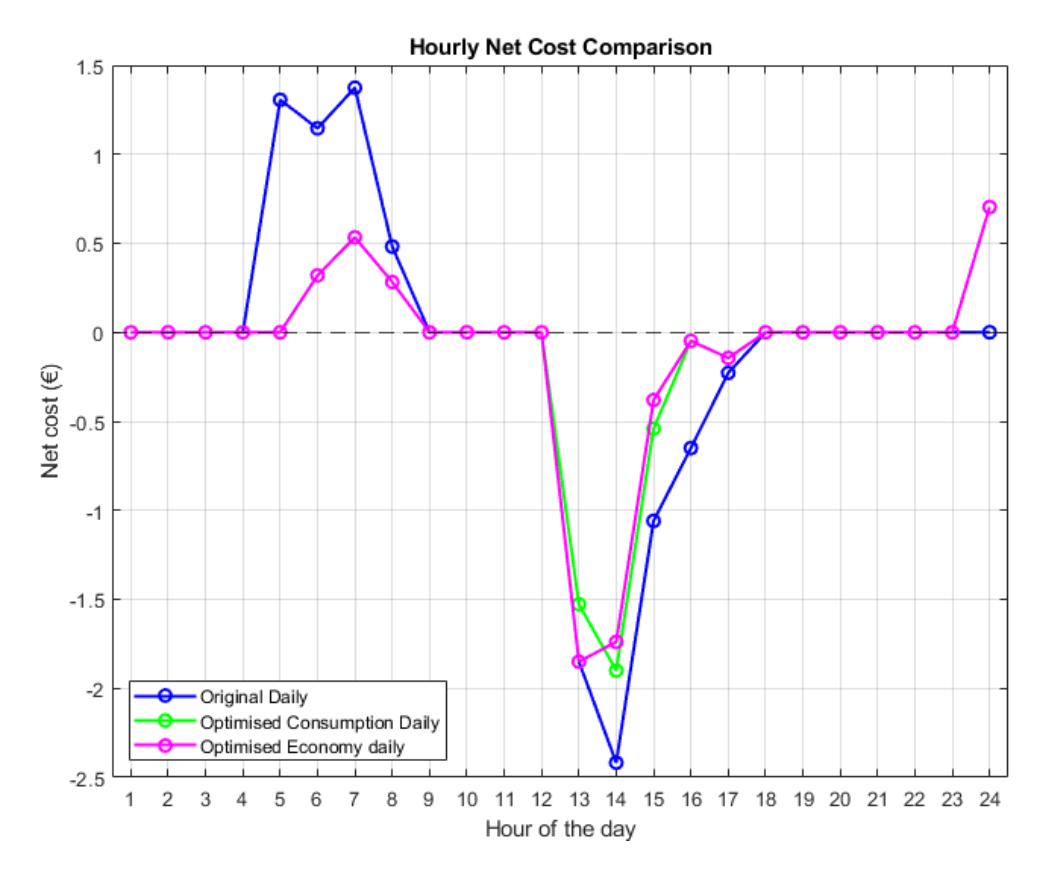


Figure 145. The hottest day hourly net cost comparison for weekdays.

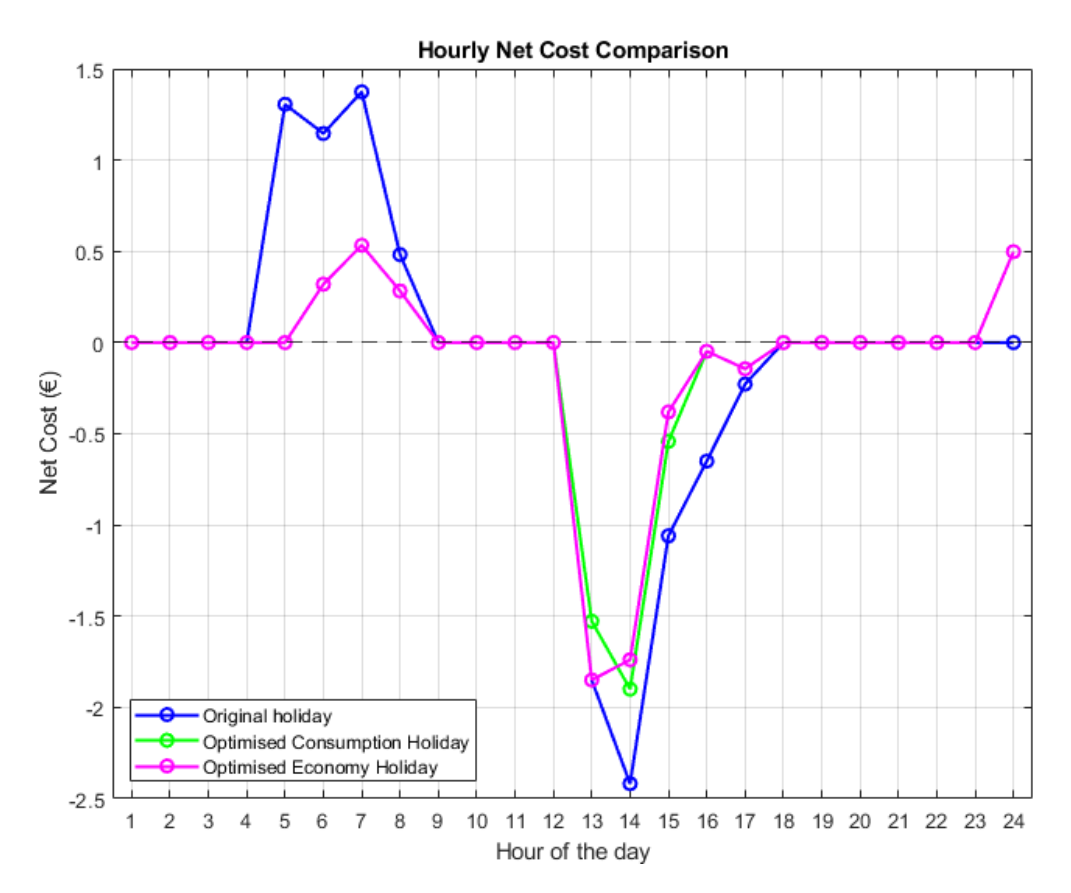


Figure 146. The hottest day hourly net cost comparison for holidays.

Table 22. The hottest day economic cost comparison.

ECONOMIC COST			
DAILY			
	ORIGINAL	OPTIMISED FOR CONSUMPTION	OPTIMIZATION FOR MAXIMUM
			NET ECONOMIC BENEFIT
Purchase cost	4.31	1.84	1.84
(€)			
Selling profit (€)	6.21	4.16	4.16
Net cost (€)	-1.90	-2.32	-2.32
Economic		0.42 (-22.4%)	0.42 (-22.4%)
saving			
PUBLIC HOLIDAYS AND WEEKENDS			
Purchase cost	4.31	1.63	1.63
(€)			
Selling profit (€)	6.21	4.16	4.16

Net cost (€)	-1.90	-2.52	-2.53
Economic		0.63 (-33%)	0.63 (-33.2%)
saving			

The energy balance and energy flows are shown in Figs. 147-152. The Table 23 is a summary of the energy flows of the hottest day.

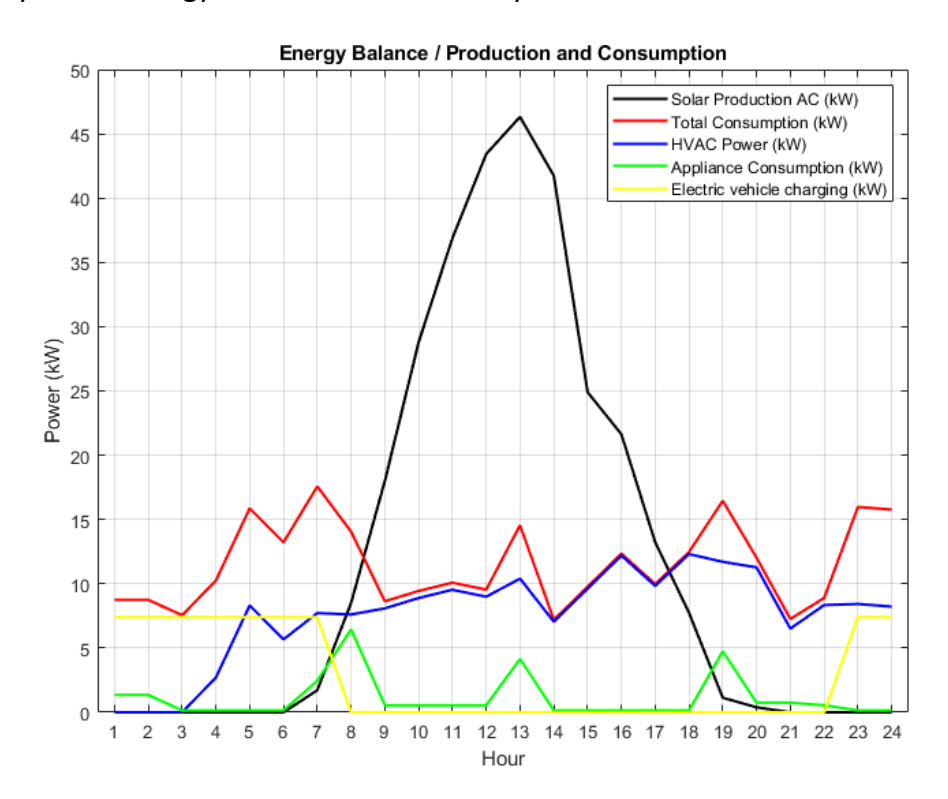


Figure 147. The hottest day original Energy Balance.

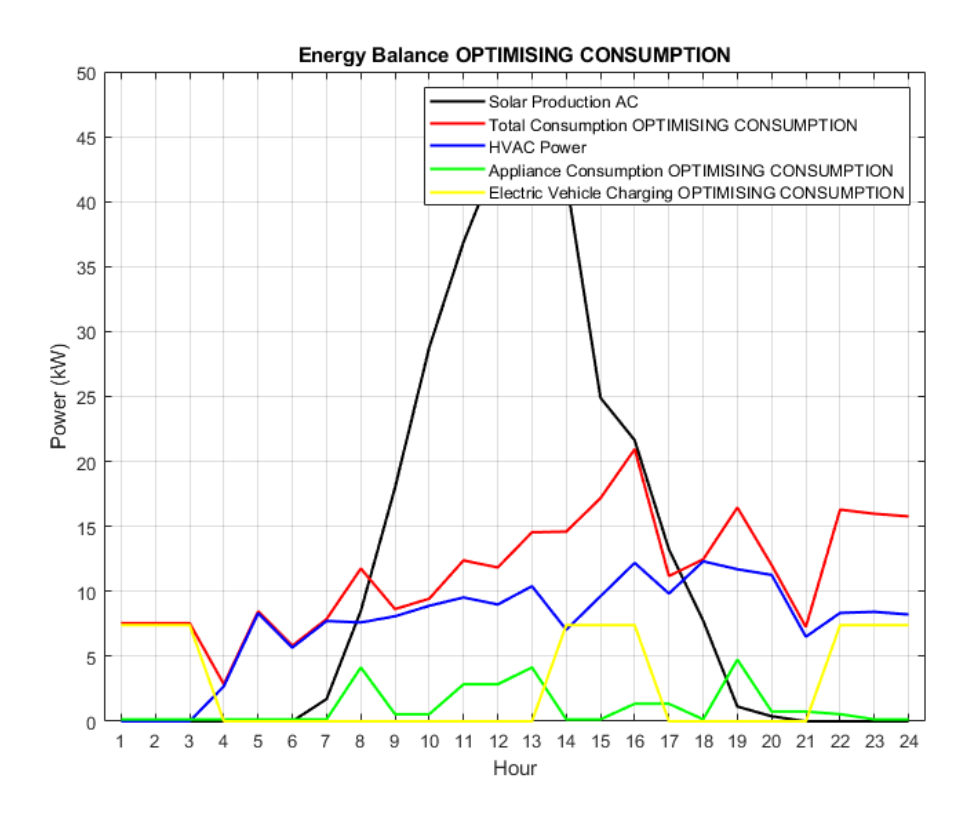


Figure 148. The hottest day Energy Balance for optimization for minimum energy consumption.

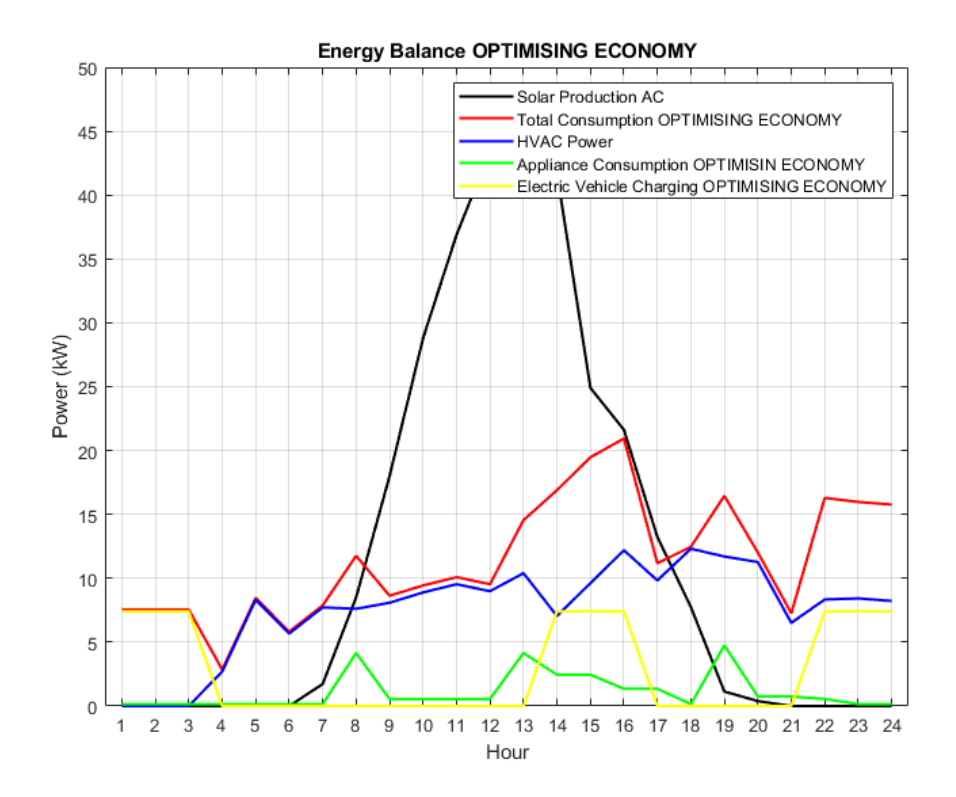


Figure 149. The hottest day Energy Balance for optimization for maximum net economic benefit.

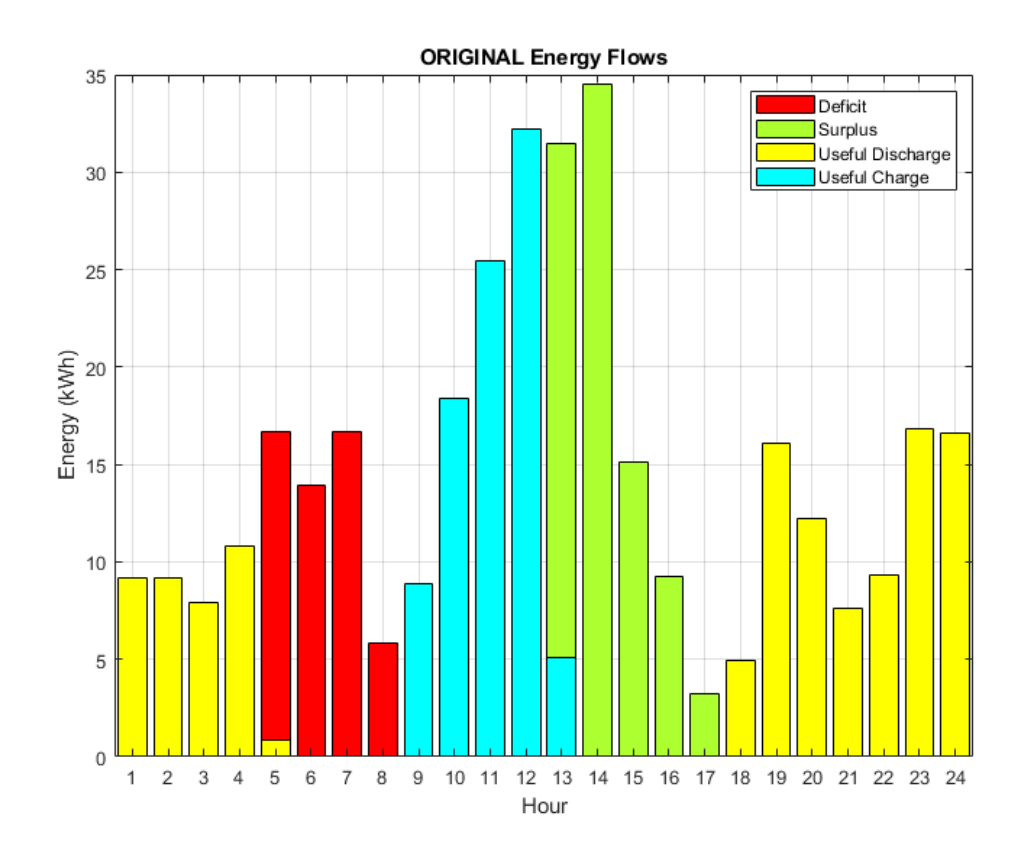


Figure 150. The hottest day original Energy Flows.

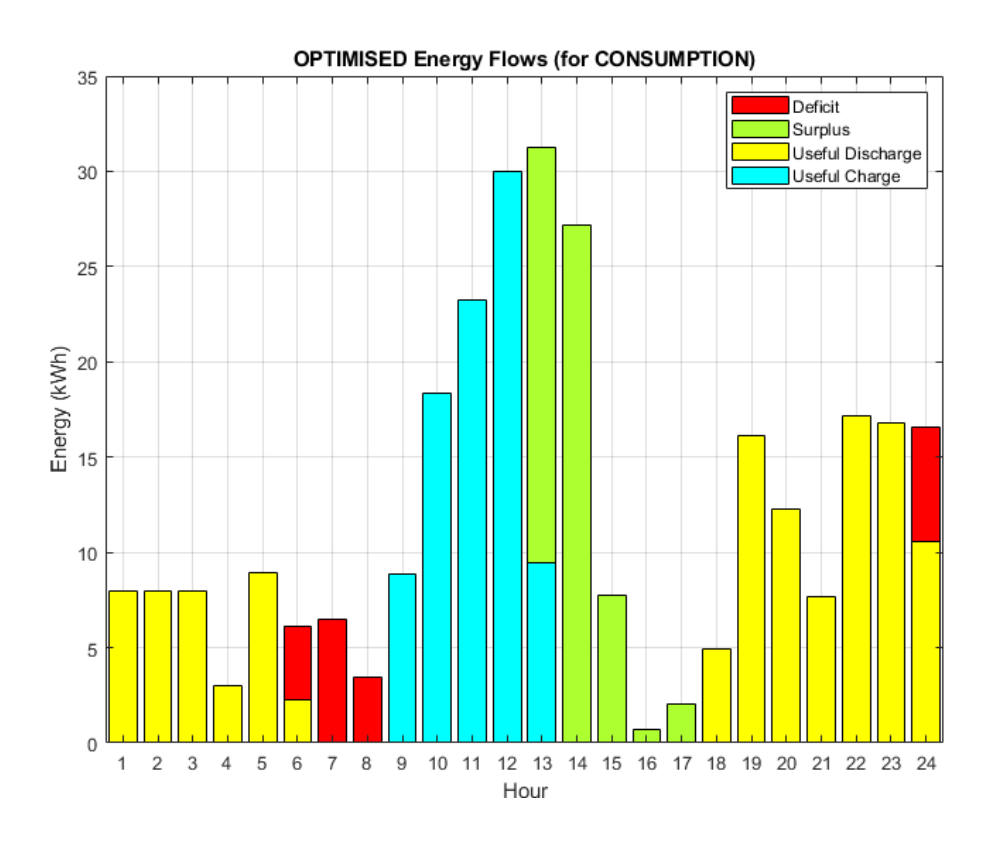


Figure 151. The hottest day Energy Flows for optimization for minimum energy consumption.

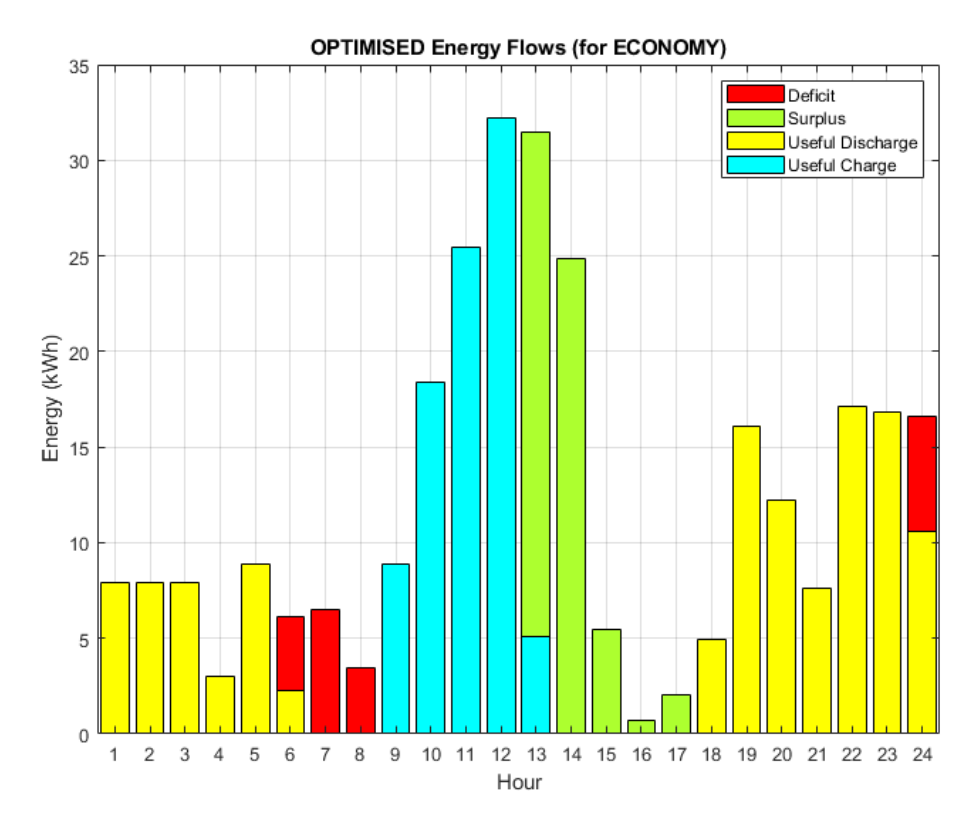


Figure 152. The hottest day Energy Flows for optimization for maximum net economic benefit.

The difference between the surplus in the optimized situations is small.

Table 23. The hottest day Energy Flows summary.

ENERGY	ORIGINAL	OPTIMIZATION FOR	OPTIMIZATION FOR	
FLOWS		MINIMUM	MAXIMUM NET	
		CONSUMPTION	ECONOMIC BENEFIT	
Surplus (kWh)	88.65	59.38	59.45	
Deficit (kWh)	52.32	19.84	19.84	
Improvement		32.48 (62.1%)	32.48 (62.1%)	

Chapter V: Conclusions and future work

This chapter summarizes the main findings of the research, highlighting the contributions of the simulation model and the optimization strategies developed. It reflects on the implications of the results for future zero-emission building design and xenergy management. This chapter also acknowledges the limitations of the current model and proposes directions for future research, including improvements in system complexity, real-time control integration, and potential applications in other building contexts.

Comparison between the cases of study

In order to make a better comparison of the results obtained, the most relevant values will be classified in tables to be able to comment on them.

EV Charging

As far as the charging of the EV is concerned, the same results are shown in Tables 8-14-20. In all cases the same results were obtained. This is because the prohibited EV charging hours do not restrict the number of hours initially proposed, which is why the same solution is arrived at. The EV is charged originally for 9 hours, and the allowed optimization schedule has more than 9 hours free, so the state of charge of the car's batteries will be the same at the end of each simulation.

In all the study days and situations before and after optimization the EV starts at 10% of its capacity, charges for 9 hours with a 7.4 kW power charger and a charging efficiency of 95%. The charging consumes 66.60 kWh, however charging performed is 63.27 kWh, so the EV ends up with 73.27 kWh out of its capacity of 77 kWh.

The prohibited hours used are 8:00-13:00 and 17:00-21:00, which makes a total of 11 hours during which the EV cannot be charged. The charging hours in the initial profile are 9, this means that there are 13 possible hours to charge the EV in the most optimal way possible while respecting the prohibited hours, as the optimizers seek to charge at least the same number of hours as the original ones, 9 in this case. However, if the forbidden schedule would leave less than 9 hours available, there is no possibility to distribute the charging in other hours trying to optimize, because there are not even

enough hours available to charge the same number of hours as in the original profile. This would mean that the optimizers would not have the same parameters as the initial situation.

Batteries

The simulation results from the zero-emissions building model in MATLAB present the performance of the battery system across three representative scenarios: a typical day, the coldest day, and the hottest day. For each scenario, three configurations were evaluated: the original (baseline) setup, an optimization strategy focused on minimizing the energy consumption deficit, and another strategy aimed at maximizing economic benefit. The results for a typical day are presented in Table 9. On a **typical day**, the baseline case shows the battery starting at 50 kWh and ending at 35.14 kWh, with 90 kWh charged and 99.62 kWh discharged. When the optimization for minimum consumption is applied, the discharge increases to 112.35 kWh, although the final state of charge (SOC) drops to 26.94 kWh. The economic optimization results in the highest energy discharge, at 114.78 kWh, but with a further reduced final SOC of 19.18 kWh. These results indicate that both optimization strategies enhance the utilization of the battery, with the economic optimization showing the most aggressive use, likely due to prioritization of financial gain, even at the expense of battery depletion.

The results for the coldest day are presented in Table 16. During the **coldest day**, where heating demands are expected to be highest, the baseline scenario achieves a discharge of 120.08 kWh with a final SOC of 13.60 kWh. Both optimization strategies increase the total discharged energy to 123.50 kWh and bring the battery down to a final SOC of 10 kWh (minimum SOC). This suggests that, under high-demand conditions, both optimizers manage to extract slightly more energy from the battery, although the gains are modest. The identical discharge values for both strategies indicate that system constraints or high demands might limit the flexibility of further optimization.

The results for the hottest day are presented in Table 21. On the **hottest day**, the baseline discharge reaches 121.76 kWh with a final SOC of 11.84 kWh. The consumption-based optimizer provides a marginal improvement, increasing discharge to 121.94 kWh. In

contrast, the economic optimizer again achieves the highest discharge at 123.50 kWh, reducing the final SOC to 10 kWh (minimum possible SOC, also close to the original final SOC). As in the coldest day scenario, economic optimization proves more effective at maximizing battery contribution, suggesting it achieves better results when making decisions aimed at saving or generating revenue based on different electricity prices.

Overall, the results demonstrate that both optimization strategies consistently outperform the original setup in terms of battery utilization. Economic optimization is particularly effective, maximizing discharge across all days. However, this comes at the cost of a significantly lower final SOC, which could have implications for battery lifetime and reserve capacity. The limited improvements seen on extreme weather days suggest the system is already close to its operational limits, leaving little room for further optimization. These insights are valuable for guiding energy management strategies in zero-emissions buildings.

Solar production and consumption

The consumption and solar production throughout each simulation can be seen in Table 28. The consumption of the loads will not be affected after applying the optimizers; however, it will be distributed more effectively to coincide with the periods of time where there is more solar generation, thus reducing the deficit of the house.

Table 24. Solar production and energy consumption summary.

DAY	CA	N-CA	EV	HVAC	Daily	PV Production
	consumption	consumption	consumption	consumption	consumption	
Typical	7 kWh	19.4 kWh	66.6 kWh	178.61 kWh	271.61 kWh	350.31 kWh
Coldest	7 kWh	19.4 kWh	66.6 kWh	261.01 kWh	354.01 kWh	237.66 kWh
Hottest	7 kWh	19.4 kWh	66.6 kWh	183.40 kWh	276.40 kWh	309.91 kWh

It is also interesting to note that the only load that varies between the cases is the HVAC load which will depend on the ambient temperature. Not changing the loads between the cases has been done deliberately in order to have a more similar basis during the different situations. The case with the highest energy consumption is the coldest day because the HVAC system must operate more than in the other situations due to the fact

that the outside temperature is the furthest away from the setpoint and for the longest time.

As discussed earlier in the theoretical framework, if the PV panel temperature increases, the generation decreases, but if the irradiance increases, the production also increases. This can be clearly observed in the solar generation between the cases, because the hottest day despite being the one with the most irradiance also has more temperature making the panel hotter, while in the coldest day the temperature of the PV panel is lower and should produce more, but the irradiance is lower. That is why the day with the highest production is the typical day which has a cooler panel temperature than the coldest day and a higher irradiance than the coldest day, but lower than the hottest day and all this makes that the typical day has the highest production of all.

Economic cost

The results for the typical day are presented in Table 10. On a **typical day**, the original scenario results in a purchase cost of $7.05 \in$ and a selling profit of $9.93 \in$, yielding a net economic gain of $-2.88 \in$. When the system is optimized for minimum consumption, the purchase cost drops significantly to $3.88 \in$. However, the selling profit also decreased to $8.21 \in$, leading to a net cost of $-4.34 \in$. This translates to an economic saving of $1.46 \in$ (a 50.6% improvement) compared to the original case.

With the economic optimization, purchase costs remain the same as the optimization for minimum consumption $(3.88\,\text{\&})$, but the selling profit increases to $8.37\,\text{\&}$. This results in a net economic cost of $-4.50\,\text{\&}$, or in other words, an economic saving of $1.62\,\text{\&}$ (56.2% improvement), outperforming the consumption optimization. This indicates that economic optimization, even without reducing energy purchases, achieves better financial performance by making more efficient use of surplus energy. In real-world applications, this suggests that prioritizing economic strategies can contribute significantly to reducing operational costs. The public holidays and weekends follow the same trend, with slightly adjusted absolute values but identical relative improvements, i.e., 50.6-49.7% for consumption and 56.2-55.2% for economy optimization.

The results for the coldest day are presented in Table 16. During **the coldest day**, which presumably involves increased heating demand, the original setup incurs the highest purchase cost of $13.48 \in$ and achieves only $2.77 \in$ in selling profit, leading to a net cost of $10.70 \in$. Both optimization strategies reduce the purchase cost significantly to $10.81 \in$ but also yield lower selling profits $(0.73 \in)$. Consequently, the net cost is reduced only slightly to $10.09 \in$ in both cases, producing a modest economic saving of $0.62 \in (5.8\%)$. This limited improvement highlights the challenge of optimizing energy costs under high-demand scenarios, such as extreme cold, where the system relies heavily on external energy sources and has fewer opportunities to sell surplus energy. It suggests that, in such cases, the effectiveness of optimization strategies is constrained by thermal demand and system limitations.

On public holidays and weekends, purchase costs slightly decrease (to 12.87 € in the original and 10.06 € in both optimizations), but the overall pattern remains consistent. Economic savings rise marginally to 0.77 € (7.6%), indicating that optimizations have a limited but measurable economic impact on high-demand days.

This case is the most complicated to optimise because it is the one with the greatest deficit since it is where most energy is consumed because as previously mentioned the outside temperature differs greatly from the desired indoor temperature. This is why the improvement obtained is limited.

The results for the hottest day are presented in Table 22. On the **hottest day**, the original system results in a purchase cost of $4.31 \in$ and a selling profit of $6.21 \in$, resulting in a net gain of $-1.90 \in$. Consumption optimization dramatically reduces purchase costs to $1.84 \in$ but also lowers selling profits to $4.16 \in$. The net cost drops to $-2.32 \in$, generating an economic saving of $0.42 \in (22.4\%)$. Although the absolute saving is small, this result reflects a meaningful relative improvement, showing that even during periods of high cooling demand, consumption-focused strategies can still enhance economic performance by effectively reducing energy purchases. However, the reduced profit from energy sales indicates a trade-off between maximizing self-consumption and taking advantage of grid feed-in opportunities.

Economic optimization yields identical results, suggesting that on this day, the flexibility in the system is limited, and both optimizations converge to the same performance. During holidays and weekends, the savings increase to 0.63 € (33%), indicating that tariff differences or demand shifts might enhance the optimization effect under altered schedules.

Overall, the economic optimization strategy consistently achieves higher net economic gains compared to the consumption-based approach, especially on typical and hot days. On the coldest day, both optimizers perform equally, likely constrained by high energy needs. Savings are most pronounced on typical days and public holidays, where tariff structures or flexible demand may allow for better scheduling.

This analysis highlights the value of intelligent control systems in zero-emission buildings—not just for energy balance, but for financial efficiency too. Economy-based optimization can significantly reduce operating costs, while still maintaining energy performance, especially under moderate weather conditions.

Energy flows

The results offer insight into how well the system aligns energy production and demand under each configuration. The results for the typical day are presented on Table 11. On a **typical day**, the original configuration shows a high energy surplus of 141.80 kWh and a deficit of 84.97 kWh. Both optimization strategies significantly reduce the deficit to 46.45 kWh while also reducing the surplus to approximately 112.60–119.60 kWh. This results in an improvement of 38.53 kWh (45.3%), which is identical for both strategies. These results demonstrate that optimization can more effectively match energy generation with demand, reducing waste and unmet needs simultaneously.

The results for the coldest day are presented on Table 17. During the **coldest day**, where heating demand is very high, the system starts with a low surplus (39.62 kWh) and a high deficit (156.33 kWh). With optimization, the deficit decreases to 122.17 kWh, and the surplus is reduced to 10.42 kWh. The overall improvement is 34.16 kWh (21.9%), again identical for both optimizers. Although the improvement is less pronounced than on

other days, it shows that optimization still provides a meaningful reduction in deficit, even under challenging conditions.

The results for the hottest day are presented on Table 23. On the **hottest day**, the baseline surplus is 88.65 kWh, and the deficit is 52.32 kWh. Optimization reduces the surplus to around 59.38–59.45 kWh and dramatically reduces the deficit to 19.84 kWh. This results in the highest relative improvement among all days: 32.48 kWh (62.1%). This suggests that during hot days, the system has greater flexibility to reallocate energy efficiently, possibly due to more predictable or consistent demand patterns (e.g., cooling systems).

Across all scenarios, both optimization strategies demonstrate a substantial reduction in energy deficit, which contributes directly to improved system efficiency. The energy surplus also decreases in each case, indicating better utilization of available resources. Interestingly, the performance of the consumption and economic optimizers is nearly identical in terms of energy flows, suggesting that both achieve similar operational alignment of energy use and production, even though their cost-based strategies differ. Also, the loads to be distributed during the simulation are relatively small and that is why the results are similar.

Comparison conclusion

Combining the analyses of battery usage, economic performance, and energy flows, it can be concluded that the optimization significantly improves system performance across all key indicators. The consumption-based optimizer prioritizes the reduction of energy waste and deficit, while the economic optimizer consistently extracts more financial value from the system—even though both achieve similar physical outcomes in terms of energy distribution.

The most notable improvements occur on the typical and hottest days, where the system has more flexibility. On the coldest day, although gains are smaller, the optimizations still provide measurable benefits, despite higher energy demand constraints. Economic savings are highest on typical days and weekends, highlighting the importance of demand scheduling and tariff-aware control systems.

In conclusion, the implementation of intelligent optimization strategies in zero-emissions buildings yields substantial improvements in energy efficiency, economic savings, and battery performance. The results clearly support the integration of such algorithms into real-world energy management systems, particularly in smart grid environments where dynamic tariffs and variable demands must be continuously balanced. These findings reinforce the importance of combining technical optimization with economic strategies to achieve both environmental and financial sustainability in building operations.

The energy consumption results observed across the three simulated scenarios—typical day, coldest day, and hottest day—are notably high due to the large volume and corresponding thermal demand of the modelled building, which has a volume of 1200 m³. This volume implies a significant internal air mass that must be conditioned, particularly during periods of extreme outdoor temperatures.

On the **coldest day**, the building exhibits the highest energy deficit (156.33 kWh) and the lowest surplus (39.62 kWh) in the base case. This is primarily driven by the elevated heating demand required to maintain indoor thermal comfort in response to very low ambient temperatures. In such conditions, heat losses through the envelope increase substantially due to the higher temperature gradient between indoor and outdoor environments. Additionally, the performance of the heat pump is less efficient in cold climates, further increasing electrical demand. The optimization strategies, although less impactful in absolute terms compared to the typical day, still manage to reduce the deficit by approximately 21.9%, demonstrating their effectiveness even under severe conditions.

Conversely, on the **hottest day**, the high energy usage is attributed to the intense cooling requirements driven by peak ambient temperatures. It has to be taken into account that the cooling load has to compensate for the outside temperature and the internal heat due to the heat generated by the occupancy of people and appliances, resulting in a deficit of 52.32 kWh in the base case. Although this scenario shows better balance compared to the coldest day, it still reflects substantial HVAC demand due to the building's size and the thermal inertia of the internal air and building materials.

Even on a **typical day**, with moderate temperatures, the system shows significant energy mismatches in the base scenario (141.80 kWh surplus and 84.97 kWh deficit), indicating that without optimization, the system generates excess energy at times when it is not needed and fails to meet demand at others. This imbalance arises from the inherent variability in generation from solar PV and consumption patterns, and it underlines the need for dynamic control.

Overall, the observed high energy flows can be attributed to the combination of large building volume, variable external climatic conditions, thermal comfort requirements, and the dynamic nature of renewable energy generation. The application of smart optimization strategies—whether aimed at reducing deficits or maximizing economic return—proves essential in aligning energy production with demand, reducing inefficiencies, and supporting the goals of a Zero Emission Building.

Future work

Possible improvements for the future would be to include a greater diversity of appliances with different restrictions, for example adding more controllable appliances, but that these must be used 3 hours non-consecutively instead of two hours at a time per day. In this way the optimization could be more significant by having more loads to rearrange throughout the day.

Other factors such as lighting should be taken into account to make the study more realistic, although due to the large consumption of electricity from other sources, it could be considered negligible if it is assumed that the lighting is provided by low energy lamps. The production of hot water is also not taken into account because it is assumed that it is provided by a solar heater that does not consume energy, although the solar heater relies on the sun to operate, so it is not possible to generate hot water when there is no sun.

Another possible improvement for the future would be to implement more constraints into the optimization process. One such constraint could ensure that the EV is charged continuously during a certain period within the allowed charging window — for example, enforcing uninterrupted charging during the early morning hours. Alternatively, a rule

could be added requiring that if charging occurs within a specific time range, the charging hours must be consecutive.

Another potential enhancement would be to implement a consumption forecasting model based on user routines. This would make it possible to predict energy demand more accurately and allow for a more efficient redistribution of energy loads. For example, charging the EV could be scheduled during periods of expected energy surplus or when prices are lower, while still ensuring that the EV reaches a minimum charge level. In cases where surplus energy is not available, charging could be reassigned to time slots with the lowest expected deficits. This predictive approach could optimize overall system performance by aligning energy use more closely with availability and pricing conditions.

This approach may lead to adjustments in the total charging duration compared to the original profile. For instance, the vehicle could be charged for fewer hours, as long as a minimum battery level is ensured. All charging would still need to comply with restricted time periods and consider technical constraints — such as preventing the battery from exceeding 100% charge. Additionally, if the vehicle remains connected after reaching full charge, the system should continue to log any excess or unused energy. This logging mechanism is already implemented, although currently without enforcing a minimum charge level.

To further improve the work in the future, it would be interesting to explore a wider range of scenarios by varying key model parameters. This includes modifying thermal variables, indoor and outdoor temperature conditions, building size, refrigerant type, and operating conditions of the compression cycle. Testing different working points of the cycle could help identify the optimal operating conditions. Additionally, improvements to the cycle itself could be implemented to enhance overall performance. Another useful enhancement would be to include thermal gains based on building orientation and the effect of shading. These adjustments would aim to have a more realistic overall energy consumption.

Further enhancements could include integrating multi-objective optimization to simultaneously consider economic return and energy autonomy or introducing time-of-use tariffs for more realistic economic modelling.

For greater accessibility, particularly for non-technical users, the code developed could be adapted into a graphical user interface (GUI) that allows easy modification of inputs and interpretation of outputs without interacting directly with the code.

References

- Brenner, L. (2025, June 23). *ResearchGate*. Retrieved from ResearchGate: https://www.researchgate.net/figure/Simplified-schematic-of-a-the-considered-refrigeration-cycle-and-b-the-corresponding fig3 353503599
- Chamarro Camazón, C. (2023, April). Renewable Energies. Solar Energy. Valladolid, Valladolid, Spain.
- Chapman, B. (2025, June 17). *Let's Talk Science*. Retrieved from How does a lithium-Ion battery work?: https://letstalkscience.ca/educational-resources/stem-explained/how-does-a-lithium-ion-battery-work
- eurostat, I. &. (2025). Consumos del Sector Residencial en España (año 2010) Información Básica (Proyecto SPAHOUSEC). IDAE .
- Fedkin, M. V. (2025, June 17). *EME 812: Utility Solar Power and Concentration*. Retrieved from EME 812: Utility Solar Power and Concentration: https://www.e-education.psu.edu/eme812/node/595
- Fernández, J. M. (2025, June 17). *Tarifaluzhora*. Retrieved from ¿Cuánto cuesta el kilovatio hora de luz (kWh) en España en 2025?: https://tarifaluzhora.es/info/precio-kwh
- Gestor. (2025, June 17). *Greening solutions*. Retrieved from La importancia de la orientacion de los paneles solares: seguidores solares: https://greening-e.com/seguidores-solares/
- Ghanavati, F., Matias, J., & Osório, G. (2024). *Towards sustainable smart cities: Integration of home energy management.* Sustainable Cities and Society 111 (2024) 105579.
- GROUP, K. (2025, June 17). *KEYTER* . Retrieved from The Four-Way Valve: A Key Component in Reversible HVAC Systems: https://www.keyter.com/the-four-way-valve-a-key-component-in-reversible-hvac-systems/

- IDAE. (2010). *Guía técnica de agua caliente sanitaria central.* Ministerio de industria, turismo y comercio.
- IDAE. (2025, June 17). *Informes Web IDAE*. Retrieved from Informe Web Consumo por usos del sector residencial 16ª edición Marzo 2025: https://informesweb.idae.es/consumo-usos-residencial/informe.php
- Kansagara, R. (2025, June 17). *Circuit Digest*. Retrieved from Introduction to Different Types of Inverter: https://circuitdigest.com/tutorial/different-types-of-inverters
- MATLABWorks. (2025, June 22). ReversibleHeatPumpExample. Retrieved from MATLAB

 Works:

 https://www.mathworks.com/help/hydro/ug/ReversibleHeatPumpExample.ht

 ml
- OMIP. (2025, June 17). OMIP. Retrieved from OMIP: https://www.omip.pt/en
- Stuart Bowden & Christiana Honsberg. (2025, June 17). *PVCDROM*. Retrieved from PVCDROM: https://www.pveducation.org/pvcdrom/solar-cell-operation/ivcurve
- Tejero González, A. (2024, May). Refrigeration and Air Conditioning. Cold Production Processes. Valladolid, Valladolid, Spain.
- Vega Maza, D. (2022, March). Technical Thermodynamics and Heat Transfer. Block 1: Fundamentals of Thermodynamics. Valladolid, Valladolid, Spain.
- Wang, S., Kong, L., Liu, C., & Cai, G. (2024). *MPC-based energy optimization and regulation for zero-carbon energy.* International Journal of Hydrogen Energy 82 (2024) 1196–1210.
- Wang, X., Mi, Z., Li, K., Huang, X., Bao, W., Song, J., Wang, C., Chen, G., & Cao, P. (2024).

 Design and transient analysis of renewable energy-based residential net-zero energy buildings with energy storage. Renewable Energy 220 (2024) 119512.